Title

Theoretical Studies of Non-Newtonian and Newtonian Fluid Flow through Porous Media

Author

Wu, Y.-S.

Publication Date

1990-02-01

LBL-28642

Lawrence Berkeley Laboratory
UNIVERSITY OF CALIFORNIA

EARTH SCIENCES DIVISION

Theoretical Studies of Non-Newtonian and Newtonian Fluid Flow through Porous Media

Y.-S. Wu
(Ph.D. Thesis)

February 1990

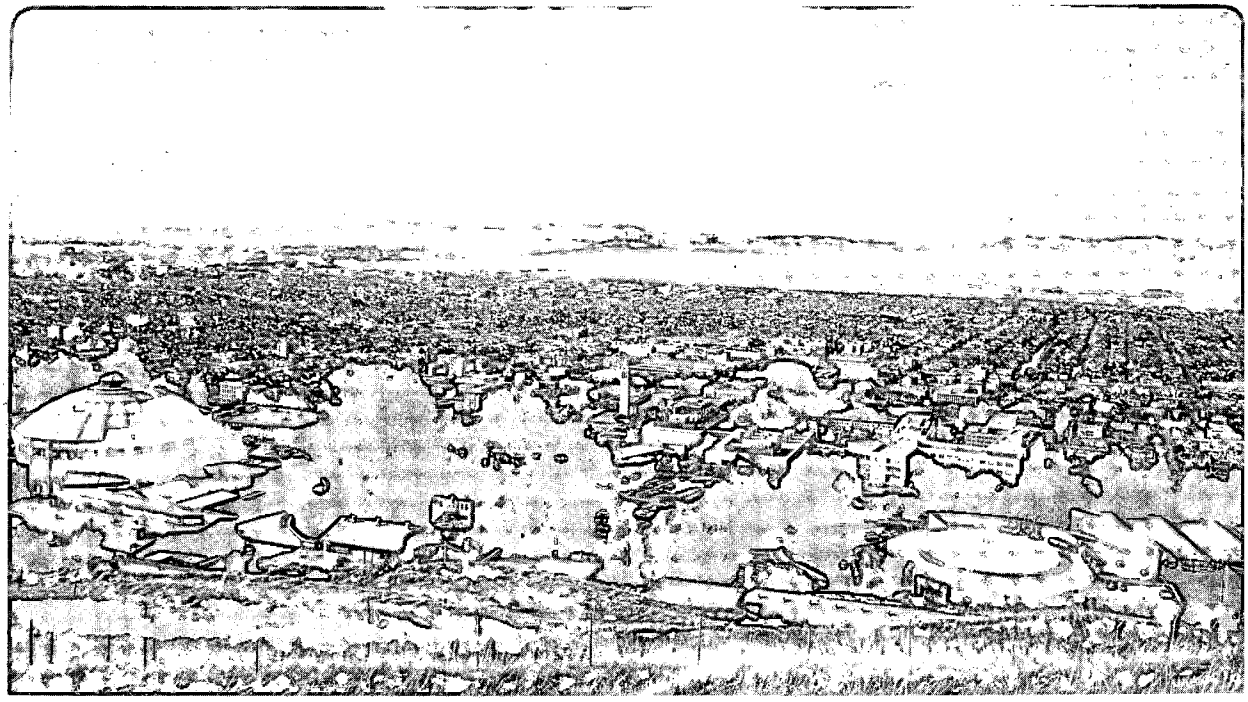

Prepared for the U.S. Department of Energy under Contract Number DE-AC03-76SF00098.

DISCLAIMER

LBL-28642

Theoretical Studies of Non-Newtonian and Newtonian Fluid Flow through Porous Media

Yu-Shu Wu

(Ph.D. Thesis)

Department of Materials Science and Mineral Engineering
University of California

and

Earth Sciences Division
Lawrence Berkeley Laboratory
University of California
Berkeley, California 94720

February 1990

This work was supported by the U.S. Department of Energy under Contract No. DE-AC03-76SF00098.

Theoretical Studies of Non-Newtonian and Newtonian Fluid Flow though Porous Media

Yu-Shu Wu

Department of Material Sciences and Mineral Engineering

University of California, Berkeley

Berkeley, California 94720

Abstract

A comprehensive theoretical study has been carried out on the flow behavior of both single and multiple phase non-Newtonian fluids in porous media. This work is divided into three parts: (1) development of numerical and analytical solutions; (2) theoretical studies of transient flow of non-Newtonian fluids in porous media; and (3) applications of well test analysis and displacement efficiency evaluation to field problems.

A fully implicit, integral finite difference model has been developed for simulation of non-Newtonian and Newtonian fluid flow through porous media. Several commonly-used rheological models of power-law and Bingham plastic non-Newtonian fluids have been incorporated in the simulator.

A Buckley-Leverett type analytical solution for one-dimensional, immiscible displacement involving non-Newtonian fluids in porous media has been developed. Based on this solution, a graphic approach for evaluating non-Newtonian displacement efficiency has been developed. The Buckley-Leverett-Welge theory is extended to flow problems with non-Newtonian fluids. An integral method is also presented for the study of transient flow of Bingham fluids in porous media. In addition, two well test analysis

methods have been developed for analyzing pressure transient tests of power-law and Bingham fluids, respectively. Applications are included to demonstrate this new technology.

The physical mechanisms involved in immiscible displacement with non-Newtonian fluids in porous media have been studied using the Buckley-Leverett type analytical solution. The results show that this kind of displacement is a complicated process and is determined by the rheological properties of the non-Newtonian fluids and the flow conditions, in addition to relative permeability data. In another study, an idealized fracture model has been used to obtain some insights into the flow of a power-law fluid in a double-porosity medium. For flow at a constant rate, non-Newtonian flow behavior in a fractured medium is characterized by two-parallel straight lines on a log-log plot of injection pressure versus time. Transient flow of a general pseudoplastic fluid has been studied numerically and it has been found that the long time pressure responses tend to be equivalent to that of a Newtonian system.

P. A. Witherspoon

Thesis Committee Chairman

Table of Contents

List of Figures

List of Tables

Nomenclature

Symbol	Description	Units
A	Cross-sectional area	m^2
A_{nm}	Surface element between V_n and V_m	m^2
b	Fracture aperture	m
B	Gogarty's Constant	$s^{(y-1)/y}$
C_f	Fluid compressibility	Pa^{-1}
C_f	Total compressibility of fracture	Pa^{-1}
C_m	Total compressibility of matrix	Pa^{-1}
C_r	Formation compressibility	Pa^{-1}
C_t	Total compressibility	Pa^{-1}
D	Half fracture spacing	m
D_p	Particle diameter of porous material	m
$\underline{D}$	Rate-of-deformation tensor	s^{-1}
D_{ij}	ijth component of $\underline{D}$	s^{-1}
D_{nm}	Distance betweenV_n and V_m	m
f_{ne}	Fractional flow of Newtonian phase	
f_{nn}	Fractional flow of non-Newtonian phase	
f(K)	Permeability function	
$\vec{F}_\beta$	Mass flux for fluid β	m/s
$F_{\beta,nm}$	Flux term of fluid β between V_n and V_m	m/s
g	Magnitude of the gravitational acceleration	m/s^2
$\vec{g}$	Gravitational acceleration vector	m/s^2
G	Minimum pressure gradient	Pa/m
h	Formation thickness	m

H	Power-law consistence	$Pa \cdot s^n$
K	Absolute permeability	m^2
K_f	Fracture permeability	m^2
K_m	Matrix permeability	m^2
k_{rne}	Relative permeability to Newtonian phase	
k_{rnn}	Relative permeability to non-Newtonian phase	
k_{rw}	Relative permeability water phase	
L	Length of a system or a core	m
m	Gogarty's permeability constant	
m	Slope of semi-log curves	Pa
M	Mass of fluid	Kg
m'	Slope of log-log curves	
M_n	Average value of mass in V_n	Kg/m^3
M_β	Mass accumulation for fluid β	Kg/m^3
$M_{\beta,n}$	Mass of fluid β in V_n	Kg
n	Power-law exponential index	
N_p	Cumulative displaced fluid	m^3
n'	Mungan's coefficient	
$\vec{n}$	Unit outward normal vector	
P_c	Capillary pressure	Pa
$P_{fw}(t)$	Wellbore flowing pressure	Pa
P_i	Initial formation pressure	Pa
P_{ne}	Pressure of Newtonian phase	Pa
P_{nn}	Pressure of non-Newtonian phase	Pa
ΔP	Pressure difference	Pa
∇P	Pressure gradient	Pa/m
q_β	Source for fluid β	$Kg/(m^3 s)$

$q_{\beta,n}$	Source for fluid β in V_n	$Kg/(m^3s)$
Q	Volumetric injection/production rate	m^3/s
Q(t)	Cumulative fluid of injection	m^3
Q_c	Cumulative mass production	Kg
$Q_m(t)$	Mass injection/production rate	Kg/s
r	Radial distance, coordinate	m
R	Radius of a tube	m
r_w	Wellbore radius	m
s	Velocity gradient function	s^{-1}
S	Saturation	
S	Surface of a volume	
S_f	Saturation at displacement front	
S_{max}	Ultimate displacement saturation	
S_{ne}	Newtonian phase saturation	
S_{neir}	Irreducible Newtonian fluid saturation	
S_{nn}	Non-Newtonian phase saturation	
S_{nnir}	Connate non-Newtonian saturation	
S_w	Water saturation	
$\bar{S}_{nn}$	Average non-Newtonian saturation	
t	Time	s
T	Tortuosity of porous media	
t^k	Time at level k	s
Δt	Time step	s
u	Darcy velocity	m/s
$\vec{u}$	Darcy velocity vector	m/s
u_{ne}	Darcy velocity of Newtonian phase	m/s
u_{nn}	Darcy velocity of non-Newtonian phase	m/s

$\vec{u}_{ne}$	Darcy flux of Newtonian phase	m/s
$\vec{u}_{nn}$	Darcy flux of non-Newtonian phase	m/s
$\vec{V}$	Velocity vector	m/s
v_i	Component of $\vec{V}$ in the x_i (i=1, 2, 3)	m/s
V_n	Volume of a system	m^3
v_p	Pore velocity	m/s
$\vec{v}_p$	Pore velocity vector	m/s
$\nabla\vec{V}$	Velocity gradient	s^{-1}
W	Width of fracture	m
x	Distance from inlet, coordinate	m
x_f	Distance to shock saturation front	m
x_i	x_1=x, x_2=y, and x_3=z	m
$x_{i,p}$	Primary variable of numerical equations	
$x_{S_{nn}}$	Distance to saturation S_{nn}	m
y	Gogarty's exponential	
y	Coordinate	m
z	Coordinate	m

Greek Symbols

α	Angle with horizontal plane	
α	Exponential Coefficient	
α_1	Williamson model coefficient	s^{-1}
α_2	Williamson model exponential	
α_2	Exponential coefficient	
$\Gamma(x)$	Gamma function or factorial function	
$\dot{\gamma}$	Shear Rate	s^{-1}

$\dot{\gamma}_a$	Average shear Rate	s^{-1}
$\dot{\gamma}_0$	Low limiting Shear Rate	s^{-1}
$\delta(t)$	Pressure penetration distance	m
θ_f	Fluid relaxation time	s
δ_1	Interpolated value of $\nabla\Phi$	Pa/m
δ_2	Interpolated value of $\nabla\Phi$	Pa/m
λ	Rigidity modulus	Pa
λ	Interporosity coefficient	
λ_{eff}	Effective mobility	$m^{1+n}/Pa{\cdot}s$
μ	viscosity	Pa·s
μ_a	Apparent viscosity	Pa·s
μ_b	Bingham plastic coefficient	Pa·s
μ_{eff}	Power-law coefficient	$Pa{\cdot}s^n{\cdot}m^{1-n}$
μ_{eqv}	Equivalent viscosity	Pa·s
μ_f	Fluid viscosity	Pa·s
μ_∞	Viscosity at infinite shear	Pa·s
μ_{max}	Higher limit viscosity	Pa·s
μ_{min}	Lower limit viscosity	Pa·s
μ_{nn}	Non-Newtonian apparent viscosity	Pa·s
μ_0	Viscosity at zero shear	Pa·s
μ_1	Viscosity at $\lvert\nabla\Phi\rvert = \delta_1$	Pa·s
μ_2	Viscosity at $\lvert\nabla\Phi\rvert = \delta_2$	Pa·s
η	$\eta = 1 + \delta(t)/r_w$	
ξ	Dimensionless aspect factor	
ρ_i	Initial fluid density	Kg/m^3
ρ_{ne}	Density of Newtonian fluid	Kg/m^3
ρ_{nn}	Density of non-Newtonian fluid	Kg/m^3

τ	Shear stress	Pa
τ_m	Meter model coefficient	Pa
τ_{rx}	Shear stress function of r	Pa
τ_w	Shear stress at wall	Pa
τ_y	Yield stress	Pa
$\tau_{½}$	Shear stress for $\mu=½\mu_0$	Pa
$\underline{\tau}$	Stress tensor	Pa
ϕ	Porosity	
Φ	Flow potential	Pa
ϕ_f	Porosity of fracture	
ϕ_i	Initial formation porosity	
ϕ_m	porosity of matrix	
$\nabla\Phi$	Flow potential gradient	Pa/m
$\nabla\Phi_e$	Effective flow potential gradient	Pa/m
ω	Storage coefficient	

Subscripts

a	Apparent
a	Average
b	Bingham fluid
e	Equivalent
eff	Effective
eqv	Equivalent
f	Fluid
f	Fracture
f	Displacement front

i	Initial
m	Mass
m	Matrix
m	Volume V_m
n	nth degree
n	Volume V_n
ne	Newtonian fluid
nm	Between V_n and V_m
nn	Non-Newtonian fluid
p	Production
rne	Relative to Newtonian fluid
rnn	Relative to non-Newtonian fluid
t	Time
t	Total
w	Wall
w	Wellbore
x	x direction
y	Yield
z	z direction
0	Zero shear stress
½	Half shear stress
∞	Infinite shear stress
β	Fluid index

Acknowledgements

I would like to take this opportunity to thank all of the people who have helped and guided me for this work during my study at Berkeley. I would first like to express my deepest gratitude to Professor P. A. Witherspoon, for his guidance and support of my research, and for accepting me as a visiting researcher and then into a graduate program at UC Berkeley, where I have had an opportunity to participate in the excellent academic environment. His enthusiasm and encouragement are behind the achievements I have made and I am very proud to be his student.

I would also like to thank Dr. Karsten Pruess for his invaluable guidance and insight, consistent encouragement and critical review of this thesis and all the research I have done at the Lawrence Berkeley Laboratory. Many results of this work are directly from discussion with Karsten. I am very fortunate to have worked with him these years. From him I have learned not only physics and numerical techniques of porous flow, but also the attitude and the philosophy for conducting research as a scientist.

Many thanks are due to Professor N. G. W. Cook for his guidance of my graduate study, for his courses of rock mechanics, and for the critical review and valuable suggestions. I am highly indebted to Professor Kent Udell for his review and help with this work.

I am grateful to all the staff in the Earth Sciences Division at the Lawrence Berkeley Laboratory for the help from them. I wish to thank Dr. T. N. Narasimhan for his courses which gave me many insights into transport phenomena in porous media. I also thank Professor Clayton Radke for his kind help to me in many ways. Thanks are due to Drs. Chin-Fu Tsang, Peter Persoff, Sally Benson, Z. X. Chen, K. Karasaki, Sunil Kumar, Hoi-Ying Holman, Iraj Javandel, Jane Long, Jahan Noorishad, Joe Wang for their help during this work.

Many friends and colleagues have given me a lot of support and encouragement during this work. I am especially grateful to Ron Falta, Mark Ripperda, Peter Fuller, Scott Gaulke, Chao Shan, Di-Wen Chen, Erika Schlueter, Lee Cox, and Don Mangold.

I am also grateful to Ellen Klahn and Diana Swantek for their help during preparing the manuscript.

To my wife, Jiamin; my child, Gordon; and my parents: many, many thanks.

This work was funded by the U. S. Dept. of Energy under Contract No. DE-AC03-76SF00098.

Chapter 1
Introduction

Even though most studies conducted on flow and transport in porous media deal with Newtonian fluids, flow of non-Newtonian fluids through porous media is encountered in many subsurface systems, involving underground natural resource recovery or storage projects. A thorough understanding of non-Newtonian flow behavior in porous media is of fundamental importance to these engineering applications. In the past three decades, a tremendous effort has been devoted to developing quantitative analysis of flow of non-Newtonian fluids through porous media. Considerable progress has been reported and much information is available in the chemical engineering, rheology and petroleum engineering literature. The theoretical investigations carried out in this field have concentrated mainly on single-phase non-Newtonian fluid flow, while the experimental attempts have been designed to provide flow analysis with rheological models for non-Newtonian fluids and porous materials of interest.

In order to apply Darcy's law to the flow of single and multiple phase non-Newtonian fluids in porous media, effective viscosities are needed for use in the Darcy equation. A significant amount of laboratory studies has been performed by many investigators in an effort to develop correlations for effective viscosities of non-Newtonian fluids with the rock parameters and flow conditions for a given fluid (Christopher and Middleman, 1965; Gogarty, 1967, and many others). In all of these studies, a power-law viscosity model has been used exclusively to approximate the flow behavior of non-Newtonian fluids, such as polymer solutions. However, there is considerable evidence from laboratory experiments and field tests that certain fluids in porous media exhibit a Bingham-type non-Newtonian behavior. In these cases, flow takes place only after the applied pressure gradients exceeds a certain minimum value.

Among the theoretical studies of transient flow of non-Newtonian fluids in porous media, van Poollen and Jargon (1969) presented a numerical study of a power-law non-Newtonian fluid flow using a finite difference method. Analytical studies of the transient flow of a power-law fluid through porous media were performed by Odeh and Yang (1979), and Ikoku and Ramey (1979). They solved the non-linear partial differential equations that govern the flow of a slightly compressible power-law fluid in porous media by using approximate linearization assumptions, and they obtained approximate closed-form analytical solutions for the wellbore pressure. Then a new well testing method was developed for power-law non-Newtonian fluid injection, based on these solutions. Their approach has been extended and improved by many authors to include: i) wellbore storage and skin effects by interfacing with a well storage numerical simulator; ii) pressure transient behavior of non-Newtonian / Newtonian fluids in composite reservoirs by a numerical method; and iii) pressure falloff behavior in a vertically fractured well. However, all of these works dealt only with power-law non-Newtonian fluids, and no studies on Bingham-type fluid flow in porous media have been reported. The analytical solutions by Odeh and Yang (1979), or Ikoku and Ramey (1979), and their followers have been found to be valid for approximations of wellbore pressures only under the condition where the power-law index, n, takes a value of between 1 and 0.6 (Vongvuthipornchai and Raghavan, 1987a). In addition, the flow of power-law fluids through fractured media may be important to some engineering applications, because many subsurface systems, such as naturally fractured petroleum and geothermal reservoirs, are fractured formations. Very little research can be found in the literature on the flow of non-Newtonian fluids in fractured media.

The power-law model has been known to be a good approximation only over a limited range of shear rates. At both very low and very high shear rates, all the fluids appear to exhibit Newtonian behavior, i.e., viscosities become constant. Even though a rheological model for general pseudoplastic non-Newtonian fluids was proposed by Meter

(Meter and Bird, 1964), no flow behavior studies have been reported using this more general viscosity function.

The behavior of multiple-phase flow, compared to single-phase flow, is much more complicated and not well understood in many respects due to the complex interactions of the different fluid phases. A fundamental understanding of immiscible displacement of Newtonian fluids in porous media has been developed by Buckley and Leverett (1942). Since then, the Buckley-Leverett fractional flow theory has been applied and generalized by various authors to study a number of more complicated problems, involving the injection of different chemicals into reservoirs. However, non-Newtonian behavior has not been considered in any of this work. There are no analytical solutions available to describe the mechanism of displacement with non-Newtonian and Newtonian fluids in porous media.

This work presents a comprehensive theoretical study of both single and multiple phase flow of non-Newtonian fluids through porous media. The emphasis in this study is to obtain some physical insights into the flow of power-law and Bingham fluids. The purpose of this study is: i) to develop analytical solutions and a general numerical simulator for both single and multiple phase non-Newtonian fluid flow in porous media; ii) to conduct systematic studies of single phase fluid transient flow and multiple phase immiscible displacement of power-law and Bingham fluids; and iii) to provide practical approaches for well testing analysis and displacement efficiency evaluation of power-law and Bingham fluids for engineering applications. Therefore, this work consists of three tasks: i) development of theoretical methods; ii) investigation of transient flow of single phase non-Newtonian fluids, and iii) investigation of immiscible displacement of separate non-Newtonian and Newtonian fluids.

Chapter 2 presents a comprehensive review of the literature on the experimental and theoretical studies of non-Newtonian fluid flow through porous media. Chapter 3 discusses the rheological models and modified Darcy's law for non-Newtonian fluids in

porous media. Based on previous laboratory results, the apparent viscosity of non-Newtonian fluids for the modified Darcy's equation in this study is assumed to be a function of flow potential gradient only for single phase flow for a given fluid and porous media. For multiple phase flow, the viscosity depends not only on flow potential gradient, but on saturation as well.

Chapter 4 describes the mathematical model and numerical approach which have been used in this study. The numerical code is a modified version of the general numerical simulator "MULKOM" (Pruess, 1983; 1988) for non-Newtonian and Newtonian fluid flow. Also, special treatment for non-Newtonian behavior of power-law, Bingham, and pseudoplastic fluids is given in this chapter.

Chapter 5 is devoted to the development of an analytical solution for immiscible displacement of non-Newtonian and Newtonian fluids in porous media. A practical graphic procedure for evaluating the analytical solution is also provided. The resulting method can be regarded as an extension of the Buckley-Leverett-Welge theory for the flow of non-Newtonian fluids through porous media. An example of the application of the analytical solution is used to verify the numerical code described in Chapter 4.

In Chapter 6, a theoretical study of the displacement of a Newtonian fluid a non-Newtonian power-law fluid is conducted using the Buckley-Leverett type analytical solution developed in Chapter 5. The physical mechanisms of immiscible displacement involving a power-law fluid are revealed in this study. The displacement process is determined by the rheological properties of power-law fluids and the flow condition, in addition to the relative permeability data.

Chapter 7 presents the investigation results of displacement involving a non-Newtonian Bingham fluid in porous media. An example of Bingham fluid displacement by a Newtonian fluid is heavy oil production in water flooding. Heavy oil often behaves like a Bingham non-Newtonian fluid under reservoir conditions. A very low rate of recovery is a common feature of high viscosity oil production in water flooding. This

work shows that the low displacement efficiency of a Bingham fluid by a Newtonian one is primarily due to the presence of the ultimate displacement saturation, which is a characteristic of immiscible displacement with a Bingham fluid. Once the saturation of the displacing phase in the two-phase flow system reaches its ultimate value, no further improvement of displacement efficiency can be obtained regardless of how long the operation continues under the same flow condition.

A systematic numerical study performed in this work is reported in Chapter 8 for transient flow of single phase power-law fluids in porous media. The numerical investigation includes i) injectivity test analysis of a power-law fluid; ii) transient flow of a power-law fluid through a fractured medium; and iii) transient flow of a pseudoplastic fluid, described by the Meter model. A better transient pressure analysis method for power-law fluid injectivity tests is discussed and recommended, which is a combination of the existing analytical approach and a numerical simulation. The two published results of well testing are analyzed by this new technique to demonstrate its general applicability to field problems. Transient flow of a power-law fluid through a fractured medium is also studied numerically using an idealized horizontal fracture model in Chapter 8. For constant flow rates, non-Newtonian flow behavior in a double-porosity medium is characterized by two-parallel straight lines on a log-log plot of wellbore pressure increase versus injection time, which are controlled by the same two dimensionless parameters as used for Newtonian flow. In the third simulation, the numerical results show that the flow behavior of pseudoplastic fluids in porous media tends towards an equivalent Newtonian system at long times. Semi-log straight lines develop on the pressure-time plots, in contrast to the log-log straight lines for power-law fluid flow, as has been discussed in the literature.

Chapter 9 presents a complete quantitative analysis for the flow of single phase Bingham non-Newtonian fluids in porous media. An integral analytical solution has been obtained for transient flow of a Bingham fluid through porous media, and its

accuracy is confirmed by comparison with the exact and numerical solutions. The flow behavior of a slightly-compressible Bingham fluid is discussed using the integral solution. In order to apply the theory to field problems, a new method of well test analysis has been developed, and its application is demonstrated by analyzing two simulated pressure drawdown and buildup tests in Chapter 9.

A summary of this work is given in Chapter 10. This study has made several contributions to the understanding of flow behavior of single and multiple phase non-Newtonian fluids in porous media. New theoretical approaches are developed for determining fluid and formation properties during power-law and Bingham non-Newtonian fluid flow in reservoirs, and also for evaluating sweep efficiency of immiscible Newtonian and non-Newtonian fluid displacement in porous media. It is believed that the analytical solutions and the general numerical simulator developed in this work will find applications in the further research on non-Newtonian fluid flow in porous media.

Chapter 2
Literature Review

2.1 Introduction

Flow of non-Newtonian fluids through porous media occurs in many subsurface systems and has found applications in certain technological areas. Previous studies on the flow of fluids through porous media were limited for the most part to Newtonian fluids (Muskat, 1946; Collins, 1961; and Scheidegger, 1974). Since the 1950's, the flow of non-Newtonian fluids through porous media has received a significant amount of attention because of its important industrial applications. In the applications related to the petroleum industry, non-Newtonian fluids, especially polymer solutions, microemulsions, and foam, are often injected into reservoirs in various enhanced oil recovery (EOR) processes. The use of polymers in water flooding can yield significant increases in the oil recovery when compared with conventional water flood methods in certain reservoirs. Therefore, polymer flooding is the most commonly used EOR technique of chemical flooding in the petroleum industry (Dauben and Menzie, 1967; Mungan, 1966; Gogarty, 1967; Harvey and Menzie, 1970; and van Poollen, 1980). The flow of polymer solutions through porous media generally behaves like a power-law non-Newtonian fluid (Savins, 1969; Gogarty; 1967; and Christopher and Middleman; 1965). There exists a considerable amount of literature and reports of a number of patents relating to the use of polymeric and chemical additives in oil recovery processes.

There is considerable evidence that the flow behavior of heavy oil is non-Newtonian and may be approximated by that of a Bingham plastic fluid. A large amount of heavy oil reservoirs have been found and developed worldwide. The non-Newtonian behavior of heavy oil flow in these oil reservoirs have been reported in the petroleum

literature (Barenblatt et al., 1984; Kasraie et al., 1989). Laboratory rheological and filtration experiments and field tests in a number of oil fields have shown that flow of heavy oil often takes place only after the applied pressure gradient exceeds a certain minimum value (Mirzadjanzade et al., 1971). The flow of heavy oil in porous media does not follow Darcy's law; and some authors explain this phenomenon as a lower limit of Darcy's law. The presence of a minimum pressure gradient usually results in a large decrease in oil recovery. Similar phenomena have been also found in gas fields of argillaceous reservoirs with interstitial water present by Mirzadjanzade et al.. There exists a threshold gas pressure gradient before gas moves, and the magnitude of the threshold pressure gradient depends on water content in pore space, decreasing as the water content decreases.

The existence of a threshold hydraulic gradient has also been observed for certain groundwater flow in saturated clay soils, or strongly argillized rocks. When the applied hydraulic gradient is below the minimum value, there is very little flow. This phenomenon has been attributed to the rheological non-Newtonian behavior caused by clay-water interactions (Bear, 1972). Mitchell (1976) discussed a number of mechanisms that are responsible for the deviations of water flow through clays from that predicted by Darcy's law.

The flow of foam in porous media is a focus of current research in many fields. Foam has been shown to be one of the most promising fluids for mobility control in underground energy recovery and underground storage projects. When flowing through porous media, foam is a discontinuous fluid, comprised of gas bubbles separated by thin liquid lamellae. The flow and behavior of foam in permeable media involve complex gas-liquid-solid interactions on the pore level, which are not completely understood at the present time. However, considerable progress has been made in recent years, and many experimental and theoretical studies of foam flow in porous media have contributed significantly to our understanding of the physics of foam transport in porous

media (Witherspoon et al. 1989; Hirasaki and Lawson, 1985; Falls et al., 1986; Ransohoff and Radke 1986). On a continuum macroscopic scale, non-Newtonian flow behavior of foam through porous materials has been referred to by all the researchers in this field. The power-law is generally used to correlate apparent viscosities of foam with other flow properties for a given porous medium and a given surfactant (Hirasaki and Lawson, 1985; Patton et al. 1983). It has also been observed experimentally that foam will start to flow in a porous medium only after the applied pressure gradient exceeds a certain threshold value (Albrecht and Marsden, 1970; and Witherspoon et al., 1989).

Drilling and hydraulic fracturing fluids used in the industry are usually non-Newtonian liquids. Therefore during well drilling or hydraulic fracturing operations, the non-Newtonian drilling muds or hydraulic fluids will infiltrate into permeable formations surrounding the wellbore, which may seriously damage the formation. The rheological behavior of drilling muds, cement slurries and hydraulic fracturing fluids often is described by a Bingham plastic or a power-law model (Cloud and Clark, 1985; Shah, 1982; Robertson et al., 1976; and Iyoho and Azar, 1981). The importance of flow into the surrounding formations of non-Newtonian fluids from the wellbore has been recognized in the industry. In fact, very little research or quantitative analysis has been reported on the formation contamination near the wellbore by such fluids in the petroleum industry, some techniques have been developed and used to remove drilling muds or fracturing agents from the borehole and the adjacent formation (Coulter et al., 1987).

2.2 Non-Newtonian Fluids

In contrast with classical fluid mechanics developed for Newtonian fluids, the theory of non-Newtonian fluid dynamics is a very new branch of applied sciences. The

increasing importance of non-Newtonian fluids has been recognized in those fields dealing with materials, whose flow behavior of stress and shear rate can not be characterized by Newton's law of viscosity (Skelland, 1967; Bohme, 1987; Astarita and Marrucci, 1974; and Crochet et al., 1984). Therefore, non-Newtonian fluid mechanics is being developed. In a broad sense, fluids are divided into two main categories: (1) Newtonian, and (2) non-Newtonian. Newtonian fluids follow Newton's law of viscous resistance and possess a constant viscosity. Non-Newtonian fluids deviate from Newton's law of viscosity, and exhibit variable viscosity. The behavior of non-Newtonian fluids is generally represented by a rheological model, or correlation of shear stress and shear rate. Examples of substances which exhibit non-Newtonian behavior include solutions and melts of high molecular weight polymers, suspensions of solids in liquids, emulsions, and materials possessing both viscous and elastic properties. There are many rheological models available for different non-Newtonian fluids in the literature (Skelland, 1967; Savins, 1969; Bird et al., 1960). Scheidegger (1974) gave a very comprehensive summary of rheological equations of various non-Newtonian fluids in porous media. The present review focuses only on those non-Newtonian fluids which are commonly encountered in porous media. The major attention here is directed to the rheological properties of flow systems of interest in studies of non-Newtonian flow through porous media.

For a Newtonian fluid, the shear stress τ is linearly related to the shear rate $\dot{\gamma}$ by *Newton's law of viscosity* (Bird et al., 1960) as,

$$\tau = -\mu\dot{\gamma} \tag{2.1}$$

where the coefficient μ is defined as dynamic viscosity of the fluid.

According to the relationships between shear stress and shear rate, non-Newtonian fluids are commonly grouped in three general classes (Skelland, 1967) : (1) time-independent non-Newtonian fluids; (2) time-dependent non-Newtonian fluids; and (3)

viscoelastic non-Newtonian fluids.

1. *Time-independent fluids* are those for which the rate of shear $\dot{\gamma}$, or the velocity gradient, is a unique but non-linear function of the instantaneous shear stress τ at that point. For the time-independent fluid, the relationship is

$$\dot{\gamma} = f(\tau)$$

The time-independent non-Newtonian fluids can be characterized by the flow curves of τ versus $\dot{\gamma}$, as shown in Figure 2.1. These are: (a) Bingham plastics, curve A; (b) pseudo-plastic fluids (shear thinning), curve B; and (c) dilatant fluids (shear thickening), curve C.

2. *Time-dependent fluids* have more complex shear stress and shear rate relationships. In these fluids, the shear rate depends not only on the shear stress, but also on shearing time, or on the previous shear stress rate history of the fluid. These materials are usually classified into two groups, thixotropic fluids and rheopectic fluids, depending upon whether the shear stress decreases or increases in time at a given shear rate and under constant temperature. Typical curves of the time-dependent behavior of non-Newtonian fluids are shown in Figure 2.2.

3. *A viscoelastic material* exhibits both elastic and viscous properties, and shows partial recovery upon the removal of the deformable shear stress. The rheological properties of such a substance at any instant will be a function of the recent history of the material and can not be described by relationships between shear stress and shear rate alone, but will require inclusion of the time derivative of both quantities.

One of the mechanical models, first proposed by Maxwell (Skelland, 1967) for viscoelastic fluids, is

$$\tau = \mu \frac{d\dot{\gamma}}{dt} - \frac{\mu}{\lambda} \frac{d\tau}{dt} \qquad (2.2)$$

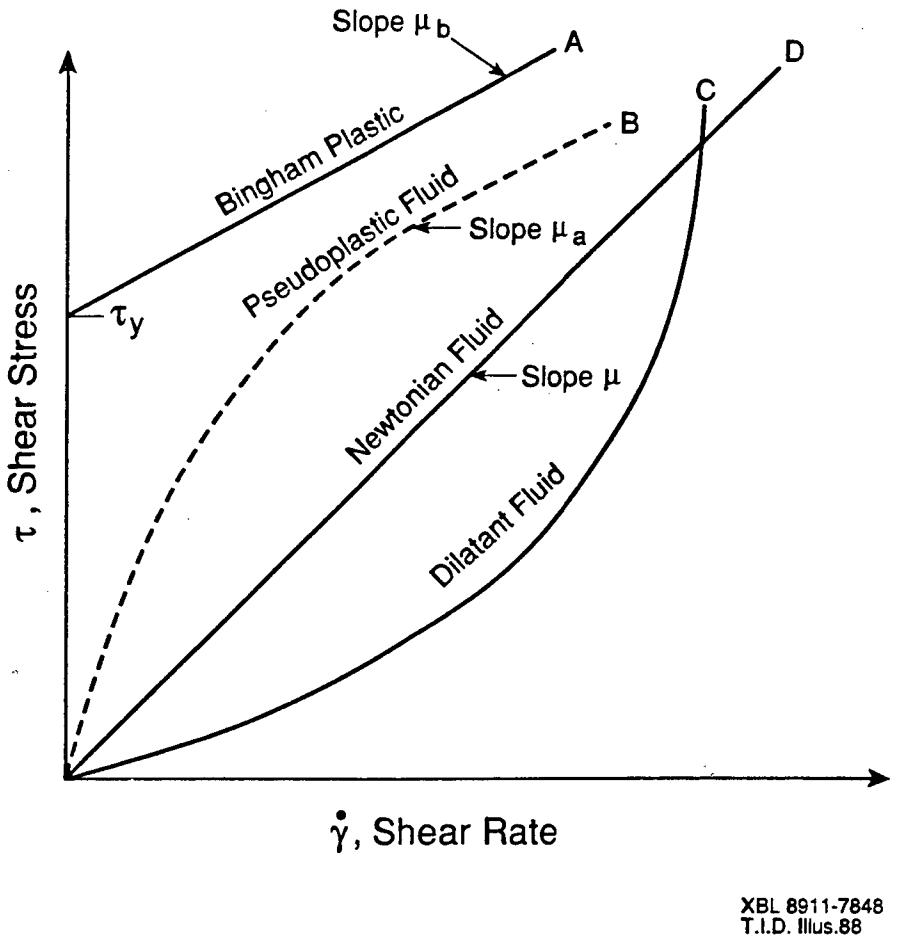

Figure 2.1 Typical Shear Stress and Shear Rate Relationships for Non-Newtonian Fluids (after Hughes and Brighton).

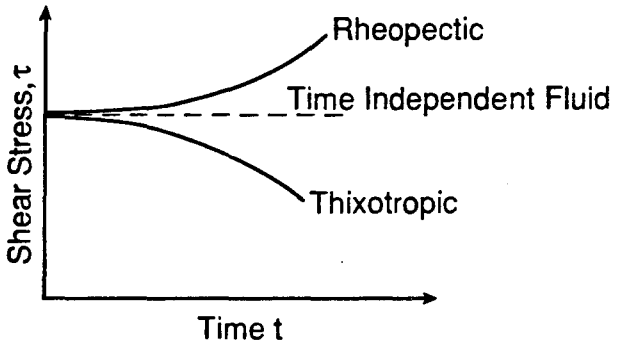

(a) Behavior of non-Newtonian fluids-under a given shear rate.

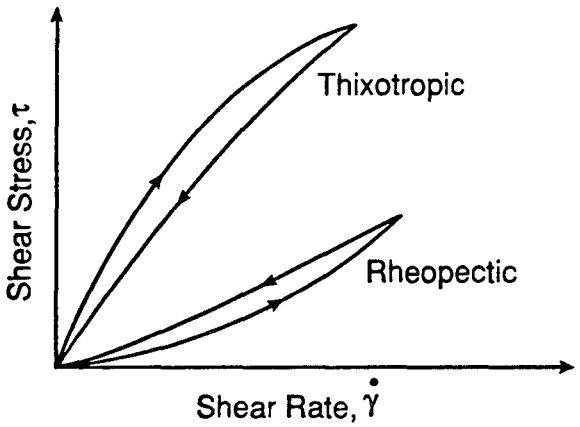

(b) Behavior of non-Newtonian fluids-shearing -history dependence.

XBL 8911-7849
T.I.D. Illus.88

Figure 2.2 Flow Curves for Time-Dependent Thixotropic and Rheopectic Non-Newtonian Fluids (after Bear; and Skelland).

where μ is viscosity, and λ is a rigidity modulus. Liquids which obey this law are known as Maxwell liquids. Another mechanical model is referred to as the Voigt model, which characterizes the rheological performance by the relationship,

$$\tau = \mu \frac{d\dot{\gamma}}{dt} + \lambda \dot{\gamma} \tag{2.3}$$

The rheological behavior of real viscoelastic fluids has been represented with some success by more or less complex combinations of generalized Maxwell and Voigt models, consisting of Maxwell or Voigt model units connected in series or in parallel.

For flow through porous media, the time-independent non-Newtonian fluids have been used almost exclusively in both experimental and theoretical studies (Savins, 1969). However, there do exist some examples for the flow of the viscoelastic non-Newtonian fluids through porous media (Sadowski, 1965; and Wissler, 1971). The effect of time-dependent non-Newtonian fluids on flow behavior in porous media have been virtually neglected in all previous investigations.

Among the most common time-independent non-Newtonian fluids (Scheidegger, 1974; Bear, 1972), Bingham plastics exhibit a finite yield stress at zero shear rate. The physical behavior of fluids with a yield stress is usually explained in terms of an internal structure in three dimensions which is capable of preventing movement when the values of shear stress are less than the yield value, τ_y, as shown in Figure 2.1. For shear stress, τ, larger than τ_y, the internal structure collapses completely, allowing shear movement to occur. The characteristics of these fluids are defined by two constants: the yield stress τ_y , which is the stress that must be exceeded for flow to begin, and the Bingham plastic viscosity μ_b , which is the slope of the straight line portion of curve A in Figure 2.1. The rheological equation for a Bingham plastic is then,

$$\tau = \tau_y - \mu_b \dot{\gamma} \tag{2.4}$$

The Bingham plastic concept has been found to closely approximate many real fluids existing in porous media, such as heavy tarry and paraffin oils (Barenblatt et al., 1984; Mirzadjanzade et al. 1971), and drilling muds and fracturing fluids (Hughes and Brighton, 1967), which are suspensions of finely divided solids in liquids.

To date the power-law, or the Ostwald-de Waele model (Bird et al., 1960), is the most widely used rheological model for flow problems in porous media. The power law model has been successfully applied to describe the flow behavior of polymer and foam solutions by a number of authors (Christopher and Middleman, 1965; McKinley et al., 1966; Gogarty, 1967; Harvey and Menzie, 1970, Mungan, 1972; Hirasaki and Pope, 1974; and many others). Originally formulated from an empirical curve-fitting function, the power law is represented by,

$$\tau = -H\dot{\gamma}^{n} \tag{2.5}$$

where n is the power-law index; and H is called the consistence coefficient. For n = 1, the fluid becomes Newtonian. A fluid which obeys Equation 2.5 is called a power-law fluid. Because of its inherent simplicity, the power-law is of considerable interest in applications and is used to approximate the rheological behavior of both shear-thinning or pseudoplastic ($n < 1$) and shear-thickening or dilatant ($n > 1$) fluids over a large range of flow conditions.

Comparing Equation 2.5 with Newton's law of viscosity, Equation 2.1, we see that such a fluid exhibits an apparent viscosity μ_a of the form:

$$\mu_a = H\dot{\gamma}^{n-1} \tag{2.6}$$

For most power-law fluids, the power-law index n is less than 1.0, and so the apparent viscosity μ_a decreases with increasing shear rate $\dot{\gamma}$. The shear-thinning behavior, which amounts to a monotonic decrease in apparent viscosity with increasing shear rate, is readily observed in the flow of polymer and foam solutions, moderately concentrated suspensions, and biological fluids.

Physically, when the fluid is at rest, fluid dispersions of asymmetric molecules or particles are probably characterized by an extensive entanglement of the particles. Progressive disentanglement should occur under the influence of shearing forces, and the particles will tend to orient themselves in the direction of shearing. This orienting effect is proportional to the shear rate and is opposed by the randomly disorienting Brownian movement. Pseudoplastic behavior should also be consistent with the existence of highly solvated molecules or particles in dispersion. Progressive shearing away of solvated layers with increasing shear rate would result in decreasing interactions between the molecules or particles and a consequent reduction in apparent viscosity.

Although the power-law equation accurately portrays the behavior of a large number of non-Newtonian fluids over a wide range of shear rate or velocity gradients, some fluids exhibit more complex behavior. In addition, at both very low and very high velocity gradients, all fluids appear to exhibit Newtonian behavior with constant viscosities μ_0 and μ_∞, respectively, as shown in Figure 2.3. Complete orientation at high shear rate and complete disorientation at very low shear rate should account for the observed Newtonian behavior in these regions. The power law predicts an infinite viscosity at vanishingly small velocity gradients.

In order to describe the entire viscosity curve, a more complex expression than the power-law model, Equation 2.5 is needed. One of the numerous proposed expressions is the extended Williamson model (Fahien, 1983),

$$\mu_a = \mu_\infty + \frac{\mu_0 - \mu_\infty}{1 + \left[\frac{\dot{\gamma}}{\alpha_1}\right]^{\alpha_2}} \tag{2.7}$$

where α_1 and α_2 are constants. For low and high values of shear rate $\dot{\gamma}$, Equation 2.7 yields $\mu_a \rightarrow \mu_0$ and $\mu_a \rightarrow \mu_\infty$, respectively.

A similar correlation of the apparent viscosity for polymer solutions was proposed by Meter (Meter and Bird, 1964),

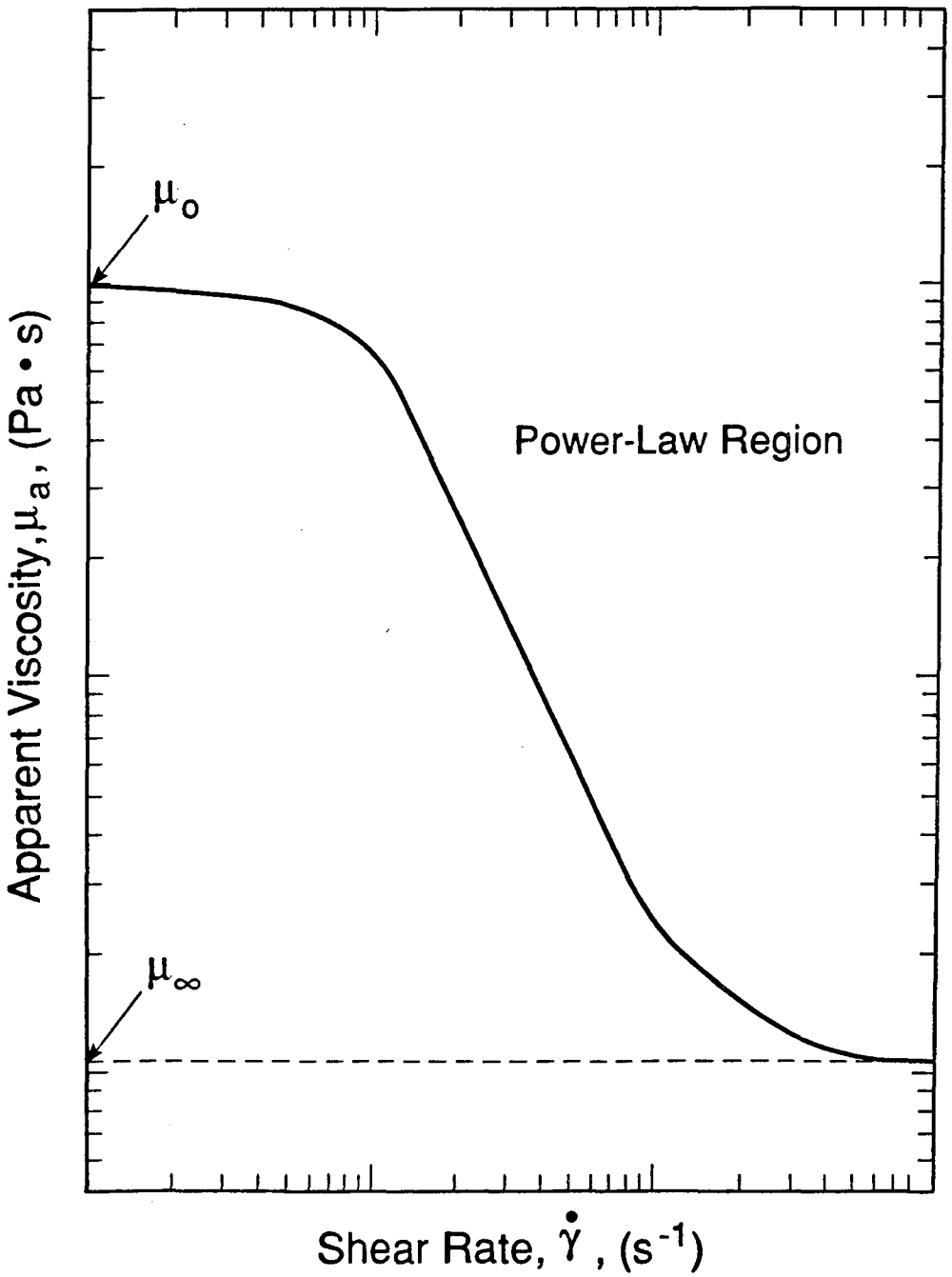

Figure 2.3 Viscosity Behavior of Pseudoplastic shear-Thinning Fluids, with Maximum and Minimum Limiting Viscosities.

$$\mu_a = \mu_\infty + \frac{\mu_0 - \mu_\infty}{1 + \left[\frac{\tau}{\tau_m}\right]^{\alpha-1}} \tag{2.8}$$

where α and τ_m are constants. Equation 2.8 has been used to investigate flow problems of polymer solutions in porous media (Lake, 1987; and Camilleri et al., 1987).

One simple relationship for describing the viscosity of a power-law fluid is called the truncated power-law model (Bird, 1965),

$$\mu_a = \mu_0 \quad \text{for } |\dot{\gamma}| \le |\dot{\gamma}_0| \tag{2.9}$$

and

$$\mu_a = H|\dot{\gamma}|^{n-1} \quad \text{for } |\dot{\gamma}| > |\dot{\gamma}_0| \tag{2.10}$$

Figure 2.4 presents the apparent viscosity as a function of shear rate for the truncated power-law model. This model was used by Vongvuthipornchai and Raghavan (1987a) in their numerical studies of the pressure falloff behavior of power-law fluid flow in a vertically fractured well.

The power law is also called a two parameter model (Bird et al., 1960), since it is characterized by the two parameters, H and n. In order that the power-law relationship be of engineering value, it is necessary for H and n to remain constant over considerable ranges of shear rate. In the general case, H and n may vary continuously with shear rate. Then, a logarithmic form of the power law should be used (Skelland, 1967), instead of Equation 2.5. However, many published laboratory studies of polymer solution flow in porous media reveal that it is a reasonable assumption to take H and n as constants.

Shear thickening behavior has been observed with dilatant materials, although these materials are far less common than pseudoplastic fluids. Volumetric dilatancy denotes an increase in total volume under shearing, whereas rheological dilatancy refers to an increase in apparent viscosity with increasing shear rate. A number of mechanisms proposed to explain the shear thickening phenomena were summarized by Savins

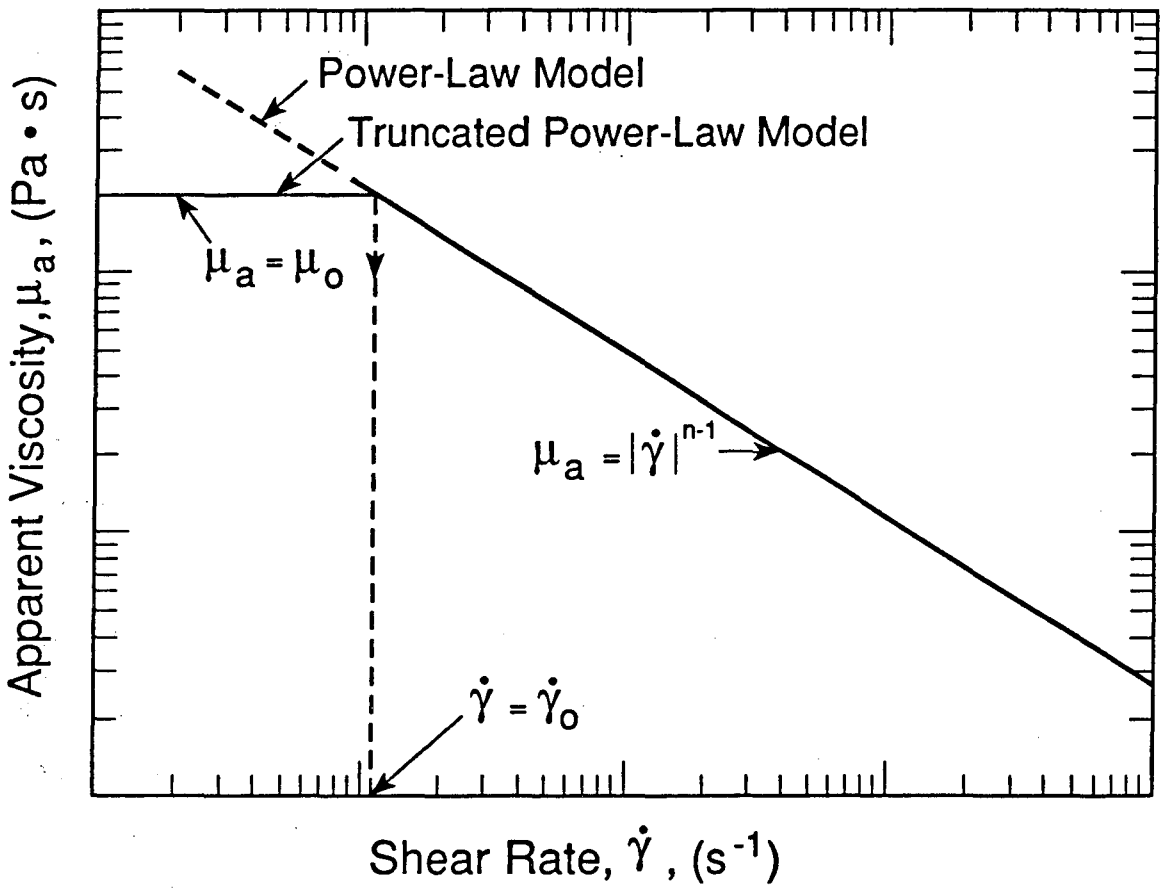

XBL 8911-7851
T.I.D. Illus.88

Figure 2.4 Viscosity Behavior of the Truncated Power-Law Model (after Vongvuthipornchai and Raghavan).

(1969). The shear thickening behavior is of particular interest in connection with non-Newtonian flow through porous media because certain dilute polymeric solutions exhibit a shear thickening response under appropriate conditions of flow, even though they show shear thinning behavior in viscometric flow. This general type of behavior has been reported in porous media flow experiments involving a variety of dilute to moderately concentrated solutions of high-molecular-weight polymers. In the case when the power-law model applies, the power-law index $n > 1$ generates a monotonically increasing shear thickening response. However, the shear thickening or dilatant phenomena may be the most controversial and least understood rheological behavior of non-Newtonian fluids.

The approaches available for rheological data analysis and characterization of non-Newtonian systems are: (1) the integration method; (2) the differentiation method (Savins, Wallick and Foster, 1962a; 1962b; 1962c) and (3) the dual differentiation-integration method (Savins, 1962). However, only the integration technique is of interest in porous media flow problems. The integral method consists of interpreting flow properties in terms of a particular model. The rheological parameters appear, on integrating, in an expression relating the pairs of observable quantities, such as volume flux and pressure. Many theoretical correlations of non-Newtonian fluid flow through porous media are based on capillary models. Consider steady laminar upward flow of a time-independent fluid through a vertical cylindrical tube with a radius R, as shown in Figure 2.5. The volumetric flow rate , Q, is (Skelland, 1967):

$$\frac{Q}{\pi R^3} = \frac{1}{\tau_w^{\,3}} \int_0^{\tau_w} \tau_{rx}^{\,2} f(\tau_{rx}) d\tau_{rx} \tag{2.11}$$

where τ_w is shear stress at the tube wall; and $f(\tau_{rx})$ is the rheological function, depending on the rheological model of the fluid; and τ_{rx} is the shear stress, given by,

$$\tau_{rx} = \frac{r\Delta P}{2L} \tag{2.12}$$

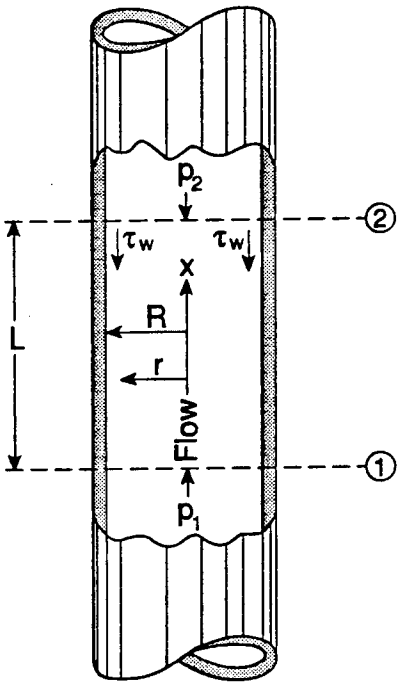

XBL 8911-7854
T.I.D. Illus.88

Figure 2.5 Stresses acting on a Cylindrical Element of Fluid of Radius R in Steady Flow through a Vertical Tube (after Skelland).

With an appropriate rheological function $f(\tau_{rx})$, as summarized by Savins (1962), Equation 2.11 relates the volumetric flow rate through a capillary and the shear stress on the wall of many useful fluids, such as Bingham plastic and power-law fluids.

2.3 Previous Work on Laboratory Studies and Rheological Models

Many studies on the flow of non-Newtonian fluids in porous media exist in chemical engineering, rheology, and petroleum engineering from the early 1960's. Because of the complexity of pore geometries in a porous medium, Darcy's law has to be used to obtain any meaningful insights into the physics of flow in porous media. Some equivalent or apparent viscosities for non-Newtonian fluid flow are needed in the Darcy equation. Therefore, a lot of experimental and theoretical investigations have been conducted to find rheological models, or correlations of apparent viscosities with flow properties for a given non-Newtonian fluid as well as a given porous material. The viscosity of a non-Newtonian fluid depends upon the shear rate, or the velocity gradient. However, it is impossible to determine the distribution of the shear rate in a microscopic sense in a porous medium, and the rheological models developed in fluid mechanics for non-Newtonian fluids cannot be applied directly to porous media. Hence, many laboratory studies were undertaken in an attempt to relate the rheological properties of a non-Newtonian fluid to the pore flow velocity of the fluid or the imposed pressure drop in a real core or in a packed porous medium.

The viscosity used in Darcy's equation for non-Newtonian fluids depends, on 1) rheological properties of the fluids, 2) characteristics of the porous medium, and 3) shear rate. Empirical attempts to establish correlations between the various dynamic properties of porous media need to introduce certain additional parameters. Theoretical considerations may be able to identify the physical significance of these parameters. The

simplest theoretical models that can be constructed for a porous medium are those consisting of capillaries. The capillary model, in which the porous medium is represented by a bundle of straight, parallel capillaries of uniform diameters, was used to derive a flow equation, the modified Darcy's law for non-Newtonian fluid flow through porous media. Under steady-state and laminar flow conditions, the momentum flux distribution in the radial direction within the capillary is first solved from the conservation of momentum. Then, by introducing a special rheological model for the non-Newtonian fluid in the momentum distribution and integrating in the radial direction, one obtains the total flow rate through the capillary. By comparing the expression for the total flow rate with Darcy's law, one can deduce a modified Darcy's law with an apparent viscosity for the special non-Newtonian fluid. The resulting equations usually involve some coefficients that need to be determined by experiments for a given fluid in a given porous medium.

In a pioneering work, Christopher and Middleman (1965) developed a modified Blake-Kozeny equation for a power-law, non-Newtonian fluid with laminar flow through packed porous media. Their theory was based on a capillary model and the Blake-Kozeny equation of permeability, and it was tested by experiment with the flow of dilute polymer solutions through packed porous material. They claimed that the accuracy of their correlation was probably acceptable for most engineering design purposes. The modified Blake-Kozeny equation is,

$$u = \left[\frac{K}{\mu_{eff}} \frac{\Delta P}{L} \right]^{\frac{1}{n}} \tag{2.13}$$

where u is the Darcy's velocity; K is permeability; $\Delta P/L$ is the pressure gradient; and μ_{eff} is given as

$$\mu_{eff} = \frac{H}{12} \left[9 + \frac{3}{n} \right]^{n} (150 K \phi)^{\frac{(1-n)}{2}} \tag{2.14}$$

Note that μ_{eff} does not have the units of viscosity. Christopher and Middleman also derived an expression for average shear rate for a power law fluid in porous media as

$$\dot{\gamma}_a = \frac{3n+1}{4n} \frac{12u}{(150K\phi)^{1/2}} \tag{2.15}$$

In order to use Equations 2.13 and 2.15, one must measure the absolute permeability K with a Newtonian fluid, measure the porosity ϕ, and determine the rheological parameters, n and H. Bird, Stewart and Lightfoot (1960) presented a similar model to Equation 2.13, except that it includes a factor of $(25/12)^{n-1}$.

Polymer solutions seem to exhibit the same general behavior with regard to the non-Newtonian apparent viscosity μ_a as a function of shear stress τ. In the limit of very small shear stress, the viscosity approaches a lower shear rate maximum value μ_0. With increasing shear stress the viscosity μ_a decreases, and if the shear stress can be increased sufficiently the viscosity reaches its upper shear rate minimum constant value, μ_∞. Hence, μ_0 and μ_∞ are measurable quantities characteristic of the fluid. A four-parameter model, Equation 2.8, was proposed by Meter (Meter and Bird, 1964) to describe the more realistic shear-thinning behavior of polymer solutions. Meter and Bird (1964) presented a practical procedure to determine the four parameters in Equation 2.8 by fitting experimental non-Newtonian viscosity data. The curve-fitting results appeared quite satisfactory.

Sadowski and Bird (1965) conducted a systematic study on non-Newtonian flow through porous media. They used a non-Newtonian viscosity μ_a in an empirical curve-fitting Ellis function, given by

$$\frac{1}{\mu_a} = \left[\frac{1}{\mu_0}\right]\left[1 + \left[\frac{\tau}{\tau_{1/2}}\right]^{\alpha-1}\right] \tag{2.16}$$

where μ_0 is zero-shear viscosity, $\tau_{1/2}$ is the shear stress at which μ_a has dropped to $\frac{1}{2}\mu_0$, and α characterizes the slope of $\log \mu_a$ vs. $\log \tau_{1/2}$ in the "power-law" region. The three

parameters μ_0, $\tau_{1/2}$, and α can be obtained by a graphical approach to the viscosity curve. By using the Blake-Kozeny-Carman equation of permeability and the capillary model, they were able to derive a modified Darcy's law as

$$u = \frac{K}{\mu_a}\frac{\Delta P}{L} \tag{2.17}$$

where the apparent or effective viscosity is defined by

$$\frac{1}{\mu_a} = \frac{1}{\mu_0}\left[1 + \frac{1}{\alpha + 3}\left[\frac{\tau_{Rh}}{\tau_{1/2}}\right]^{\alpha-1}\right] \tag{2.18}$$

with $\tau_{Rh} = (\Delta P/L)\,[D_p\phi/6(1-\phi)]$, and D_p is the particle diameter.

In an experimental study of the flow through porous media of fourteen different polymer solutions, Sadowski (1965) found that the shear-sensitive viscosities of these fluids were characterized by the three-parameter Ellis model (2.16). The modified Darcy's law (2.17) was used successfully to correlate the constant volumetric flow rate to the rheological properties for polymer solutions with low and medium molecular weight. Sadowski also pointed out that the results depended on the experimental procedure. If the flow rate of the fluid passing through the packed bed was held constant, the observed results were both steady and reversible. If the pressure drop across the packed bed was held constant, for very small or very large polymer solution concentrations, the observed results were unsteady and irreversible. The explanation for the unsteady and irreversible flow behavior observed for constant pressure drop was that polymer adsorption and gel formation occurred throughout the bed.

Another modified form of Darcy's law for calculating non-Newtonian fluid flow in porous media was obtained by McKinley et al. (1966) as

$$\vec{u} = -F(\tau)\frac{K}{\mu_0}\nabla P \tag{2.19}$$

where μ_0 is the apparent viscosity at some convenient reference stress τ_0 . The dimensionless viscosity ratio, $F(\tau)$, is defined as

$$F(\tau) = \frac{\mu_0}{\mu(\tau)} \tag{2.20}$$

Here the shear stress τ is given by

$$\tau = \alpha_0 \left[\frac{K}{\phi}\right]^{1/2} |\nabla P| \tag{2.21}$$

The constant α_0 and the dimensionless viscosity ratio $F(\tau)$ are determined experimentally from capillary measurements for a given type of rock and a given fluid. This model was developed by direct analogy with the flow through a uniform capillary and was confirmed experimentally by the authors.

A universal equation for the prediction of the average velocity in the flow of non-Newtonian fluids through packed beds and porous media was proposed by Kozicki et al. (1967). This general average velocity-pressure gradient relationship was also based on the Blake-Kozeny equation and the capillary model, and was confirmed experimentally for various non-Newtonian fluids. The modification of Darcy's law is expressed in terms of the flow potential gradient $\nabla\Phi$ and the apparent viscosity μ_a , as

$$\vec{u} = -\frac{K}{\mu_a}\nabla\Phi \tag{2.22}$$

for zero "slip" velocity on the pore wall. The apparent viscosity is defined as

$$\mu_a = \frac{\tau_w^{1+\xi}}{(1+\xi)\int_{\tau_y}^{\tau_w} \frac{\tau^\xi}{\mu}\, d\tau} \tag{2.23}$$

where τ_w is the shear stress at the wall, ξ is a dimensionless aspect factor, τ_y is the yield stress, T is the tortuosity of the porous medium, and μ is the viscosity of the non-Newtonian fluid as a function of shear stress. In reducing the general expressions (2.22)

and (2.23) to specific situations, the authors set the aspect factor $\xi = 3$ to arrive at results in agreement with the available experimental data.

An in-depth laboratory study of the rheological adsorption and oil displacement characteristics of polymer solutions was reported by Mungan et al. (1966). One of the most important contributions to the understanding of the rheological behavior of non-Newtonian fluid flow through porous media was made by Gogarty (1967a, 1967b). By using a number of real cores and consolidated porous media in experiments, he correlated the rheological and flow data to obtain a useful relationship for shear rate and pore velocity in porous material. The average shear rate $\dot{\gamma}_a$ is defined as a ratio of the pore velocity and a characteristic length for the porous medium, and it is then modified by an exponent y,

$$\dot{\gamma}_a = \left[\frac{B\, u}{f(K)\, (K/\phi)^{1/2}} \right]^y \tag{2.24}$$

where B is a constant determined from experiments. The exponent y accounts for the possible deviation between the slope of the apparent viscosity-shear rate curve from a capillary viscometer experiment, and the slope of the corresponding curve for the same fluid, but determined from an experiment with the porous medium. The function f(K) is a linear function of the logarithm of the permeability,

$$f(K) = m \log\left[\frac{K}{K_r} \right] + p \tag{2.25}$$

Here the constants m and p depend on the fluid type in a given kind of rock; and K_r is some reference permeability.

Gogarty proved experimentally that the apparent viscosity for use in the Darcy's equation was a function only of the shear rate, as defined by Equation 2.24,

$$\mu_a = F(\dot{\gamma}_a) \tag{2.26}$$

This rheological model was found to fit data for fluids whose character changed rapidly with shear rate from Newtonian to non-Newtonian. Flow experiments were performed with permeabilities in the range from 0.069 darcy through 0.425 darcy, and porosities in the range from 17% through 21.7%.

In contrast with the above work dealing with one-dimensional flow, Benis (1968) presented a theory to consider non-Newtonian fluid flow through two-dimensional narrow channels. The equations were solved numerically for the case of a power-law fluid. This method may be interesting for flow problems in fractured reservoirs.

Viscoelastic effects for non-Newtonian flow in porous media were observed and studied by Wissler (1971). He used a third-order perturbation technique to analyze the flow of a viscoelastic fluid in a converging-diverging channel and concluded that the actual pressure gradient would exceed the purely viscous gradient by a certain factor. The modified Darcy's law for a visco-inelastic, power-law fluid can then be used.

An important experimental study on flow of polymer solutions through porous media was reported by Dauben and Menzie (1967). They observed that the apparent viscosities of polyethylene oxide solutions under certain conditions was much higher than would be predicted from solution viscosity measurements. These polymer solutions exhibited dilatant behavior in porous media in contrast with the pseudoplastic behavior in simple flow systems. Glass bead packs were used as the porous material. The shear rate they derived is

$$\dot{\gamma} = \frac{12(2)^{1/2} v_p (L-\phi)}{D_p \phi} \tag{2.27}$$

where v_p is the pore velocity of flow, L is the spacing of the parallel plate instrument, and D_p is the diameter of the glass beads.

Harvey and Menzie (1970) developed a method for investigating the flow through unconsolidated porous media of high molecular weight polymer solutions. By

introducing the "pseudo Reynolds number" and the "effective particle diameter", they successfully analyzed experimental data for three different polymer solutions. From experiments conducted over a period of years under reservoir flow conditions, Jennings et al. (1971) found that viscoelastic behavior also contributed to the mobility control activity of some polymers. Complex flow behavior of viscoelastic fluids can result in very large flow resistances at high flow rates in porous media. However, viscoelastic flow is not significant under reservoir flow conditions.

Mungan (1972) tested three partially hydrolized polyacrylamide polymers under experimental conditions and observed that the polymers exhibited pseudoplastic behavior over an eight-order-magnitude range of shear rates. The correlation for shear rate that he used is

$$\dot{\gamma} = \frac{3n' + 1}{4n'} \cdot \frac{4v_p}{R} \tag{2.28}$$

where R is the radius of the equivalent capillary of the porous medium, n′ is the slope of the log-log plot of shear stress τ vs. $4v_p/R$. All of Mungan's experimental data show that the apparent viscosity of the polymers is a function solely of the shear rate defined in Equation 2.28.

A detailed analysis of factors influencing mobility and adsorption in the flow of polymer solutions through porous media was provided by Hirasaki and Pope (1974). The pseudoplastic behavior was modeled with the modified Blake-Kozeny equation for the power-law fluid, and the apparent viscosity was defined as

$$\mu_a = H \dot{\gamma}^{n-1} \tag{2.29}$$

where the shear rate is given by

$$\dot{\gamma} = \left[\frac{3n + 1}{4n} \right]^{\frac{n}{n-1}} \frac{12\, u}{(150k\phi)^{1/2}} \tag{2.30}$$

A model to include dilatant behavior in the modified Blake-Kozeny equation was given as

$$\mu_a = \frac{\mu_{eff}\, u^{n-1}}{\left[1 - \dfrac{\theta_f\, u}{(1-\phi)(150k/\phi)^{1/2}}\right]} \tag{2.31}$$

where μ_{eff} is defined in Equation 2.14, and θ_f is the fluid relaxation time.

A new experimental technique was recently developed by Cohen and Christ (1986) for determining mobility reduction as a result of polymer adsorption in the flow of polymer solutions through porous media. The experimental data were analyzed by correlating mobility with fluid shear stress, τ_w, at the pore wall, under adsorbing and non-adsorbing conditions. Among many investigations conducted on the flow of polymer solutions in porous media, one of the most extensive studies was presented by Sorbie et al. (1987). They used both experimental and theoretical approaches to look at adsorption, dispersion, inaccessible-volume effects, and non-Newtonian behavior as well.

2.4 Previous Work on Analysis of Flow through Porous Media

The subject of transient flow of non-Newtonian fluids in porous media is relatively new to many applications. Almost all of the analytical and numerical investigations have focused on the flow of one-dimensional, single-phase power-law fluids. The first paper in this area was published by van Poollen and Jargon (1969). They derived an equation that described the flow of a power-law non-Newtonian fluid in porous media. An analytical solution for steady state flow was obtained, and the unsteady-state flow was studied by a finite difference model. They found that drawdown curves for a power-law fluid did not exhibit the semi-log straight-line relationship that exists for Newtonian fluid flow in a homogeneous medium. A number of transient well tests were used to examine the

theory.

Patton et al. (1971) presented an analytical solution to the linear polymer flood problem and also a numerical model utilizing a stream tube approach that could be used to simulate linear or five-spot polymer floods. However, the effects of non-Newtonian behavior were neglected. A more comprehensive three-phase and three-dimensional finite difference numerical code for polymer flooding was developed by Bondor et al. (1972). This code represented the polymer solution as a fourth component fully miscible with the aqueous phase, in addition to the three other components, oil, water and gas. The rheological behavior of the polymer solution was included in the code by extending the modified Blake-Kozeny model to the multiphase flow problem. The apparent viscosity μ_a was modeled as that similar to the Meter model (2.8). As shown in Figure 2.6, the formulation is

$$\mu_a = \begin{cases} \mu_{max} & \text{, low velocities} \\ \mu_{eff}\, u^{n-1} & \text{, pseudoplastic region} \\ \mu_{min} & \text{, high velocities} \end{cases} \qquad (2.32)$$

where the coefficient μ_{eff} is also given by Equation 2.14. However, to take into account the effects of multiphase flow, the permeability and porosity are replaced by an effective permeability to water phase, $(K\, k_{rw})$, and an effective porosity $(\phi\, S_w)$, respectively. Here k_{rw} is the relative permeability to water, and S_w is the saturation of the water phase. This simulator also incorporated the adsorption of polymer, the reduction of rock permeability to the aqueous phase, and the dispersion of the polymer plug. The result was shown to represent the displacement as observed in a physical experiment.

Pressure transient theory of flow of non-Newtonian power-law fluids in porous media was developed by Odeh and Yang (1979) and Ikoku and Ramey (1979). They simultaneously derived a partial differential equation for flow of power-law fluids through porous media using similar linearization procedures, and obtained approximate analytical solutions. Then, new well test analysis techniques were proposed for

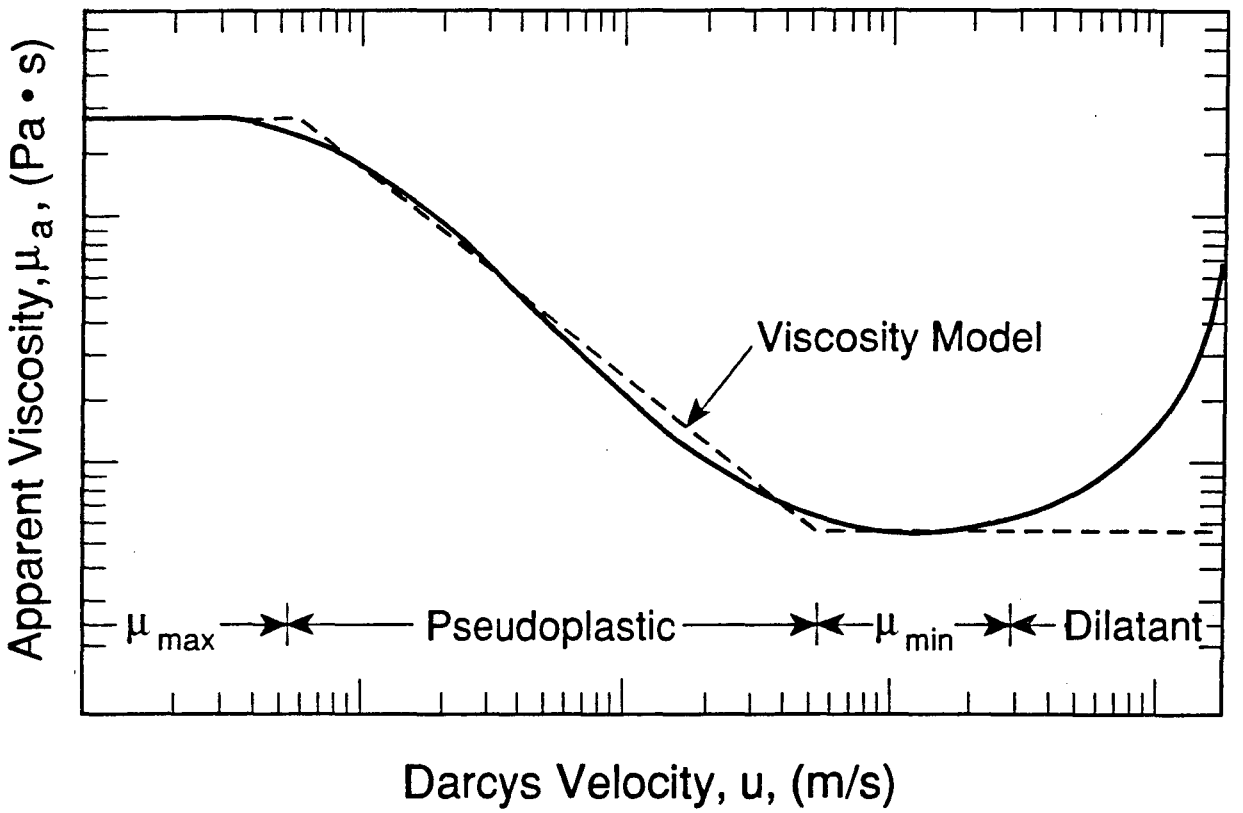

Figure 2.6 Rheological Behavior of Polymer Solution in Porous Media (after Bondor et. al).

interpreting pressure data observed during injectivity and falloff tests in reservoirs. The problem with this theory is the assumption used to linearize the governing equation, which requires

$$\left[-\frac{\partial P}{\partial r}\right]^{1/n} \approx \left[\frac{\mu_{eff}}{K}\right]^{1/n} \frac{Q}{2\pi rh} \tag{2.33}$$

where Q is the volumetric injection rate; and h is the thickness of formation. This is equivalent to assuming that the flow rate is constant at each radial location and that a steady-state viscosity profile exists. It has been shown numerically that this solution introduces significant errors by Vongvuthipornchai and Raghavan (1987a) when the power-law index $n < 0.6$. Generally, the linearized solution can not be used for pressure falloff test analysis when the power-law index $n < 0.5$.

In another paper, Ikoku and Ramey (1980) extended their theory to include wellbore storage and skin effects using a numerical wellbore storage simulator. Pressure responses with storage and skin effects were obtained in terms of Duhamel's integral, which was solved numerically. This work was furthered by Vongvuthipornchai and Raghavan (1987b). They developed an approximate analytical solution in the Laplace domain, and a long-time asymptotic solution in the real domain for this problem. The solution in the Laplace domain was evaluated by a numerical inversion technique (Stehfest, 1970), and was used to examine pressure falloff behavior dominated by storage and skin effects.

The linearized governing equation derived by Odeh and Yang (1979) for a power-law fluid was solved by McDonald (1979) using a finite difference model. He found that very fine grids were needed for power-law flow calculations, and the coarser meshes led to unacceptable truncation errors.

Pressure transient behavior during non-Newtonian power-law fluid and Newtonian fluid displacement has also been studied using numerical methods. Lund and Ikoku

(1981) applied the partial differential equation for radial flow of power-law fluids by Ikoku and Ramey (1979) to non-Newtonian and Newtonian fluids in composite reservoirs. The non-Newtonian fluid was injected to displace the Newtonian fluid under a piston-like displacement process. Polymer flooding projects are usually characterized by composite systems with moving banks of different fluids surrounding injection wells. Theory and analysis including a moving displacement front are more realistic than single-phase flow solutions. The well testing method of Ikoku and Ramey was extended to multiphase flow of non-Newtonian and Newtonian fluids by Gencer and Ikoku (1984). They used a numerical model to investigate the pressure behavior of power-law fluids during two-phase flow and gave an example for analysis of simulated injectivity and falloff test data.

A detailed numerical study of the flow of non-Newtonian power-law fluids in a vertically fractured well was reported by Vongvuthipornchai and Raghavan (1987a). They presented a new numerical analysis technique for fractured well tests, and also examined the general pressure falloff behavior in unfractured wells after the injection of non-Newtonian power-law fluids.

A more sophisticated numerical simulator of compositional micellar/polymer flow was developed by Camilleri et al. (1987a). This model took into account many important process properties, such as polymer inaccessible pore volume, permeability reduction, adsorption, residual saturations, relative permeability, phase, and non-Newtonian behavior as well. The phase behavior was modeled by four pseudocomponents: surfactant, alcohol, oil, and brine (Camilleri et al., 1987b). The polymer apparent viscosity was calculated from the Meter model, and the shear rate equation used was Equation 2.30 from the work of Hirasaki and Pope (1974). This new phase behavior code was used to match many simulated and experimental data, and satisfactory results were obtained (Camilleri et al., 1987c). The success of closely matching experimental phase concentration histories showed that this code provided a good description of the physical

processes occurring during the displacement of oil by surfactant.

Compared with studies conducted on flow of non-Newtonian power-law fluids, there are only a few publications dealing with flow problems in porous media involving non-Newtonian Bingham fluids (Barenblatt et al., 1984; Scheidegger, 1974). However, it has long been observed in heavy oil development and in laboratory experiments that there exists a minimum pressure gradient for heavy oil to start flow (Mirzadjanzade et al., 1971). Similar phenomena occur when groundwater flows in strongly argillized rocks and in clay soils (Bear, 1972). In such cases, the formulation of Darcy's law has been modified as

$$\vec{u} = -\frac{K}{\mu_b}\left(1 - \frac{G}{|\nabla P|}\right)\nabla P \qquad |\nabla P| > G \tag{2.34a}$$

$$\vec{u} = 0 \qquad |\nabla P| \le G \tag{2.34b}$$

where G is the minimum pressure gradient. The physical meaning of G can be found by considering flow of a Bingham fluid through a capillary with radius R. Then, the Bingham equation was solved by Buckingham (Scheidegger, 1974; Skelland, 1967) to give the average flow velocity over the cross-section of the tube. By comparing this velocity with the result from Darcy's law, we can obtain

$$G = \frac{\tau_y}{3R/8} = \frac{\tau_y}{d} \tag{2.35}$$

where d is a characteristic pore size of a porous medium, d = 3R/8. Therefore, physically, the minimum pressure gradient G is the pressure gradient corresponding to the yield stress τ_y in a porous medium.

In the petroleum and groundwater literature, very few solutions or analysis methods consider non-Newtonian Bingham plastic behavior, based on the modified Darcy's law (2.34). As pointed out by Scheidegger, "the mathematical difficulties in the integration of such flow equations become very great so that no solution for practical

cases seems to be available."

2.5 Conclusions from Literature Survey

To date considerable progress has been made in understanding the flow of non-Newtonian fluids through porous media. The experimental and theoretical studies performed in this field have focused on single-phase flow behavior. Solutions for single-phase non-Newtonian fluid flow are very useful in providing fundamentals for well testing analysis techniques, which are widely used in petroleum reservoir engineering and groundwater hydrology to determine reservoir and fluid properties. The main goals of the laboratory investigations are to correlate rheological properties with flow conditions for a particular non-Newtonian fluid in a given porous medium. An apparent viscosity is also needed in Darcy's equation for further study of the flow behavior. The general procedure in the experimental studies is to find a relationship between the most important physical quantities, such as shear rate, shear stress, and pressure gradient for the fluid of interest. This is normally done by using a capillary model to approximate the porous system. The remaining unknown parameters are left to be determined from flow experiments. The primary objectives of the theoretical studies are to develop well testing analysis methods for field applications. Based on theoretical pressure responses calculated from analytical or numerical solutions, the transient pressure analysis methods developed for non-Newtonian flow will permit approximate estimations of fluid and formation properties by matching observed pressure data from wells.

Despite considerable advances over the past three decades in studying the flow of non-Newtonian fluids through porous media, it is obvious that further studies are needed in understanding the physics of non-Newtonian flow in a complicated porous system. It has been well-documented that pseudoplastic fluids exhibit Newtonian behavior at high and low velocities. Even for single-phase non-Newtonian fluids, few theoretical

investigations including such complicated phenomena have been published that are based on the more realistic rheological model of Meter, Equation 2.8. The flow behavior of pseudoplastic fluids in porous media is still poorly understood. Also there are no techniques or theories available for analysis of non-Newtonian flow behavior in a fracture system. However, many underground formations for energy recovery or for waste storage have been found to be naturally fractured reservoirs.

At present, there is no standard approach in the petroleum engineering or groundwater literature for analyzing well test data for Bingham-type fluids. Interpretation of transient pressure responses with Bingham flow in porous media will be very important for heavy oil development, for groundwater flow evaluation in certain clay formations, and for foam flow analysis. A thorough study of Bingham-type fluid flow in reservoir conditions is needed not only for engineering applications, but also for the physical insights of transport behavior.

Non-Newtonian and Newtonian fluid immiscible displacement occurs in many EOR processes. These operations involve the injection of non-Newtonian fluids, such as polymer and foam solutions, or heavy oil production by waterflooding. However, very little research has been published on multiple phase flow of both non-Newtonian and Newtonian fluids in porous media, and there are no analytical solutions available for such flow. Even using numerical methods, very few studies have been performed to look at the physics of displacement. As a result, the mechanisms of immiscible displacement involving non-Newtonian fluids is still not well understood. Until we are able to predict how immiscible flow is affected by the properties of non-Newtonian fluids, it seems unlikely that a realistic theoretical model can be developed to describe the complex problems when such fluids are present.

It should be pointed out that non-Newtonian behavior is only one important factor that affects the flow of these fluids through porous media. There are many other factors which also have effects on the flow behavior. These include adsorption on pore surfaces

of rock, dispersion, inaccessible pore volume, viscous fingering, and lithology of the formation of interest, etc. A complete understanding of the flow behavior of non-Newtonian fluids in porous media with consideration of all these physical phenomena will be possible only after much more theoretical and experimental studies have been performed.

Chapter 3
Rheological Model

The *rheological model or condition* is the connection between shear stress and shear rate in the fluid (and their time derivatives). For flow in porous media, the rheological model is usually referred to the correlation of apparent viscosities of a non-Newtonian fluid and flow conditions for a given porous material. For an incompressible Newtonian fluid, Newton's law defining the dynamic viscosity μ is generalized to the following form (Savins, 1962; Fahien, 1983):

$$\underline{\tau} = -2\,\mu\,\underline{D} \tag{3.1}$$

where $\underline{\tau}$ is the stress tensor and $\underline{D}$ is the "rate-of-strain" tensor, or "rate-of-deformation" tensor. It is defined as

$$\underline{D} = \frac{1}{2}\left(\nabla\vec{V} + \nabla\vec{V}^{T}\right) \tag{3.2}$$

or

$$D_{ij} = \frac{1}{2}\left[\frac{\partial v_i}{\partial x_j} + \frac{\partial v_j}{\partial x_i}\right] \tag{3.3}$$

where $\nabla\vec{V}$ is the velocity gradient, and D_{ij} is the (i, j) component of the tensor $\underline{D}$ (i, j = 1, 2 ,3), $\nabla\vec{V}^{T}$ is the transpose of $\nabla\vec{V}$, and v_i is the component of vector $\vec{V}_i$ in the x_i direction ($x_1 = x$, $x_2 = y$, $x_3 = z$). The ijth component of tensor $\nabla\vec{V}$ is given by

$$\left(\nabla\vec{V}\right)_{ij} = \frac{\partial v_i}{\partial x_j} \tag{3.4}$$

For an incompressible non-Newtonian fluid, termed as the generalized Newtonian fluid in fluid mechanics (Astarita and Marrucci; 1974), Newton's law of viscosity can be modified to read

$$\underline{\tau} = -2\,\mu_a(s)\,\underline{D} \tag{3.5}$$

where μ_a is an apparent or effective viscosity which varies with the velocity gradient function s, which is defined as

$$s = 2\sum_i \sum_j D_{ij}\,D_{ji} \tag{3.6}$$

Several forms of the $\mu_a(s)$ function in Equation 3.5 have been proposed in the literature and are widely used in flow calculations. Among the rheological models for non-Newtonian fluids, only the power-law and Bingham models have been extensively used in research on porous media flow problems.

In this study, Darcy's law is assumed to be applicable to describe the flow of non-Newtonian fluids in porous media, in the form:

$$\vec{u} = -\frac{K}{\mu_{nn}}\nabla\Phi \tag{3.7}$$

where the non-Newtonian behavior is taken into account by the apparent viscosity μ_{nn}, and the flow potential Φ is defined as (Narasimhan, 1982; and Hubbert, 1956),

$$\Phi = \rho_{nn}\left[\int_{P_0}^{P}\frac{dP}{\rho_{nn}(P)} - z\,g\right] \tag{3.8}$$

where P_0 is a reference pressure; and the positive z-direction is chosen to be downward in the Cartesian coordinates (x, y, z).

Since theoretical and experimental considerations of non-Newtonian flow are based on an analysis of the microscopic properties of flow, we need to use the concept of "pore velocity". The pore velocity is defined to represent the "real" flow velocity along flow channels. However, it is physically meaningful only in an average or statistical sense because the actual velocity of the fluid will change within one flow channel and from one flow channel to another. In practice, it is generally assumed the porous medium is

isotropic in so far as the distribution of the porosity over the section is concerned. A commonly accepted hypothesis for the connection between pore velocity $\vec{v}_p$ and Darcy's velocity $\vec{u}$ is the Dupuit-Forchheimer assumption (Scheidegger, 1974; Marsily, 1986):

$$\vec{v}_p = \frac{\vec{u}}{\phi} = -\frac{K}{\mu_{nn}\phi}\nabla\Phi \tag{3.9}$$

By definition, the viscosity of a non-Newtonian fluid is a function of the shear rate. For single-phase flow of non-Newtonian fluids through porous media, it has been shown experimentally that shear rate depends only on the pore velocity for a given porous material and the particular fluid used (Gogarty, 1967; Savins, 1969; Hirasaki and Pope, 1974). For simplicity in the analytical and numerical solutions, it is better to correlate the non-Newtonian viscosity directly to the flow potential gradient. For single phase flow problems through porous media, the flow potential has been traditionally used as the primary dependent variable from its easily-measurable property. If we also want to use the potential as a primary variable in study of a non-Newtonian flow problem, it is logical to express all the other dependent variables in terms of functions of the flow potential and flow potential gradient. Non-Newtonian viscosities in a flow system change with the pore velocity, and the pore velocity changes accordingly with flow potential gradient, which is described by the Dupuit-Forchheimer formulation, Equation 3.9 and Darcy's law, Equation 3.7. Therefore,the treatment of non-Newtonian viscosities as functions of flow potential gradient will become necessary in the development of the calculable numerical and analytical solutions in Chapters 4-7. Specifically, it would be extremely difficult to relate viscosity of a Bingham fluid with pore velocity in a flow study from Equation 2.34. This treatment can be verified to be valid by representing the pore velocity v_p by Equation 3.9 as follows:

$$\mu_{nn} = f(v_p) = f\left[-\frac{K}{\mu_{nn}\phi}\nabla\Phi\right]$$

This equation implicitly states that the apparent viscosity used in Darcy's law for a non-Newtonian fluid is a function of the potential gradient only. Therefore, it is assumed in this work that the apparent viscosity μ_{nn} in the modified Darcy's equation 3.7 depends only on the potential gradient for the flow system under consideration,

$$\mu_{nn} = \mu_{nn}(\nabla\Phi) \tag{3.10}$$

For flow of a power-law fluid in porous media, a comparison of Equation 2.13 with Equation 3.7 leads to the following explicit relationship,

$$\mu_{nn} = \mu_{eff}\left[\frac{K}{\mu_{eff}}|\nabla\Phi|\right]^{\frac{n-1}{n}} \tag{3.11}$$

where μ_{eff} is defined in Equation 2.14.

If the four-parameter model by Meter (Meter and Bird, 1964) is used to describe the rheological behavior of shear-thinning fluids, one may choose the shear rate in a form (Hirasaki and Pope, 1974),

$$\dot{\gamma} = \left[\frac{3n+1}{4n}\right]^{n/(n-1)}\left[\frac{4K|\nabla\Phi|}{\phi\mu_{nn}[8K/\phi]^{1/2}}\right] \tag{3.12}$$

Using Equation 3.12 in the Meter model (2.8) will result in (Camilleri et al., 1987a),

$$\mu_{nn} = \mu_{\infty} + \frac{\mu_0 - \mu_{\infty}}{1 + \left[\frac{\dot{\gamma}}{\dot{\gamma}_{1/2}}\right]^{\beta-1}} \tag{3.13}$$

where the constants μ_0, μ_{∞}, and $\dot{\gamma}_{1/2}$ are defined in Equations 2.7 and 2.8, and the constant β may be different from α in Equation 2.8. Then, Equation 3.13 gives an implicit expression for the viscosity μ_{nn} as a function of the potential gradient in the Meter model.

For purposes of numerical simulation, the flow of Bingham fluids is best represented by a constant viscosity and a threshold pressure gradient, as in Equation

2.34. However, formally it is also possible to treat Bingham fluids as having a $|\nabla\Phi|$ dependent viscosity, which will be used to evaluate the analytical solution for immiscible displacement in Chapter 7. From Darcy's law (2.34), we have

$$\mu_{nn} = \frac{\mu_b}{1 - \frac{G}{|\nabla\Phi|}} \quad , \text{for } |\nabla\Phi| > G \tag{3.14a}$$

and

$$\mu_{nn} = \infty \quad , \text{for } |\nabla\Phi| \leq G \tag{3.14b}$$

where G is the minimum potential gradient. Flow takes place only after the applied potential gradient exceeds the value of G.

Similarly, many viscosity functions can be derived in terms of the potential gradient from rheological models available in the literature for flow of non-Newtonian fluids in porous media, such as those given by Scheidegger (1974).

All the viscosity models discussed above for non-Newtonian fluids were obtained originally from an analysis of experimental data or from the capillary analog for a porous medium, and they are valid only for single phase flow in porous media. The interest of this work is not only in single phase flow, but also in multiple phase flow. Therefore, the previously modified versions of Darcy's law for single non-Newtonian fluids are extended to include the effects of multiple phase flow on the viscosity of non-Newtonian fluids. The permeabilities, which are constants for single phase non-Newtonian fluid flow, may become functions of other dependent variables, such as saturation, from the inherent complexities of multiple phase flow. Since the viscosity of a non-Newtonian fluid is a flow property, it depends on the shear rate among other parameters for the multiphase flow case. Physically, it is reasonable to assume that the shear rate of a non-Newtonian fluid in multiple phase flow is also a function of the pore velocity of that fluid only for a given fluid and a given porous medium, based on the results for single phase non-Newtonian flow. The average shear rate, or pore velocity,

during multiple phase flow in a porous medium is determined by the local potential gradient in the direction of flow and also by the local saturation of the flowing phase. Hence, the apparent viscosity of non-Newtonian fluids for multiple phase flow is supposed to be a function of both flow potential gradient and saturation. For a given porous medium in the study, this may be expressed by

$$\mu_{nn} = \mu_{nn} (\nabla\Phi, S_{nn}) \tag{3.15}$$

This correlation should be obtained from experiments with non-Newtonian multiple phase flow where relative permeability and capillary pressure are known. A simpler way to find the dependence of viscosity on flow potential gradient and saturation may be to modify the viscosity function that is available for the single phase non-Newtonian fluid (Gencer and Ikuko, 1984; and Bondor et al., 1972). In this method, the corresponding permeability for single phase flow is replaced by the effective permeability (Kk_{rnn}), and porosity by (ϕS_{nn}) in the single phase viscosity function.

Chapter 4
Mathematical Model

4.1 Introduction

Conservation of mass, momentum and energy governs the behavior of fluid flow through porous media. The physical laws at the pore level in a porous medium are simple and well-known. In practice, however, only the global behavior of the system is of interest. Due to the complexity of pore geometries, the macroscopic behavior is not easily deduced from that on the pore level. Any attempts to directly apply the Navier-Stokes equation to flow problems in porous media will face the difficulties of poorly-defined pore geometries and the complex phenomena of physical and chemical interactions between fluids or between fluids and solids, which cannot be solved at the present time. Therefore, the macroscopic continuum approach has been used prevalently both theoretically and in applications. Almost all theories on flow phenomena occurring in porous media lead to macroscopic laws applicable to a finite volume of the system under consideration whose dimensions are large compared with those of pores. Consequently, these laws lead to equations in which the medium is treated as if it were continuous and characterized by the local values of a certain number of parameters defined for all points.

It should be pointed out that recent theoretical developments in new cellular-automaton models (lattice-gas) have provided an alternative approach for building microscopic models in hydrodynamics (Frisch et al., 1986). They introduced an entire discrete lattice-gas model for the numerical solution of the two-dimensional Navier-Stokes equation. The macroscopic behavior of the lattice-gas automaton asymptotically approaches continuum flow. This new theory has been extended to develop a new and

generally applicable computational model of immiscible two-phase flow and applied to the study of flow in porous media (Rothman et al., 1988). However, it seems that there is a long way before this new technique can find engineering applications in the industry.

The physical laws governing equilibrium and flow of several fluids in a porous medium are represented mathematically on the macroscopic level by a set of partial differential equations, which generally are non-linear when multiple phase or non-Newtonian fluids are involved. Solutions of the governing differential equations can often be obtained only by numerical methods. Under very special cases with appropriate idealizations, analytical solutions may be possible, such as in the case of the Buckley-Leverett solution for a linear waterflood situation.

The governing equations used for non-Newtonian and Newtonian fluid flow in this study are similar to those of multiple phase flow in porous media, and Darcy's law is assumed to be valid and to include the effects of the rheological properties of non-Newtonian fluids on flow behavior. In the present work, the flow system is assumed to be isothermal, so that the energy conservation equation is not required.

4.2 Governing Equations for Non-Newtonian and Newtonian Fluid Flow

Consider an arbitrary volume V_n of a porous medium with porosity ϕ, filled with a Newtonian fluid of density ρ_{ne} and a non-Newtonian fluid of density ρ_{nn}, bounded by surface S (Figure 4.1). It is assumed that the non-Newtonian and Newtonian fluids are immiscible, and no mass transfer occurs between the two phases. The formal development and notations used here for the governing equations follow the work in the "TOUGH User's Guide" by Pruess (1987). The law of conservation of mass for each fluid states that the sum of the net fluxes crossing the boundary plus the generation rate of the mass of the fluid must be equal to the rate of the mass accumulated in the domain for the fluid, in an integral form,

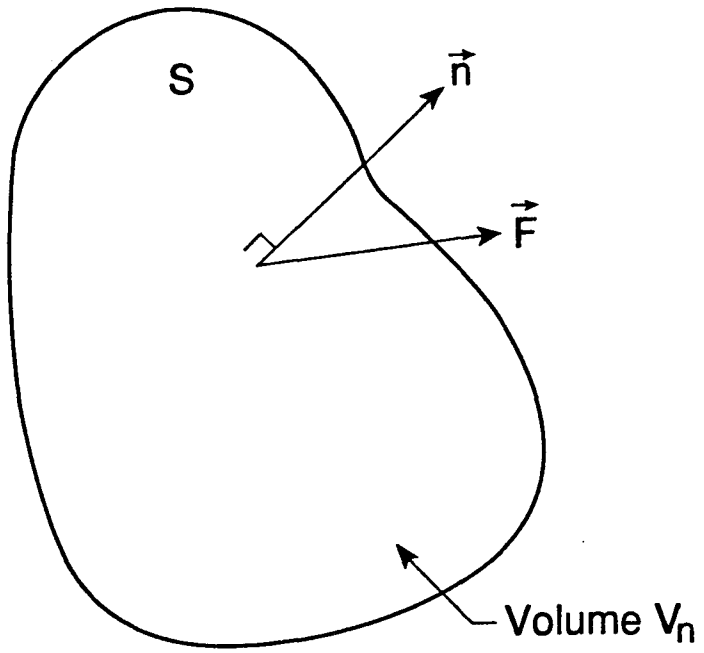

XBL 8911-7855
T.I.D. Illus.88

Figure 4.1 Arbitrary Volume of Formation in a Flow Field Bounded by Surface S.

$$\frac{d}{dt}\iiint_{V_n} M_\beta \, dV = -\iint_S \vec{F}_\beta \cdot \vec{n} \, dS + \iiint_{V_n} q_\beta \, dV \tag{4.1}$$

Where for Newtonian fluid $\beta = ne$, for non-Newtonian fluid $\beta = nn$, $\vec{n}$ is the unit outward normal vector on surface S, and q_β is source terms for fluid β. The mass accumulation terms M_β for Newtonian and non-Newtonian fluids ($\beta = ne, nn$) are

$$M_\beta = \phi \, S_\beta \, \rho_\beta \tag{4.2}$$

where S_β is the saturation of phase β ($\beta = ne, nn$), and ρ_β is density of phase β ($\beta = ne, nn$).

The mass flux terms $\vec{F}_\beta$ in Equation 4.1 are described by Darcy's law for Newtonian and non-Newtonian fluids as

$$\vec{F}_\beta = -K \frac{k_{r\beta}}{\mu_\beta} \rho_\beta (\nabla P_\beta - \rho_\beta \vec{g}) \tag{4.3}$$

where K is absolute permeability, $k_{r\beta}$ is relative permeability to phase β, μ_β is dynamic viscosity of phase β, P_β is pressure in phase β, and $\vec{g}$ is gravitational acceleration.

Upon applying the Gauss theorem to Equation 4.1, the surface integral on the right side of Equation 4.1 can be transformed into a volume integral,

$$\frac{d}{dt}\iiint_{V_n} M_\beta \, dV = \iiint_{V_n} (- \operatorname{div} \vec{F}_\beta + q_\beta) \, dV \tag{4.4}$$

Since Equation 4.4 is valid for any arbitrary region in the flow system, it follows that

$$\frac{\partial M_\beta}{\partial t} = - \operatorname{div} \vec{F}_\beta + q_\beta \tag{4.5}$$

This is a differential form of the governing equations for mass conservation of non-Newtonian and Newtonian fluids.

From the definition of saturation, it follows that

$$S_{ne} + S_{nn} = 1 \tag{4.6}$$

This constraint condition is always valid in a two phase flow problem.

The governing equations for flow of single-phase non-Newtonian fluids in porous media can always be considered as a special case of the multiphase equations. They are readily derived from Equations 4.1, or 4.5 by setting $S_{ne} = 0$, and $S_{nn} = 1$.

4.3 Constitutive Equations

The mass transport governing Equations 4.1, or 4.5 need to be supplemented with constitutive equations, which express all the parameters as functions of a set of primary thermodynamic variables of interest (P_β, S_β). The following relationships will be used to complete the statement of multiple phase flow of non-Newtonian and Newtonian fluids through porous media.

Equations of state of the densities for Newtonian and non-Newtonian fluids are, respectively,

$$\rho_{ne} = \rho_{ne} (P_{ne}) \tag{4.7}$$

$$\rho_{nn} = \rho_{nn} (P_{nn}) \tag{4.8}$$

The difference in pressure between the two phases may be described in terms of capillary pressure,

$$P_c (S_{nn}) = P_{ne} - P_{nn} \tag{4.9}$$

and the capillary pressure P_c is determined experimentally as a function of saturation only.

The relative permeabilities are also assumed to be functions of fluid saturation only (Honarpour et al., 1986),

$$k_{rne} = k_{rne}(S_{nn}) \tag{4.10}$$

$$k_{rnn} = k_{rnn}(S_{nn}) \tag{4.11}$$

As pointed out by other workers (Bird et al. , 1960), the permeability for single-phase non-Newtonian fluid flow should be obtained from core experiments with Newtonian fluids. In order to reduce the uncertainties when non-Newtonian flow is involved, the relative permeability data for multiphase flow of non-Newtonian fluids should also be determined by using Newtonian fluids in the laboratory experiment.

4.4 Numerical Model

When a non-Newtonian fluid is involved in a flow problem, the apparent viscosity as used in Darcy's law depends on the pore velocity, or the potential gradient. Therefore, the governing integral or partial differential equations are highly non-linear. Solutions for such problems can only be found by numerical methods. However, under some special circumstances, analytical and approximate analytical solutions are possible. Both analytical and numerical methods have been employed in this work in order to provide a general theoretical approach to analysis of the flow behavior of non-Newtonian fluids.

The numerical technique in this work is the "integral finite difference" method (Narasimhan and Witherspoon, 1976). A modified version of the "MULKOM" family of multi-phase, multi-component codes (Pruess, 1983; 1988) for non-Newtonian and Newtonian fluid flow has been developed in analyzing flow problems of single and multiple phase non-Newtonian fluids in porous media. The input data and running procedures are similar to those for the code "MULKOM-GWF", which was developed to model the flow of gas, water and foam solutions in porous media (Pruess and Wu, 1988). This simulator for Newtonian fluid flow calculations has been validated by Pruess and

his co-workers at Lawrence Berkeley Laboratory. MULKOM has been used extensively for fundamental and applied research on geothermal reservoirs, oil and gas fields, nuclear waste repositories, and for the design and analysis of laboratory experiments (Pruess, 1988).

Based on the integral finite difference method, the mass balance equations for each phase are expressed in terms of the integral difference equations, which are fully implicit to provide stability and time step tolerance in highly non-linear problems (Thomas, 1982). Thermodynamic properties are represented by averages over explicitly defined finite subdomains, while fluxes of mass across surface segments are evaluated by finite difference approximations. The mass balance difference equations are solved simultaneously, using the Newton/Raphson iteration procedure.

The capillary pressures and relative permeabilities are treated as functions of saturation, and can be specified differently for different flow regions. Thermophysical properties of water and gas (methane) substance, such as density and viscosity, are represented within experimental accuracy by the steam table equations given by the International Formulation Committee (1967) and by Vargaftik (1975), respectively. The rheological properties for non-Newtonian viscosity need special treatments and depend on the rheological models used. A number of the common viscosity functions have been implemented in the codes, such as the power-law and Bingham models.

A brief description of the numerical method used in this non-Newtonian flow version of MULKOM is included in the following section for completeness. It is almost identical to that given in the TOUGH code (Pruess, 1987). The continuum Equation 4.1 is discretized in space using the "integral finite difference" scheme. Introducing an appropriate volume average, it follows that

$$\iiint_{V_n} M \, dV = V_n M_n \tag{4.12}$$

Where M is a volume-normalized extensive quantity, and M_n is the average value of M over the domain V_n. The surface integrals are approximated as a discrete sum of averages over surface segments A_{nm}:

$$-\iint_{S_n} \vec{F} \cdot \vec{n}\, dS = \sum_m A_{nm} F_{nm} \tag{4.13}$$

Here F_{nm} is the average value of the (inward) normal component of $\vec{F}$ over the surface segment A_{nm} between volume elements V_n and V_m. This is expressed in terms of averages over parameters for elements V_n and V_m. For the basic Darcy flux term, Equation 4.3, we have

$$F_{\beta,nm} = -K_{nm} \left[\frac{k_{r\beta}\, \rho_\beta}{\mu_\beta} \right]_{nm} \left[\frac{P_{\beta,n} - P_{\beta,m}}{D_{nm}} - \rho_{\beta,nm}\, g_{nm} \right] \tag{4.14}$$

where the subscripts (nm) denote a suitable averaging (interpolation, harmonic weighting, upstream weighting). D_{nm} is the distance between the nodal points n and m, and g_{nm} is the component of gravitational acceleration in the direction from m to n.

Substituting Equations 4.12, and 4.13 into the governing Equation 4.1, a set of first-order ordinary differential equations in time is obtained,

$$\frac{dM_{\beta,n}}{dt} = \frac{1}{V_n} \sum_m A_{nm} F_{\beta,nm} + q_{\beta,n} \tag{4.15}$$

Time is discretized as a first order difference, and the flux and sink and source terms on the right hand side of Equation 4.15 are evaluated at the new time level, $t^{k+1} = t^k + \Delta t$, to obtain the numerical stability needed for an efficient calculation of multi-phase flow. This treatment of flux terms is known as "fully implicit," because the fluxes are expressed in terms of the unknown thermodynamic parameters at time level t^{k+1}, so that these unknowns are only implicitly defined in the resulting equations. The time discretization results in the following set of coupled non-linear, algebraic equations:

$$R_{\beta,n}^{k+1} = M_{\beta,n}^{k+1} - M_{\beta,n}^{k} -$$

$$\frac{\Delta t}{V_n}\left\{\sum_m A_{nm} F_{\beta,nm}^{k+1} + V_n (q_{\beta,n})^{k+1}\right\} = 0 \qquad (4.16)$$

Following Pruess (1987), "the entire geometric information of the space discretization in Equation 4.16 is provided in the form of a list of grid block volumes V_n, interface areas A_{nm}, nodal distances D_{nm} and components g_{nm} of gravitational acceleration along nodal lines. There is no reference whatsoever to a global system of coordinates, or to the dimensionality of a particular flow problem. The discretized equations are in fact valid for arbitrary irregular discretizations in one, two or three dimensions, and for porous as well as for fractured media. This flexibility should be used with caution, however, because the accuracy of the solutions depends on the accuracy with which the various interface parameters in equations, such as in Equation 4.14, can be expressed in terms of average conditions in grid blocks. A sufficient condition for this to be possible is that there exists approximate thermodynamic equilibrium in (almost) all grid blocks at (almost) all times. For systems of regular grid clocks referenced to global coordinates (such as r-z, x-y-z), Equation 4.16 is identical to a conventional finite difference formulation."

For each volume element (grid block) V_n there are two equations for the primary thermodynamic variables, P_{nn} and S_{nn}, if the problem is two-phase flow of one Newtonian and one non-Newtonian fluid. For a flow system which is discretized into N grid blocks, Equation 4.16 represents a set of 2N algebraic equations. The unknowns are the 2N independent primary variables x_i (i=1, 2, 3, ..., 2N) which completely define the state of the flow system at time level t^{k+1}. These equations are solved by Newton/Raphson iteration, which is implemented as follows. An iteration index p is used here, and the residuals are expanded in terms of the primary variables $x_{i,p}$ at iteration level p:

$$R_{\beta,n}{}^{k+1}(x_{i,p+1}) = R_{\beta,n}{}^{k+1}(x_{i,p}) +$$

$$\sum_i \left.\frac{\partial R_{\beta,n}{}^{k+1}}{\partial x_i}\right|_p (x_{i,p+1} - x_{i,p})$$

$$+ \cdots = 0 \qquad (4.17)$$

Retaining only terms up to first order, a set of 2N linear equations for the increments $(x_{i,p+1} - x_{i,p})$ is obtained :

$$-\sum_i \left.\frac{\partial R_{\beta,n}{}^{k+1}}{\partial x_i}\right|_p (x_{i,p+1} - x_{i,p}) = R_{\beta,n}{}^{k+1}(x_{i,p}) \qquad (4.18)$$

All terms $\frac{\partial R_n}{\partial x_i}$ in the Jacobian matrix are evaluated by numerical differentiation. Equation 4.18 is solved with the Harwell subroutine package "MA 28" (Duff,1977). Iteration is continued until the residuals $R_n{}^{k+1}$ are reduced below a preset convergence tolerance.

4.5 Treatment of Non-Newtonian Behavior

The apparent viscosity functions for non-Newtonian fluids in porous media depend on the pore velocity, or the potential gradient, in a complex way, as discussed in Chapters 2 and 3. The rheological correlations for different non-Newtonian fluids are quite different. Therefore, it is impossible to develop a general numerical scheme that can be universally applied to various non-Newtonian fluids. Instead, a special treatment for the particular fluid of interest has to be worked out. However, for some fluids, such as power-law, Bingham plastic, pseudoplastic fluids, which are most often encountered in porous media, the numerical treatment developed in this work will be discussed here. The implementation of the treatment for these three non-Newtonian fluids in the code "MULKOM", is given in Appendix F.

4.5.1 Power-Law Fluid

The power-law model, Equation 3.11, is the most widely used to describe the rheological property of shear-thinning fluids, such as polymer and foam solutions. The power-law index n ranges between 0 and 1 for a shear thinning fluid, and the viscosity becomes infinite as the flow potential gradient tends to zero. Therefore, direct use of Equation 3.11 in the calculation will cause numerical difficulties. A formulation incorporated in the code for a power-law fluid is to use a linear interpolation when the potential gradient is very small. As shown in Figure 4.2, the viscosity for a small value of potential gradient is calculated by

$$\mu_{nn} = \mu_1 + \frac{\mu_1 - \mu_2}{\delta_1 - \delta_2} (|\nabla\Phi| - \delta_1) \tag{4.19}$$

for $|\nabla\Phi| \le \delta_1$. Where the interpolation parameters δ_1 and δ_2 are defined in Figure 4.2. If the potential gradient is larger than δ_1, Equation 3.11 is used in the code. In order to maintain the continuities in the viscosity and its derivative at (δ_1, μ_1), the difference in values of δ_1 and δ_2 should be chosen sufficiently small. Then, the values for μ_1, and μ_2 may be taken as

$$\mu_j = \mu_{eff} \left[\frac{K}{\mu_{eff}} \delta_j \right]^{\frac{n-1}{n}} \qquad (j = 1, 2) \tag{4.20}$$

The numerical tests show that the treatment of power-law fluids by Equation 4.19 works very well for a power-law fluid flow problem with various potential gradients. The accuracy of this scheme has been confirmed by a number of runs. Another way for the linear interpolation at small potential gradient is to use the tangential slope $\mu_{nn}'|_{\delta_1}$ in (4.19) instead of the the chord slope used. In the numerical studies of transient flow problems of power-law fluids in Chapter 8, the values of the interpolation parameters are taken as $\delta_1 = 10$ (Pa/m), and $\delta_1 - \delta_2 = 10^{-7}$ (Pa/m).

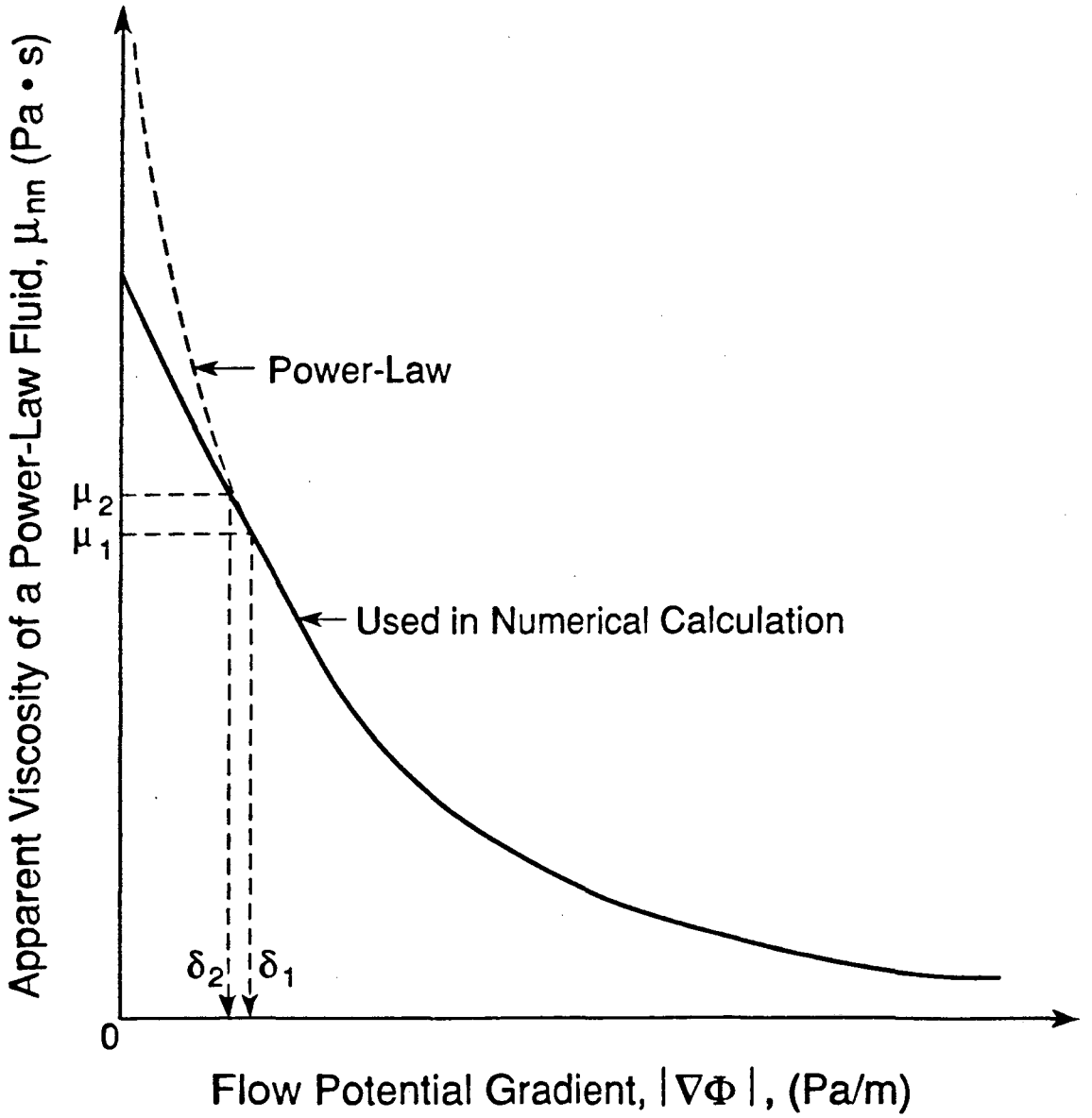

Figure 4.2 Schematic of Linear Interpolation of Viscosities of Power-Law Fluids with Small Flow Potential Gradient.

A similar treatment is also incorporated in the numerical code and used for the modeling transient flow of power-law fluids through fractured media in Chapter 8. In that application, the viscosity function for a power-law fluid is given by Equation C.8, derived in Appendix C, instead of Equation 3.11 for porous media flow.

4.5.2 Bingham Fluid

The apparent viscosity of Bingham fluids, as given by Equation 3.14, has a similar behavior to that of a power-law fluid. As the potential gradient decreases and comes close to the minimum potential gradient G, the viscosity tends to be infinite. It is possible to use a linear interpolation approximation for the viscosity when the potential gradient nears G to overcome the associated numerical difficulties. However, a much better approach that has been found is to introduce an effective potential gradient $\nabla\Phi_e$, whose scalar component in the x direction, flow direction, is defined as

$$\left[\nabla\Phi_e\right]_x = \begin{cases} (\nabla\Phi)_x - G & (\nabla\Phi)_x > G \\ (\nabla\Phi)_x + G & (\nabla\Phi)_x \le -G \\ 0 & -G \le (\nabla\Phi)_x \le G \end{cases} \tag{4.21}$$

where $(\nabla\Phi)_x$ is the scalar component of the potential gradient $\nabla\Phi$. As shown in Figure 4.3, Darcy's law as used in the code for a Bingham fluid is

$$\vec{u} = -\frac{K}{\mu_b}\nabla\Phi_e \tag{4.22}$$

and replaces Equation 2.34 in Chapter 9 in the numerical calculations. This treatment of the code using the effective potential gradient has proven to be the most efficient when simulating Bingham fluid flow in porous media.

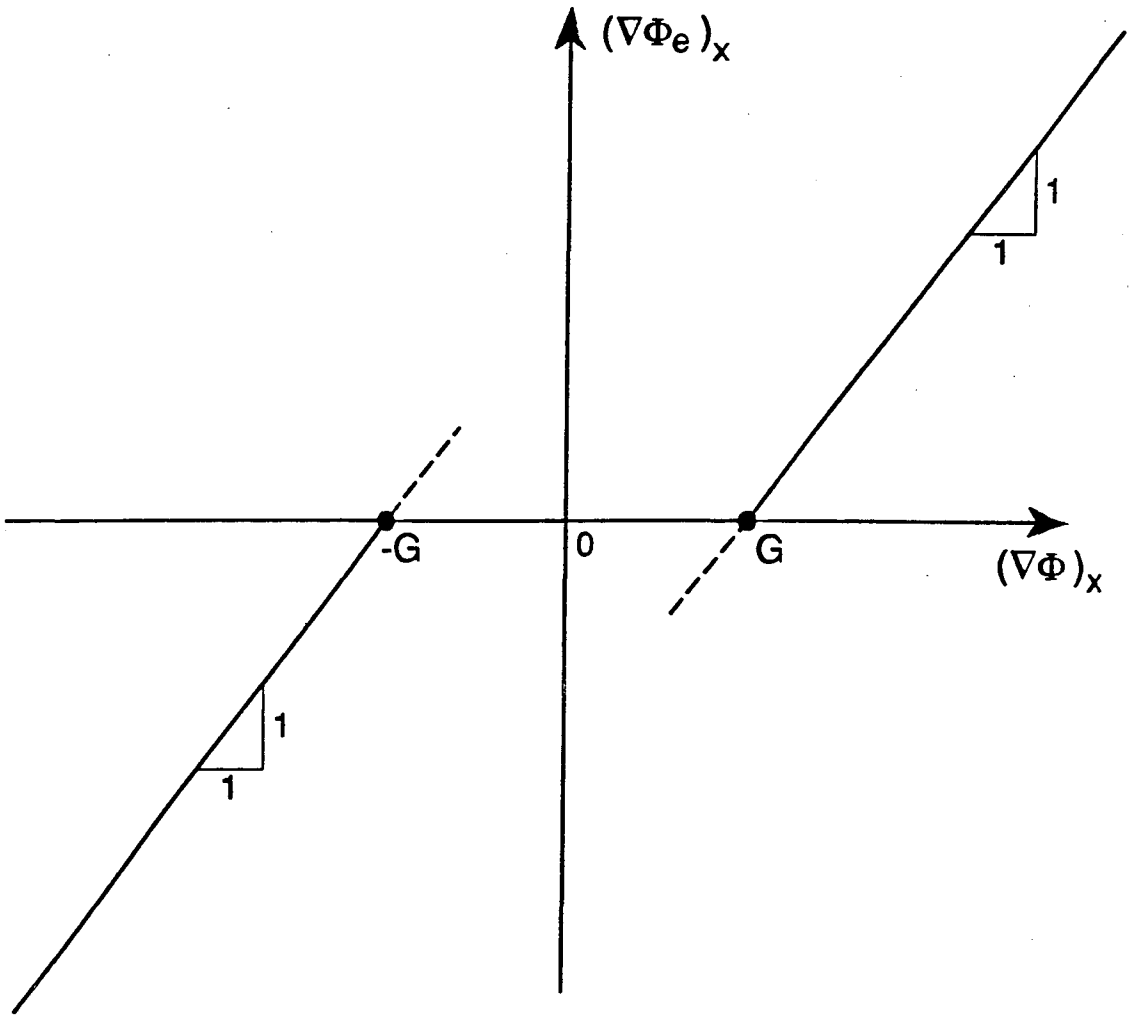

XBL 8912-7929
T.I.D.Illus.88

Figure 4.3 Effective Potential Gradient for a Bingham Fluid, the Dashed Linear Extension for Numerical Calculation of Derivatives When $(\nabla\Phi)$ is near + G or - G.

Modeling of Bingham fluid flow in porous media is a very difficult problem numerically because of the minimum pressure gradient phenomenon. For a single well flow problem with a uniform initial pressure distribution in the formation, the fluid in many grids near wellbore maybe change from immobile to mobile within only one time step at early transient times after the well is put into production. With each Newton-Raphson iteration during a time step, pressure disturbance may penetrate one more grid. As a result, more Newton-Raphson iterations for convergence at each time step are then needed in the calculation. Therefore, no explicit formula can be used in the code, and we have to use some fully implicit numerical scheme to handle the non-linear convergent problem with Bingham fluids.

4.5.3 General Pseudoplastic Fluid

In this study, a general pseudoplastic fluid is defined as a fluid whose apparent viscosity is described by the Meter four-parameter model, Equation 3.13, (Meter and Bird, 1964). The shear rate, $\dot{\gamma}$, in Equation 3.13 for single phase one-dimensional flow of a power law fluid is given by Equation 3.12 (Camilleri et al., 1987a; Hirasaki and Pope, 1974). For the special cases, where $\mu_0 = \mu_\infty$, or, $\beta = 1$, the fluid becomes Newtonian.

For a horizontal flow problem, ignoring the effects of gravity on shear rate in Equation 3.12, and introducing the resulting shear rate function into Equation 3.13, one can obtain

$$\mu_{nn}{}^{\beta} + C_n \left[-\frac{\partial P}{\partial x}\right]^{\beta-1} \mu_{nn} - \mu_0 \mu_{nn}{}^{\beta-1} - \mu_\infty C_n \left[-\frac{\partial P}{\partial x}\right]^{\beta-1} = 0 \qquad (4.23)$$

Note that $(-\partial P/\partial x) \geq 0$ for injection and C_n is

$$C_n = \left[\frac{\left(\frac{3n+1}{4n} \right)^{n/(n-1)}}{\dot{\gamma}_{1/2}} \left(\frac{2K}{\phi} \right)^{1/2} \right]^{\beta-1} \tag{4.24}$$

Equation 4.23 implicitly defines the viscosity μ_{nn} as a function of the pressure gradient $(-\partial P/\partial x)$. For the pseudoplastic fluid in porous media, this has been implemented in the numerical code to correlate apparent viscosity of the psuedoplastic fluid with pressure gradient in the numerical study of Chapter 8.

One may try to use Equations 3.12 and 3.13 directly in the code by using the values of viscosity from the previous iteration in calculation of the current iteration in order to avoid solving the non-linear algebraic equation 4.23 for μ_{nn} from $(-\partial P/\partial x)$ at each iteration. However, numerical tests have shown that the convergence is even slower than the above method because of the highly non-linear relationship between viscosity and pressure gradient. The fully implicit treatment used in this work gives satisfactory convergence.

Chapter 5
Analytical Solution for Immiscible Displacement

5.1 Introduction

Immiscible and miscible flow of multiple phase fluids through porous media, as compared with single phase flow, is much more complicated and is not well understood in many areas due to the complex interactions of the different fluid phases. Many contributions to this subject have been made since the 1940's. In the petroleum industry, the simultaneous flow of oil, gas and water in reservoirs is important in connection with the production of oil and gas. The flow of moisture in unsaturated soils (i.e., the simultaneous flow of water and air) is often encountered in soil science. Multiple phase flow of water, hydrocarbons, air and chemicals is also involved in evaluating problems of underground contamination.

The study of multiple phase flow in porous media has been divided into different parts according to the flow behavior prevalent in each part. The most important distinction is whether the fluids are miscible or immiscible, leading to "miscible" and "immiscible" displacement in porous media (Scheidegger, 1974; Marle, 1981; Stalkup, 1983). These two types of displacement are limiting cases that can be investigated theoretically. In miscible displacement, the two fluids are completely soluble in each other. The interfacial tension between the two fluids is zero, and the two fluids dissolve in each other. Whereas in immiscible displacement, we have a simultaneous flow of two or more immiscible fluids or phases in the porous medium. The interfacial tension between the fluids is nonzero, and distinct fluid-fluid interfaces separate the fluids within the pore space.

Immiscible displacement is involved in most of the EOR methods in the petroleum industry. Most EOR processes consist of injecting a fluid (gas or liquid) into a reservoir to displace the in-situ oil or gas. A fundamental understanding of immiscible displacement of Newtonian fluids in porous media was contributed by Buckley and Leverett (1942) in their classical study of the fractional flow theory. The Buckley-Leverett solution gives a saturation profile with a sharp front along the flow direction, but ignores capillary pressure and gravity effects. As time progresses, the saturation becomes a multiple-valued function of the distance coordinate, x, which can be overcome by material balance considerations. Where the initial saturation is uniform, a simple graphic approach developed by Welge (1952) can be used to determine the sharp saturation front without difficulty. Effects of gravity and capillary pressure on linear waterflood was included by Fayers and Sheldon (1959), Hovanessian and Fayers (1961), by numerical models. More recently, some special analytical solutions of immiscible displacement including the effects of capillary pressure were obtained by Yortsos and Fokas (1983) and Chen (1988).

The Buckley-Leverett fractional flow theory has been applied and generalized by various authors to study the EOR problems (Pope 1980), surfactant flooding (Larson and Hirasaki, 1978; Hirasaki, 1981), polymer flooding (Patton, Coats and Colegrone, 1971), the mechanism of chemical methods (Larson, Davis and Scriven, 1982), detergent flooding (Fayers and Perrine, 1959), displacement of oil and water by alcohol (Wachmann, 1964 ; Taber, Kamath and Reed, 1961), displacement of viscous oil by hot water and chemical additive (Karakas, Saneie, and Yortsos, 1986), and alkaline flooding (deZabala, Vislocky, Rubin and Radke, 1982). An extension to more than two immiscible phases dubbed "coherence theory" was described by Helfferich (1981). However, no non-Newtonian behavior has been considered in any of these extensive investigations.

The state of the art in the mathematical modeling of immiscible Newtonian fluid displacement processes has advanced considerably since the 1950's (Douglas et al.,

1959; Peaceman et al., 1962; Coats, 1987; Aziz and Settari, 1979; Thomas, 1982, and Peaceman, 1977). A large number of numerical models have been developed to simulate the process of waterflooding under quite general conditions. The approaches usually followed in simulating immiscible flow include derivation of mass, momentum, and energy conservation equations for the displacing and displaced phases, plus the construction of certain numerical schemes for the solution of the resulting partial differential or integral equations with proper boundary and initial conditions. However, the numerical modeling cannot replace the analytical methods completely, since i) the numerical codes need checking against an analytical solution, and ii) the analytical solution if available provides a better insight into the physics of the transport phenomena occurring within the porous media.

Immiscible displacement of Non-Newtonian and Newtonian fluids occurs in many EOR processes, such as the injection of non-Newtonian fluids, especially, polymer solutions, microemulsions, macroemulsions, foam solutions, and heavy oil displacement by waterflooding. As mentioned in Chapter 2, almost all theoretical studies on non-Newtonian fluid flow in porous media have focused on single phase flow. Very little research has been carried out on multiple phase flow of non-Newtonian and Newtonian fluids through porous media. There are no analytical solutions available on this subject for theoretical studies or for engineering applications, and the physics of immiscible flow with non-Newtonian fluids is poorly understood.

In this chapter, analytical solutions to describe displacement mechanisms of non-Newtonian / Newtonian fluids in porous media will be developed for the one-dimensional linear flow case. A practical procedure to evaluate the behavior of non-Newtonian and Newtonian linear displacement is also provided, based on the analytical solutions, which is similar to the graphic method of Welge (1952). The result can be regarded as an extension of the Buckley-Leverett theory for flow of non-Newtonian fluids in porous media. The analytical results reveal how the saturation profile and the

displacement efficiency are controlled not only by the relative permeabilities, as in the Buckley-Leverett solution, but also by the inherent complexities of non-Newtonian fluids.

The results of this analytical solution will have applications in two areas. First, they can be used to study the displacement mechanism of non-Newtonian and Newtonian fluids in porous media. The second application is demonstrated in this chapter. The analytical solution will be used to verify the numerical simulator developed for non-Newtonian flow in Chapter 4. The results from the numerical code and the analytical solution for a power-law fluid displacement problem are found to be in excellent agreement with each other.

5.2 Mathematical Formulation

Two-phase flow of non-Newtonian and Newtonian fluids is considered in a homogeneous and isotropic porous medium. There is no mass transfer between non-Newtonian and Newtonian fluids, and dispersion and adsorption on the rock are ignored. The governing equations are given by Equation 4.5,

$$-\nabla \cdot (\rho_{ne} \vec{u}_{ne}) = \frac{\partial}{\partial t} (\rho_{ne} S_{ne} \phi) \tag{5.1}$$

for the Newtonian fluid,

$$-\nabla \cdot (\rho_{nn} \vec{u}_{nn}) = \frac{\partial}{\partial t} (\rho_{nn} S_{nn} \phi) \tag{5.2}$$

for the non-Newtonian fluid. The flow for Newtonian and non-Newtonian phases is described by a multiple phase extension of Darcy's law, Equation 3.7

$$\vec{u}_{ne} = -K \frac{k_{rne}}{\mu_{ne}} (\nabla P_{ne} - \rho_{ne} \vec{g}) \tag{5.3}$$

and

$$\vec{u}_{nn} = -K \frac{k_{rnn}}{\mu_{nn}} (\nabla P_{nn} - \rho_{nn} \vec{g}) \tag{5.4}$$

The pressures in the two phases depend on the capillary pressure,

$$P_c (S_{nn}) = P_{ne} - P_{nn} \tag{5.5}$$

k_{ne}, k_{nn} and P_c are assumed to be functions of saturation only. Also, from the definition of saturation, we have

$$S_{ne} + S_{nn} = 1 \tag{5.6}$$

5.3 Analytical Solution for Non-Newtonian and Newtonian Fluid Displacement

For the derivation of the analytical solution, the following additional assumptions are made:

1. the two fluids and the porous medium are incompressible,
2. the capillary pressure gradient is negligible,
3. the viscosity of non-Newtonian fluids is a function of pressure gradient and saturation only, as described in Equation 3.15,
4 one-dimensional linear flow.

The flow system is a semi-infinite linear reservoir with a constant cross-sectional area A, as shown in Figure 5.1. The system is initially saturated with a Newtonian fluid, and a non-Newtonian fluid is injected. It is further assumed that gravity segregation is negligible and stable displacement exists near the displacement front. Equations 5.1 and 5.2 can then be changed to read

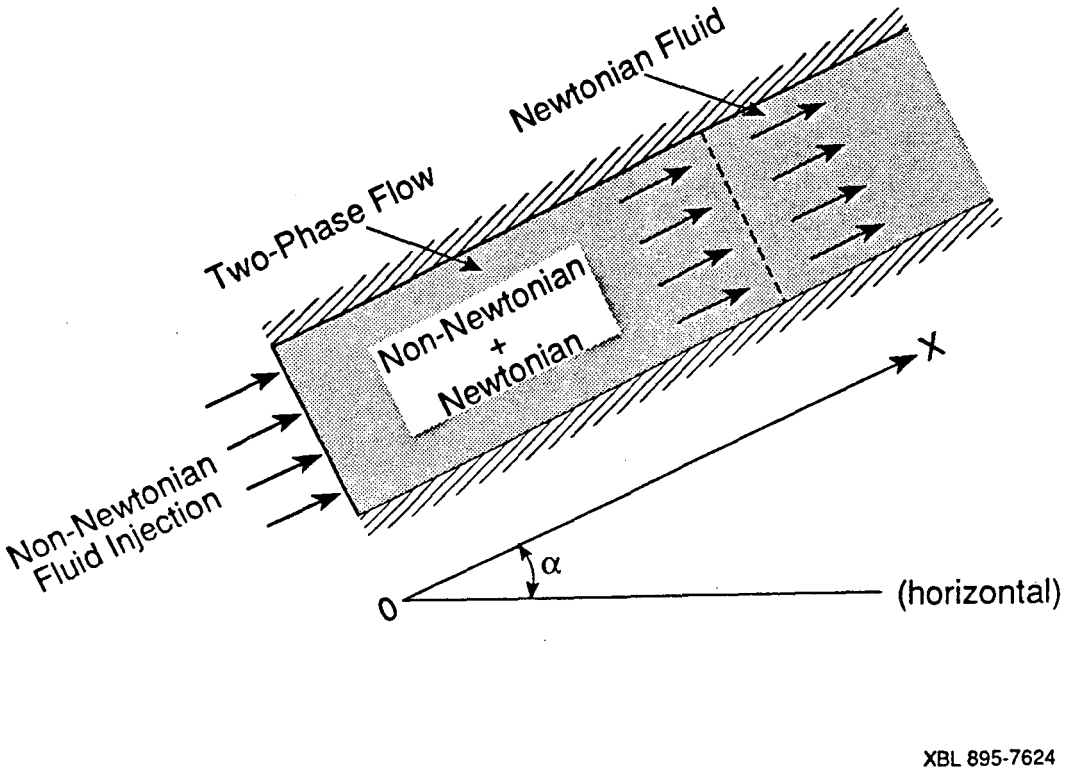

Figure 5.1 Schematic of Displacement of a Newtonian Fluid by a Non-Newtonian Fluid.

$$-\frac{\partial u_{ne}}{\partial x} = \phi \frac{\partial S_{ne}}{\partial t} \tag{5.7}$$

and

$$-\frac{\partial u_{nn}}{\partial x} = \phi \frac{\partial S_{nn}}{\partial t} \tag{5.8}$$

where u_{ne} and u_{nn} are the volumetric flow velocities of Newtonian and Newtonian fluids, respectively. For the Newtonian phase, the flow velocity is

$$u_{ne} = -K \frac{k_{rne}}{\mu_{ne}} \left[\frac{\partial P}{\partial x} + \rho_{ne} g \sin \alpha \right] \tag{5.9}$$

and for the non-Newtonian phase,

$$u_{nn} = -K \frac{k_{rnn}}{\mu_{nn}} \left[\frac{\partial P}{\partial x} + \rho_{nn} g \sin \alpha \right] \tag{5.10}$$

To complete the mathematical description of the physical problem, the initial and boundary conditions must be specified. Initially, the Newtonian fluid is at its maximum saturation in the system.

$$S_{ne}(x, 0) = 1 - S_{nnir} \tag{5.11}$$

where S_{nnir} is the initial immobile non-Newtonian fluid saturation. For most practical field problems, S_{nnir} is usually zero, which can be treated as a special case.

In this problem, we are concerned with continuously injecting a non-Newtonian fluid at a known rate $q(t)$, which can be a function of injection time t. The boundary conditions at $x = 0$ are:

$$u_{nn}(0, t) = \frac{q(t)}{A} \tag{5.12}$$

$$u_{ne}(0, t) = 0 \tag{5.13}$$

In this semi-infinite system, the following condition must be imposed as $x \rightarrow \infty$,

$$S_{ne} \rightarrow 1 - S_{nnir} \tag{5.14}$$

and

$$S_{nn} \rightarrow S_{nnir} \tag{5.15}$$

The solution procedure follows the work by Buckley and Leverett (1942), as outlined by Willhite (1986). The fractional flow concept is also used to simplify the governing equations in terms of saturation only in this study. The fractional flow of a phase is defined as a volume fraction of the phase flowing at x and t to the total volume of the flowing phases (Willhite, 1986). For the Newtonian phase, this can be written

$$f_{ne} = \frac{u_{ne}}{u_{ne} + u_{nn}} = \frac{u_{ne}}{u(t)} \tag{5.16}$$

and for the non-Newtonian phase,

$$f_{nn} = \frac{u_{nn}}{u_{ne} + u_{nn}} = \frac{u_{nn}}{u(t)} \tag{5.17}$$

where $u(t) = u_{ne} + u_{nn}$. From a volume balance, the sum of Equations 5.16 and 5.17 yields

$$f_{ne} + f_{nn} = 1 \tag{5.18}$$

The fractional flow function for the non-Newtonian phase may be written in the following form (Willhite, 1986):

$$f_{nn} = \frac{1}{1 + \left[\frac{k_{rne}(S_{nn})}{k_{rnn}(S_{nn})}\right]\left[\frac{\mu_{nn}(\partial\Phi/\partial x,\, S_{nn})}{\mu_{ne}}\right]} + \frac{\frac{A\,K\,k_{rne}(S_{nn})}{\mu_{ne} q(t)}(\rho_{ne} - \rho_{nn})\, g \sin(\alpha)}{1 + \left[\frac{k_{rne}(S_{nn})}{k_{rnn}(S_{nn})}\right]\left[\frac{\mu_{nn}(\partial\Phi/\partial x,\, S_{nn})}{\mu_{ne}}\right]} \tag{5.19}$$

where the component of the potential gradient $\nabla\Phi$ along the x coordinate for the non-Newtonian fluid is

$$\frac{\partial\Phi}{\partial x} = \frac{\partial P}{\partial x} + \rho_{nn}\, g \sin\alpha \tag{5.20}$$

Here α is the angle between the horizontal plane and the flow direction of the x coordinate. Equation 5.19 indicates that the fractional flow f_{nn} for the non-Newtonian phase is generally a function of both saturation and potential gradient.

However, for a given injection rate, and given fluid and rock properties, the potential gradient at a given time can be shown to be a function of saturation only (Appendix A),

$$q(t) + A\,K\left[\frac{k_{rne}(S_{nn})}{\mu_{ne}} + \frac{k_{rnn}(S_{nn})}{\mu_{nn}(\partial\Phi/\partial x,\, S_{nn})}\right]\frac{\partial P}{\partial x}$$

$$+ K\left[\frac{\rho_{ne}k_{rne}(S_{nn})}{\mu_{ne}} + \frac{\rho_{nn}k_{rnn}(S_{nn})}{\mu_{nn}(\partial\Phi/\partial x,\, S_{nn})}\right] g \sin(\alpha) = 0 \tag{5.21}$$

This shows that the flow potential gradient and the saturation are dependent on each other for this particular displacement system. Therefore, the potential gradient in the system is implicitly defined as a function of saturation by Equation 5.21.

The governing Equations 5.7 and 5.8 subject to the boundary and initial conditions (5.11)-(5.15) can be solved to obtain the following solution (see Appendix A):

$$\left[\frac{dx}{dt}\right]_{S_{nn}} = \frac{q(t)}{\phi\, A}\left[\frac{\partial f_{nn}}{\partial S_{nn}}\right]_t \tag{5.22}$$

This is the frontal advance equation for the non-Newtonian displacement, and is in the same form as the Buckley-Leverett equation. The difference is the dependence of the fractional flow f_{nn} for the non-Newtonian displacement on saturation not only through the relative permeability, but also through the non-Newtonian phase viscosity, as described by Equation 5.19. Equation 5.22 shows that, for a given time and a given

injection rate, a particular non-Newtonian fluid saturation profile propagates through the porous medium at a constant velocity. As in the Buckley-Leverett theory, the saturation for a vanishing capillary pressure gradient will in general become a triple-valued function of distance near the displacement front (Cardwell,1959). Equation 5.22 will then fail to describe the velocity of the shock saturation front, since $\partial f_{nn}/\partial S_{nn}$ does not exist on the front because of the discontinuity in S_{nn} at that point. Consideration of material balance across the shock front (Sheldon, et al., 1959) provides the velocity of the front,

$$\left[\frac{dx}{dt}\right]_{S_f} = \frac{q(t)}{A\,\phi}\left[\frac{f^{+}_{nn} - f^{-}_{nn}}{S^{+}_{nn} - S^{-}_{nn}}\right] \tag{5.23}$$

where S_f is the front saturation of the displacing non-Newtonian phase. The superscripts "+" and "-" refer to values ahead of and behind the front, respectively.

The location $x_{S_{nn}}$ of any saturation S_{nn} traveling from the inlet at time t can be determined by integrating Equation 5.22 with respect to time, which yields

$$x_{S_{nn}} = \frac{Q(t)}{A\,\phi}\left[\frac{\partial f_{nn}}{\partial S_{nn}}\right]_{S_{nn}} \tag{5.24}$$

where Q(t) is the cumulative volume of the injected fluid,

$$Q(t) = \int_0^t q(\lambda)\, d\lambda \tag{5.25}$$

A direct use of Equation 5.24 , given x and t, will result in a multiple-valued saturation distribution, which can be handled by a mass balance calculation , as in the Buckley-Leverett solution. An alternative graphic method of evaluating the above solution will be discussed in the next Section.

5.4 Graphical Evaluation of Linear Displacement Solution

The fractional flow of the displacing non-Newtonian phase is a function of its saturation only, after taking into account the constraint condition (5.21). Therefore, the Welge (1952) graphic method can be shown (Appendix B) to apply to a non-Newtonian fluid displacement by an integration of the mass balance of the fluid injected into the system and incorporating the result of Equation 5.24. The only additional work is to take into account the contribution of a velocity-dependent apparent viscosity of the non-Newtonian fluid on the fractional flow curve.

At the moving saturation front, we have (see Appendix B),

$$\left[\frac{\partial f_{nn}}{\partial S_{nn}}\right]_{S_f} = \frac{f_{nn}|_{S_f} - f_{nn}|_{S_{nnir}}}{S_f - S_{nnir}} \tag{5.26}$$

and the average saturation in the displaced zone is given by,

$$\left[\frac{\partial f_{nn}}{\partial S_{nn}}\right]_{S_f} = \frac{1}{\bar{S}_{nn} - S_{nnir}} \tag{5.27}$$

where $\bar{S}_{nn}$ is the average saturation of the non-Newtonian phase in the swept zone. To satisfy both Equations 5.26 and 5.27, a simple geometric construction can be used (see Figure 5.2). On a curve of fractional flow f_{nn} versus saturation S_{nn}, draw the tangent to the fractional flow curve, from the point $(S_{nn} = S_{nnir}, f_{nn} = 0)$. The point of tangency has coordinates $(S_{nn} = S_f, f_{nn} = f_{nn}|_{S_f})$, and the extrapolated tangent must intercept the line $f_{nn} = 1$ at the point $(S = \bar{S}_{nn}, f_{nn} = 1)$. Therefore, the graphic method of Welge applies if the fractional flow curves are provided for the non-Newtonian displacement process. The only difference is in the determination of the non-Newtonian fractional flow curve because we have to include the effects of the apparent viscosity of non-Newtonian fluids, which are also a function of saturation.

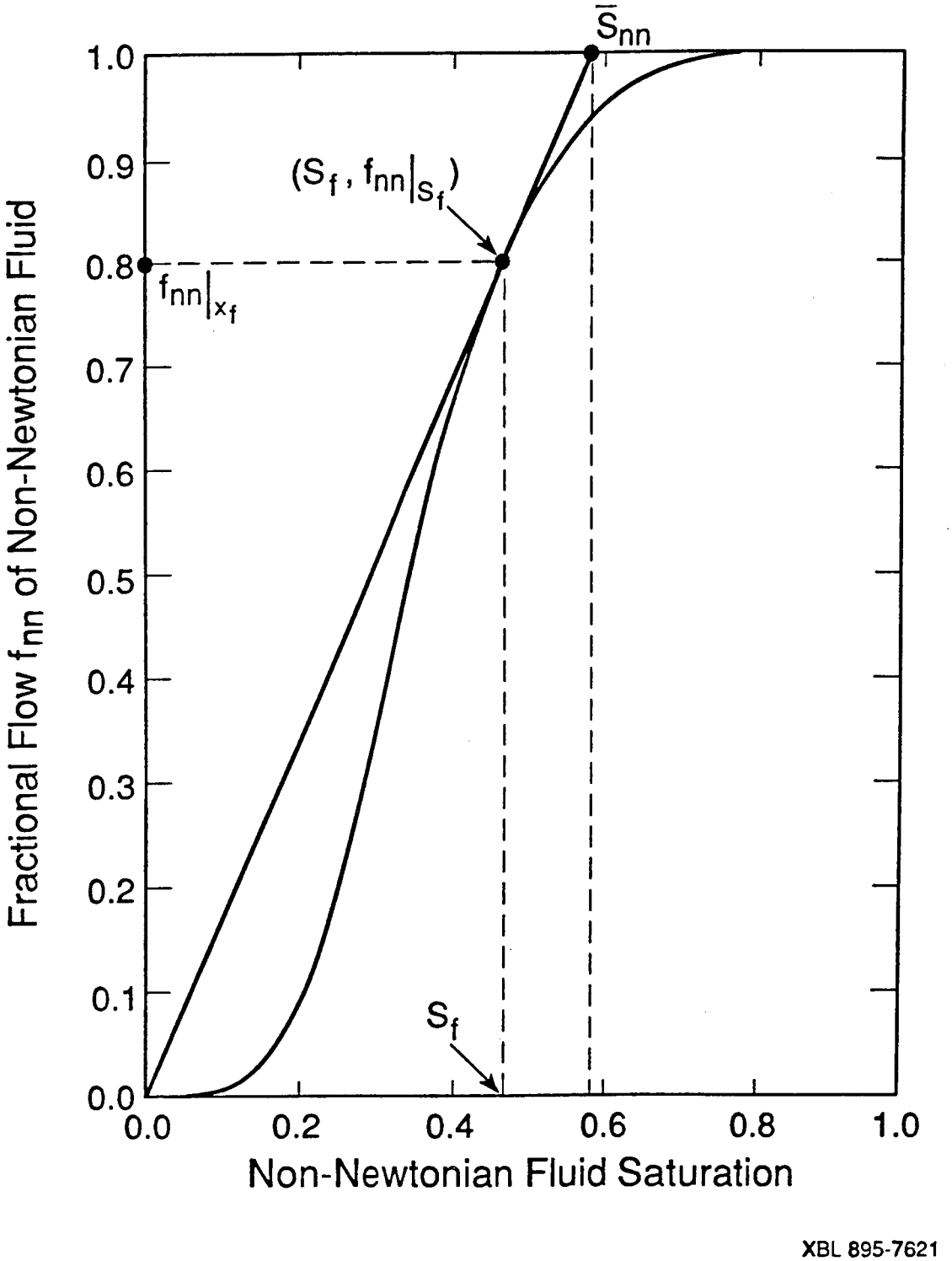

Figure 5.2 Method of Determining Shock Front and Average Displacing Non-Newtonian Phase Saturations from Fractional Flow Curves.

With given relative permeability data and the rheological model μ_{nn}, the general procedure for evaluating the flow behavior of non-Newtonian one-dimensional linear displacement is as follows:

1. Solve pressure gradients $(-\partial P/\partial x)$ with respect to various saturations, from Equation 5.21 for different injection rates and plot the relationship between pressure gradient and saturation corresponding to the injection rate, as shown in Figure 5.3. This requires use of the apparent non-Newtonian viscosity model, such as Equation 3.15 for the fluid of interest.

2. Calculate the fractional flow, f_{nn}, by Equation 5.19 using the pressure gradients from Figure 5.3 to calculate the corresponding potential gradients. Then use the rheological viscosity model to compute the non-Newtonian phase viscosity. An example of fractional flow curves is shown in Figure 5.4.

3. Calculate the derivatives of fractional flow, $\partial f_{nn}/\partial S_{nn}$, with respect to saturation from Figure 5.4. These are shown in Figure 5.5.

4. Determine the shock front saturations from Figure 5.5, as illustrated in Figure 5.2.

5. Calculate the saturation profile for $S_f < S_{nn} < 1 - S_{neir}$ from $x = 0$ to $x = x_f$ according to Equation 5.24 for a given injection rate and using the corresponding potential gradients from Figure 5.5. This profile is shown in Figure 5.6.

6. Determine the average saturation in the swept zone from Figure 5.4, as illustrated in Figure 5.2. This can be used to calculate the cumulative Newtonian fluid displaced, N_p, for the swept region,

$$N_p = A \phi x_f (\bar{S}_{nn} - S_{nnir}) \tag{5.28}$$

The above procedure has been computer-programmed for use in this work.

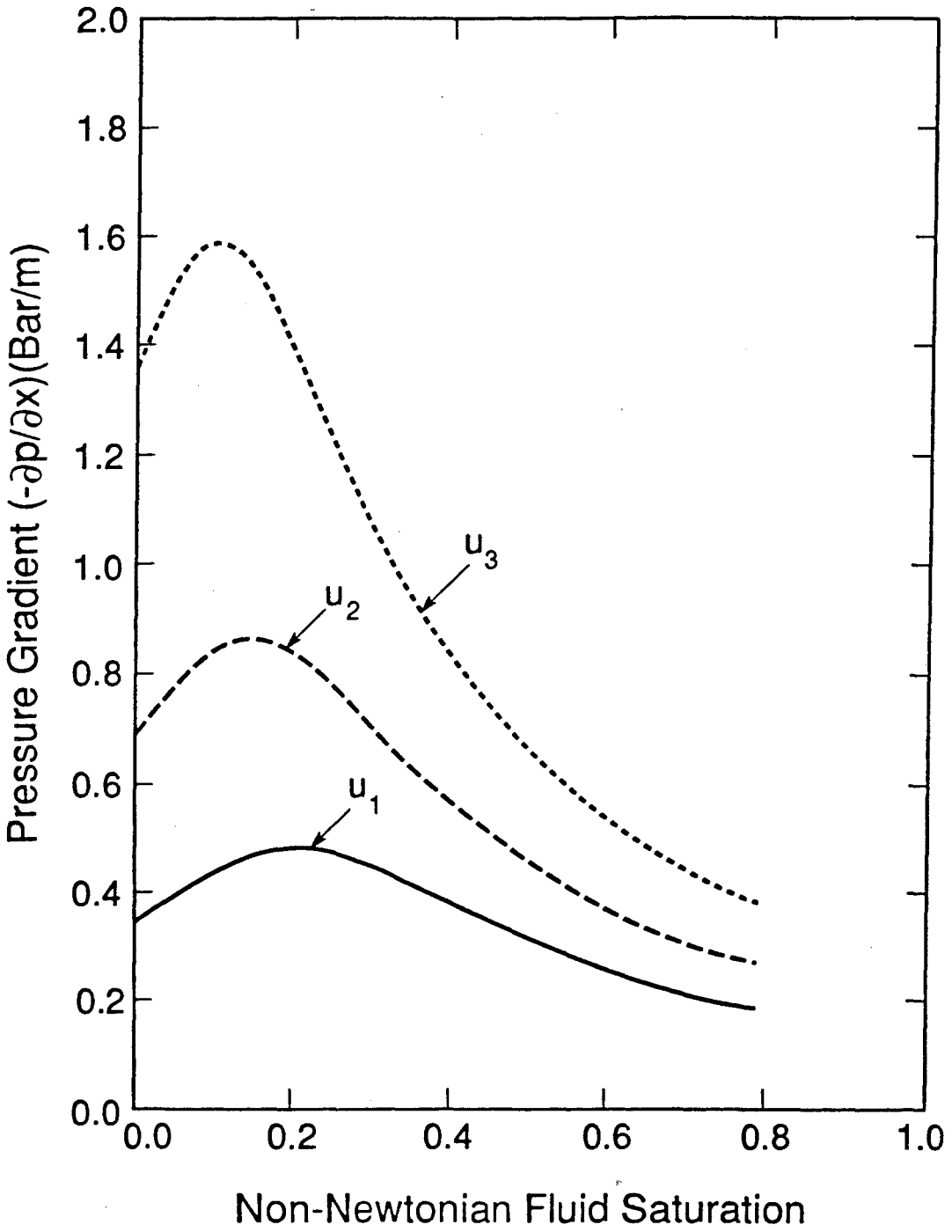

Figure 5.3 Pressure Gradients versus Displacing Non-Newtonian Phase Saturation for Different Injection Rates.

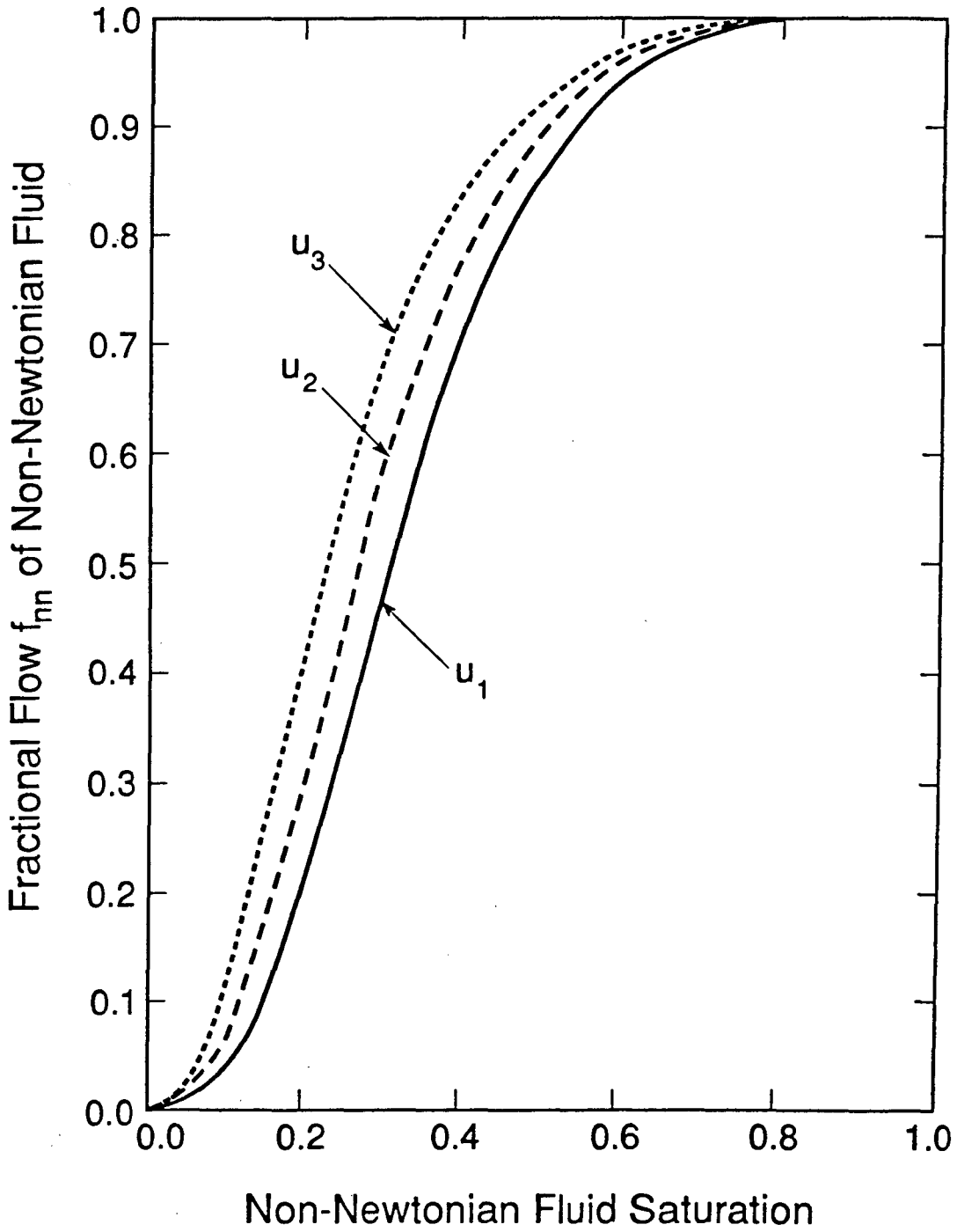

Figure 5.4 Fractional Flow Curves of Non-Newtonian Fluids for Different Injection Rates.

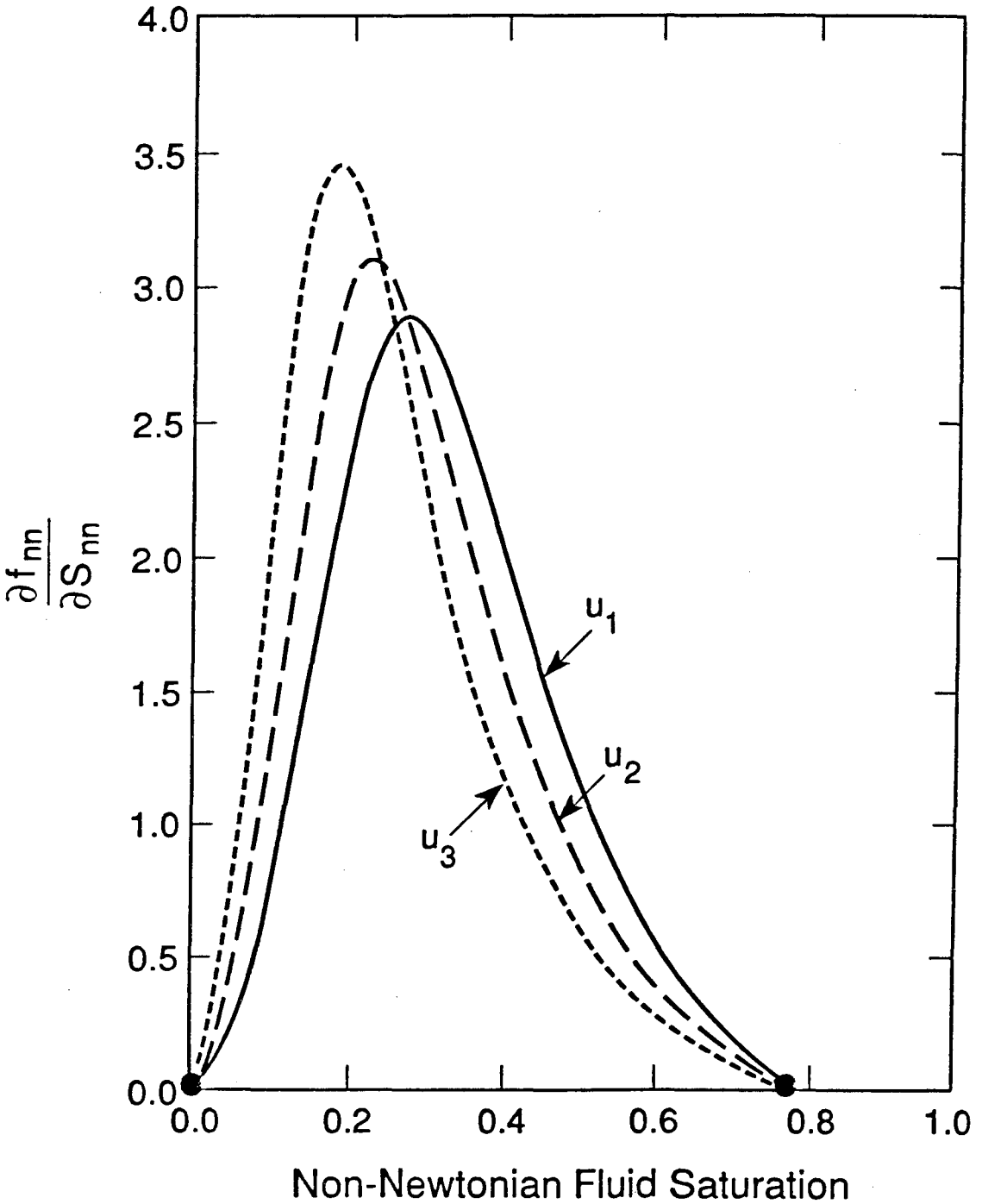

Figure 5.5 Derivatives of Fractional Flow with Respect to Non-Newtonian Phase Saturation for Different Injection Rates.

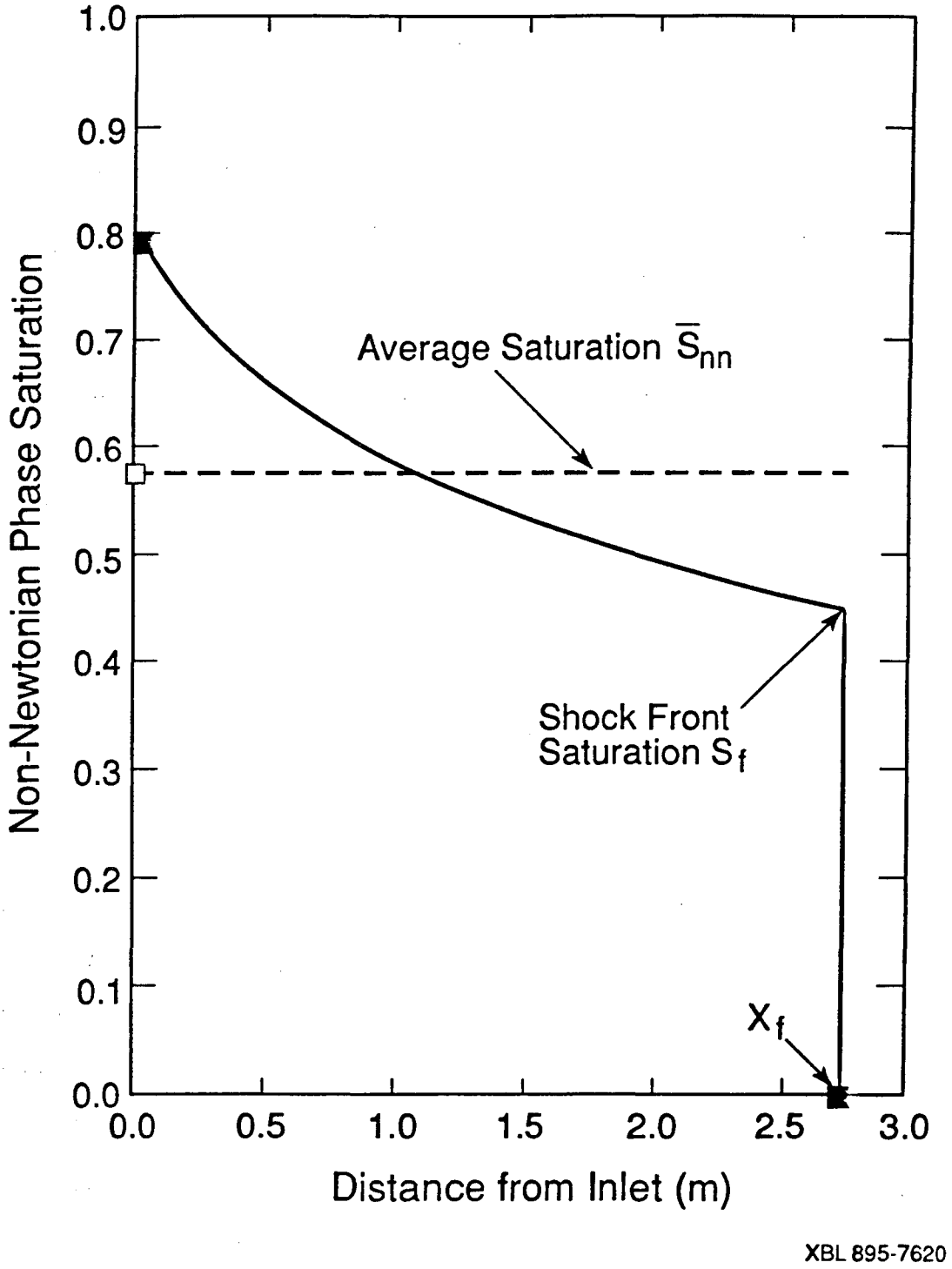

Figure 5.6 Saturation Distributions of Non-Newtonian Fluids in the System at a Given Injection Time.

5.5 Verification of the Numerical Method

The numerical simulator discussed in Chapter 4, which is a modified version of MULKOM (Pruess, 1983) has the ability to model multiple phase flow of non-Newtonian and Newtonian fluids in porous media under a wide range of operating conditions and using different rheological models for non-Newtonian fluid behavior. Here the power-law model has been used to check the code. The validity of the numerical results from this code has been tested for immiscible displacement of a Newtonian fluid by a non-Newtonian power-law fluid using the Buckley-Leverett-type solution described above. The example of interest is a one-dimensional linear flow problem of incompressible two-phase fluids in a semi-infinite, horizontal, homogeneous and isotropic porous medium. A constant injection rate is maintained at the inlet ($x = 0$) from time $t = 0$. Initially, the reservoir is fully saturated with only the Newtonian liquid. The relative permeability curve used for both the analytical and numerical calculations is shown in Figure 5.7. Capillary effects are assumed to be negligible.

In order to reduce the effects of discretization in the finite system, a very fine mesh spacing ($\Delta x = .0125m$) was chosen for the first 240 elements, then the mesh spacing was increased by a factor of 1.5 to the 290th element. The analytical solution for the non-Newtonian displacement was evaluated using the computerized-graphic method outlined in the previous section. The power-law non-Newtonian fluid has been used extensively in the study of non-Newtonian fluid flow through porous media both theoretically and experimentally. Therefore, a power-law liquid was used as a displacing agent to drive the initially saturated Newtonian liquid in the porous medium.

The properties of rock and fluids are given in Table 5.1. The rheological model for a power-law fluid, Equation 3.11 is used here. For the two phase flow problem, a modification for μ_{eff} , defined in Equation 2.14, is made by replacing K by Kk_{rnn} and ϕ by $\phi(S_{nn} - S_{nnir})$, to obtain

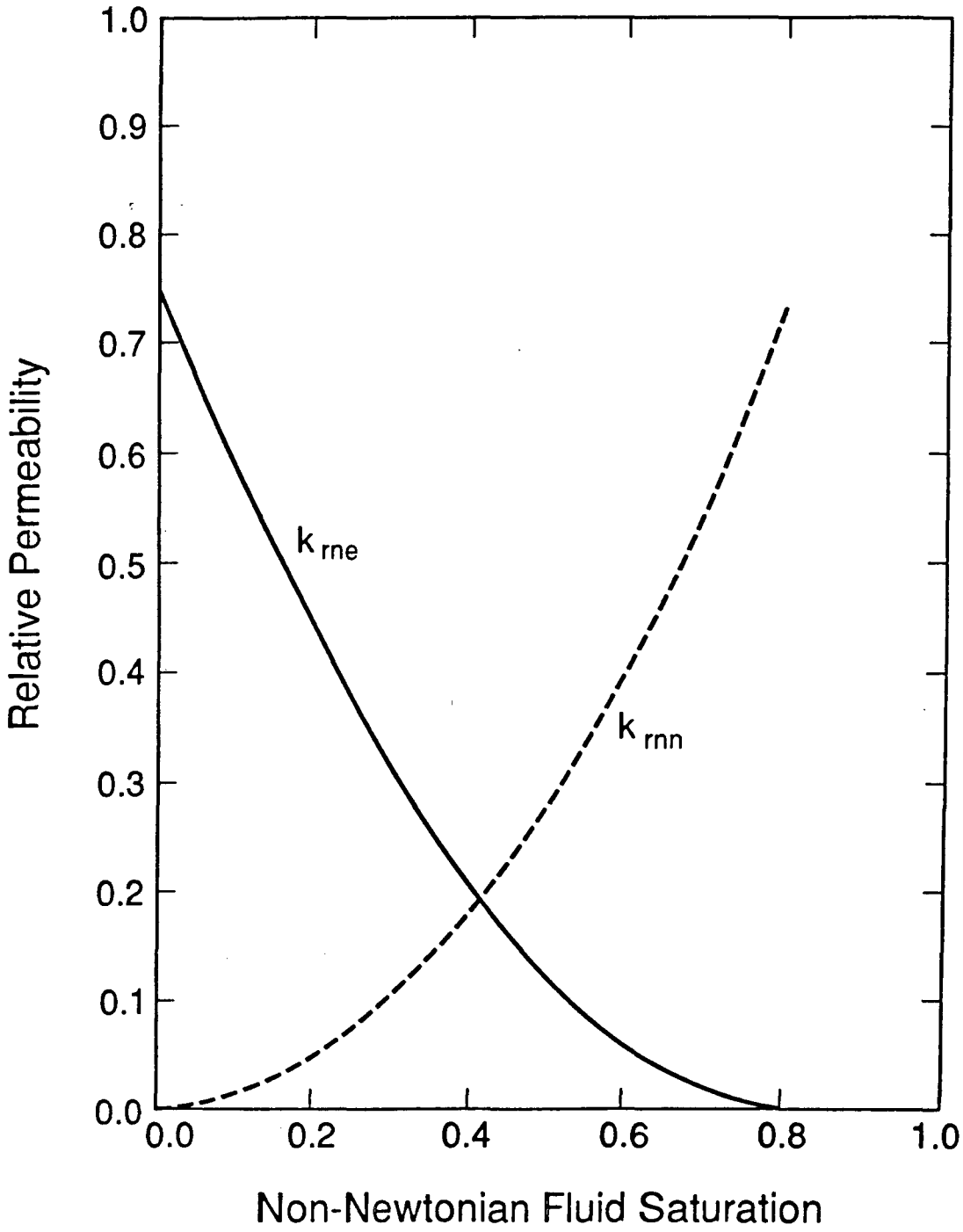

Figure 5.7 Relative Permeability Functions Used for Code Verification.

Table 5.1

Parameters for Linear Power-Law Fluid Displacement

Porosity	ϕ=0.20
Permeability	K=1 darcy
Cross-Sectional Area	1 m^2
Injection Rate	$q=0.8233\times10^{-5} m^3/s$
Injection Time	T=10 hrs
Displaced Phase Viscosity	μ_{ne}=5 cp
Irreducible Newtonian Saturation	S_{neir}=0.20
Initial Non-Newtonian Saturation	S_{nnir}=0.00
Power-Law Index	n=0.5
Power-Law Coefficient	H=0.01 $Pa\cdot s^n$

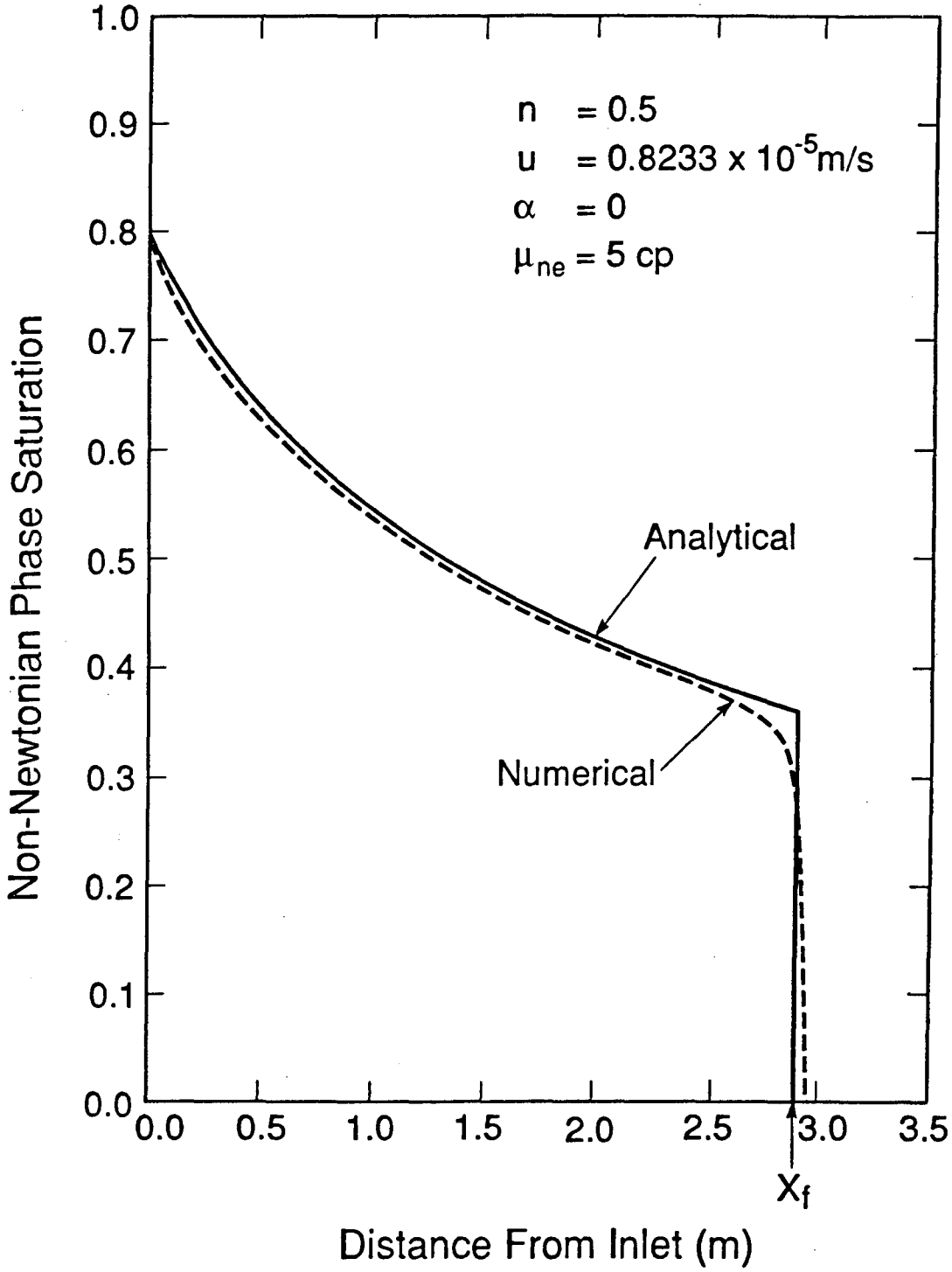

Figure 5.8 Comparison of Saturation Profiles Calculated from Analytical and Numerical Solutions after 10 Hours of Injection of a Power-Law Fluid.

XBL 893-7522
T.I.D. Illus. 88
3/29/89

$$\mu_{eff} = \frac{H}{12}(9+\frac{3}{n})^n\left[150Kk_{rnn}(S_{nn})\phi(S_{nn}-S_{nnir})\right]^{\frac{1-n}{2}} \tag{5.29}$$

If we use a power-law index of $n = 0.5$, then the pressure gradients for this horizontal flow problem can be derived from Equation 5.21 as,

$$-\frac{\partial P}{\partial x} = \frac{1}{2}\left\{\left[\frac{\left[\frac{Kk_{rne}}{\mu_{ne}}\right]^2}{\frac{Kk_{rnn}}{\mu_{eff}}} + \frac{4q}{\left[\frac{Kk_{rnn}}{\mu_{eff}}\right]^{1/2}}\right]^{1/2} - \frac{\frac{Kk_{rne}}{\mu_{ne}}}{\left[\frac{Kk_{rnn}}{\mu_{eff}}\right]^{1/2}}\right\} \tag{5.30}$$

Equation 5.30 is employed in calculating the fractional flow f_{nn} to incorporate non-Newtonian effects of a power-law fluid in the analytical solution. A comparison of the saturation profiles from the numerical and the analytical solutions after 10 hours of non-Newtonian fluid injection into the system is given in Figure 5.8. This shows that the numerical results are in excellent agreement with the analytical prediction. Considering the complexity introduced when non-Newtonian fluids are involved in a multiple phase flow problem, Figure 5.8 provides an excellent indication that the numerical model is correct in describing the multiple phase immiscible displacement of a Newtonian fluid by a non-Newtonian fluid in porous media. Viscosity profiles for the non-Newtonian fluid are given in Figure 5.9, and also show good agreement between the analytical and numerical results over the whole swept region, $x < x_f$. Only at the shock advancing saturation front does the numerical solution deviate somewhat from the analytical solution, which is typical of "smearing" effect from numerical dispersion.

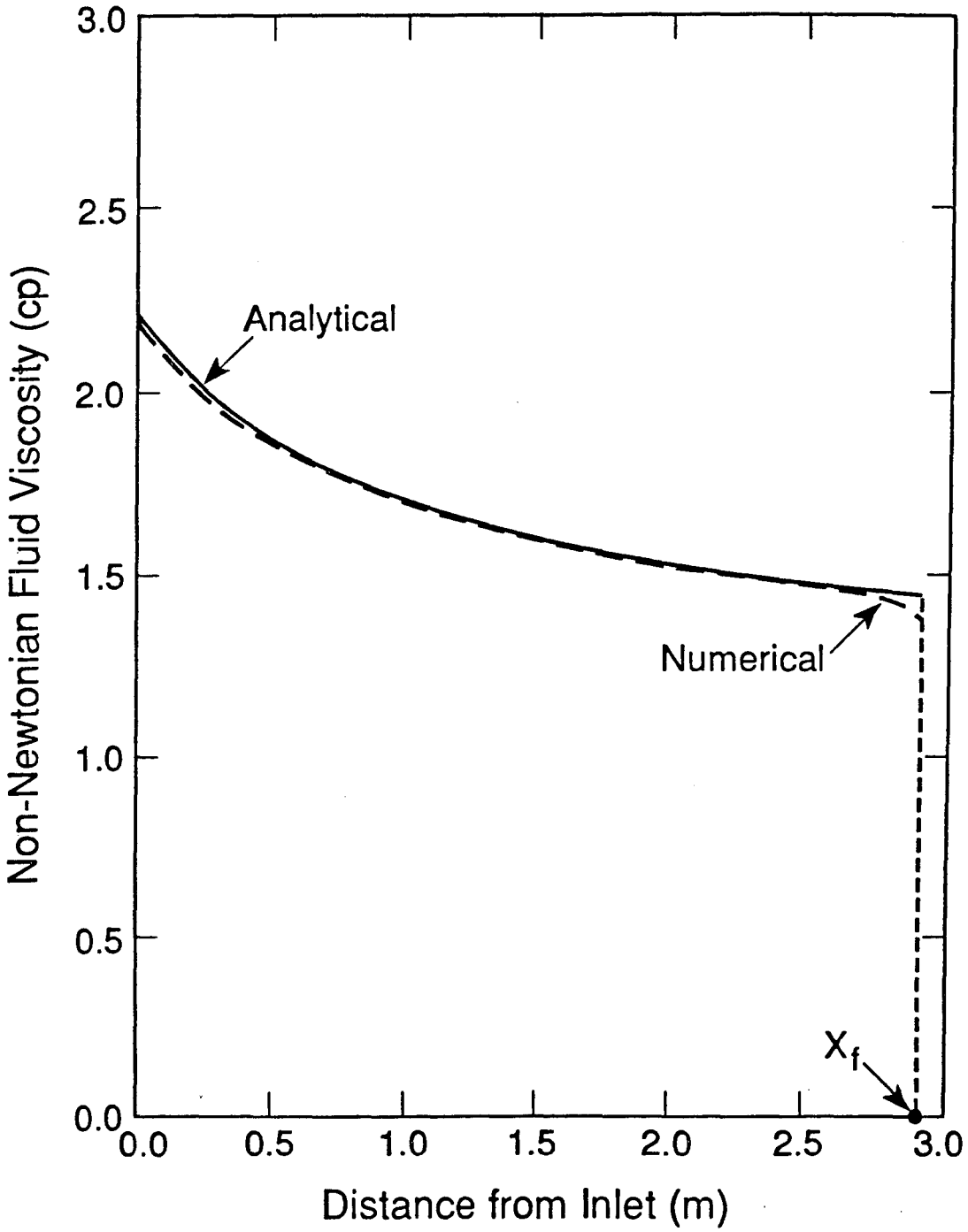

Figure 5.9 Comparison of Apparent Viscosity Profiles Calculated from Analytical and Numerical Solutions after 10 Hours of Injection of a Power-Law Fluid.

XBL 895-7623

Chapter 6
Immiscible Displacement of a Newtonian Fluid by a Power-Law Non-Newtonian Fluid

6.1 Introduction

A physical example of a Newtonian fluid being displaced by a non-Newtonian power-law fluid in porous media is the recovery of oil by polymer flooding in EOR processes. Since almost all theoretical studies on non-Newtonian power-law fluid flow in porous media have been focused on single phase flow, the displacement mechanisms with power-law fluids are not well understood. In this chapter, a theoretical study of immiscible displacement of a Newtonian fluid by a power-law fluid will be presented using the analytical solution developed in Chapter 5.

In the stabilized displacement of Newtonian fluids where capillary pressure is ignored, the process is described by the Buckley and Leverett theory. Under the stabilized condition, the displacement data for linear floods are not affected by the length of the system or injection rate. The saturation distribution at a time is uniquely determined by the fractional flow curve for the given reservoir rock and fluid properties (Sheldon et al., 1959). The sweep efficiency is independent of flow rate as long as the displacement process is stable (Willhite, 1986; Yortsos and Huang, 1986; and Bentsen, 1985). However, the Buckley-Leverett frontal advance theory has certain limitations in applications. Some are from its assumptions used in developing the solution, such as isotropic and homogenous porous media, incompressible fluids, and strictly one-dimensional flow. One important phenomenon associated with frontal movement that has been ignored in the theory is the frontal instability and viscous fingering (Collins, 1961; Scheidegger, 1974). Instability of a displacement front has been found to be strongly dependent on

mobility ratio in both the macroscopic analysis (Chen and Whitson; 1988) and the microscopic model (Collins, 1961). The inhomogeneous nature of a porous medium or certain perturbation will initiate the instability and hence fingering, but gravity, capillarity, and diffusion may act to eliminate the fingers as they are formed.

The displacement process becomes more complicated when a non-Newtonian fluid is involved. Under the idealized condition of the Buckley-Leverett theory, the immiscible displacement is still determined by the fractional flow curve if the capillary pressure effects are ignored. The fractional flow function, as defined by Equation 5.19, depends not only on the relative permeabilities, as in the Buckley-Leverett frontal theory, but also on the rheological behavior of the non-Newtonian fluid. Therefore, the sweep efficiency with a non-Newtonian fluid as the displacing phase will be affected by the rheological behavior of the non-Newtonian fluid, in addition to the effects of relative permeability. All these factors are included in the analytical solution of Chapter 5, and the basic displacement behavior can now be analyzed as discussed below.

6.2 Evaluation of Analytical Solution.

The physical flow model is a one-dimensional linear porous medium, which is initially saturated only with a Newtonian Fluid. A constant volumetric injection rate of a power-law fluid is imposed at the inlet, $x = 0$, from $t = 0$. The relative permeability curves used for all calculations in this chapter are shown in Figure 6.1, and the properties of rock and fluids are given in Table 6.1. The solution (5.24) is evaluated to obtain the saturation profiles by the computerized-graphic method, as outlined in Section 5.4. The apparent viscosity for the power-law fluid is represented by Equations 3.11 and 5.29. In order to calculate the fractional flow function from Equation 5.19, the constraint condition (5.21) is needed to correlate the potential gradient with the saturation for this

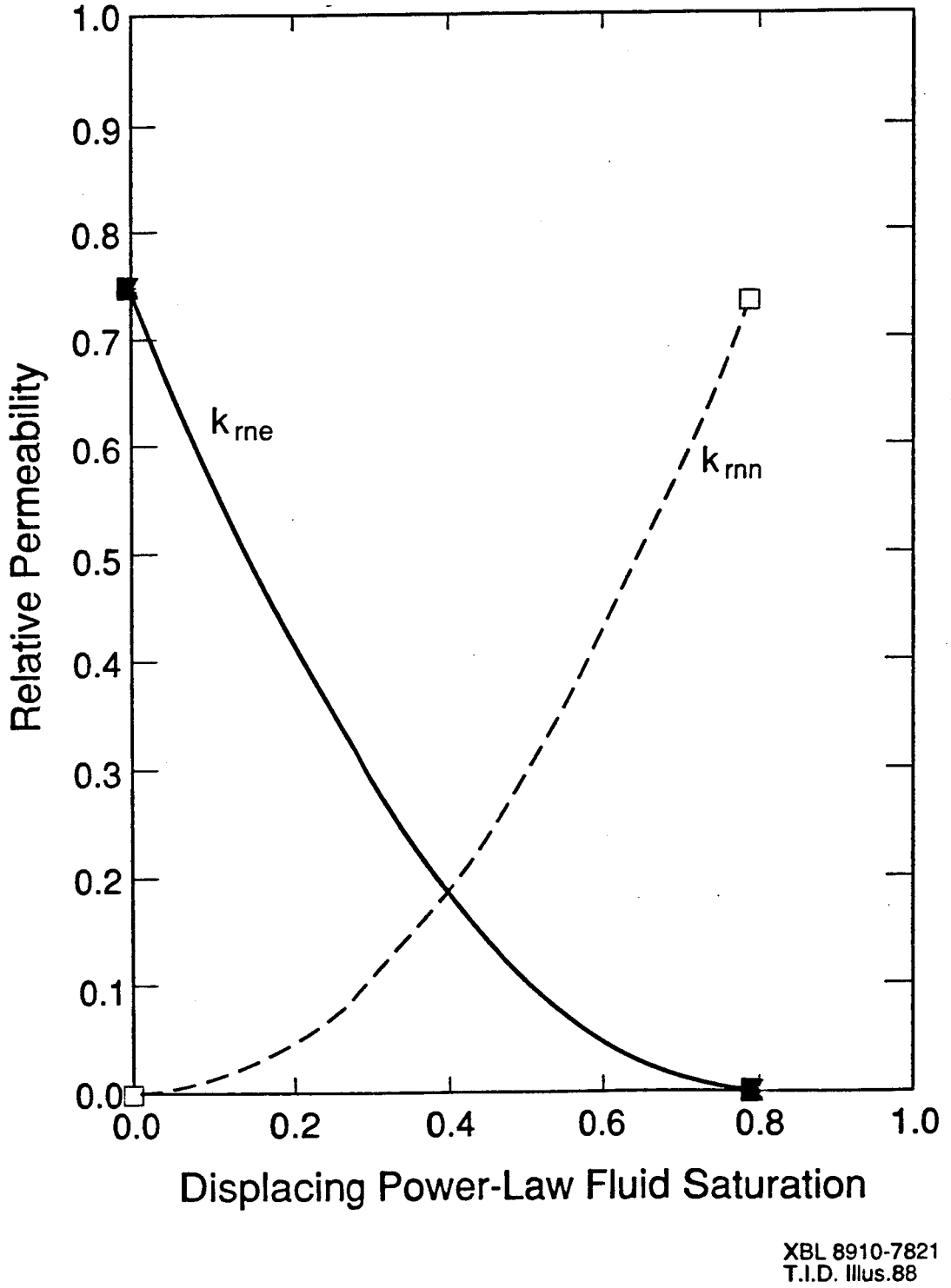

Figure 6.1 Relative Permeability Functions Used for Evaluation of Displacement by a Power-Law Fluid.

Table 6.1

Parameters for Linear Power-Law Fluid Displacement

Porosity	ϕ=0.20
Permeability	K=1 darcy
Cross-Sectional Area	1 m^2
Injection Rate	$q=1.0\times10^{-5} m^3/s$
Injection Time	T=10 hrs
Displaced Phase Viscosity	μ_{ne}=4 cp
Irreducible Saturation	S_{neir}=0.20
Power-Law Index	n=0.5
Power-Law Coefficient	H=0.01 $Pa \cdot s^n$

one-dimensional linear flow problem. Introducing Equations 3.11, and 5.20 into Equation 5.21, we can obtain the following relationship for the pressure gradient corresponding to a particular value of S_{nn} ,

$$\frac{Kk_{re}(S_{nn})}{\mu_{ne}}\left[-\frac{\partial P}{\partial x}\right]_{S_{nn}} + \left[\frac{Kk_{rn}(S_{nn})}{\mu_{eff}}\right]^{1/n}\left[\left[-\frac{\partial P}{\partial x}\right]_{S_{nn}} - \rho_{nn}\, g \sin(\alpha)\right]^{1/n} - \left[\frac{q}{A} + \frac{Kk_{re}(S_{nn})}{\mu_{ne}}\rho_{ne}\, g \sin(\alpha)\right] = 0 \qquad (6.1)$$

where μ_{eff} is defined in Equation 5.29. Equation 6.1 is incorporated in the calculation of the fractional flow to solve potential gradients corresponding to saturations under different flow conditions.

6.3 Displacement of a Newtonian Fluid by a Power-Law Non-Newtonian Fluid

For a given operating condition, non-Newtonian fluid displacement in porous media is controlled not only by relative permeability data, as in Newtonian fluid displacement, but also by the rheological properties of the non-Newtonian fluid. Some fundamental aspects of power-law non-Newtonian fluid displacement will be discussed in this section using the results from the analytical solution.

6.3.1 Effects of Non-Newtonian Rheological Properties

There are two parameters that characterize the flow behavior of a power-law fluid, which are the exponential index, n, and the coefficient, H. For a pseudoplastic shear-thinning fluid, $0 < n < 1$. If $n = 1$, the fluid is Newtonian. The effect of the power-law

index , n, on linear horizontal displacement can be quite significant. Figure 6.2 shows that pressure gradients are changed significantly as a function of saturation for different values of n. At both high and low values for the non-Newtonian phase saturation, the pressure gradients are smaller because the flow resistance decreases as the flow tends to single phase flow. The apparent viscosities of several non-Newtonian fluids with different power-law indices n are given in Figure 6.3, and the resulting fractional flow curves are shown in Figure 6.4. Figure 6.5 presents the derivatives of the fractional flow function with respect to saturation for different values of n. Saturation profiles after a 10-hour injection period in the system are plotted in Figure 6.6. Note the significant decreases in sweep efficiency as the power-law index n is reduced.

Since the power-law index, n, is usually determined by experiment or from well test analysis, some errors cannot be avoided in determining the values of n. These results show how difficult it will be to use a numerical code to match experimental data from non-Newtonian displacement investigations in the laboratory, because of the extreme sensitivity of the core saturation distribution to the value of n. The sensitivity of the displacement behavior to the power-index suggests that in determining the index for flow through porous media, it may be helpful to match experimental saturation profiles using the analytical solution.

The effects of the consistence coefficient, H, are also examined. From Equation 3.11, the apparent viscosity of a power-law fluid for this linear displacement can be expressed as,

$$\mu_{nn} = H^{1/n}\left[\frac{1}{12}[9 + 3/n]^{n}(150Kk_{rnn}\phi(S_{nn}-S_{nnir}))^{(1-n)/2}\right]^{1/n}\left[Kk_{rnn}|\nabla\Phi|\right]^{(n-1)/n} \quad (6.2)$$

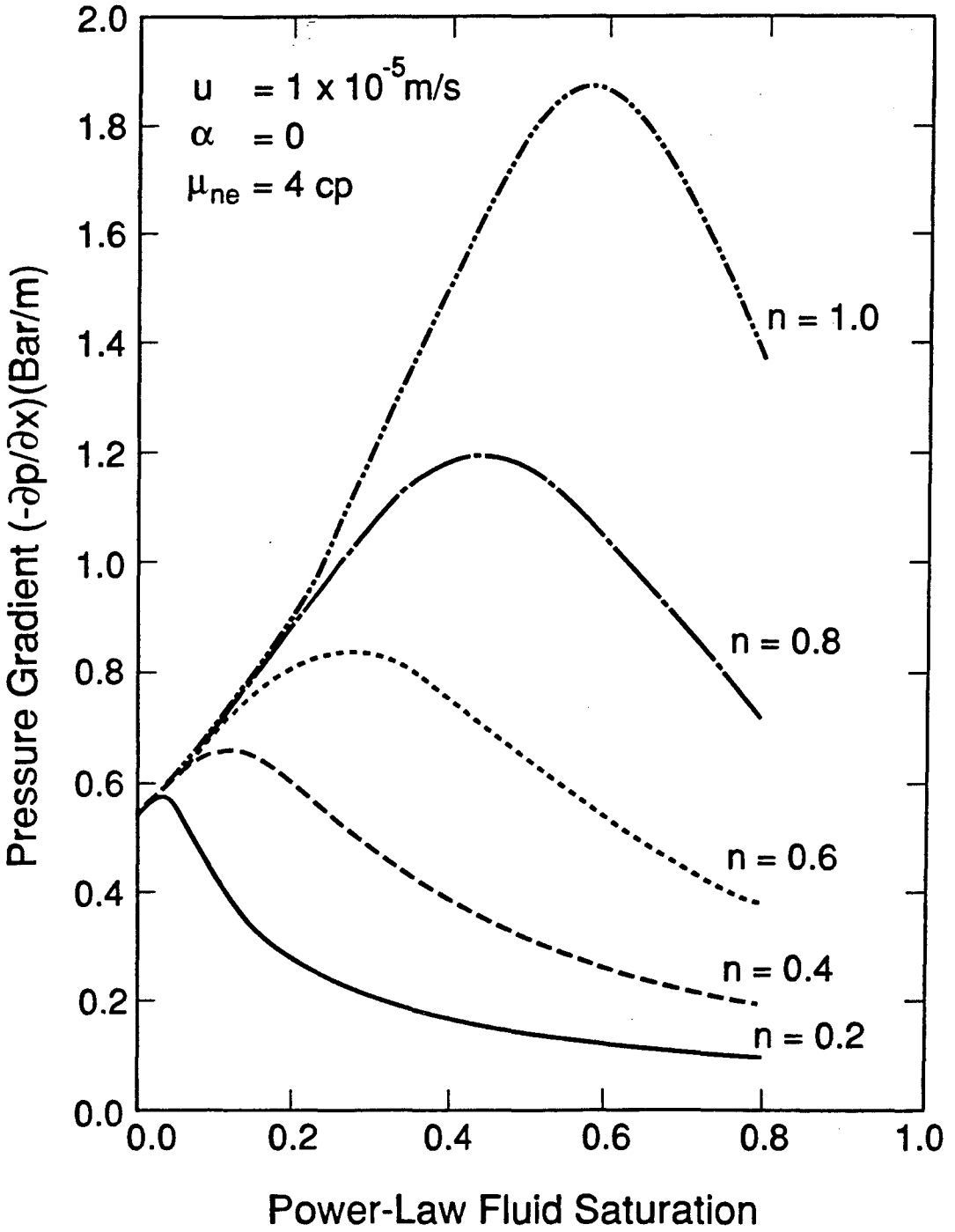

XBL 893-7519
T.I.D. Illus. 88
3/29/89

Figure 6.2 Effects of the Power-Law Index on Pressure Gradients.

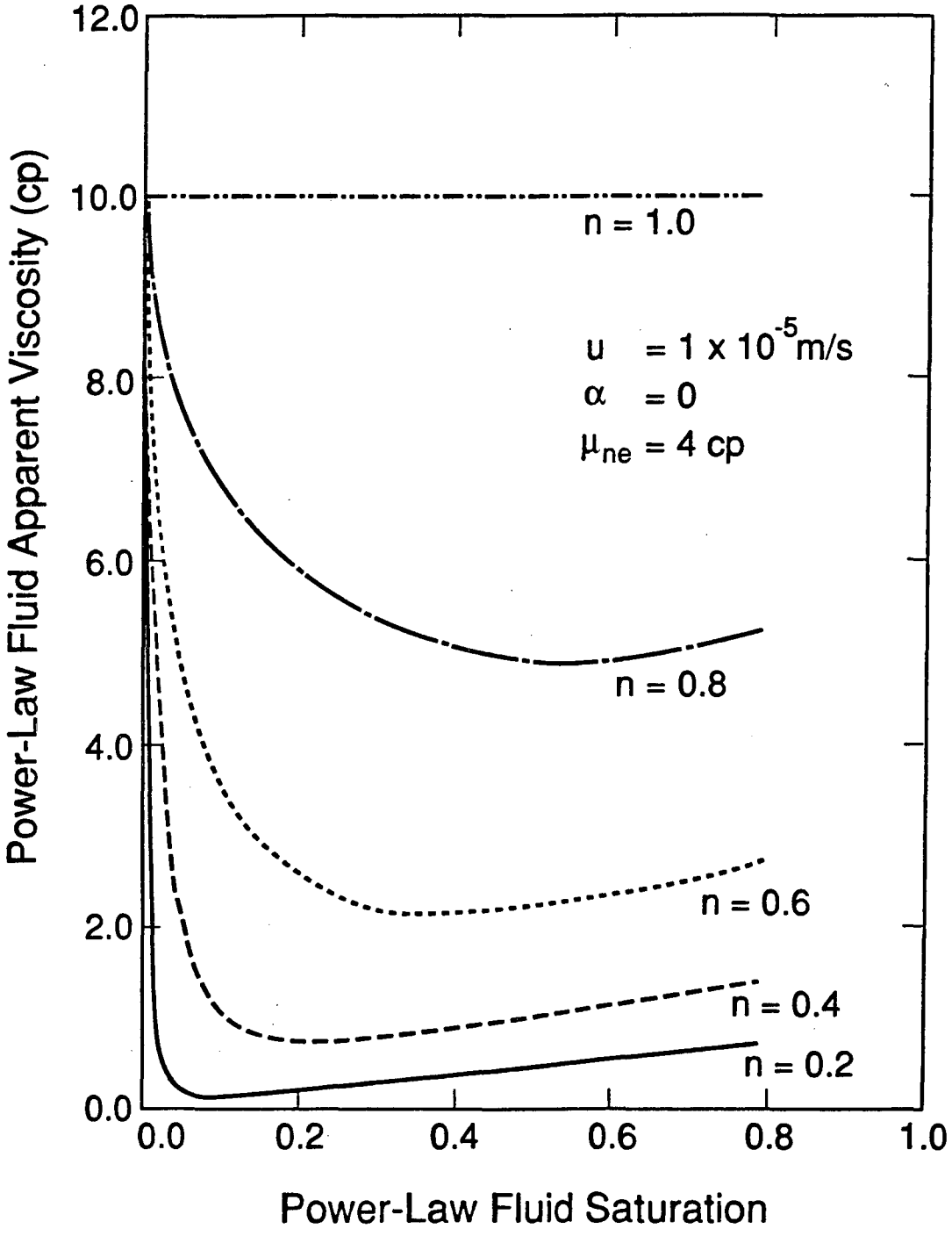

Figure 6.3 Effects of the Power-Law Index on Non-Newtonian Phase Apparent Viscosity.

XBL 893-7517
T.I.D. Illus. 88
3/29/89

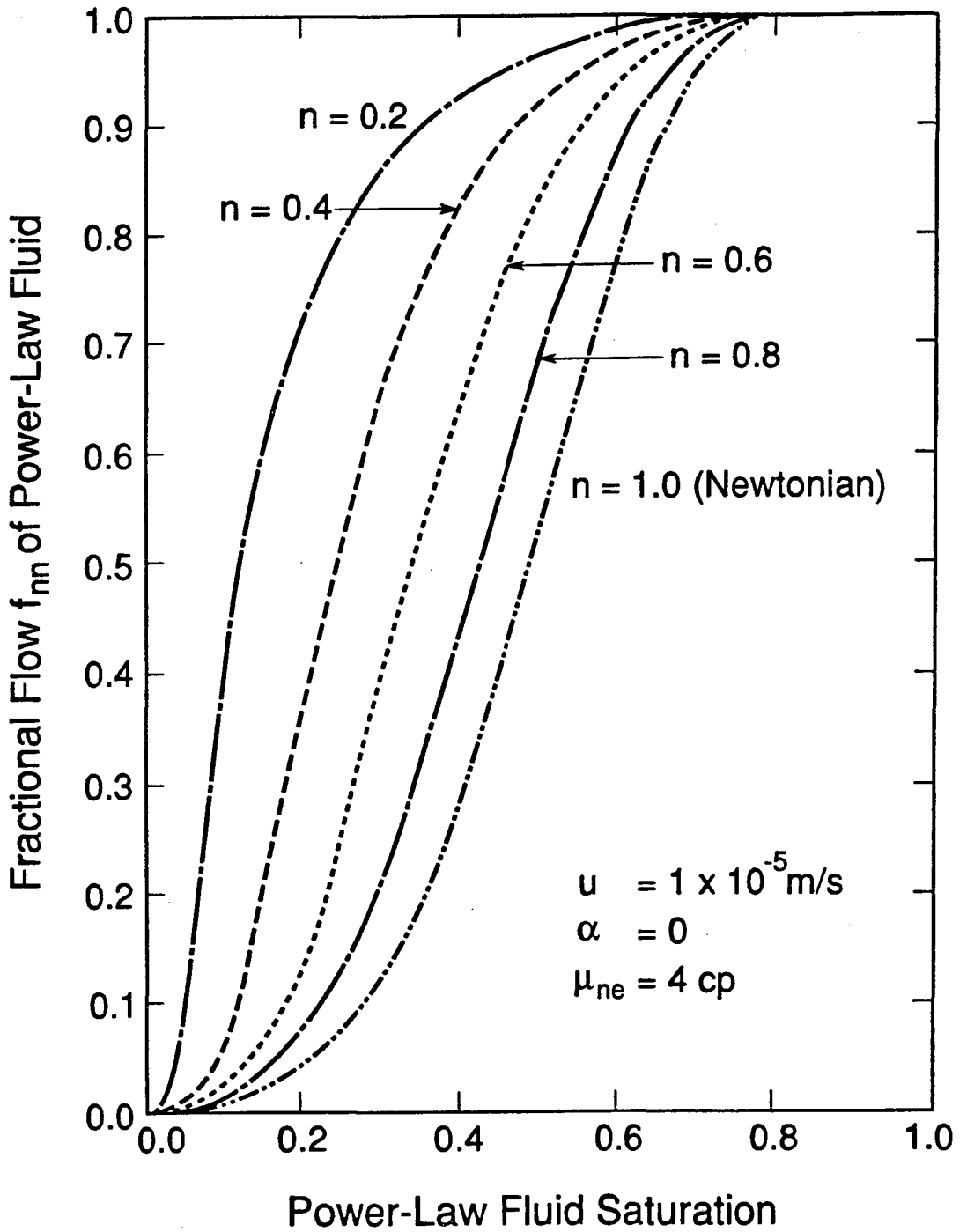

XBL 893-7518
T.I.D. Illus. 88
3/29/89

Figure 6.4 Effects of the Power-Law Index on Non-Newtonian Phase Fractional Flow.

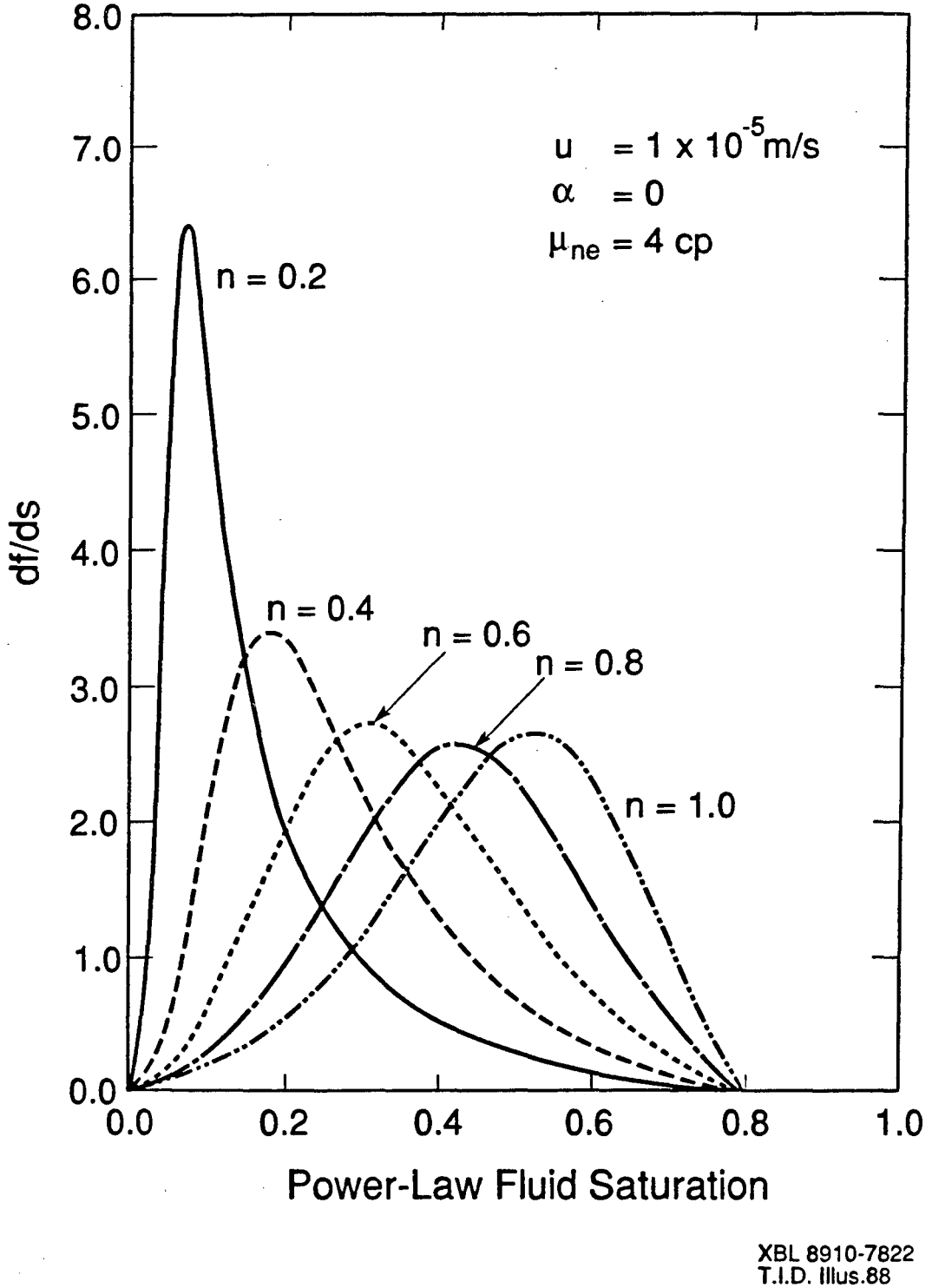

Figure 6.5 Effects of the Power-Law Index on Derivative of Fractional Flow with Respect to Non-Newtonian Phase Saturation.

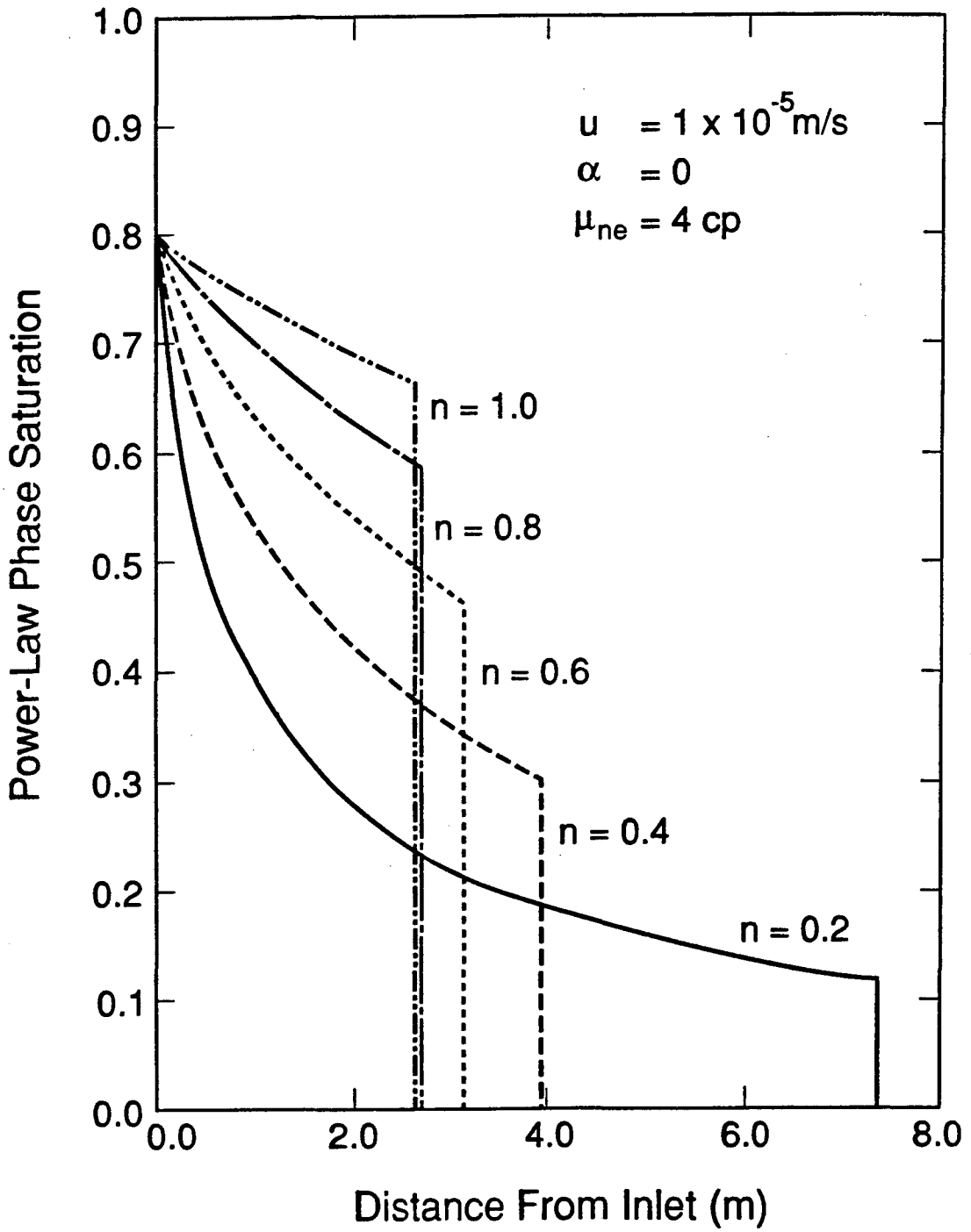

XBL 893-7520
T.I.D. Illus. 88
3/29/89

Figure 6.6 Non-Newtonian Phase Saturation Distributions, Effects of the Power-Law Index on Displacement Efficiency

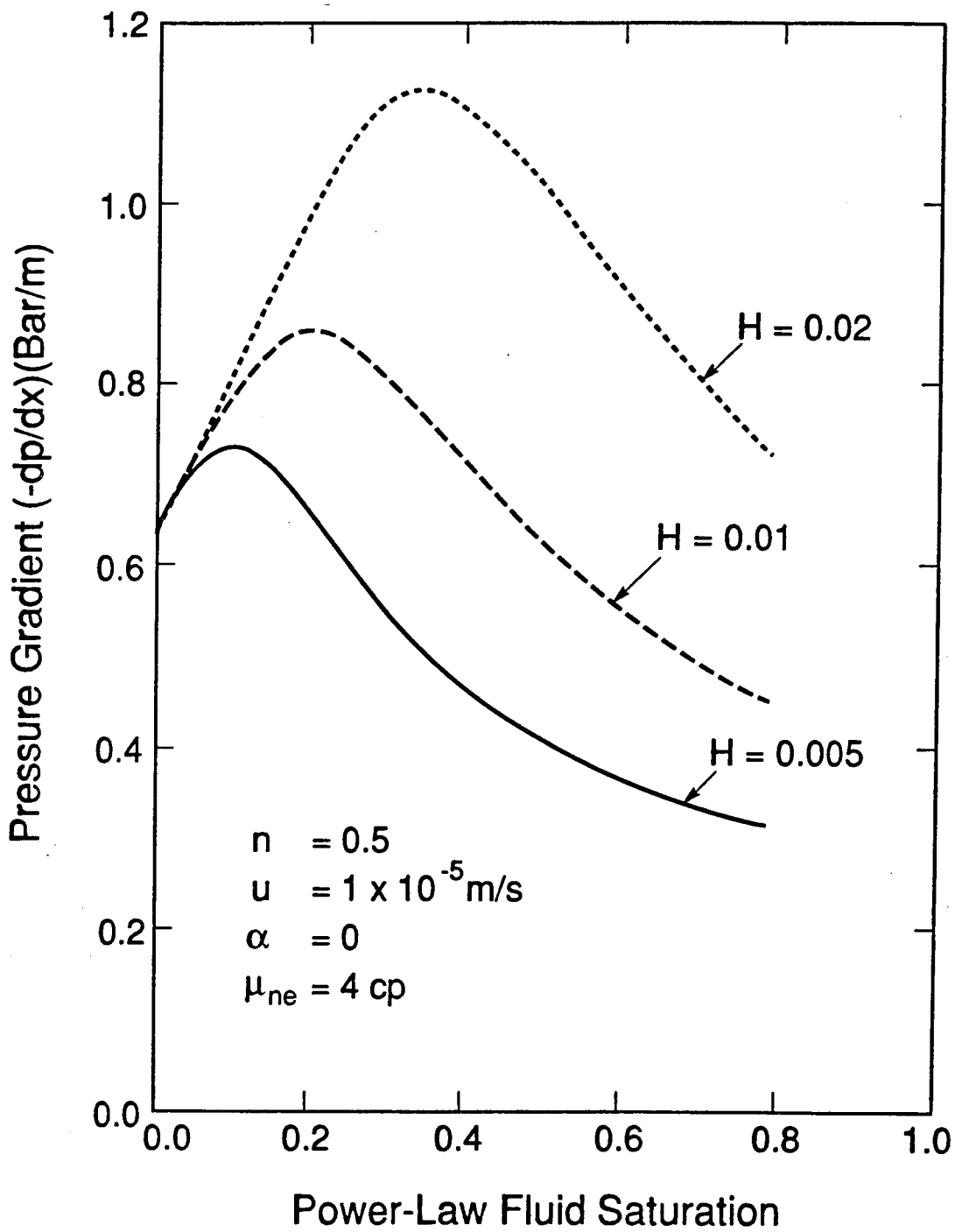

XBL 8911-7842
T.I.D. Illus. 88

Figure 6.7 Pressure Gradients versus Displacing Power-Law Fluid Phase Saturation, Effects of the Coefficient H.

Therefore, H acts a scaling factor of the viscosity for a given power-law index, n. The pressure gradients and the viscosities as functions of saturation are shown in Figures 6.7 and 6.8 for the three values of H. The corresponding fractional flow and its derivatives are given in Figures 6.9 and 6.10, respectively. Figure 6.9 exhibits the linear-scaling effect of H. The resulting saturation profiles after 10 hours of injection are shown in Figure 6.11. The horizontal lines in this figure are the average saturations in the swept zone, which reflect the sweep efficiency. The results indicate that the effects of H on the displacement process are also significant.

6.3.2 Effect of Injection Rates

For a stable Newtonian displacement in porous media based on the Buckley-Leverett theory, the injection rate has no effect on displacement efficiency or sweep efficiency. When a non-Newtonian fluid is involved, changes in the injection rate will result in changes in the pore velocity, or in the shear rate, which will affect the viscosity of the non-Newtonian phase and therefore alter the fractional flow curve. The fluid and rock parameters used for the calculations in this section are similar to those used in the previous section, as given in Table 6.1 and any differences are indicated on the figures to follow. Figure 6.12 gives non-Newtonian viscosity versus saturation curves for three different injection rates in a semi-infinite linear horizontal system. The calculated saturation profiles corresponding to the injection rates are shown in Figure 6.13. Since the only variable parameter in this calculation is the injection rate, the saturation distributions in Figure 6.12 indicate that the injection rate has a significant effect on displacement. For a displacement process with this type of shear thinning fluid, the lower the injection rate, the larger the viscosity of the displacing phase, and the higher the displacement efficiency will be.

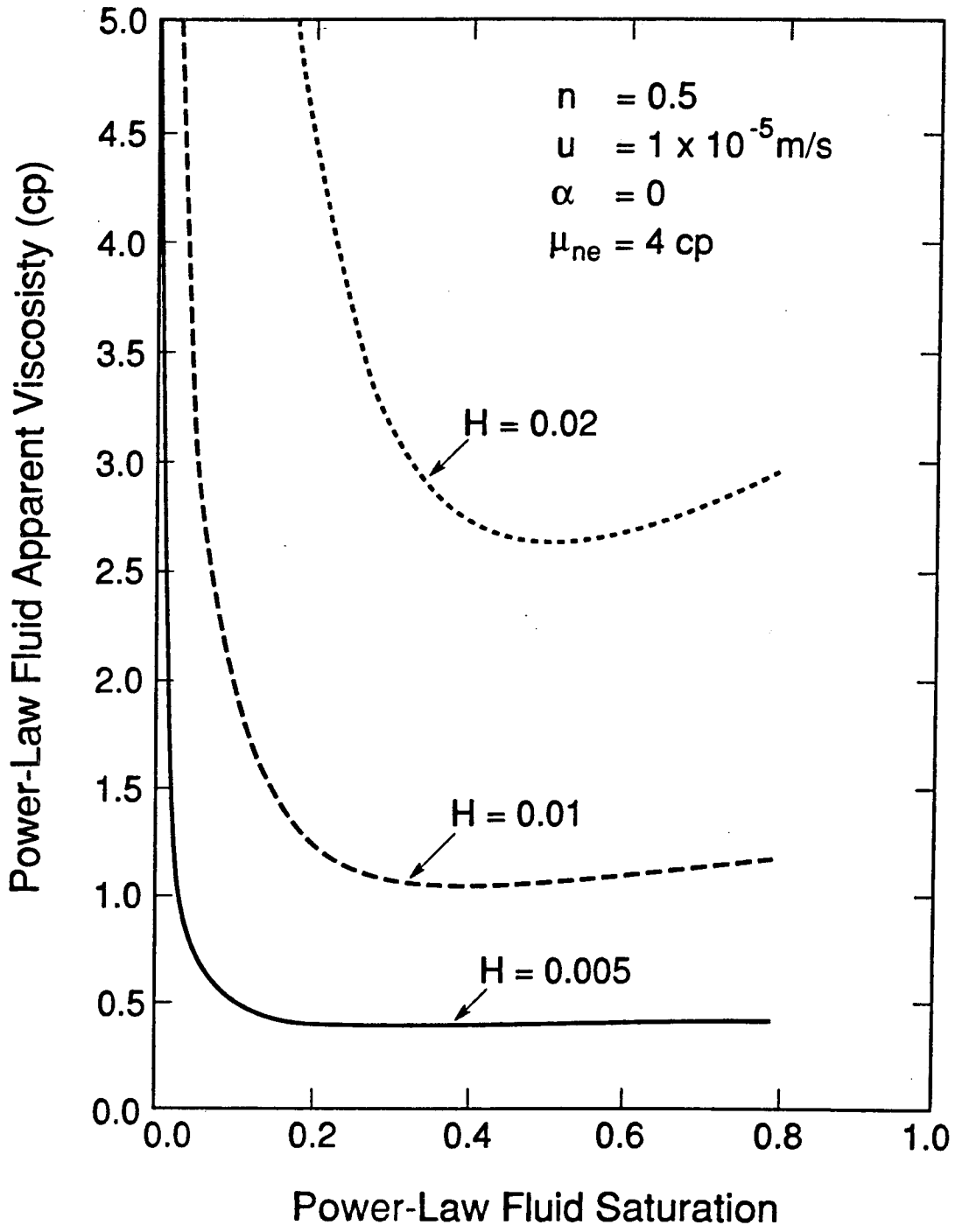

XBL 8911-7843
T.I.D. Illus. 88

Figure 6.8 Effects of the Coefficient H on the Non-Newtonian Apparent Viscosity.

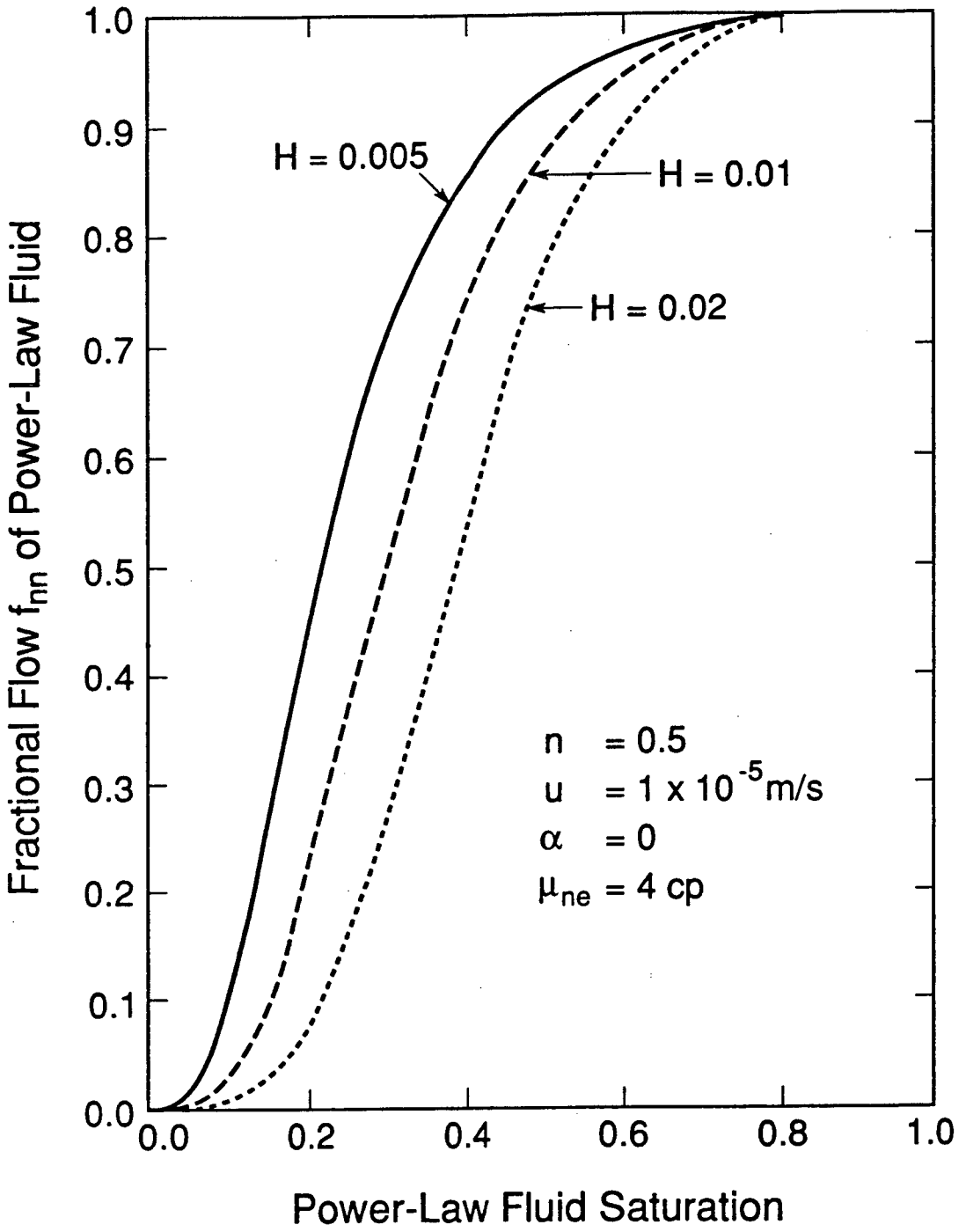

XBL 8911-7844
T.I.D. Illus. 88

Figure 6.9 Effects of the Coefficient H on Non-Newtonian Phase Fractional Flow.

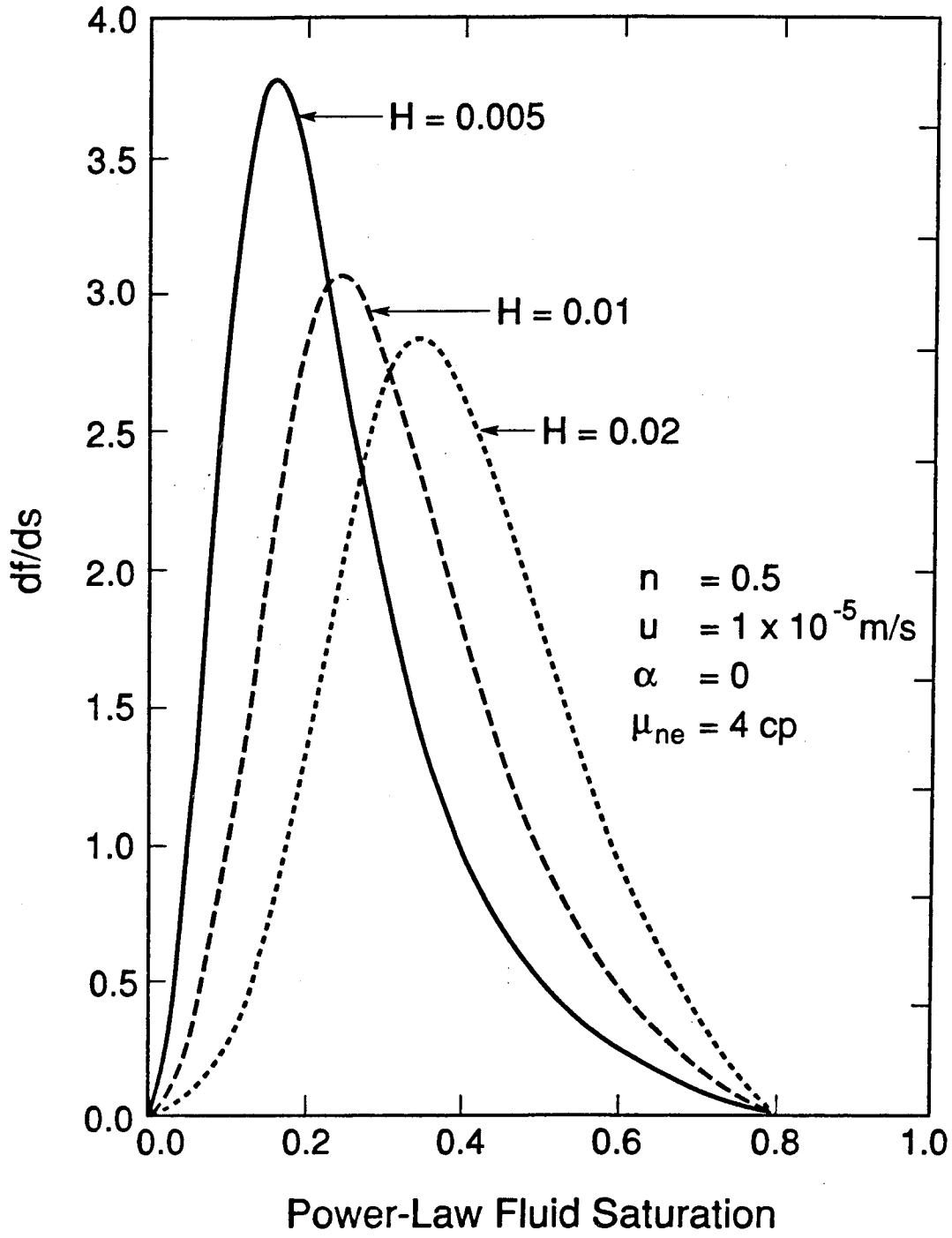

XBL 8911-7845
T.I.D. Illus. 88

Figure 6.10 Effects of the Coefficient H on Derivative of Fractional Flow with Respect to Non-Newtonian Phase Saturation.

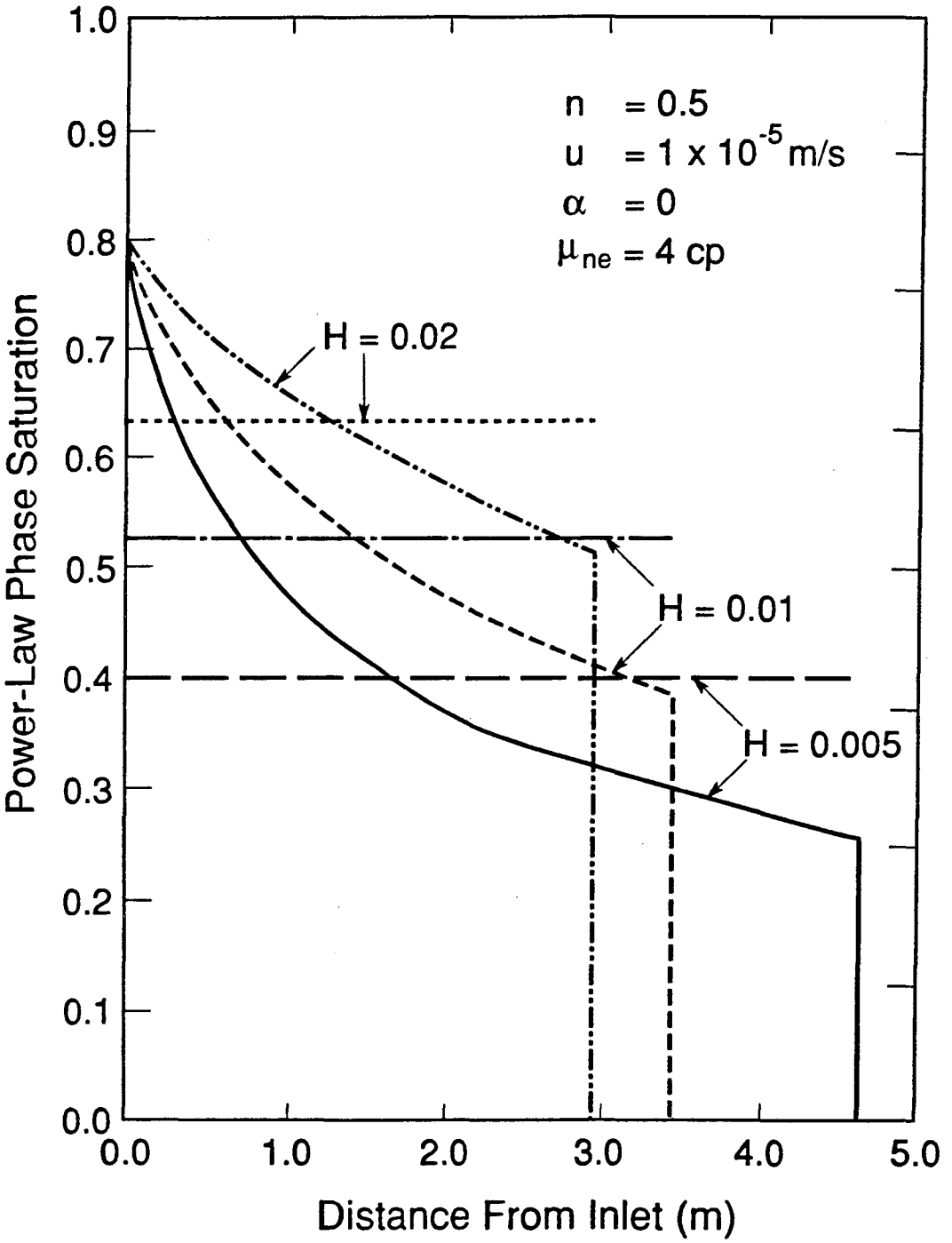

Figure 6.11 Non-Newtonian Phase Saturation Distributions,

Effects of the Coefficient H on Displacement Efficiency.

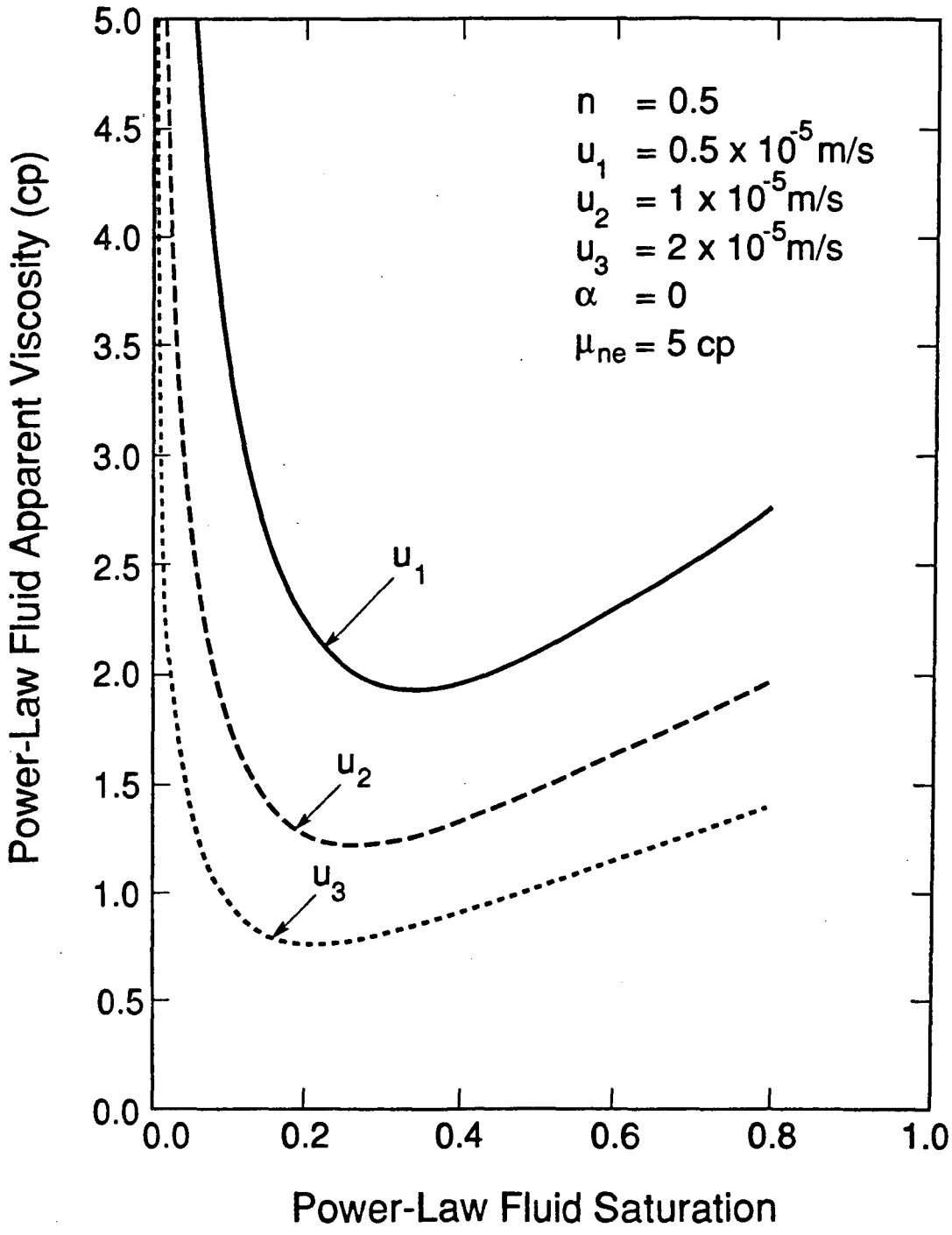

XBL 893-7513
T.I.D. Illus. 88
3/29/89

Figure 6.12 Effects of Injection Rates on Non-Newtonian Phase Apparent Viscosities.

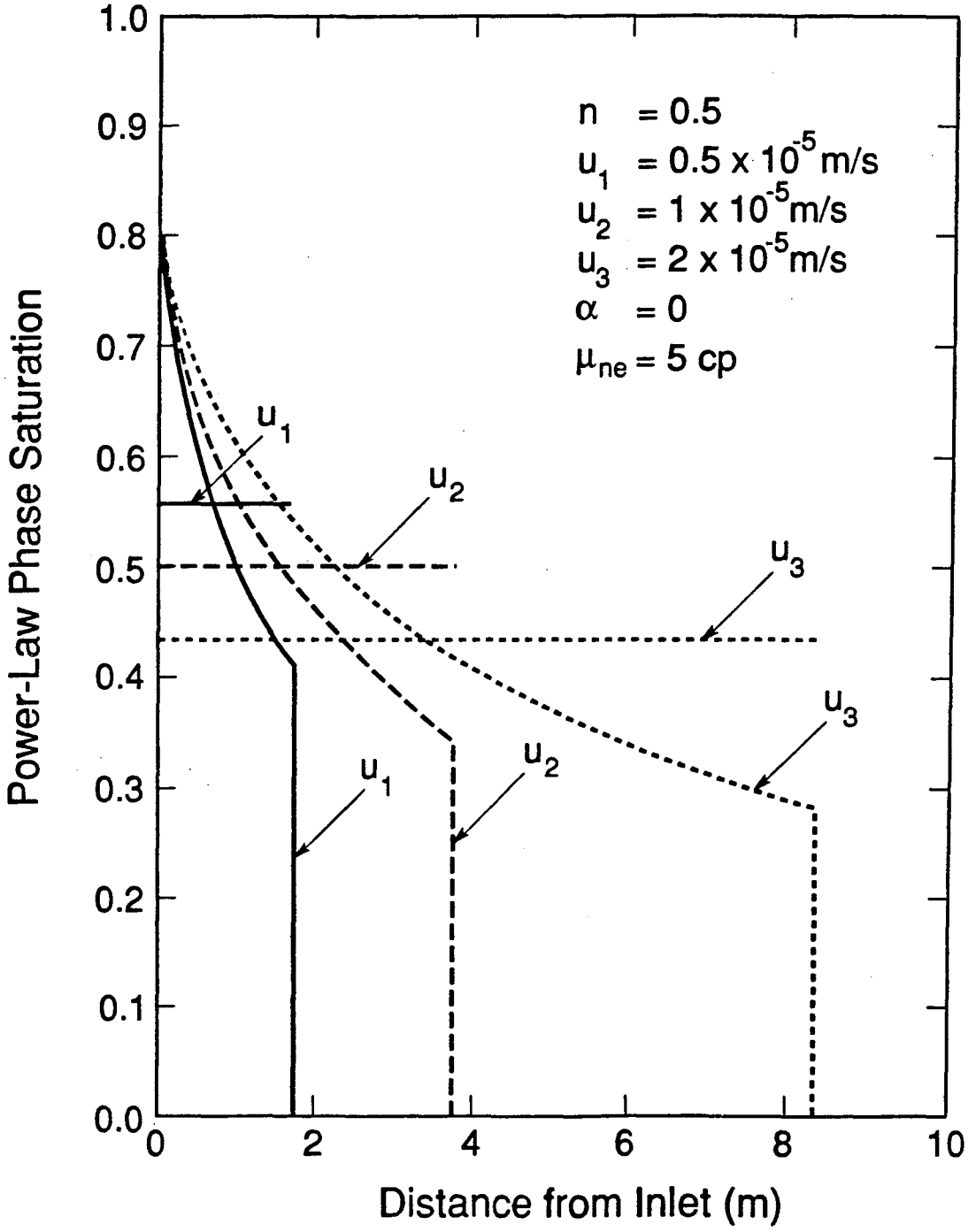

XBL 893-7514
T.I.D. Illus. 88
3/29/89

Figure 6.13 Non-Newtonian Phase Saturation Distributions, Effects of Injection Rates on Displacement Efficiency.

6.3.3 Effect of Gravity

It is expected that gravity may have more effect on non-Newtonian displacement than on Newtonian displacement because it influences the mobility by affecting the non-Newtonian phase viscosity, in addition to occurring in the potential gradient term. This can be demonstrated by the following example. A power-law non-Newtonian fluid is injected upwards ($\alpha=\pi/2$) , horizontally ($\alpha=0$) , and downwards ($\alpha=-\pi/2$) , to displace a heavier in-situ Newtonian fluid. This is a potential application of foam flooding in oil recovery. The fractional flow curves are given in Figure 6.14. Since counterflow may occur physically at very low or very high displacing phase saturations under the effects of gravity, we will have the situations in which $f_{nn} > 1$ for upflow and $f_{nn} < 0$ for downflow. The final saturation distributions in Figure 6.15 show the significance of effects of gravity on non-Newtonian displacement in porous media. For this particular problem, the upflow displacement results in the lowest efficiency since the gravity helps the lighter displacing phase flow faster, and its viscosity becomes smaller, as shown in Figure 6.16.

6.3.4 Conclusions

In summary, the calculated analytical results for displacement with a power-law fluid reveal that the non-Newtonian displacement is a complicated process. The displacement process is controlled by the rheological properties of the particular non-Newtonian fluid used, the injection condition in addition to relative permeability, and is more sensitive to gravity effects as well. The power-law index, n, has the most significant effect on immiscible displacement involving a power-law fluid. The magnitude of the consistence coefficient, H, serves as a scaling factor, which also has a

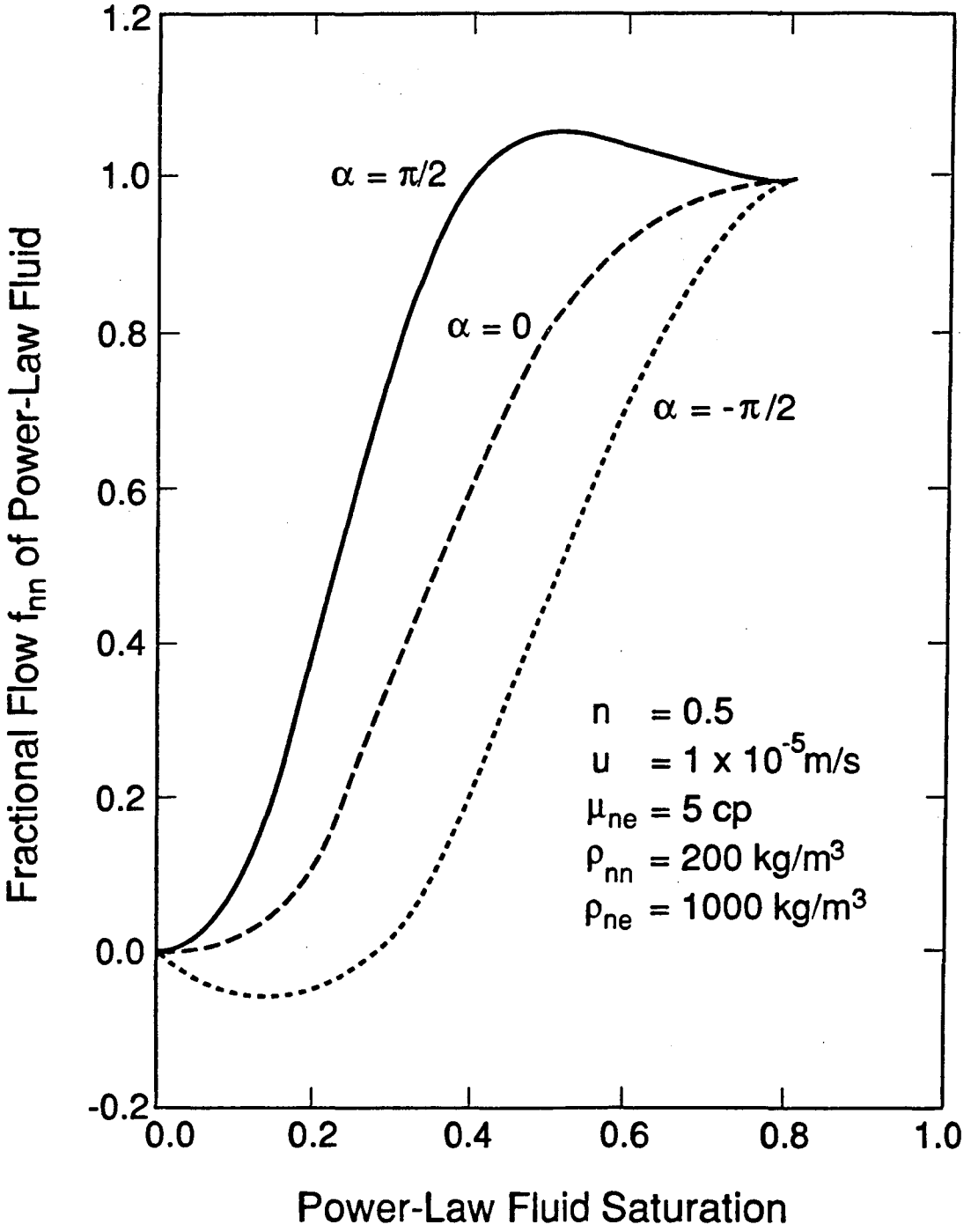

XBL 893-7515
T.I.D. Illus. 88
3/29/89

Figure 6.14 Fractional Flow Curves of a Power-Law Fluid Including Gravity Effects.

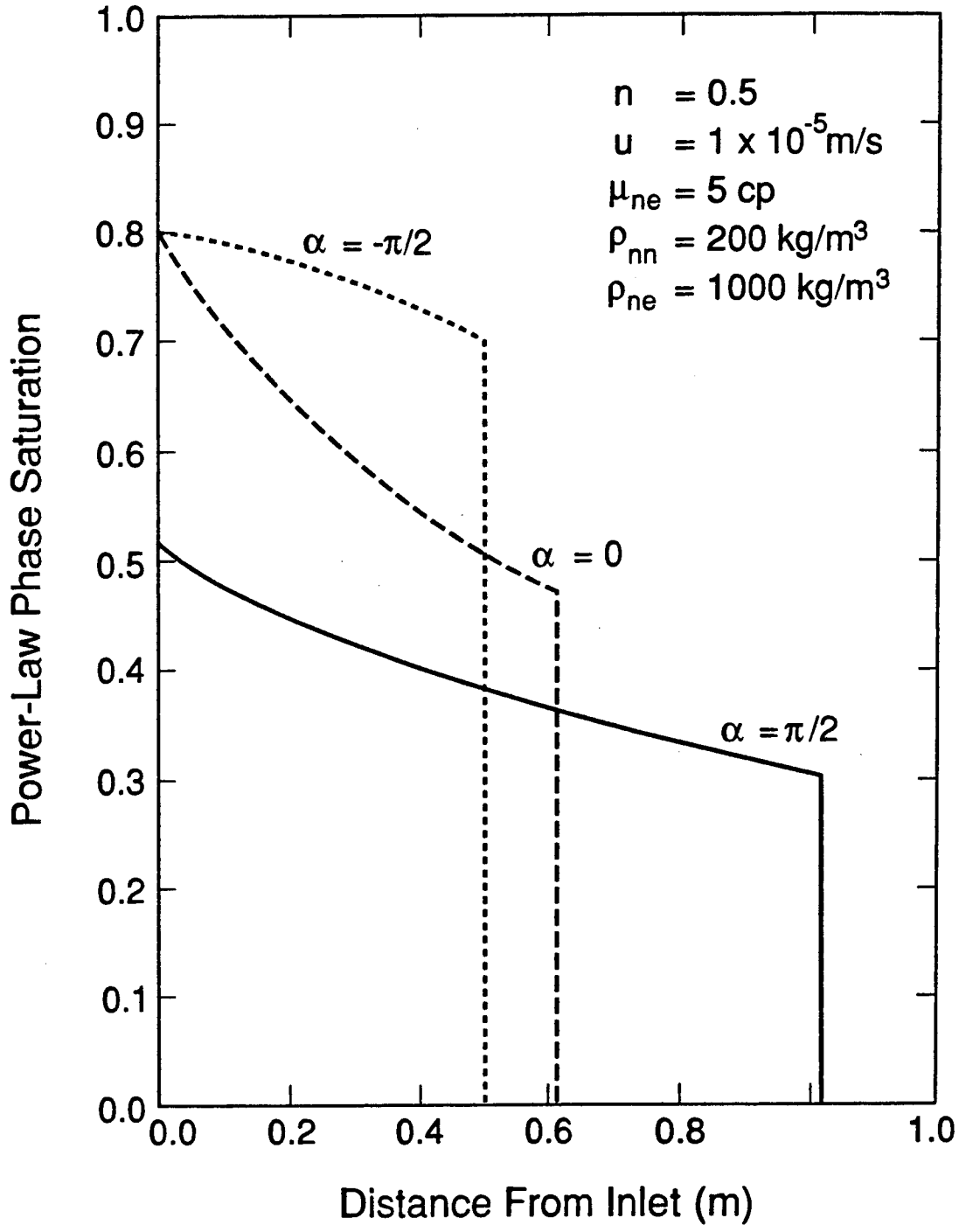

XBL 893-7516
T.I.D. Illus. 88
3/29/89

Figure 6.15 Non-Newtonian Phase Saturation Distributions, Effects of Gravity Rates on Displacement Efficiency.

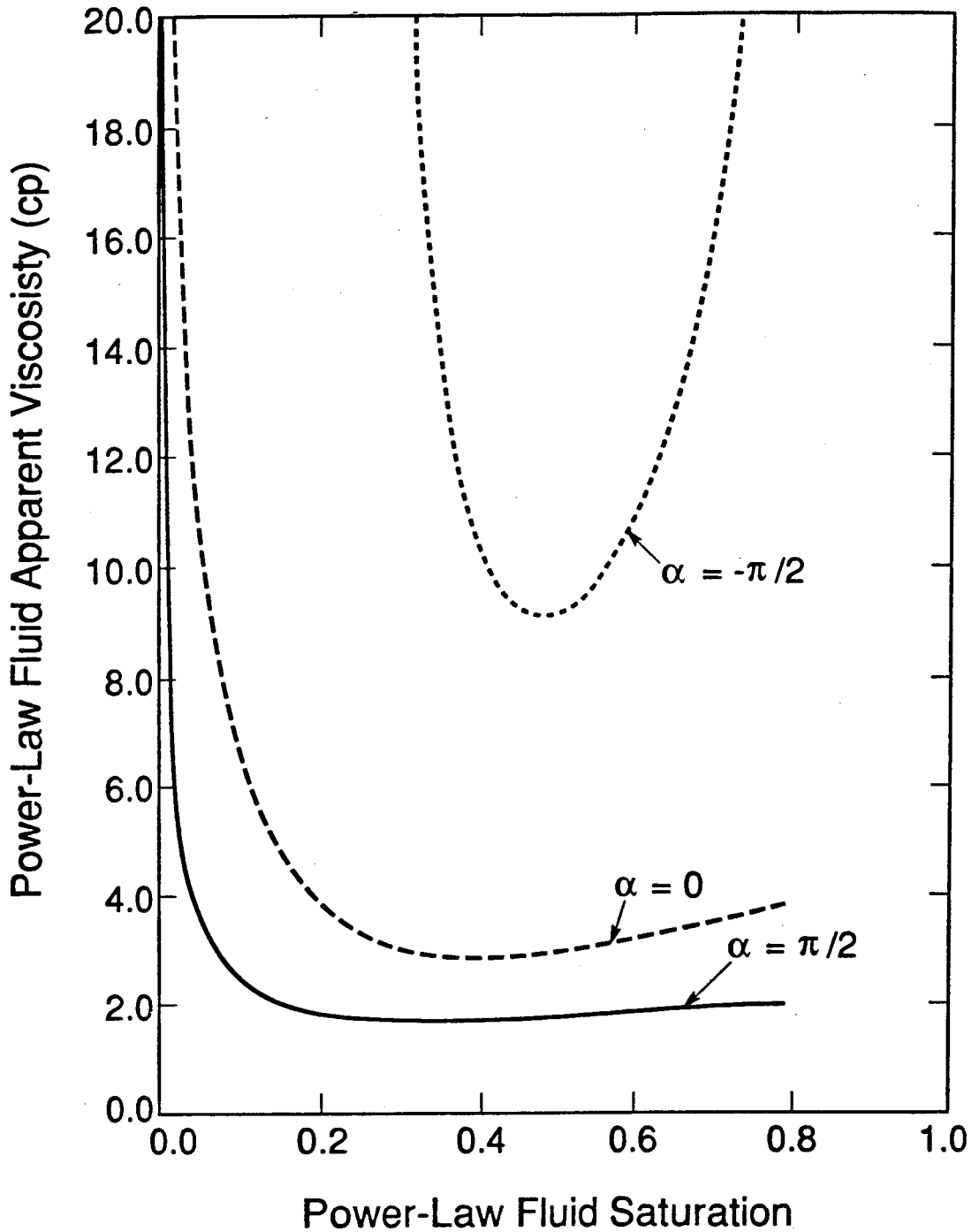

XBL 8911-7847
T.I.D. Illus. 88

Figure 6.16 Effects of Injection Rates on Non-Newtonian Phase Apparent Viscosities.

significant effect on the displacement efficiency.

For the displacement of a Newtonian fluid by a shear-thinning power-law fluid, the sweep efficiency can be improved by reducing injection rates of the power-law fluid. Then, the apparent viscosity of the displacing non-Newtonian fluid will increase, and more percentage of the Newtonian fluid will be driven out of the system. Also, a better displacement can be obtained under the influence of gravity to decrease the flow potential gradient in the flow direction which results in an increase in the apparent viscosity of the displacing power-law fluid.

Chapter 7
Immiscible Displacement of a Bingham Non-Newtonian Fluid by a Newtonian Fluid

7.1 Introduction

In this chapter, the analytical solution developed in Chapter 5 is used to study the physical mechanisms of a Bingham-type non-Newtonian fluid being displaced by a Newtonian fluid. One application of this study is to look at the production process of heavy oil by waterflooding. Many heavy oil reservoirs have been found worldwide and have contributed a considerable percentage of oil to the supply market. A common feature of the highly viscous heavy oil production is the low percentage of oil recovery, which is caused by the high oil viscosity and the effects of the minimum pressure gradient existing at reservoir conditions. The non-Newtonian behavior of heavy oil flow through porous media has been noted in the literature (Mirzadjanzade et al., 1971; Kasraie et al., 1989). The flow of heavy oil in many reservoirs has been observed to exhibit a kind of Bingham-type behavior, i. e., a threshold minimum pressure gradient G must be exceeded before flow starts (Barenblatt et al., 1984). Even with a value of only a few hundredths of a bar per meter for the minimum pressure gradient, it was reported that a very large stagnant zone in the heavy oil formation developed during production, and a significant decrease in oil recovery resulted. In order to increase the rate of heavy oil recovery, many efforts have been made, and various thermal recovery techniques, such as steam flooding, have been developed by industry (Chu, 1987). A number of laboratory experiments and theoretical studies have been published on thermal recovery in porous media. Analytical models (Marx and Langenheim, 1959; Ramey, 1959; Mandl and Volek, 1969) and numerical simulators (Coats et al., 1974; Coats, 1978; 1980) were

used to predict the thermal displacement performance. However, heavy oil viscosities were treated as a function of temperature only, and the effects of non-Newtonian behavior were neglected completely in all these studies.

The physical mechanisms behind the displacement of a Bingham type fluid are of fundamental importance to many engineering designs, such as heavy oil production by water flooding, or drilling mud invasion into a permeable formation during the drilling operations. However, very few studies have been reported on multiple phase flow involving a Bingham fluid in porous media. The immiscible displacement behavior with a Bingham non-Newtonian fluid is the least understood in the literature. Therefore, the purpose of this chapter is to obtain some insights into the physics behind the displacement of a Bingham fluid by a Newtonian fluid under isothermal conditions using the general solution for immiscible non-Newtonian flow developed in Chapter 5.

7.2 Evaluation of Analytical Solution.

The flow physical model is a one-dimensional linear porous system with a constant cross-sectional area, A. Initially, the system is saturated with only a Bingham fluid, and a Newtonian fluid is injected at a constant volumetric rate at the inlet, $x = 0$, from $t = 0$. The relative permeabilities used in this chapter are given as functions of saturation of the displacing Newtonian fluid by Figure 7.1. The fluid and rock properties are summarized in Table 7.1, and the effects of capillary pressure gradient are ignored.

The rheological model for the flow of a single-phase Bingham plastic fluid in porous media, Equation 3.14, is extended to this two-phase flow problem,

$$\mu_{nn} = \frac{\mu_b}{1 - \dfrac{G}{|\partial\Phi/\partial x|}} \tag{7.1a}$$

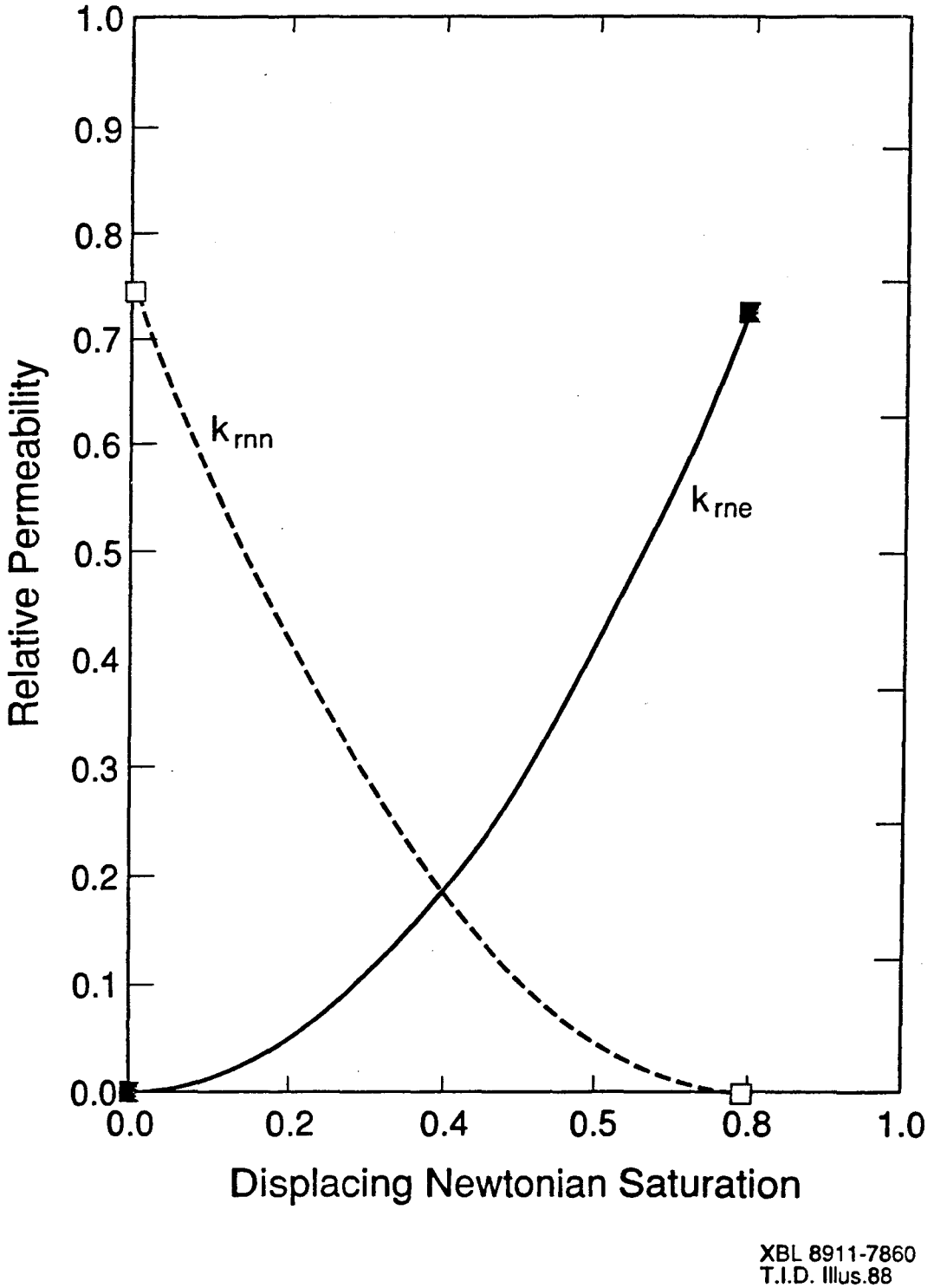

Figure 7.1 Relative Permeability Functions Used for Evaluation of Displacement of a Bingham Fluid.

Table 7.1

Parameters for Linear Bingham Fluid Displacement

Porosity	ϕ=0.20
Permeability	K=1 darcy
Cross-Sectional Area	1 m^2
Injection Rate	$q=1.0\times10^{-6} m^3/s$
Injection Time	T=10 hrs
Displacing Newtonian Viscosity	μ_{ne}=1 cp
Irreducible Saturation	S_{nnir}=0.20
Bingham Plastic Coefficient	μ_b= 4.0 cp
Minimum Pressure Gradient	G= 10,000 Pa/m

for $|\partial\Phi/\partial x| > G$, and

$$\mu_{nn} = \infty \tag{7.1b}$$

for $|\partial\Phi/\partial x| \le G$. For a particular saturation S_{ne} of the Newtonian phase, the corresponding flow potential gradient for the non-Newtonian phase can be derived by introducing Equation 7.1a in Equation 5.21 as

$$-\left[\frac{\partial\Phi}{\partial x}\right]_{S_{ne}} = -\rho_{nn}\, g \sin(\alpha) + \frac{\dfrac{q}{AK} + \dfrac{k_{rnn}(S_{ne})}{\mu_b} G + \dfrac{k_{rne}(S_{ne})}{\mu_{ne}} \rho_{ne}\, g \sin(\alpha) + \dfrac{k_{rnn}(S_{ne})}{\mu_b} \rho_{nn}\, g \sin(\alpha)}{\dfrac{k_{rne}(S_{ne})}{\mu_{ne}} + \dfrac{k_{rnn}(S_{ne})}{\mu_b}} \tag{7.2}$$

The apparent viscosity for the Bingham fluid is determined by using Equation 7.2 in 7.1, and then the fractional flow curves are calculated from Equation 5.19, in which S_{nn} is replaced by S_{ne} for this problem.

7.3 Displacement of a Bingham Non-Newtonian Fluid by a Newtonian Fluid

For the given operating conditions similar to those used in the Buckley-Leverett theory, the non-Newtonian fluid displacement is described by the analytical solution in chapter 5. The displacement involving a Bingham fluid is also determined only by the fractional flow function, which is controlled not only by relative permeability effects, as in Newtonian fluid displacement, but also by the non-Newtonian rheological properties of Bingham fluids. Some fundamental behavior of Bingham type non-Newtonian fluid displacement will be discussed in this section.

7.3.1 Effect of Non-Newtonian Rheological Properties

A Bingham fluid is characterized by the two parameters, the minimum potential gradient, G , and the Bingham plastic coefficient, μ_b. For a porous media flow problem, the two parameters should be determined by laboratory experiments or well tests. A well testing analysis technique will be discussed in Chapter 9 for determining the Bingham flow properties in porous media. The physical significance of the minimum pressure gradient G is described by Equation 2.35, which is related to the yield stress of the fluid and the characteristic length of the pore space in the porous medium. The range of values for the minimum potential gradient G is quite diversified for different reservoirs. A reasonable value of G is of the order of 10^4 Pa/m for heavy oil flow (Mirzadjanzade et al., 1971), and it may exceed 3.0×10^5 Pa/m for groundwater flow in certain clay soils (Bear, 1972). Therefore, various values of G are used to examine its effects on the linear horizontal displacement process.

The pressure gradients as functions of saturation for the displacing Newtonian phase at different values of minimum pressure gradients are given in Figure 7.2. The corresponding apparent viscosities of the Bingham fluids are shown in Figure 7.3. The basic displacement behavior with a Bingham plastic fluid in porous media, as revealed by Figures 7.4, 7.5 and 7.6, is that there exists an ultimate or maximum displacement saturation, S_{max} , for the displacing Newtonian phase. The maximum displacement saturation is reflected at the point of a fractional flow curve, at which $f_{ne} = 1.0$ in Figure 7.4. The derivative of the fractional flow function with respect to saturation is discontinuous when the displacing phase reaches its maximum value S_{max}, as shown in Figure 7.5. The resulting saturation distribution is given by Figure 7.6 showing effects of the minimum pressure gradient G. It is obvious that the sweep efficiency decreases rapidly as G increases, as described by the corresponding horizontal lines in Figure 7.6. For Newtonian displacement, the ultimate saturation for the displacing fluid is equal

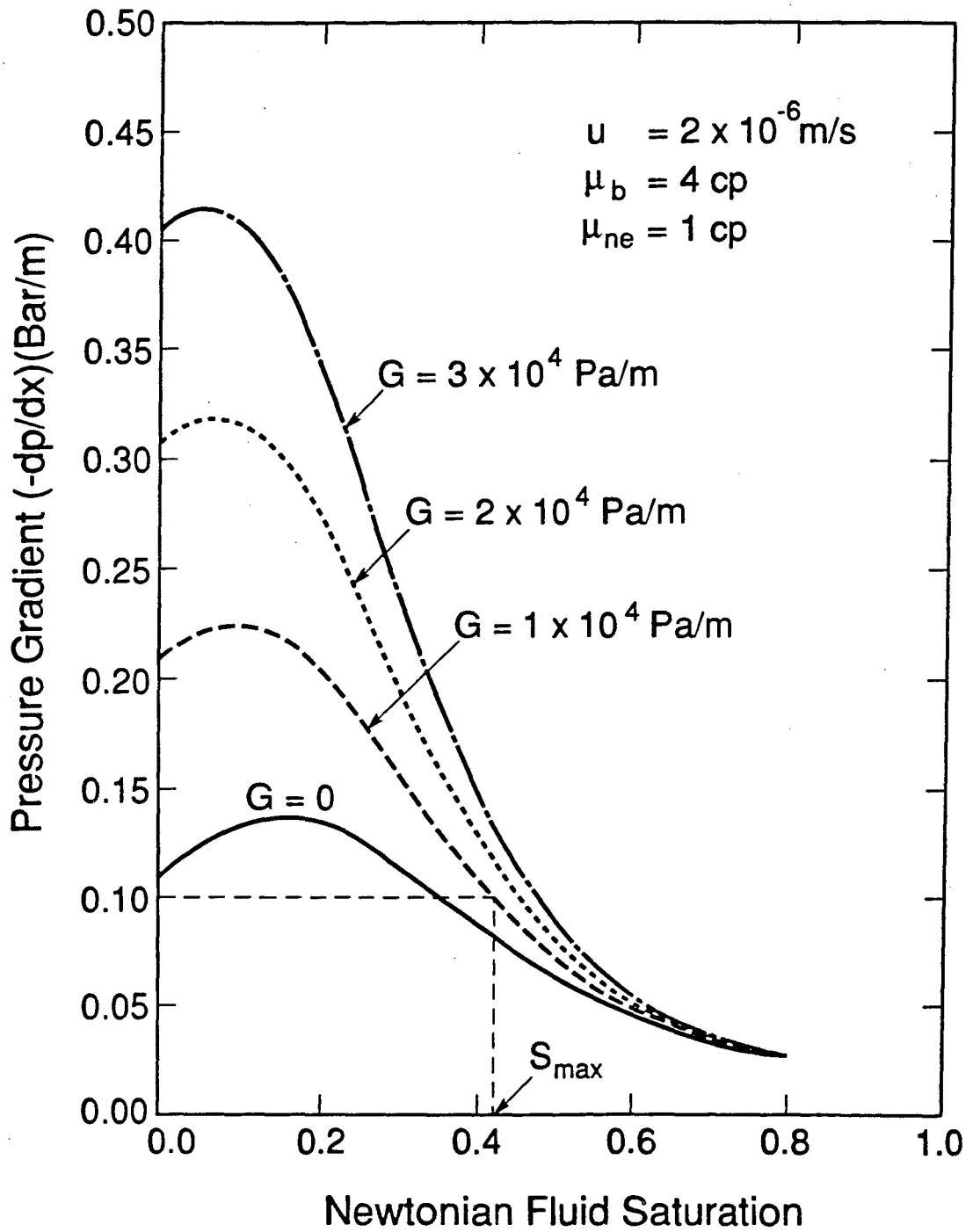

XBL 8911-7861
T.I.D. Illus. 88

Figure 7.2 Pressure Gradients versus Newtonian Fluid Saturation, Effects of the Minimum Pressure Gradient.

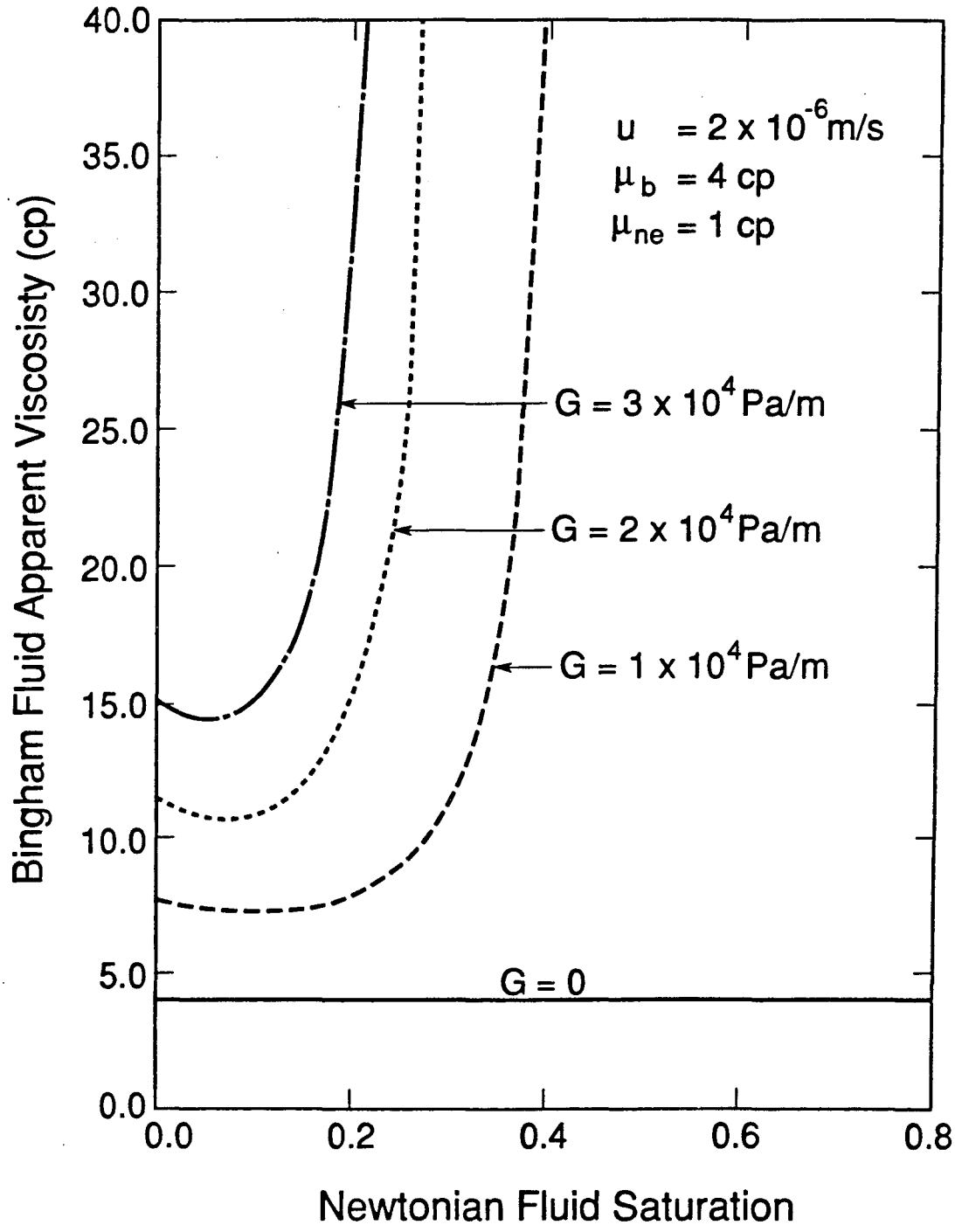

XBL 8911-7862
T.I.D. Illus. 88

Figure 7.3 Effects of the Minimum Pressure Gradient on Bingham Phase Apparent Viscosities.

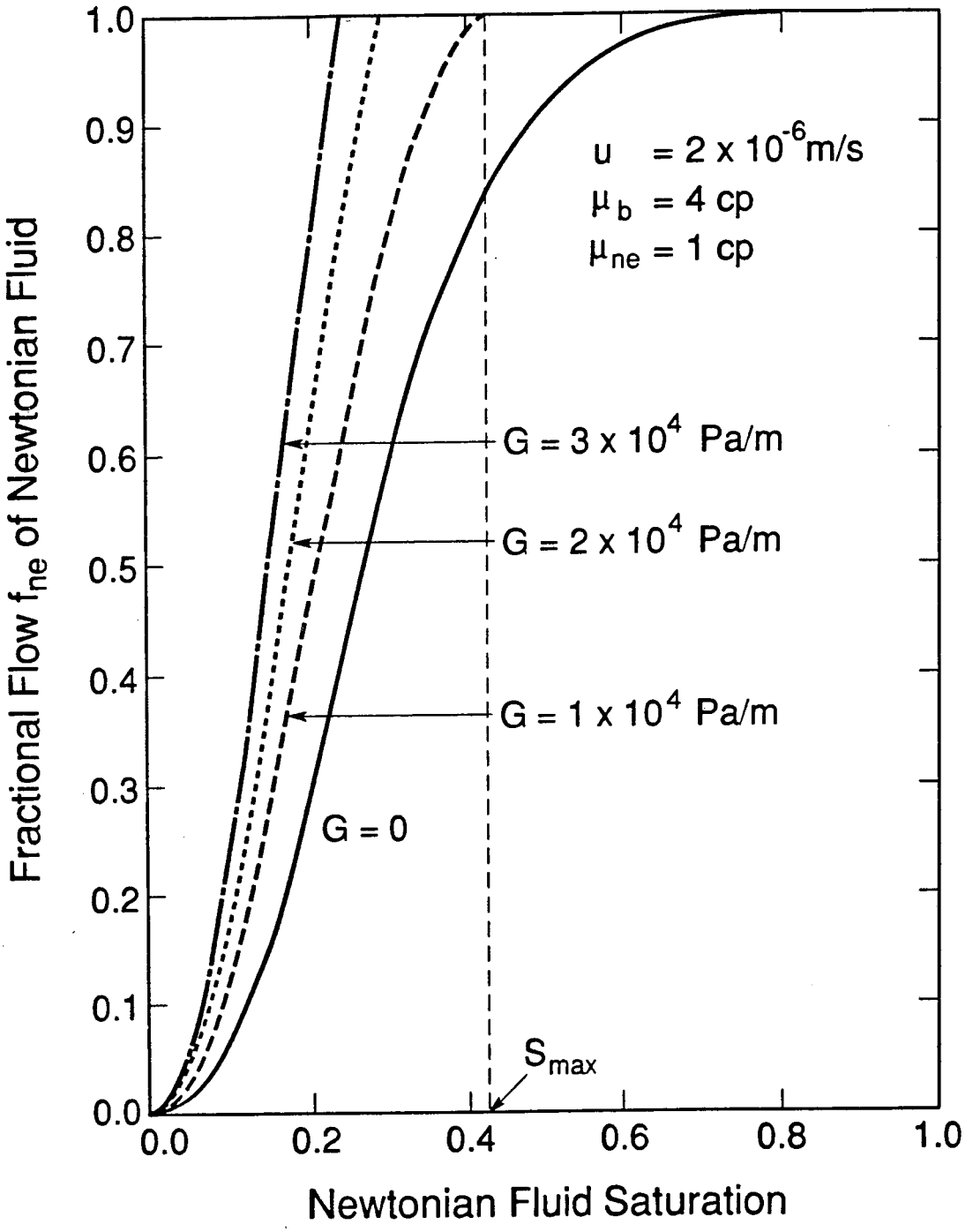

XBL 8911-7863
T.I.D. Illus. 88

Figure 7.4 Fractional Flow Curves for a Bingham Fluid Displaced by a Newtonian Fluid, Effects of the Minimum Pressure Gradient.

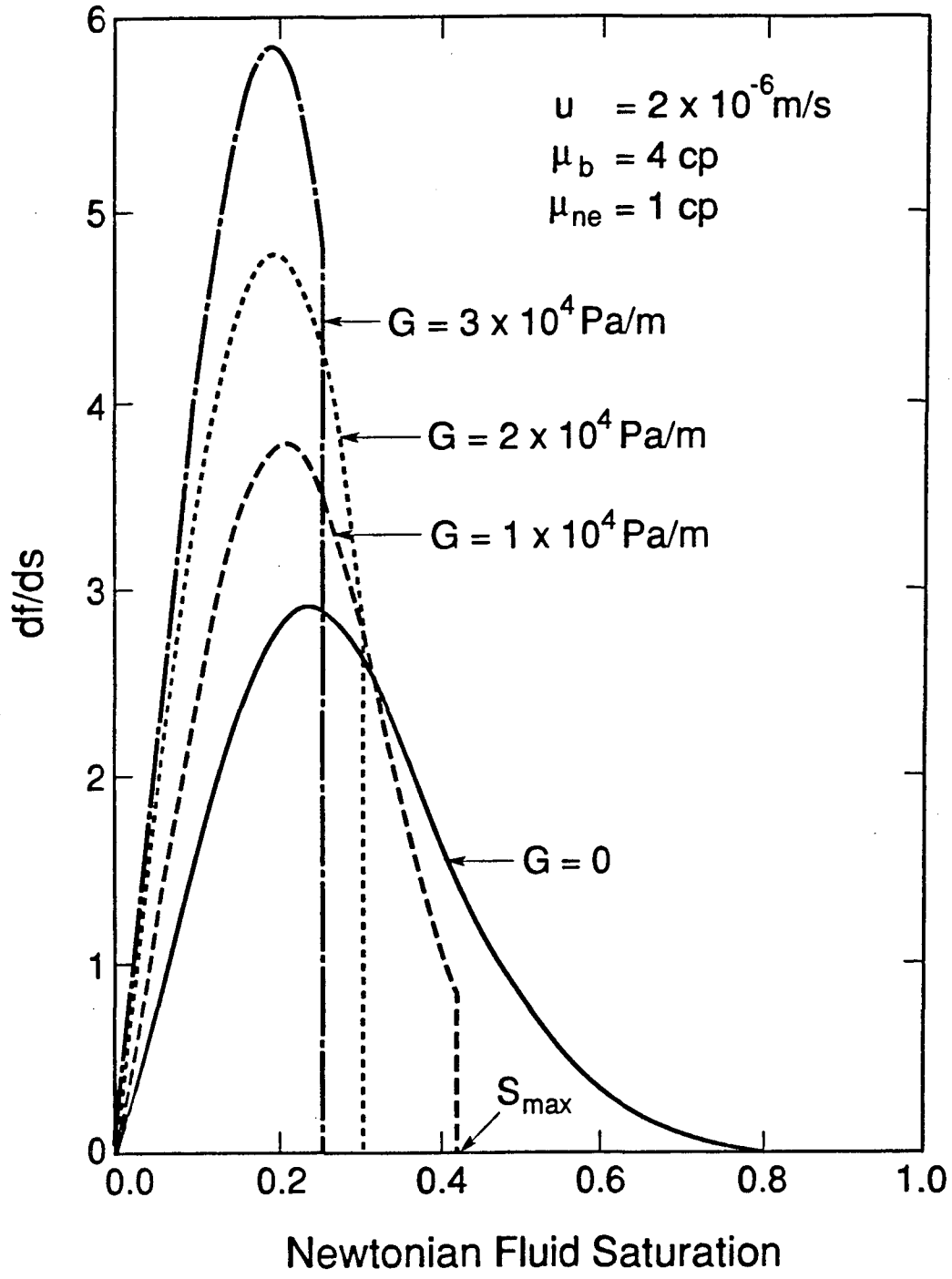

XBL 8911-7864
T.I.D. Illus. 88

Figure 7.5 Effects of the Minimum Pressure Gradient on Derivative of Fractional Flow with Respect to Newtonian Saturation.

theoretically to the total mobile saturation of the in-situ fluid, such as that of the curve (G = 0) in Figure 7.6.

Physically, the phenomenon of ultimate displacement saturation occurs as the flow potential gradient approaches the minimum pressure gradient, at which the apparent viscosity is infinite. Then the only flowing phase is the displacing Newtonian fluid. Consequently, once the maximum saturation has been reached for a flow system, no improvement of sweep efficiency can be obtained no matter how long the displacement process continues, as shown in Figure 7.6. The flow condition is more complicated in reservoirs than in this linear semi-infinite system. Since oil wells are usually drilled according to certain patterns, there always exist some low flow rate or low potential gradient stagnation zones between production and injection wells. The presence of the ultimate displacement saturation for a Bingham fluid indicates that no oil can be driven out of these regions. Therefore, the ultimate displacement saturation phenomenon is also responsible for the low oil recovery observed in heavy oil reservoirs developed by water-flooding, in addition to effects of the high oil viscosity.

The effects of the other rheological parameter, the Bingham plastic coefficient μ_b, are shown in Figures 7.7, 7.8 and 7.9. It is interesting to note that the ultimate displacement saturations hardly change as μ_b changes. However, the average saturations in the swept zones are quite different for a different value of μ_b from Figure 7.9. The ultimate displacement saturation is essentially determined by the minimum pressure gradient G and also by the pressure gradient which is very close to the minimum pressure gradient G, as described by Equations 7.1 and 7.2. The changes in μ_b have little effects on the ultimate displacement saturation since the flow potential gradient used in Equation 7.1a, calculated from Equation 7.2, hardly varies with μ_b as $\partial P/\partial x \rightarrow G$.

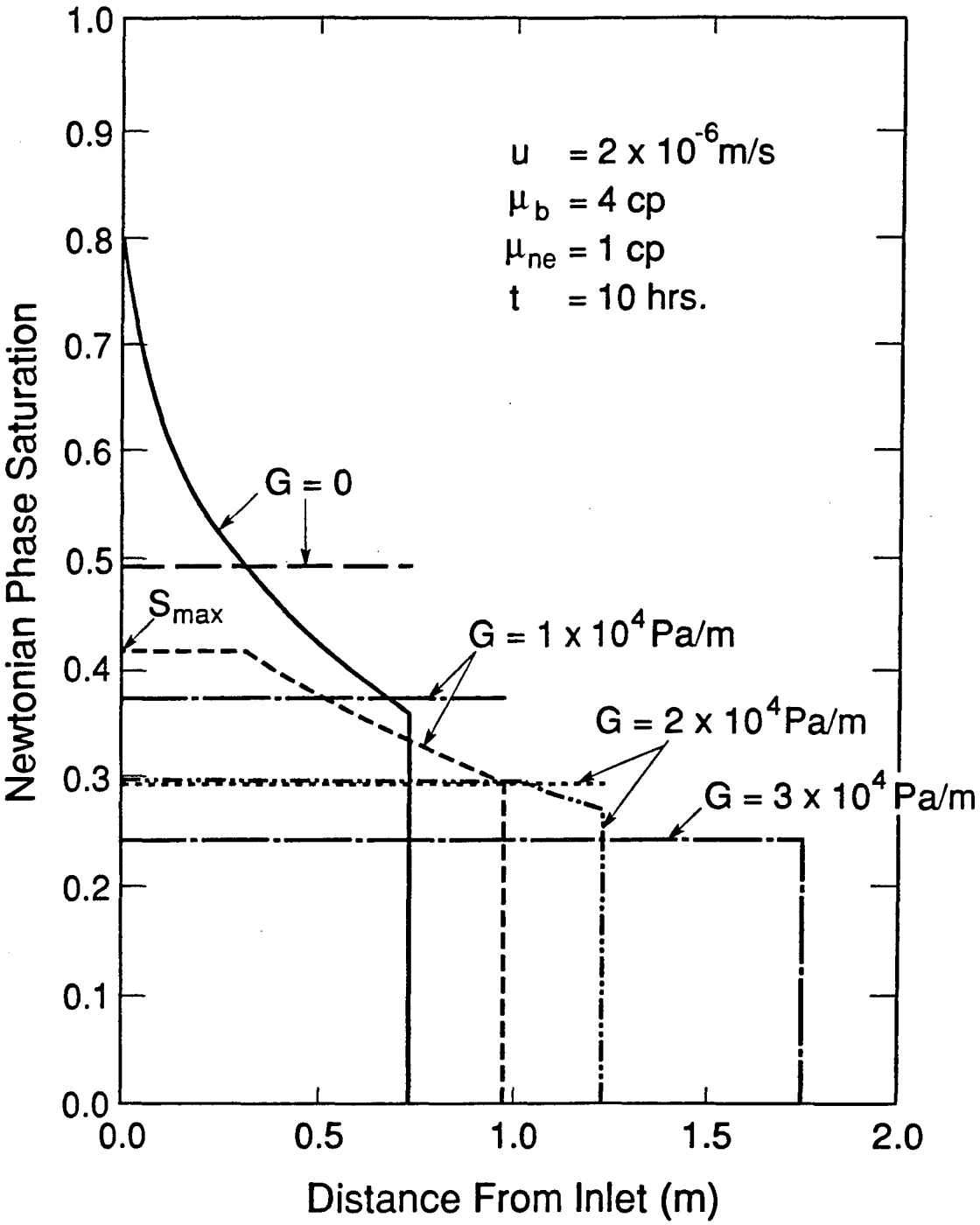

XBL 8911-7865
T.I.D. Illus.88

Figure 7.6 Newtonian Phase Saturation Distributions, Effects of the Minimum Pressure Gradient on Displacement Efficiency of a Bingham Fluid by a Newtonian Fluid.

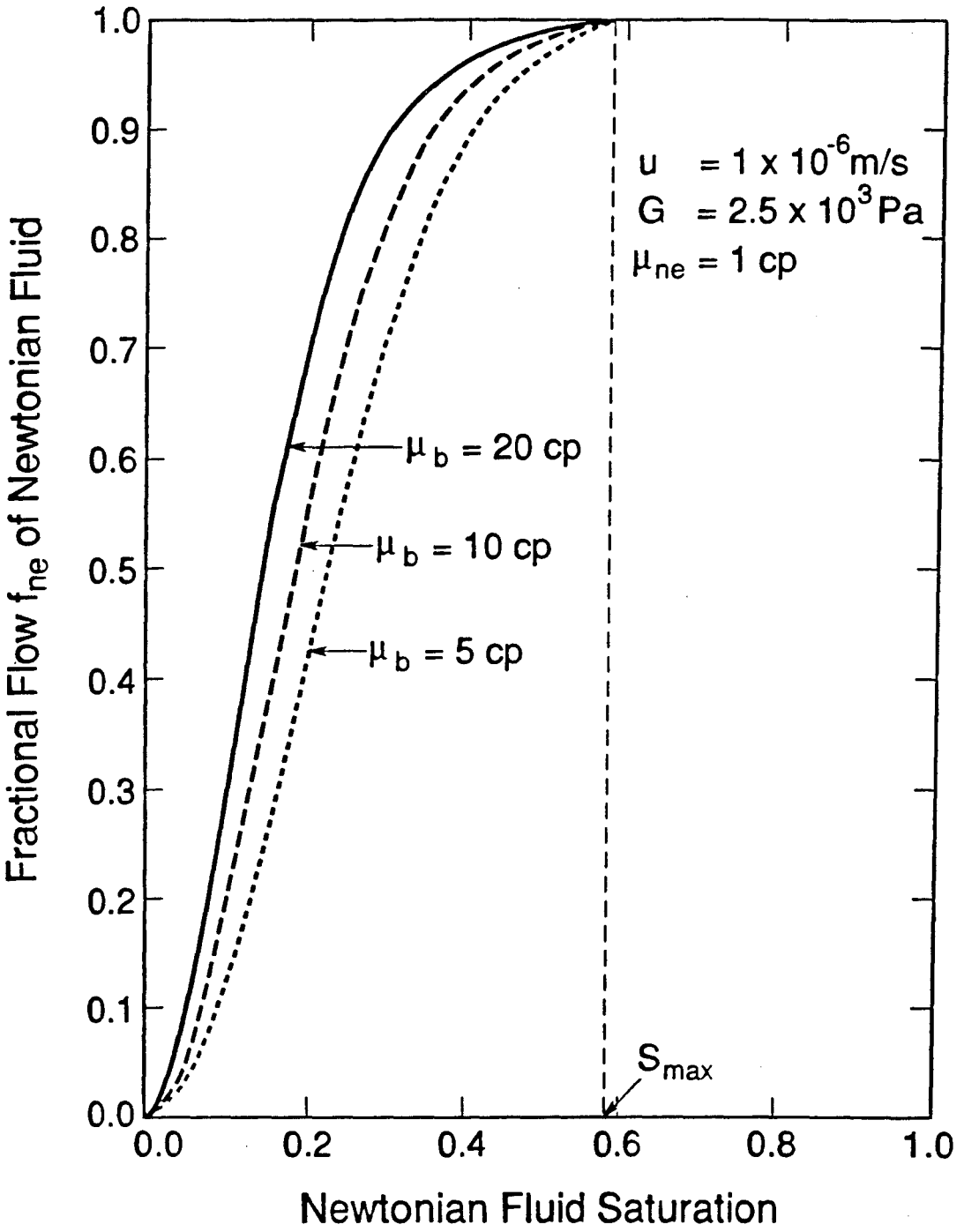

XBL 8911-7866
T.I.D. Illus. 88

Figure 7.7 Fractional Flow Curves for a Bingham Fluid Displaced by a Newtonian Fluid, Effects of Bingham's Coefficient μ_b .

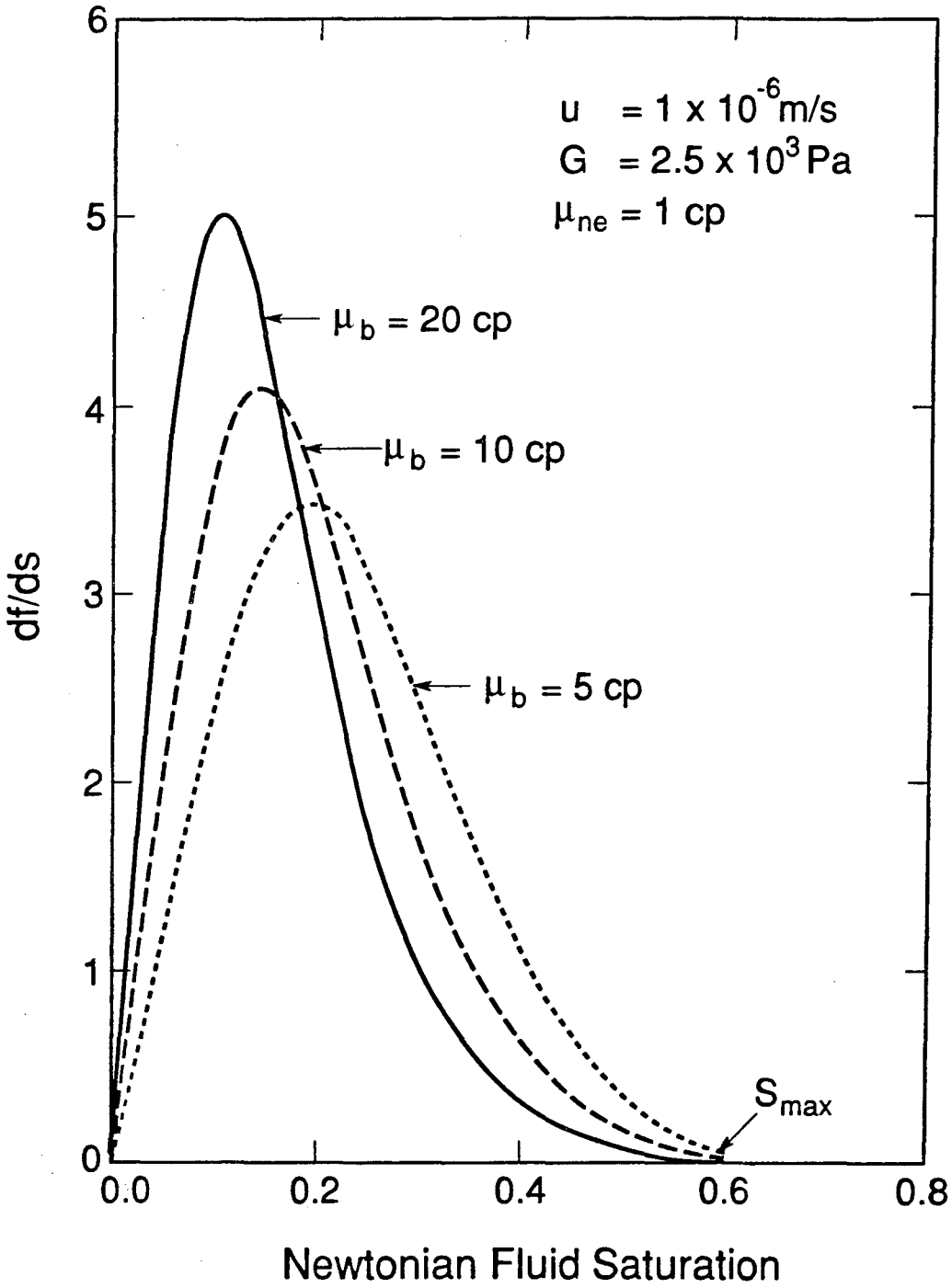

XBL 8911-7867
T.I.D. Illus. 88

Figure 7.8 Effects of Bingham's Coefficient μ_b on Derivative of Fractional Flow with Respect to Newtonian Saturation.

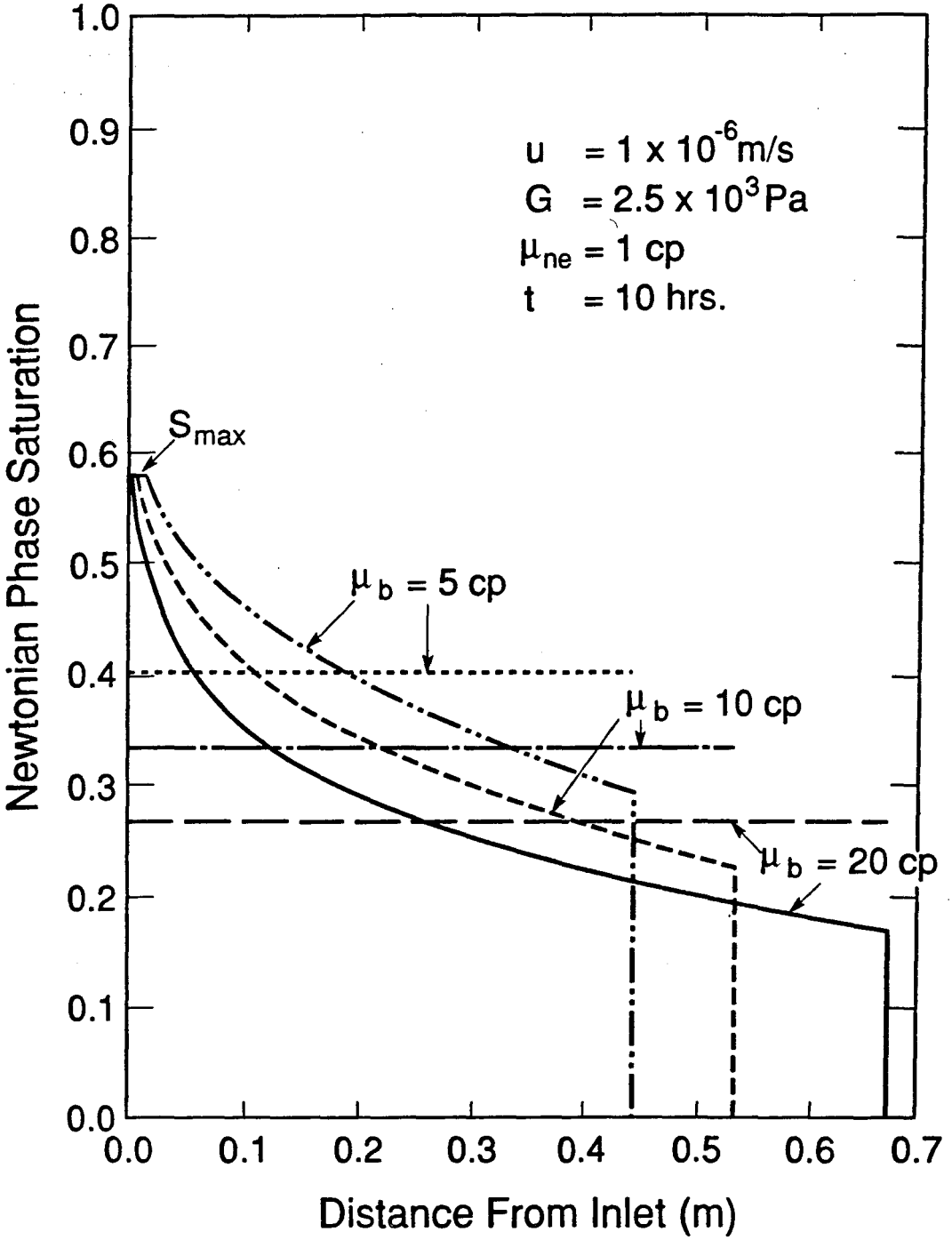

XBL 8911-7868
T.I.D. Illus.88

Figure 7.9 Newtonian Phase Saturation Distributions, Effects of Bingham's Coefficient μ_b on Displacement Efficiency of a Bingham Fluid by a Newtonian Fluid.

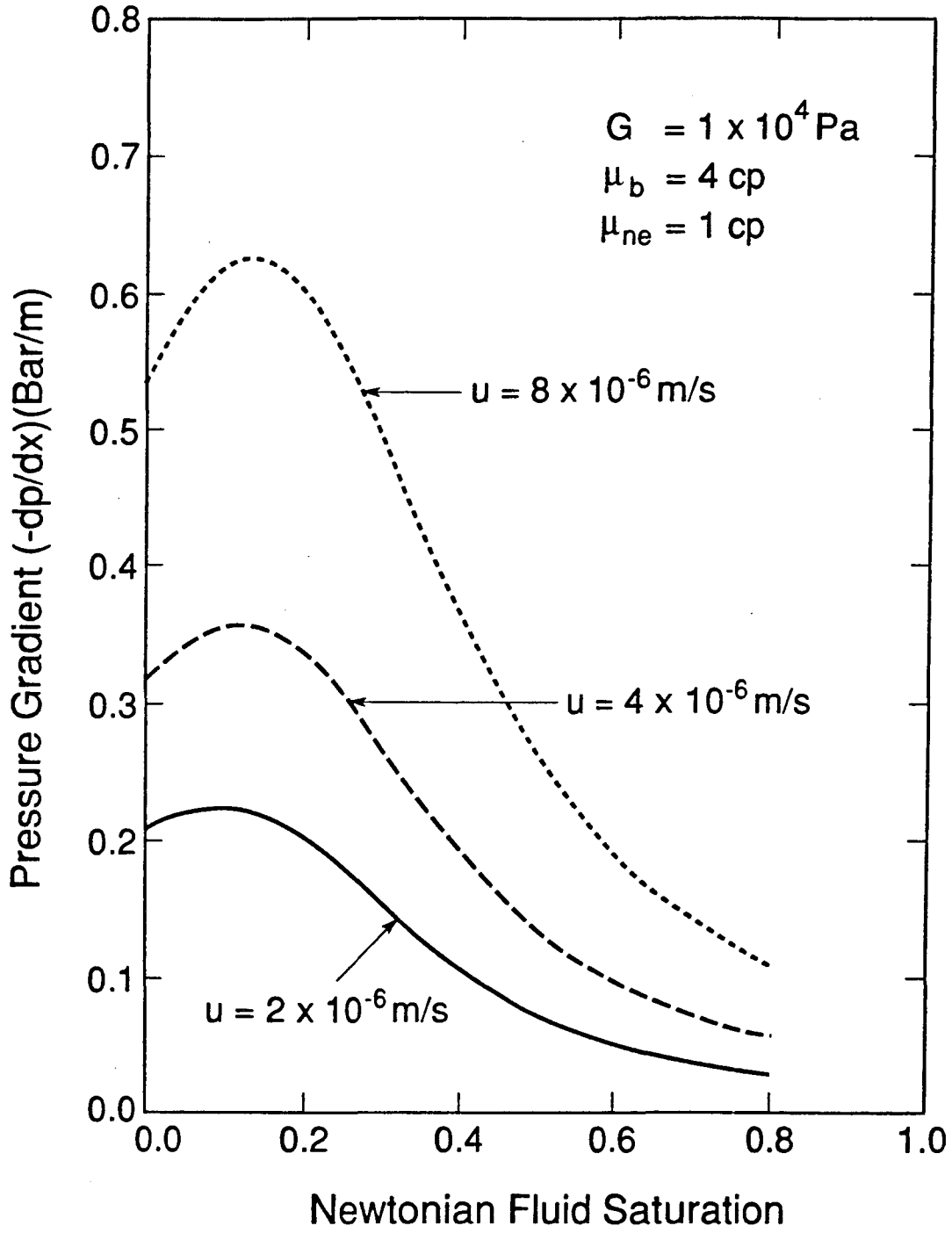

XBL 8911-7869
T.I.D. Illus. 88

Figure 7.10 Pressure Gradients versus Newtonian Fluid Saturation, Effects of Injection Rates.

7.3.2 Effect of Injection Rates

In this problem, a Bingham fluid in the horizontal porous medium is displaced by water. If the water injection rate at the inlet is increased, the pressure gradient in the system will increase, and the apparent viscosity for the Bingham fluid will be reduced. Therefore, a better sweep efficiency will result.

The pressure gradients and apparent viscosities as functions of the displacing Newtonian phase saturation for different water injection rates are shown in Figures 7.10 and 7.11, respectively. Accordingly, the fractional flow functions and their derivatives with respect to saturation are given in Figures 7.12 and 7.13, which do exhibit the significant effects by the injection rate. Figure 7.14 presents the saturation profiles after injection of 10 hours with the different rates. It is encouraging to note that both the sweep efficiency and the ultimate displacement saturation can be greatly improved by only increasing the injection rate for the same flow condition.

7.3.3 Effect of Gravity

The effects of gravity on Bingham fluid displacement by a Newtonian fluid can be examined by considering the following example. A heavier Newtonian fluid with density $\rho_{ne} = 1{,}000$ Kg/m is used to displace a Bingham fluid with density $\rho_{nn} = 850$ Kg/m. The flow directions are upward ($\alpha = \pi/2$), horizontal ($\alpha = 0$), and downward ($\alpha = -\pi/2$). This is similar to using water to drive heavy oil in reservoirs. The fractional flow curves are shown in Figure 7.15, and the resulting saturation distribution is described by Figure 7.16 for this particular problem. The difference in density of the two fluids is small, so the influence of gravity on displacement efficiency is not very significant. However, gravity does change the ultimate displacement saturation, as shown in Figure 7.16. The

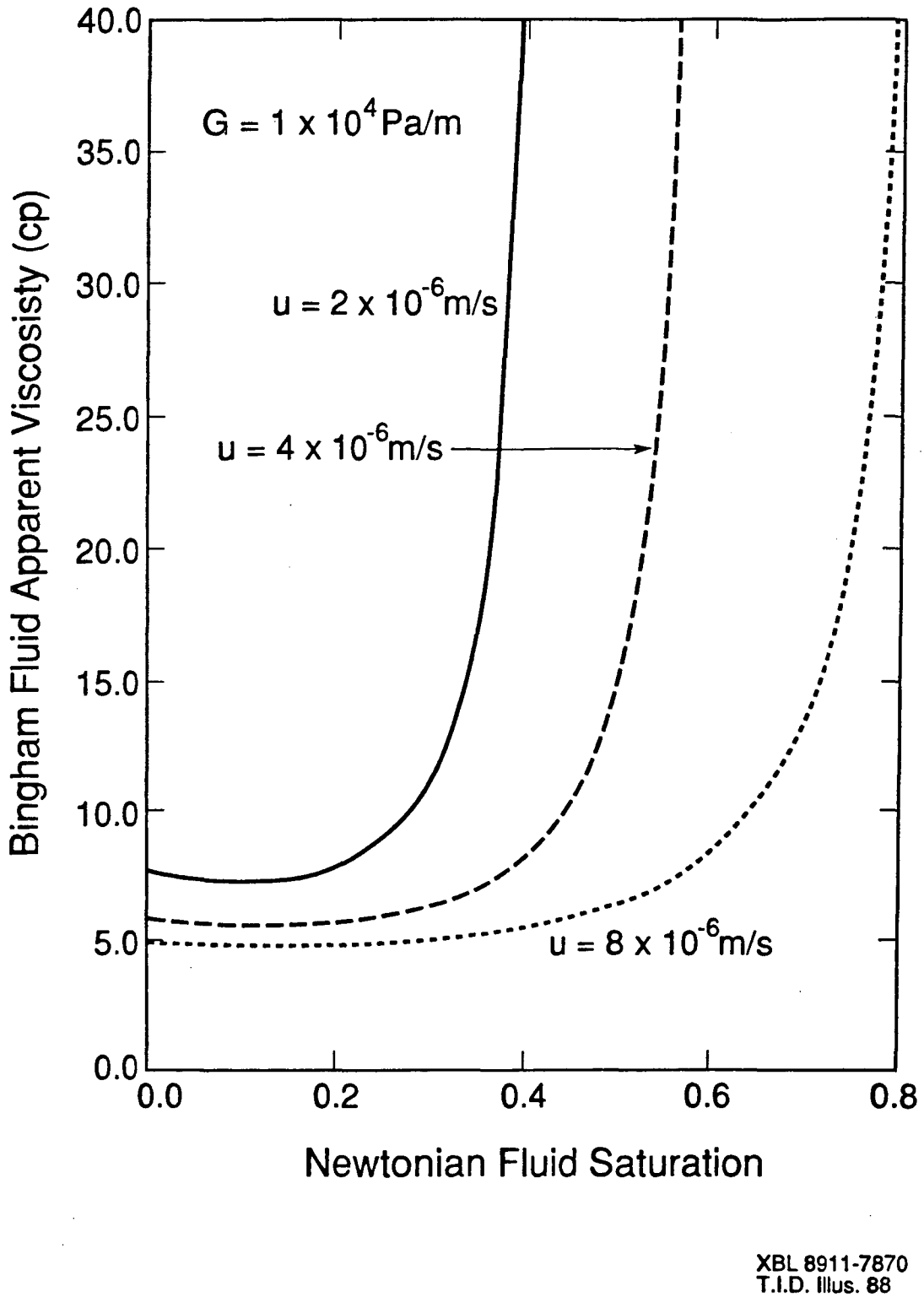

Figure 7.11 Effects of Injection Rates on Bingham Phase Apparent Viscosities.

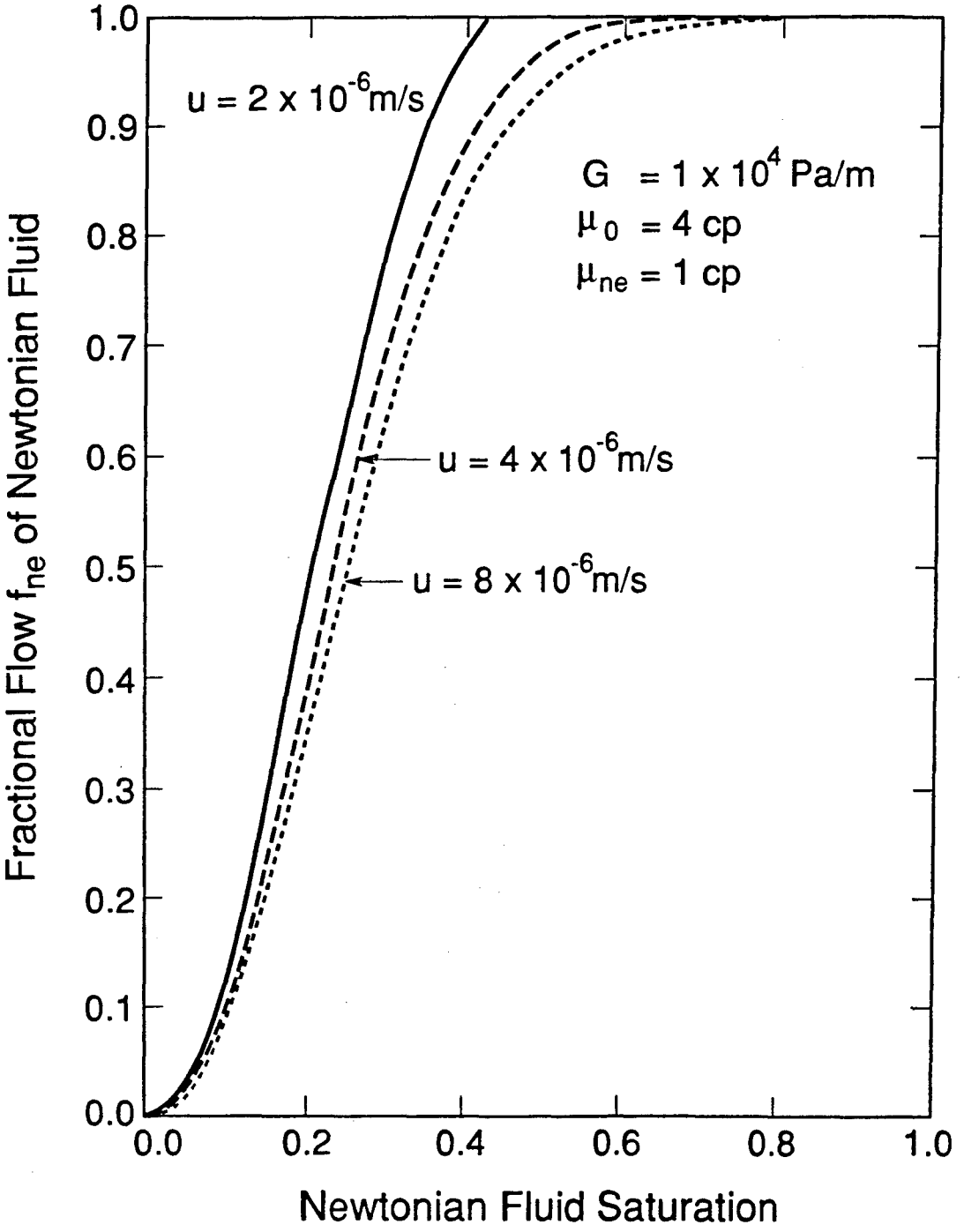

XBL 8911-7871
T.I.D. Illus. 88

Figure 7.12 Fractional Flow Curves for a Bingham Fluid Displaced by a Newtonian Fluid, Effects of injection Rates.

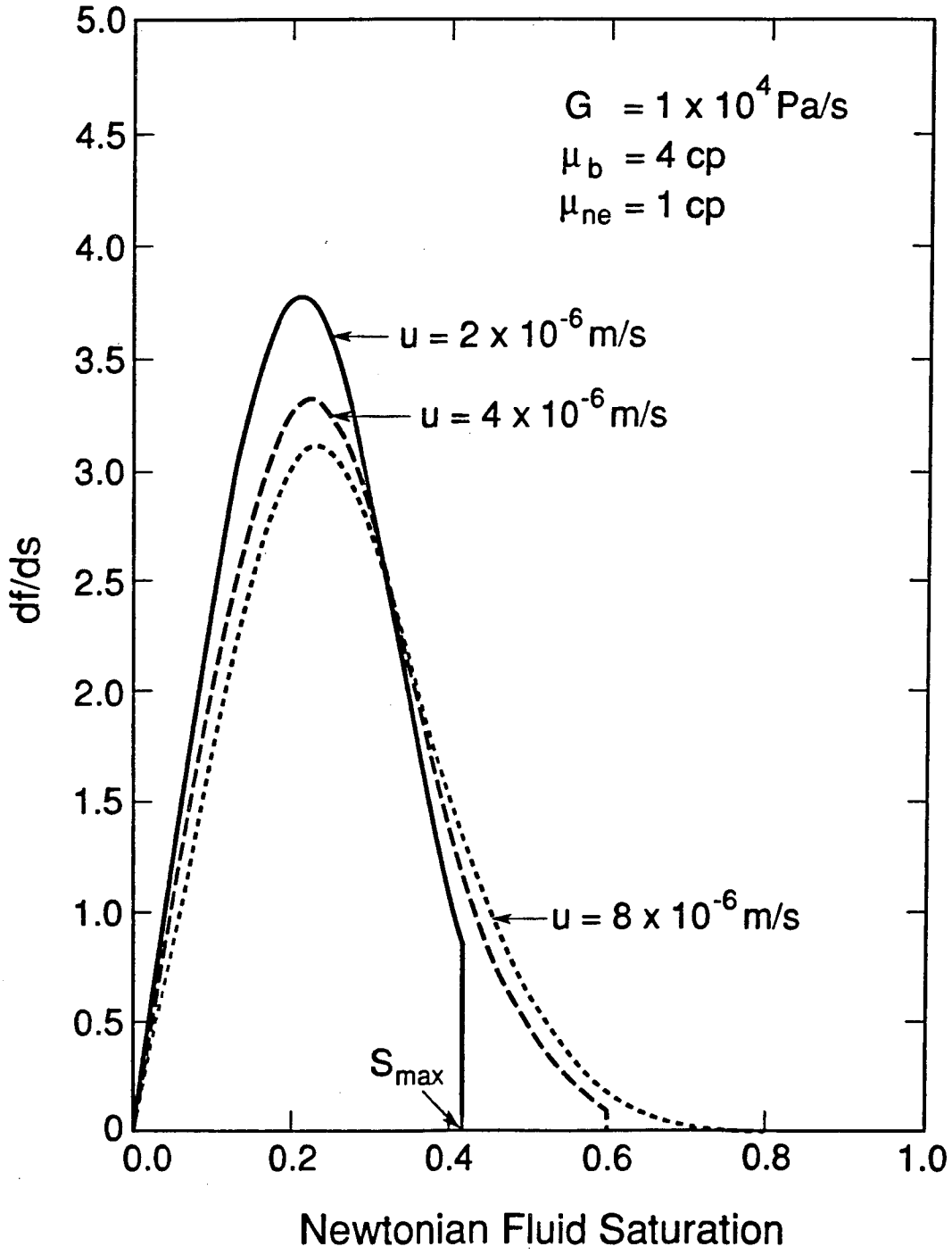

XBL 8911-7873
T.I.D. Illus. 88

Figure 7.13 Effects of Injection Rates on Derivative of Fractional Flow with Respect to Newtonian Saturation.

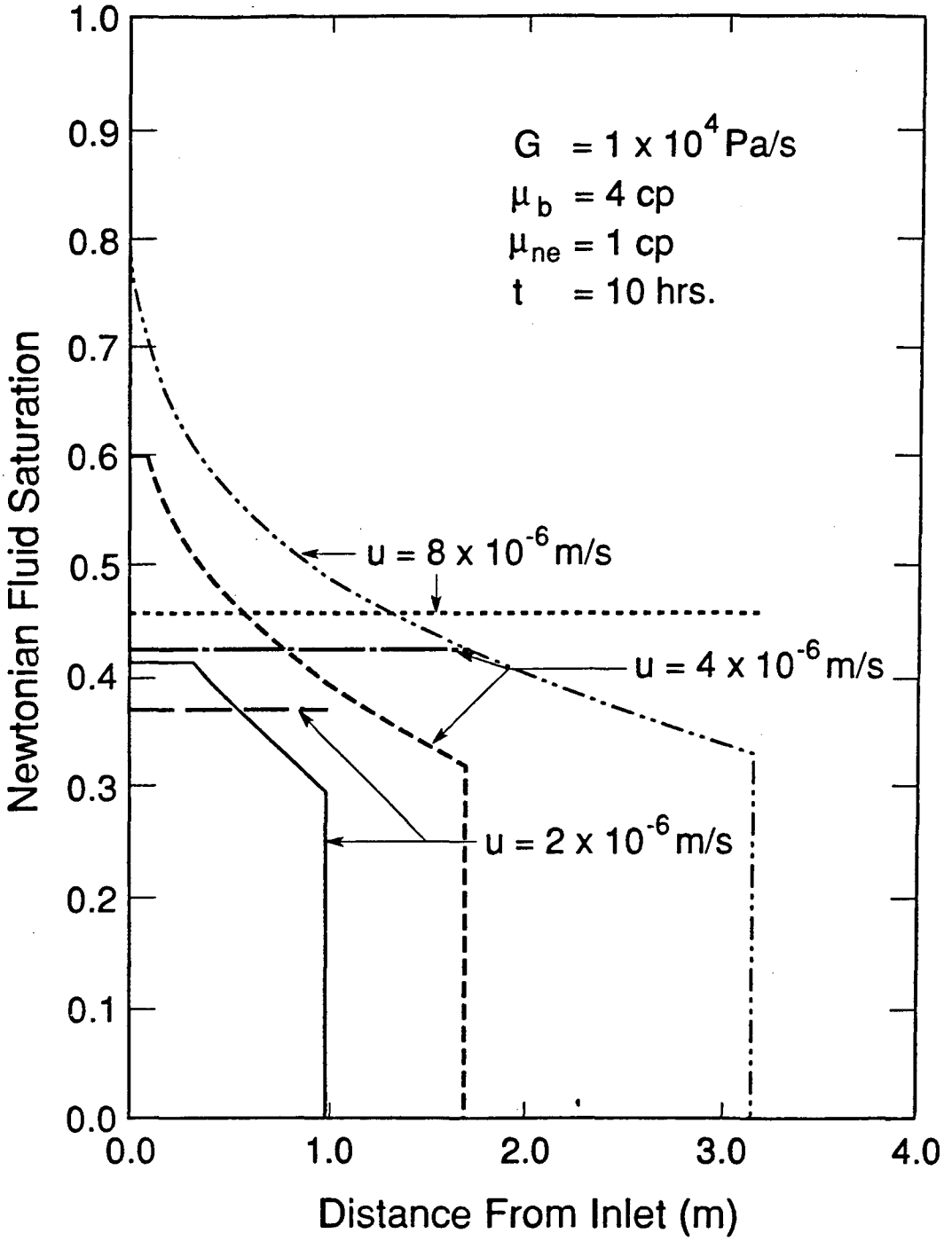

Figure 7.14 Newtonian Phase Saturation Distributions, Effects of Injection Rates on Displacement Efficiency of a Bingham Fluid by a Newtonian Fluid.

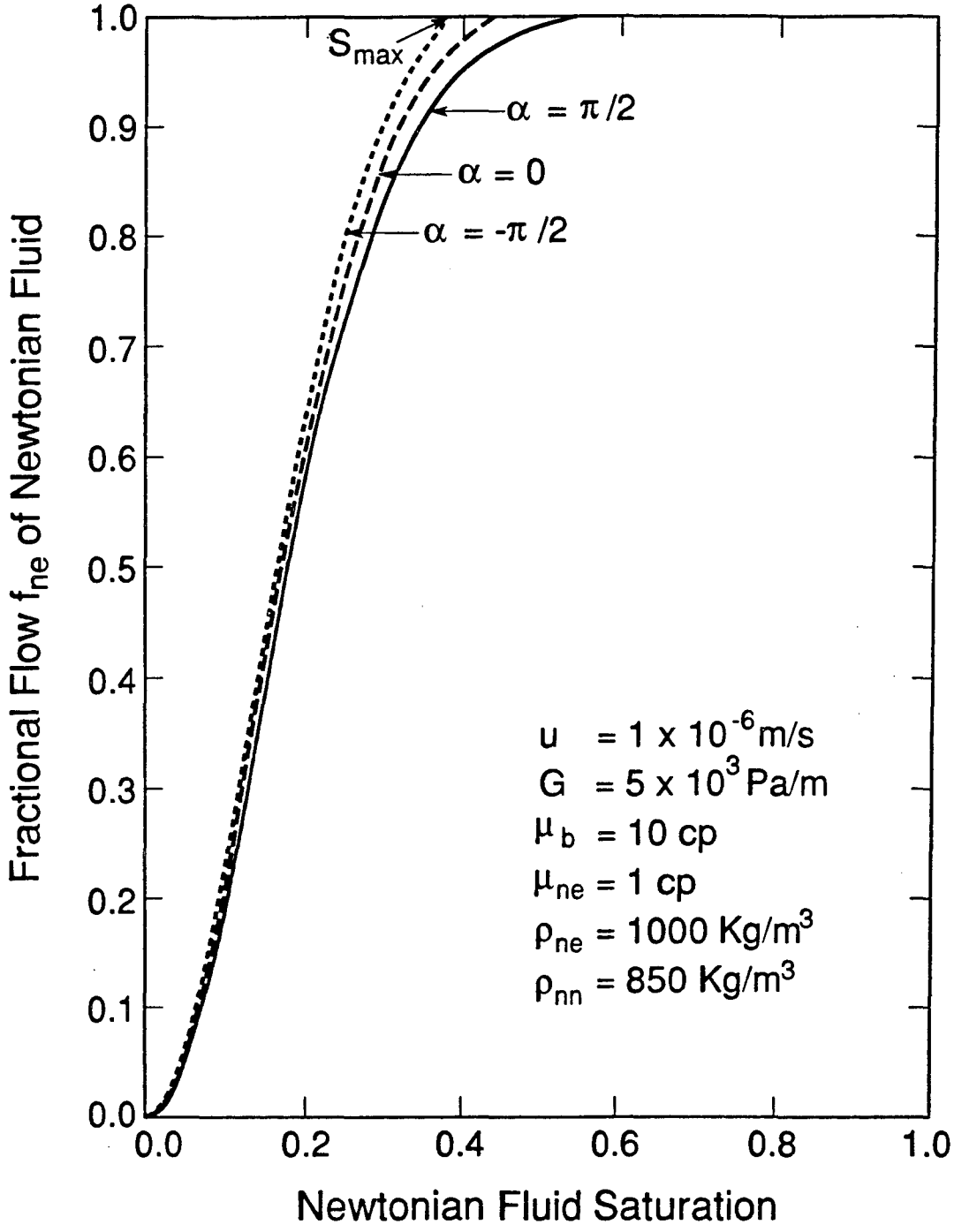

XBL 8911-7875
T.I.D. Illus. 88

Figure 7.15 Fractional Flow Curves for a Bingham Fluid Displaced by a Newtonian Fluid, Effects of Gravity.

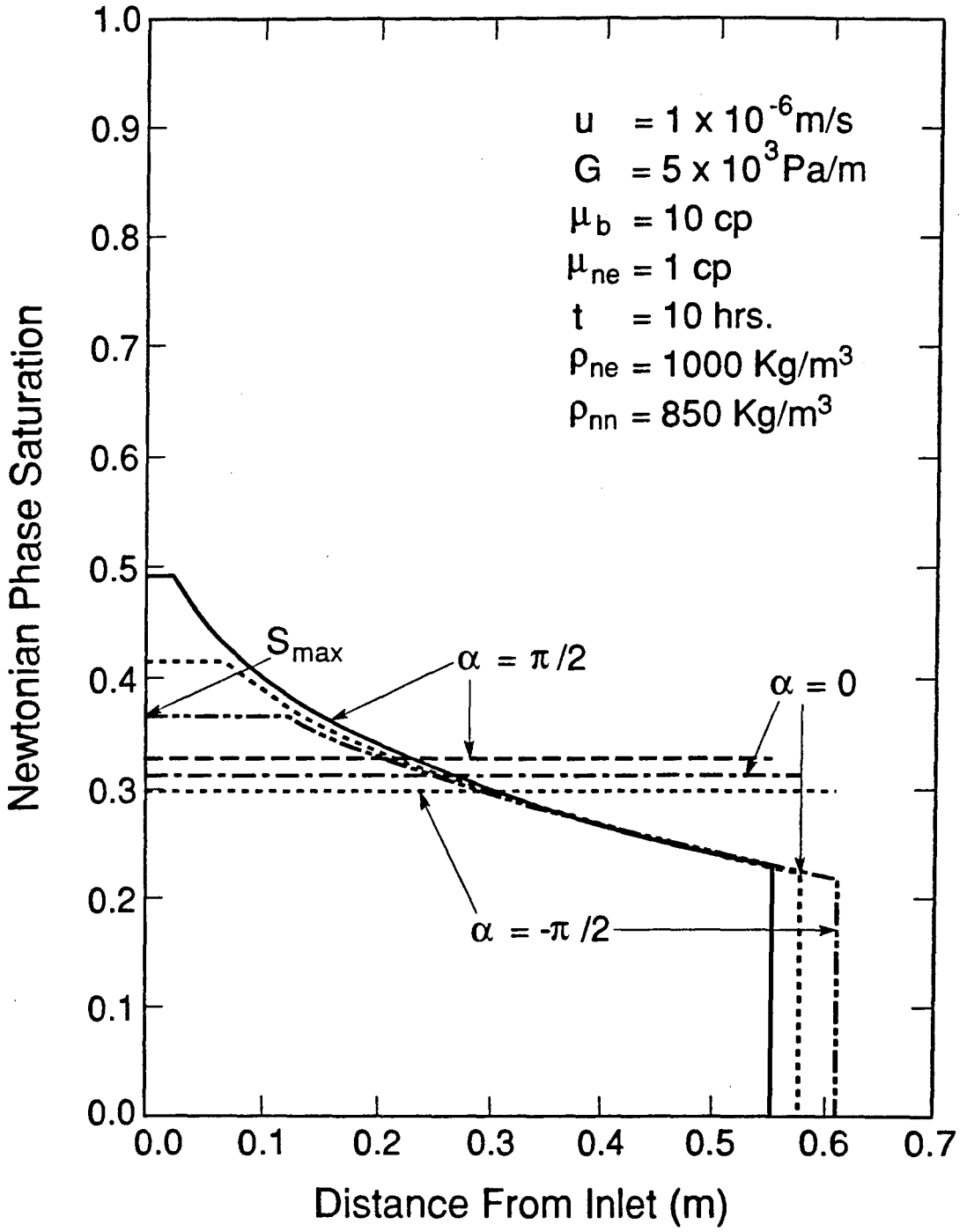

XBL 8911-7876
T.I.D. Illus. 88

Figure 7.16 Newtonian Phase Saturation Distributions, Effects of Gravity on Displacement Efficiency of a Bingham Fluid by a Newtonian Fluid.

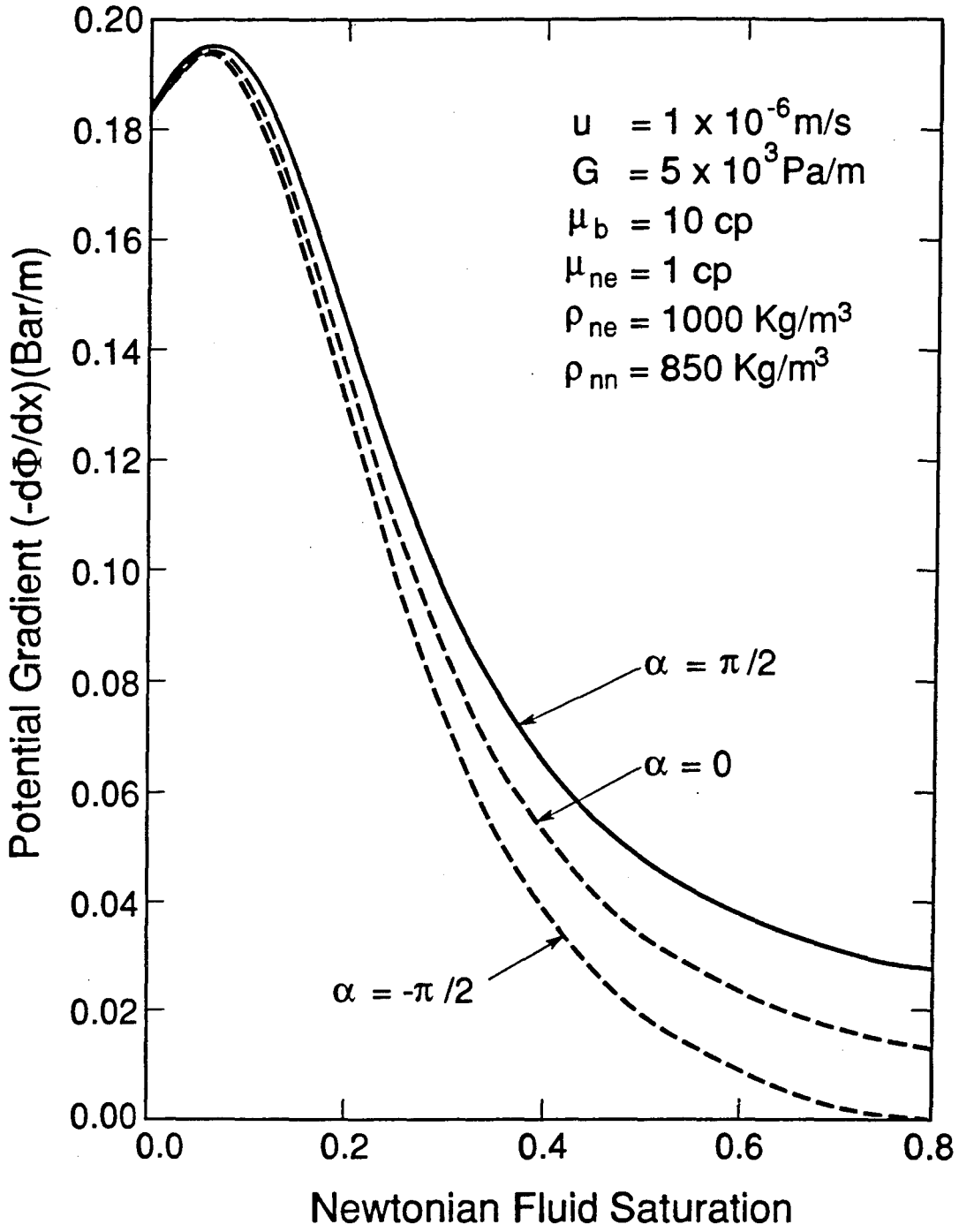

Figure 7.17 Effects of Gravity on Bingham Phase Apparent Viscosities.

best displacement performance is obtained by the upward flow calculation. Since the gravity resists the upward flow of the heavier displacing phase, the flow potential gradient must be larger in order to maintain the same flow rate, as shown in Figure 7.17. Consequently, a decrease in the apparent viscosity of the Bingham fluid for upward flow as the flow potential gradient increases results in a better sweep efficiency.

A more significant effect of gravity can be found if a gas phase with density $\rho_{ne} = 10\ kg/m^3$ is used to displace a heavier Bingham fluid. The results are shown in Figures 7.18 and 7.19. It is obvious that the best displacement is given by the downward injection under the gravity effect for this case. Of course, this is a very poor situation for application of the theory because gas is a very compressible fluid, but it dose give us some approximate insight for the displacement.

7.3.4 Conclusions

In summary, the fundamental feature of immiscible displacement involving a Bingham plastic fluid is that there exists an ultimate displacement saturation, which is essentially determined by the minimum pressure gradient G and the flow rate. Once the saturation approaches the ultimate saturation in the formation, no improvement can be obtained, regardless of how long the displacement lasts for a given operating condition. A simple way to gain a better sweep efficiency is to increase injection rates, then the apparent viscosity of the displaced Bingham fluid can be reduced. Gravity may have a significant effect on the displacement process if the difference in density of the two fluids is large. For a given flow rate, a better displacement can also be obtained by using gravity to increase the flow potential gradient in the flow direction.

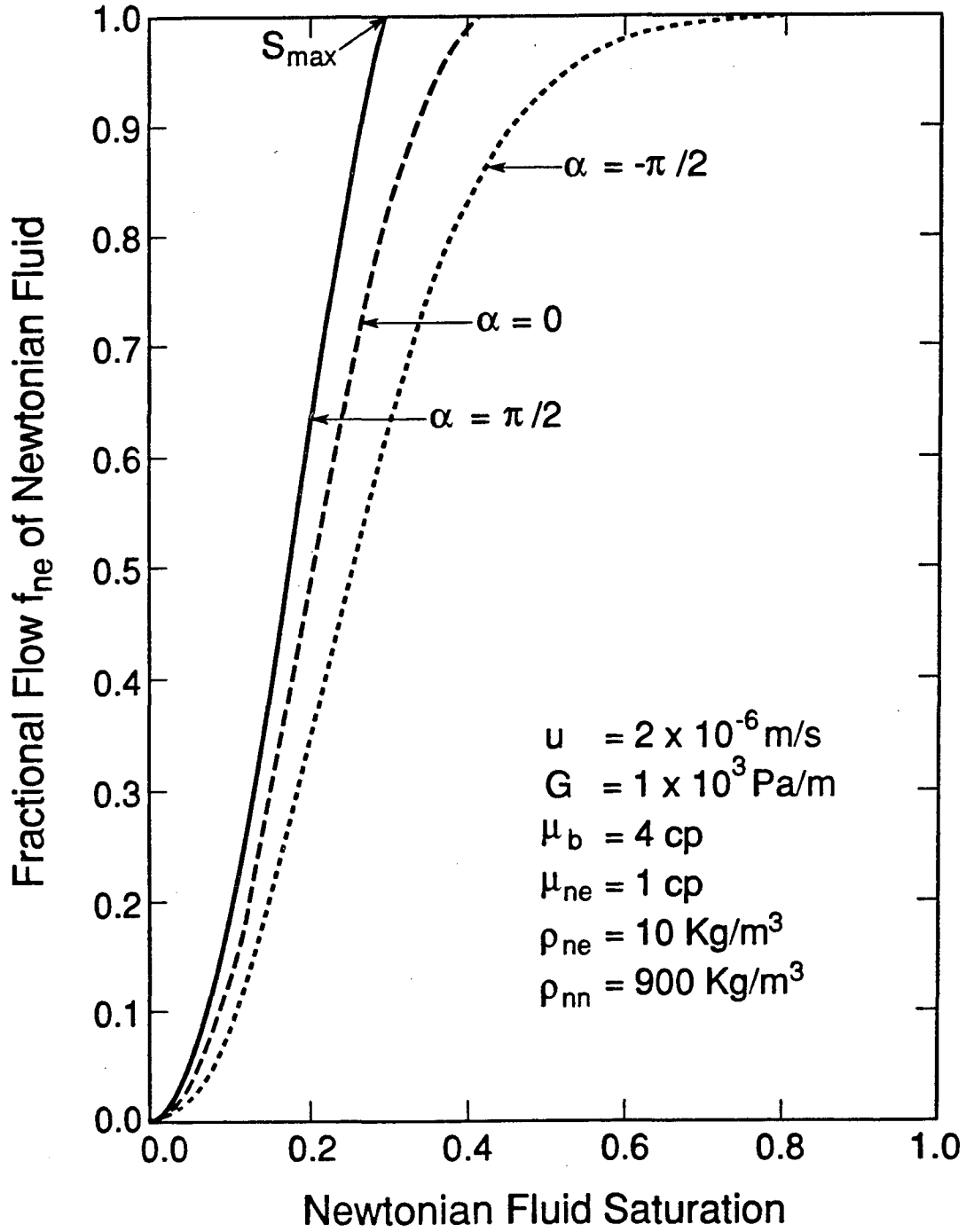

XBL 8911-7877
T.I.D. Illus. 88

Figure 7.18 Fractional Flow Curves for a Bingham Fluid Displaced by a Gas, Effects of Gravity.

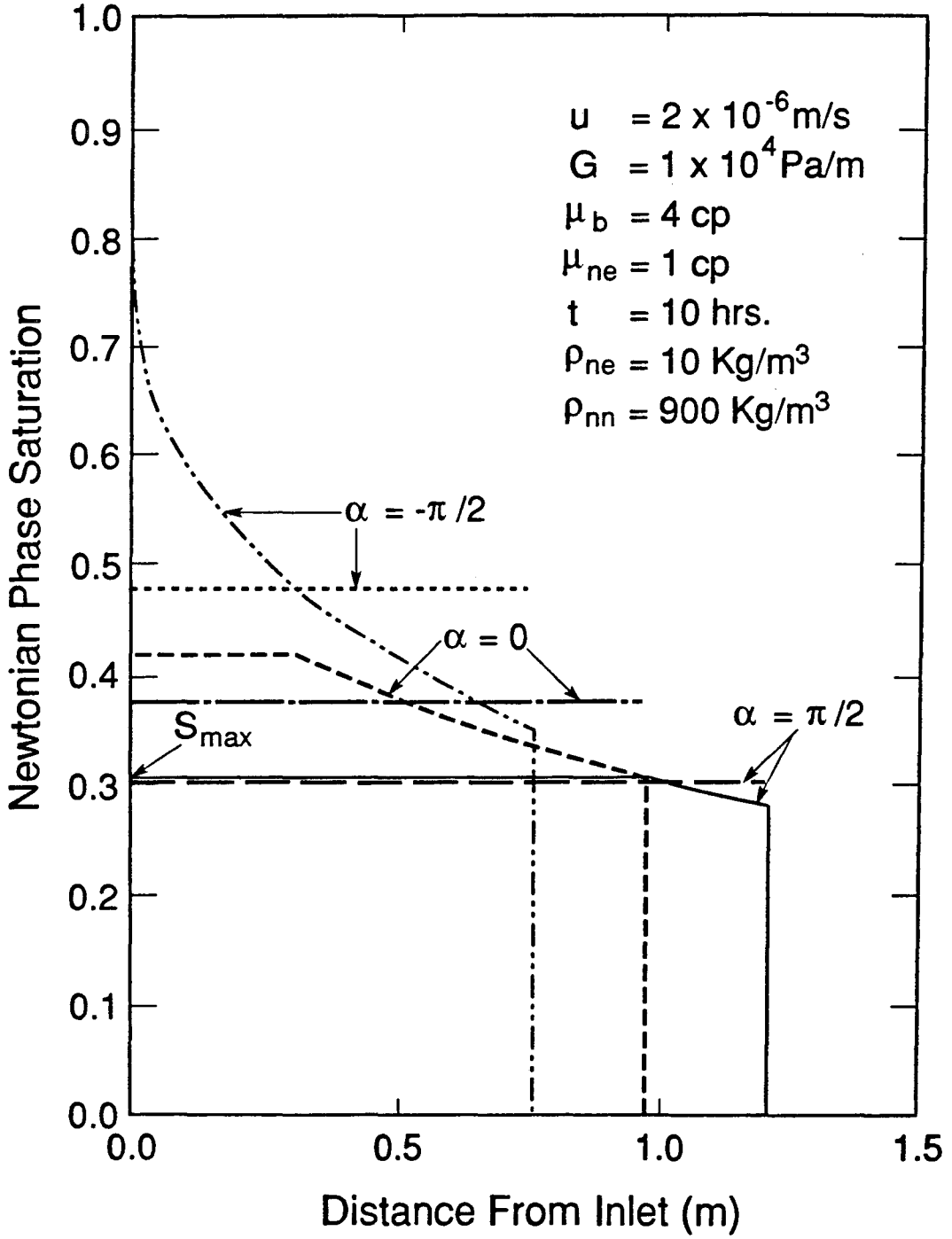

Figure 7.19 Newtonian Phase Saturation Distributions, Effects of Gravity on Displacement Efficiency of a Bingham Fluid by a Gas.

Chapter 8
Numerical Studies of Transient Flow of a Single-Phase Power-Law Non-Newtonian Fluid

8.1 Introduction

As reviewed in Chapter 2, considerable progress has been made since the early 1960's in understanding the flow of a single-phase power-law non-Newtonian fluid through porous media. Among many researchers, Odeh and Yang (1979), Ikoku and Ramey (1979) made the major contributions to the analysis of flow behavior and well tests of power-law fluids in porous media. By using a linearization assumption that there exists a steady-state viscosity profile in the reservoir, as given by Equation 2.33, they obtained approximate analytical solutions. Based on these solutions, a number of analytical and numerical methods have been developed to interpret well testing data during injectivity and falloff tests of power-law fluids.

Vongvuthipornchai and Raghavan (1987a) examined the approximate solutions by Odeh and Yang, and Ikoku and Ramey, and found that the solutions would give large errors in analyzing pressure falloff behavior when the power-law index $n < 0.6$. It has been found from laboratory experiments and field tests that the in-situ rheological properties of polymer solutions in reservoirs may be quite different from the laboratory-measured values (Castagno et al., 1984; 1987). Changes in the non-Newtonian parameters of polymer solutions under reservoir condition may be caused by degradation in polymer concentration due to adsorption on the pore surface, or by effects of different shear rate distributions for flow through different pore geometries. In general, the two parameters, power-law index, n, and the consistency coefficient, H, are both unknowns in a well testing problem with a power-law fluid injection. Therefore, the conditions for

the application of their methods may not be satisfied, and a direct use of the transient pressure analysis methods available for power-law fluid flow may result in significant errors in the predicted fluid and formation properties.

The flow of power-law fluids in fractured media is of interest in many applications, such as in EOR operations by polymer-flooding in naturally fractured petroleum reservoirs, or in the use of foam as a blocking agent in a fractured medium for underground energy and waste storage purposes. Very little research has been published on the flow of non-Newtonian fluids through fracture systems. In the petroleum literature, Luan (1981) extended the work of Ikoku and Ramey (1979) to the flow problem of power-law fluids in naturally fractured reservoirs (Warren and Root, 1963). He was able to obtain an approximate analytical solution by using the linearization assumption, Equation 2.33, for the fracture system and a constant viscosity for the power-law fluid in calculating interporosity flow between matrix and fracture.

Pseudoplastic fluid flow in porous media shows more complicated behavior than that predicted by the power-law. It has been observed in many laboratory experiments that any pseudoplastic fluid exhibits Newtonian behavior at high or low shear rates (Savins, 1969; Fahien,1983, Christopher and Middleman, 1965). Therefore, a more realistic rheological model, such as the Meter model, for general pseudoplastic fluids (Meter and Bird, 1964), should be used in further studies of power-law fluid flow through porous media. It should be possible to obtain a more comprehensive look at transport phenomena including Newtonian behavior at very high and very low shear rates during a pseudoplastic fluid flow in porous media.

This chapter presents the following numerical studies: 1) well testing analysis during a power-law fluid injection; 2) transient flow of a power-law fluid through a fractured medium; and 3) transient flow of a general pseudoplastic non-Newtonian fluid, described by the Meter model, through a porous medium. The numerical simulator, outlined in Chapter 4, is used here to simulate single phase non-Newtonian flow.

8.2 Well Testing Analysis of Power-Law Fluid Injection

The transient pressure analysis technique recommended in this work is a combination of the existing analytical method with numerical simulation. First, a log-log plot of the observed pressure increase at the wellbore versus the injection time is used to obtain an approximate value of n. The long time approximate analytical solution (Ikoku and Ramey, 1979) is

$$\log\left[P_{wf}(t) - P_i\right] = \left[\frac{1-n}{3-n}\right]\log(t) + \log\left[\frac{\left[\frac{Q}{2\pi h}\right]^{\frac{n+1}{3-n}}\left[\frac{\mu_{eff}}{K}\right]^{\frac{2}{3-n}}\left[\frac{(3-n)^2}{n\phi C_t}\right]^{\frac{1-n}{3-n}}}{(1-n)\,\Gamma\left[\frac{2}{3-n}\right]}\right] \tag{8.1}$$

where $P_{wf}(t)$ is the wellbore flowing pressure; P_i is the initial constant pressure in the formation; h is the thickness of the formation; Q is a constant volumetric injection rate; C_t is total system compressibility; and μ_{eff} is defined in Equation 2.14.

Equation 8.1 indicates that at long injection times, a graph of log $(P_{wf} - P_i)$ versus log (t) yields a straight line with a slope

$$m' = \frac{1-n}{3-n} \tag{8.2}$$

which can be used to obtain a first-order approximation for n. The intercept at t = 1 second, ΔP_1, can give the effective mobility λ_{eff} from,

$$\lambda_{eff} = \frac{K}{\mu_{eff}} = \frac{\left[\frac{Q}{2\pi h}\right]^{\frac{n+1}{2}}\left[\frac{(3-n)^2}{n\phi C_t}\right]^{\frac{1-n}{2}}}{\left[\Delta P_1\,(1-n)\,\Gamma\left[2/(3-n)\right]\right]^{\frac{3-n}{2}}} \tag{8.3}$$

The modified Darcy's law for this horizontal radial flow can be obtained by substituting Equation 3.11 into 3.7,

$$u = \left[\frac{K}{\mu_{eff}} \left[-\frac{\partial P}{\partial r} \right] \right]^{1/n} \tag{8.4}$$

Therefore, as long as the straight line occurs in the log-log plot of a well test, the power-law index n and the effective mobility λ_{eff} can be calculated from the slope and intercept of the straight line if the porosity and compressibility are known. Then, the problem is well-posed for a numerical calculation since the parameters in Equation 8.4 are defined. The observed pressure data can be matched by the numerical calculation using the value of n, and λ_{eff} obtained as an initial guess.

An injection test example is given here to illustrate the approach used. The well test data used are from the published data of a simulated polymer injection test (Ikoku and Ramey, 1979), and are in Table 8.1. The pressure responses, $\Delta P = (P_{wf} - P_i)$, versus time are shown by the circles in Figure 8.1, which yields a straight line with a slope $m' = 0.25$. Then

$$m' = \frac{1-n}{3-n} = 0.25$$

and this gives, $n = 0.33$. Also, the intercept, $\Delta P_1 = 4.64 \times 10^5$ Pa, can be determined at t = 1 second, from Figure 8.1. Ikoku and Ramey obtained the following effective mobility,

$$\lambda_{eff} = 6.37 \times 10^{-8} m^{1.33}/Pa \cdot s$$

Since $n = 0.33 < 0.60$, these results need to be checked according to Vongvuthi-pornchai and Raghavan (1987a). When the same parameters are input into the numerical model, the resulting pressure increase is given by the lower solid line on Figure 8.1. This would be the wellbore injection behavior if the fluid and formation flow properties were those determined above. The difference in the pressure responses shown in Figure 8.1 is 22 % and indicates that the prediction by the approximate analytical solution introduces

Table 8.1

Parameters for Well Testing Analysis of Polymer Injection Test

Initial Pressure	$P_i=3\times10^6$Pa
Initial Porosity	$\phi_i=0.15$
Formation thickness	h=4.877m
Total Compressibility	$C_t=9.674\times10^{-10}Pa^{-1}$
Production Rate	$Q=1.84\times10^{-4}m^3/s$
Power-Law Index	n=0.33
Wellbore Radius	$r_w=0.0762$m

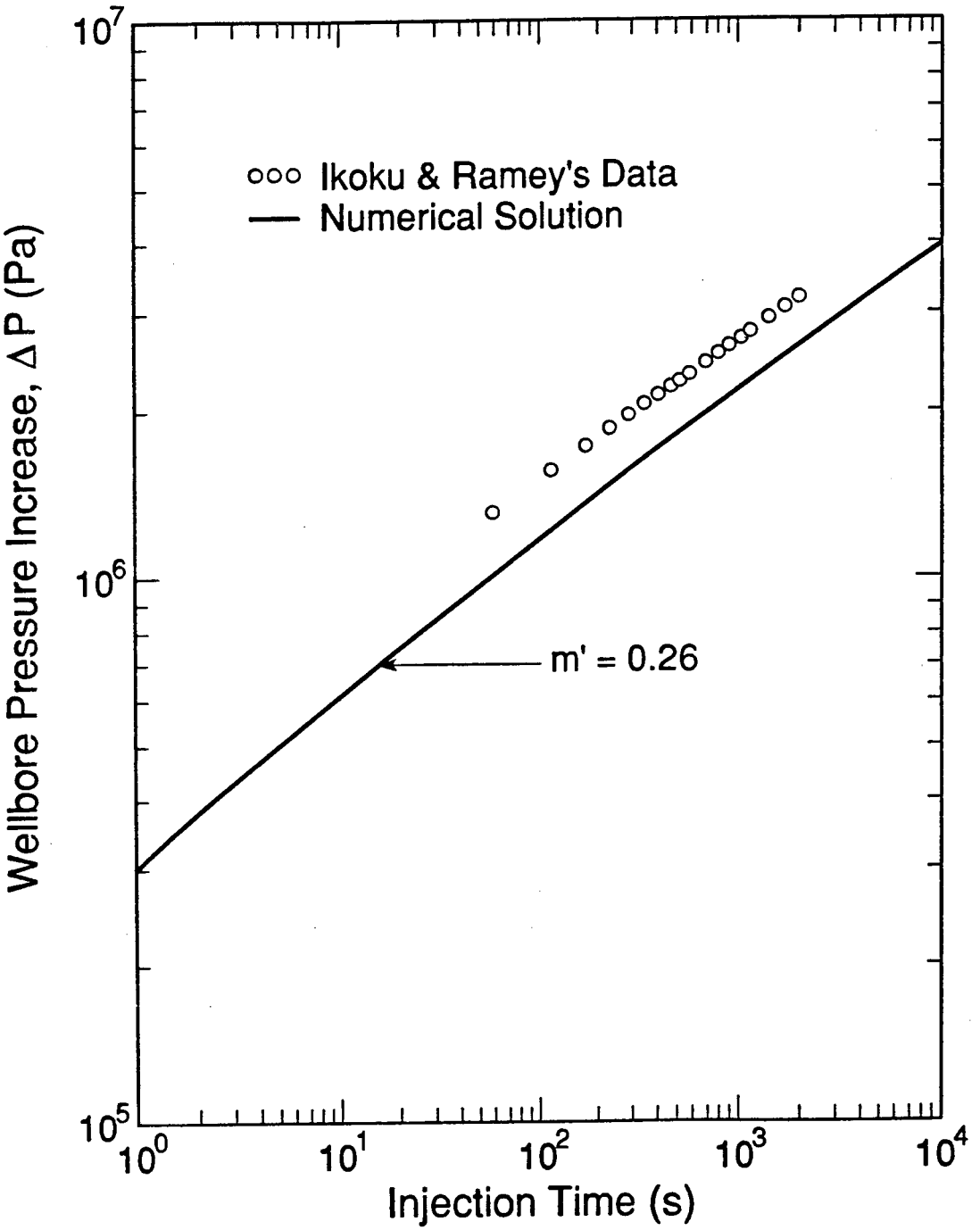

XBL 8912-7911
T.I.D. Illus.88

Figure 8.1 Logarithm of Pressure Increase versus Logarithm of Injection Time for a Power-Law Fluid Injectivity Test (data from Ikoku and Ramey).

a very large error for this test. However, the straight lines do develop for both curves in Figure 8.1, and are almost parallel with each other. Therefore, the slope of the straight line in the approximate solution gives a good approximation of the power-law index, n. we shall use n = 0.33, and adjust the effective mobility value to match the test data. The numerical results for two more test runs are shown in Figure 8.2, which are in good agreement with those from the polymer injection example. The effective mobility used in this calculation is

$$\lambda_{eff} = 4.53\times10^{-8} m^{1.33}/Pa\cdot s$$

This means that the actual effective mobility is only 70 % of that determined by Ikoku and Ramey, and indicates that the approximate analytical solution introduces an error of 40 % in the calculation of the effective mobility, λ_{eff}.

The next example is a field test that was performed on biopolymer injection (Odeh and Yang, 1979). The pressure transient data are plotted on Figure 8.3 and formation properties are listed in Table 8.2. The slope of the log-log straight line part of the wellbore pressure increase versus injection time in Figure 8.3 is determined as $m' = 0.21$, and then, $n = 0.46$. The intercept, $\Delta P_1 = 6.236\times10^5$ Pa is found at a time of 1 second. A tentative effective mobility can be calculated by Equation 8.3 as

$$\lambda_{eff} = \frac{\left[\frac{8.059\times10^{-4}}{2\times\pi\times4.419}\right]^{\frac{1+.46}{2}}\left[\frac{(3-.46)^2}{.46\times.22\times2.176\times10^{-9}}\right]^{\frac{1-.46}{2}}}{\left[6.235\times10^5\,\Gamma\left[\frac{2}{3-.46}\right]\right]^{\frac{3-.46}{2}}}$$

$$= 1.514\times10^{-8}(m^{1.46}/Pa\cdot s)$$

Using these values of n and λ_{eff}, and the parameters in Table 8.2, we have the pressure responses at the wellbore as shown by the bottom solid curve of Figure 8.4. Obviously, this result is unacceptable with an error in pressure increase by a factor of 5, when compared with the actual field data. However, the log-log straight line of the

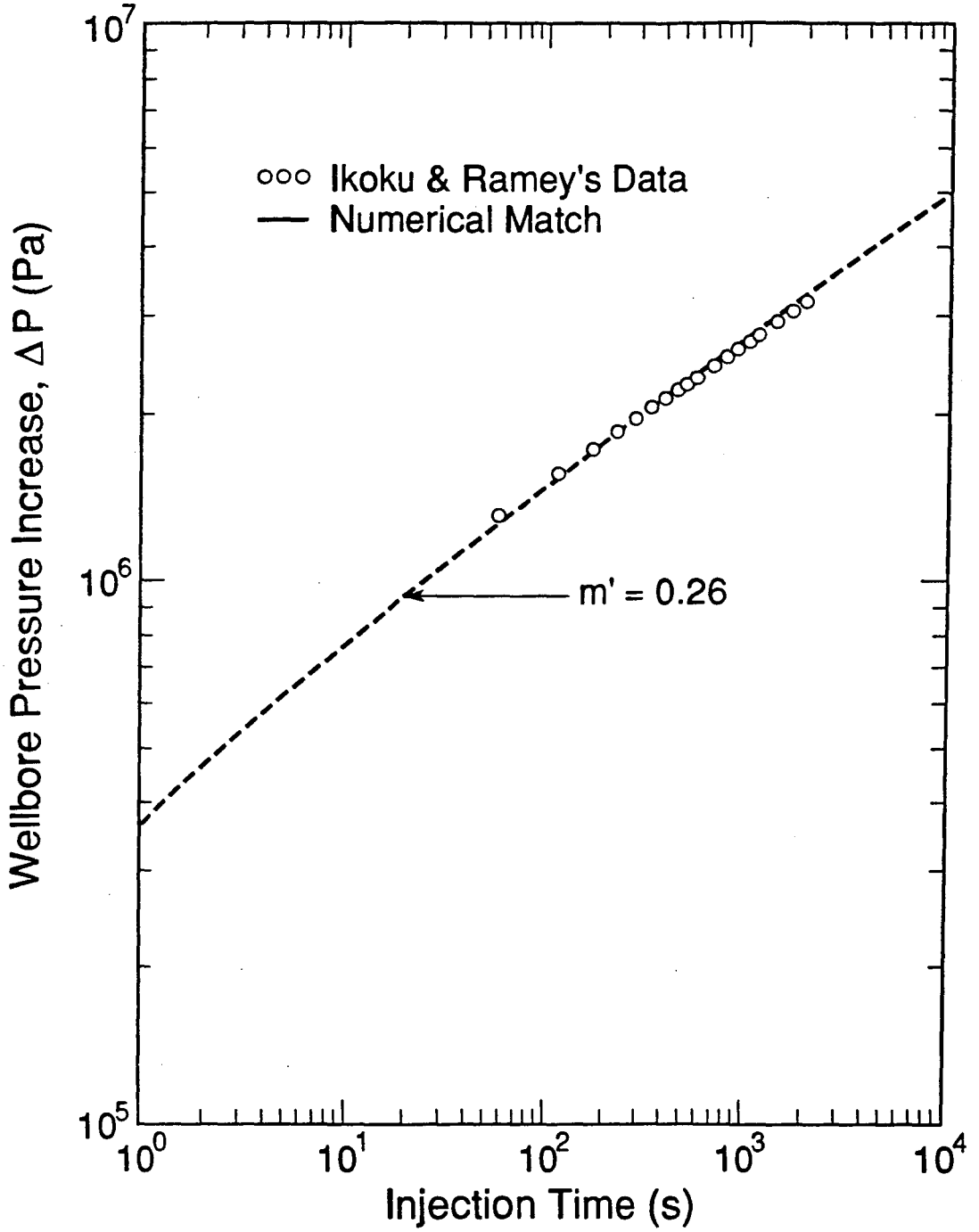

XBL 8912-7912
T.I.D. Illus.88

Figure 8.2. Numerical Matching Curve of Pressure Increase versus Injection Time for a Power-Law Fluid Injectivity Test (data from Ikoku and Ramey).

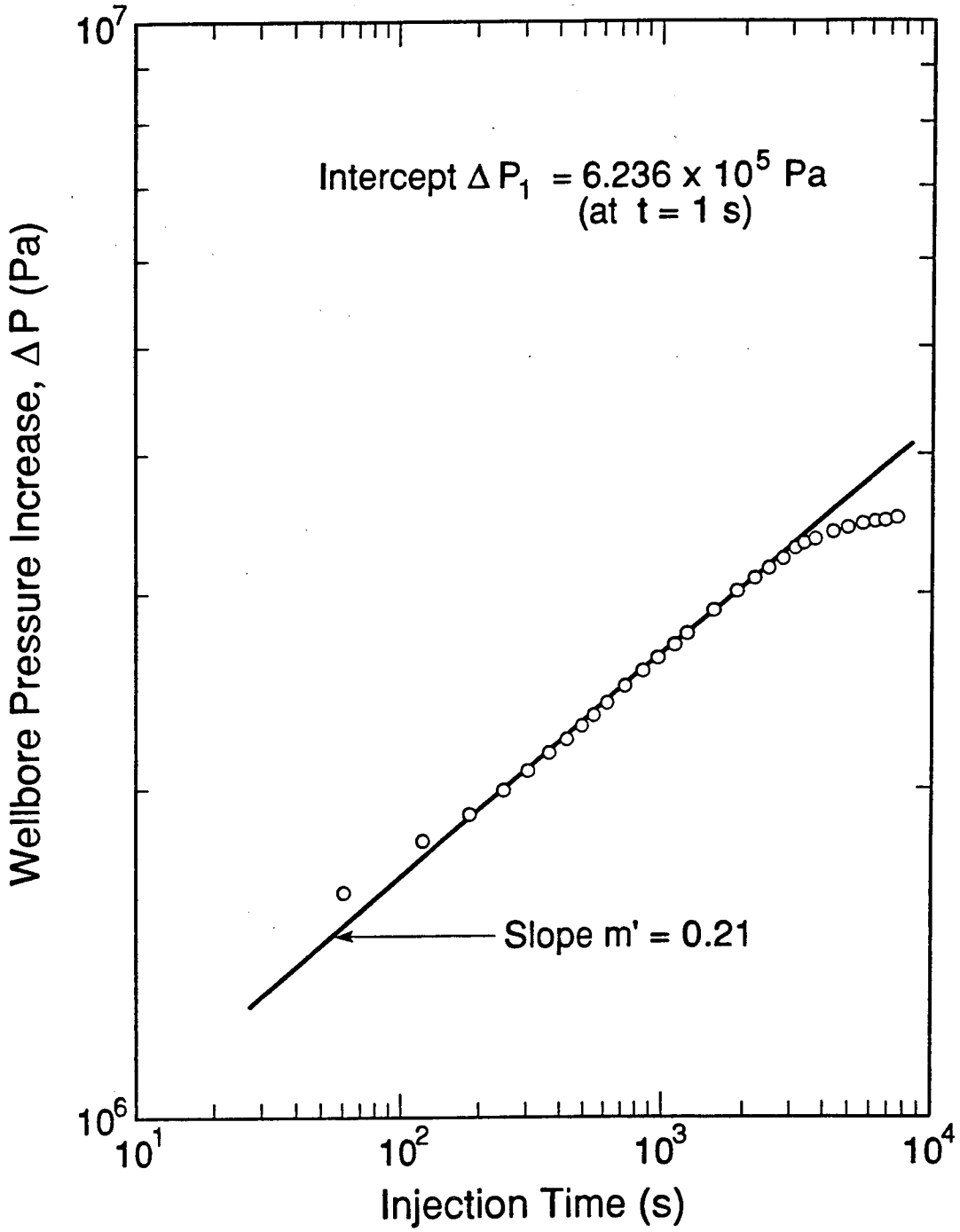

Figure 8.3 Logarithm of Pressure Increase versus Logarithm of Injection Time for a Biopolymer Injectivity Test (data from Odeh and Yang).

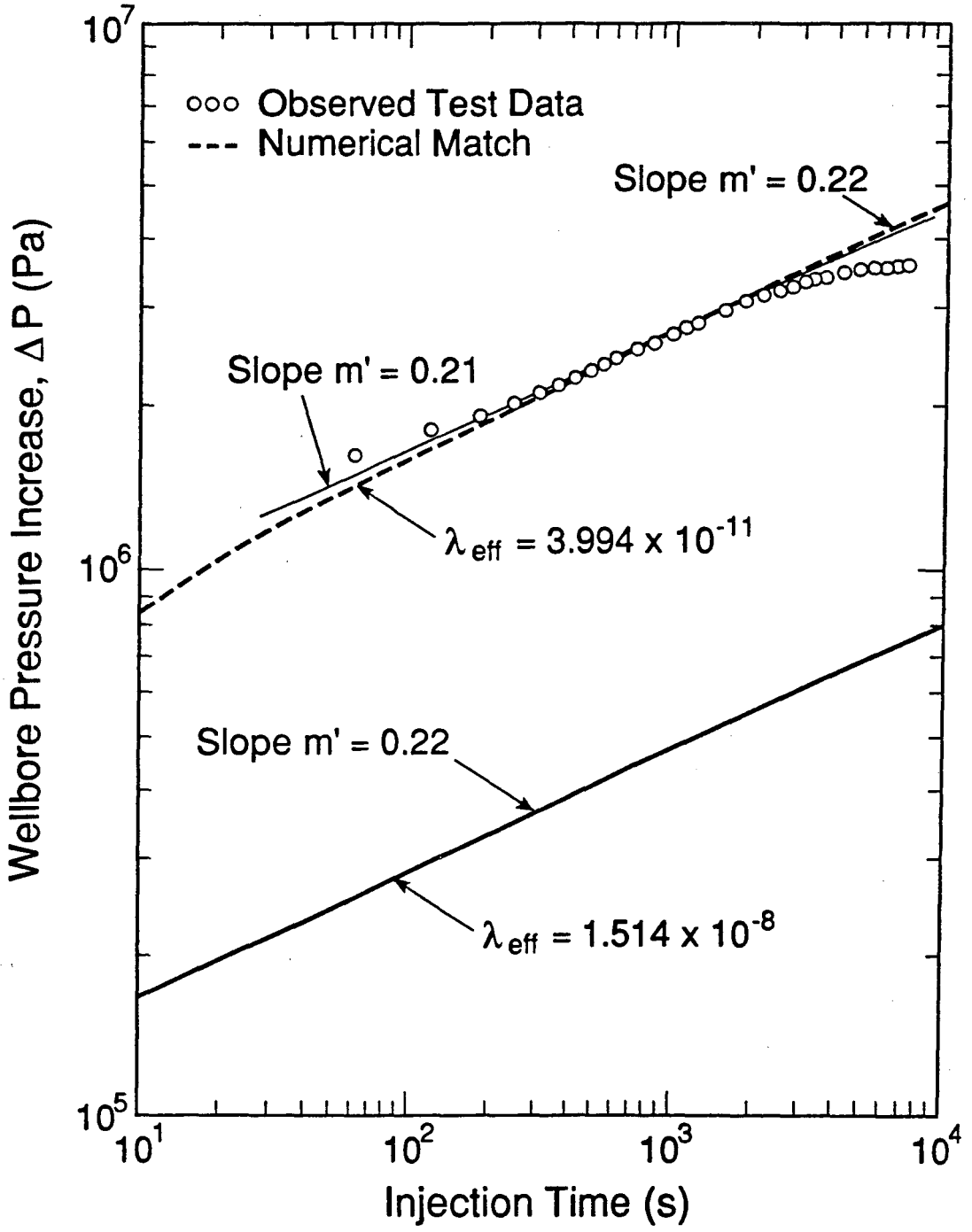

XBL 8912-7914
T.I.D. Illus.88

Figure 8.4 Numerical Matching Curve of Pressure Increase versus Injection Time for a Biopolymer Fluid Injectivity Test (data from Odeh and Yang).

Table 8.2
Parameters for Well Testing Analysis of Biopolymer Injection

Initial Pressure	$P_i=2.606\times10^{6}Pa$
Initial Porosity	$\phi_i=0.22$
Formation thickness	h=4.419m
Total Compressibility	$C_t=2.176\times10^{-10}Pa^{-1}$
Production Rate	$Q=8.059\times10^{-4}m^3/s$
Permeability	$K=8.684\times10^{-14}m^2$
Wellbore Radius	$r_w=0.0762m$

pressure-time curve, with a slope $m' = 0.22$ is approximately parallel with that of the observed curve where the slope $m' = 0.21$. Therefore, the long time asymptotic solution by Ikoku and Ramey again gives a good approximation for the power-law index n. We shall use n = 0.46, and adjust λ_{eff}. In four more test runs, the result is shown by the dashed curve in Figure 8.4, and this yields an effective mobility $\lambda_{eff} = 3.99 \times 10^{-11}$, and a slope $m' = 0.22$. For this case, the permeability was known, K = 88 md, from a core analysis. Then, if the power-law model, Equation 3.11, holds for flow in the reservoir, we can calculate the consistency, $H = 0.019$ Pa·s$^{.46}$. These results further illustrate the errors that can occur in the analysis of field data using the approximate analytical solutions of Ikoku and Ramey (1979), Odeh and Yang (1979).

8.3 Transient Flow of a Power-Law Fluid through a Fractured Medium

A numerical study of the flow of a power-law non-Newtonian fluid in a fractured medium is performed in order to obtain some insight into its flow behavior. We shall assume the standard model of parallel smooth sides for the fractures (see Figure 8.5). This is the simplest model, and is often used to approximate more complicated fracture networks in reservoirs. The rheological model for a power-law fluid, Equation 3.11, is used for flow in the matrix system. However, because of the two-dimensional nature of flow through a fracture, the modified Darcy's law, such as Equation 2.13 derived from the capillary model, cannot be employed directly in fracture flow. Therefore, a modified Darcy's equation for a power-law fluid in a parallel-plate fracture is derived in Appendix C and is used in this chapter. The fracture model used in this study is given in Figure 8.5 for a horizontal system of parallel-plate fractures. It can be shown (see Appendix C) that the modified Darcy's law for the flow of a power-law fluid in fractures can also be described by Equation 3.7. However, we may use the same form of the viscosity

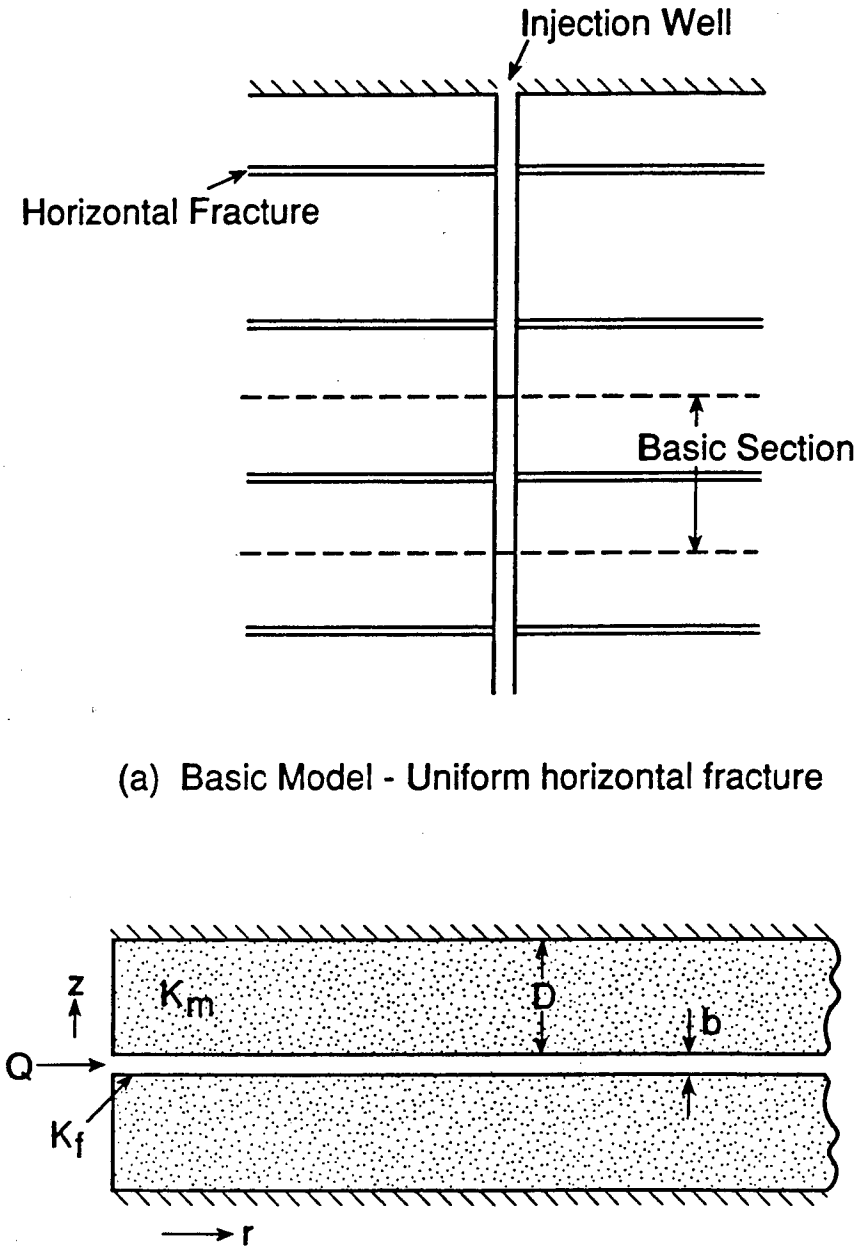

Figure 8.5 Schematic of a Horizontal Fracture System.

function as in Equation 3.11. Here, μ_{eff} is replaced by

$$\mu_{eff}^{*} = H\left[\frac{2n+1}{3n}\right]^{n}\left[\frac{b}{2K_f}\right]^{n-1} \tag{8.5}$$

where b is aperture of the fracture, and K_f is the effective fracture permeability used in the Darcy's equation, defined by Equation C.6.

Flow through fractured media is of fundamental importance in many subsurface systems, such as the exploitation of hydrocarbon and geothermal energy, and underground waste storage in naturally fractured reservoirs. The study of fluid flow in naturally fractured reservoirs has been a challenging task, and considerable progress has been made since the 1960's (Barenblatt et al., 1960; and Warren and Root, 1963). Most studies of flow in fractured reservoirs use the double-porosity concept and consider that global flow occurs primarily through the high-permeability, low-effective-porosity fracture system surrounding blocks of rock matrix. The matrix blocks contain the majority of the formation storage volume and act as local source or sink terms connected to the fracture system. The fractures are interconnected and provide the main fluid flow path to injection or production wells.

A very important characteristic of a double-porosity system is the nature of the fluid exchange between the two constitutive media, the so-called interporosity flow. The conventional treatment of the interporosity flow between matrix and fractures resorts to an approximation that a quasi-steady state exists in the matrix elements at all times, with the interporosity flow rate being proportional to the difference of the average pressures in matrix and fractures. The quasi-steady assumption was originally proposed by Barenblatt et al. and Warren and Root and has been used by many subsequent authors. For isothermal single phase Newtonian fluid flow, this assumption was shown to give accurate results by Kazemi (1969) using a numerical model. However, for more complicated flow problems, such as those involving heat exchange between matrix and fractures, and

for multiple phase flow with strong mobility effects, transient interporosity flow conditions may last a long time (decades) before reaching quasi-steady state. Under these conditions, it is necessary to treat the flow inside the blocks and at the block-fracture interface as a transient process. Pruess and Narasimhan (1982, 1985) developed a "multiple interacting continua" technique (MINC), in which fully transient flow in the matrix and between matrix blocks and fractures is described by a numerical method. Using appropriate subgridding in the matrix blocks, it is possible to resolve the details of the gradients (of pressure, temperature, etc.) which drive the interporosity flow. The MINC-method has been successfully applied to a number of geothermal reservoir (Pruess, 1983a) and multiple phase flow problems (Wu and Pruess, 1986).

For the flow of a single phase power-law fluid in a fractured medium, the apparent viscosity of the fluid inside the matrix and at the matrix-fracture interfaces depends on the pore velocity, or pressure gradient, as described by Equation 3.11. One should expect a strong effect of the non-linearity in non-Newtonian viscosity on flow behavior. Therefore, the MINC-method will be used in simulating the interporosity flow of a power-law fluid. Also, a comparison of the MINC-calculations with the conventional double-porosity results is given here to demonstrate that the double-porosity approximation is generally not suitable in simulating non-Newtonian fluid flow in fractured media.

Let us first consider a simple case. A power-law fluid is injected into a horizontal fracture system with impermeable matrix blocks such that the system is equivalent to a porous medium. Pressure responses for injection only into the fracture system and for injection into the porous medium can be compared. The equivalent porosities and permeabilities for the fractured and porous systems are taken to be the same, respectively (see Table 8.3). The only differences in the input parameters for the two runs are the viscosity functions, as given in Equations 3.11 and C.8, and their dependence on the inherent effects of the distinctly different geometries of these two systems. The wellbore pressure increases $\Delta P = (P_{wf} - P_i)$ during injection of the power-law fluid are

Table 8.3

Parameters for Power-Law Fluid Injection in a Fracture System

Initial Pressure	$P_i=3\times10^{6}Pa$
Fracture Aperture	$b=2.3\times10^{-4}m$
Half Fracture Spacing	$D=0.5m$
Matrix Porosity	$\phi_m=2.3\times10^{-4}$
Effective Fracture Porosity	$\phi_f=2.3\times10^{-4}$
Matrix Permeability	$K_m=1.014\times10^{-12}m^2$
Effective Fracture Permeability	$K_f=1.014\times10^{-12}m^2$
Fluid Compressibility	$C_f=4.557\times10^{-10}Pa^{-1}$
Rock Compressibility	$C_r=5.443\times10^{-10}Pa^{-1}$
Initial Fluid Density	$\rho_i=972.78Kg/m^3$
Injection Rate	$Q_m=5\times10^{-3}Kg/s$
Wellbore Radius	$r_w=0.0762m$
Power-Law Index	$n=.5$
Power-Law Coefficient	$H=0.05Pa\cdot s^n$

shown in Figure 8.6. It is interesting to note that a log-log straight line also develops on the fracture flow curve after the early transient period, and its slope is $m' = 0.20$. From Equation 8.2, we can write

$$m' = \frac{1-n}{3-n} = \frac{1-0.5}{3-0.5} = 0.20$$

This indicates that the same well test analysis method, as discussed in Section 8.2, may apply to the flow of power-law fluids in purely-fractured media.

It is important to note on Figure 8.6 that a larger injection pressure is needed in order to maintain the same injection rate for flow in the porous model as in the fracture network. If a Newtonian fluid were used, the injection pressures for both systems would be exactly the same. For this particular problem, however, the flow of the power-law fluid in the porous media suffers more flow resistance than in the single fracture, even with the same equivalent porosities and permeabilities. This can be seen in Figure 8.7, which gives the apparent viscosities for the non-Newtonian fluid as it flows through either media under the same conditions. The viscosities for flow in the porous model are always higher than in the fracture. This suggests that the viscosity function, Equation 3.11 for porous media flow, cannot be extended to flow problems in fractures.

Let us now consider the flow of a power-law fluid in a fracture system where the matrix blocks are permeable. The same horizontal fracture model is used, as shown in Figure 8.5. The matrix subgridding in this numerical simulation employs the MINC-technique and is generated by a mesh generator - GMINC (Pruess, 1983b). The basic section of the horizontal fracture system is first partitioned into "primary" volume elements (or grid blocks) such as would be employed for a porous medium. The interblock flow connections are then assigned to the fracture continuum, and each primary grid block is sub-divided into a sequence of "secondary" volume elements. Here, the secondary elements are a number of horizontal layers parallel to the fracture in each primary element. The flow inside the matrix system and between matrix blocks and fractures is

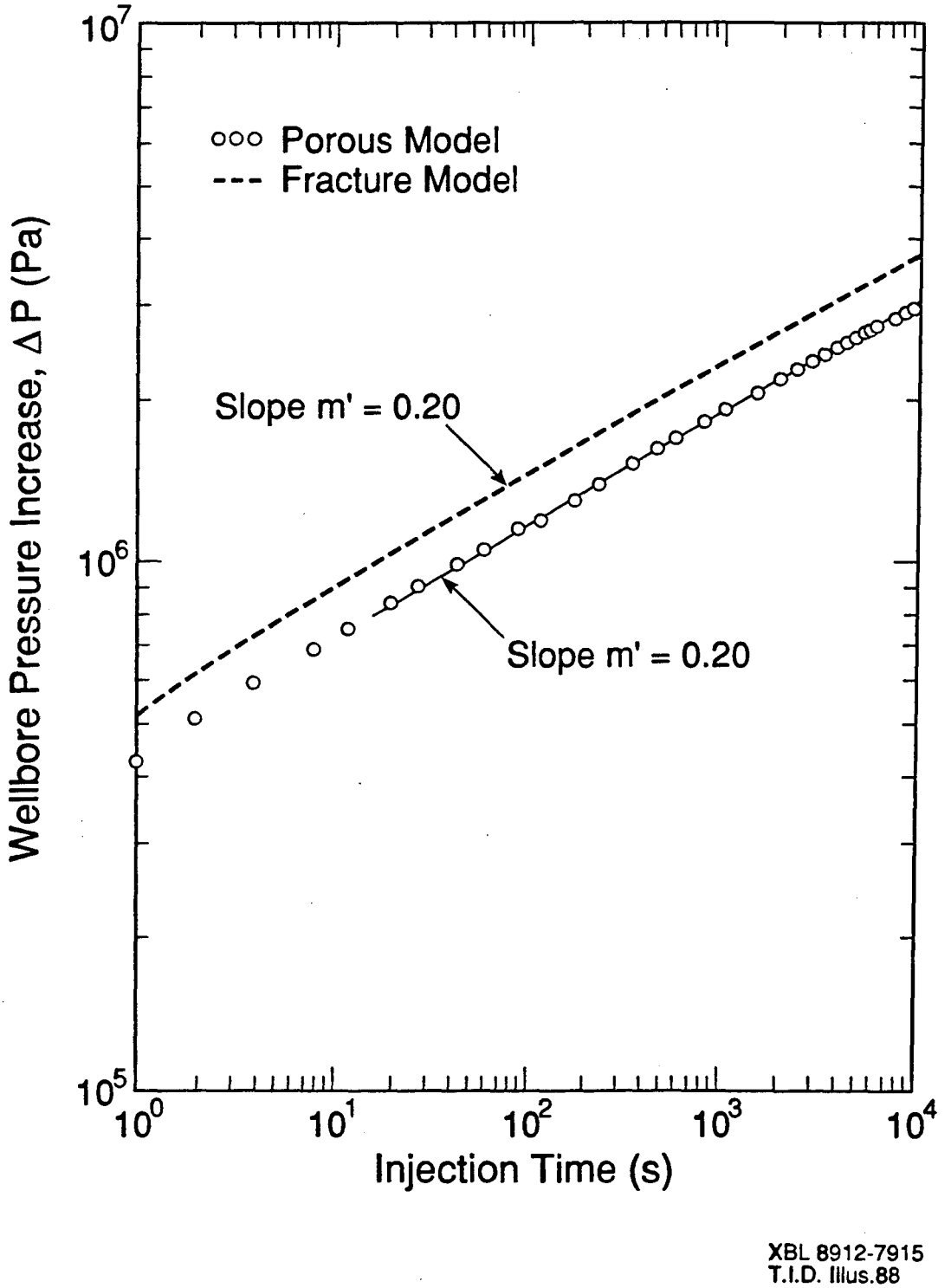

Figure 8.6 Comparison of Transient Pressures of a Pure Fracture System and an Equivalent Porous medium.

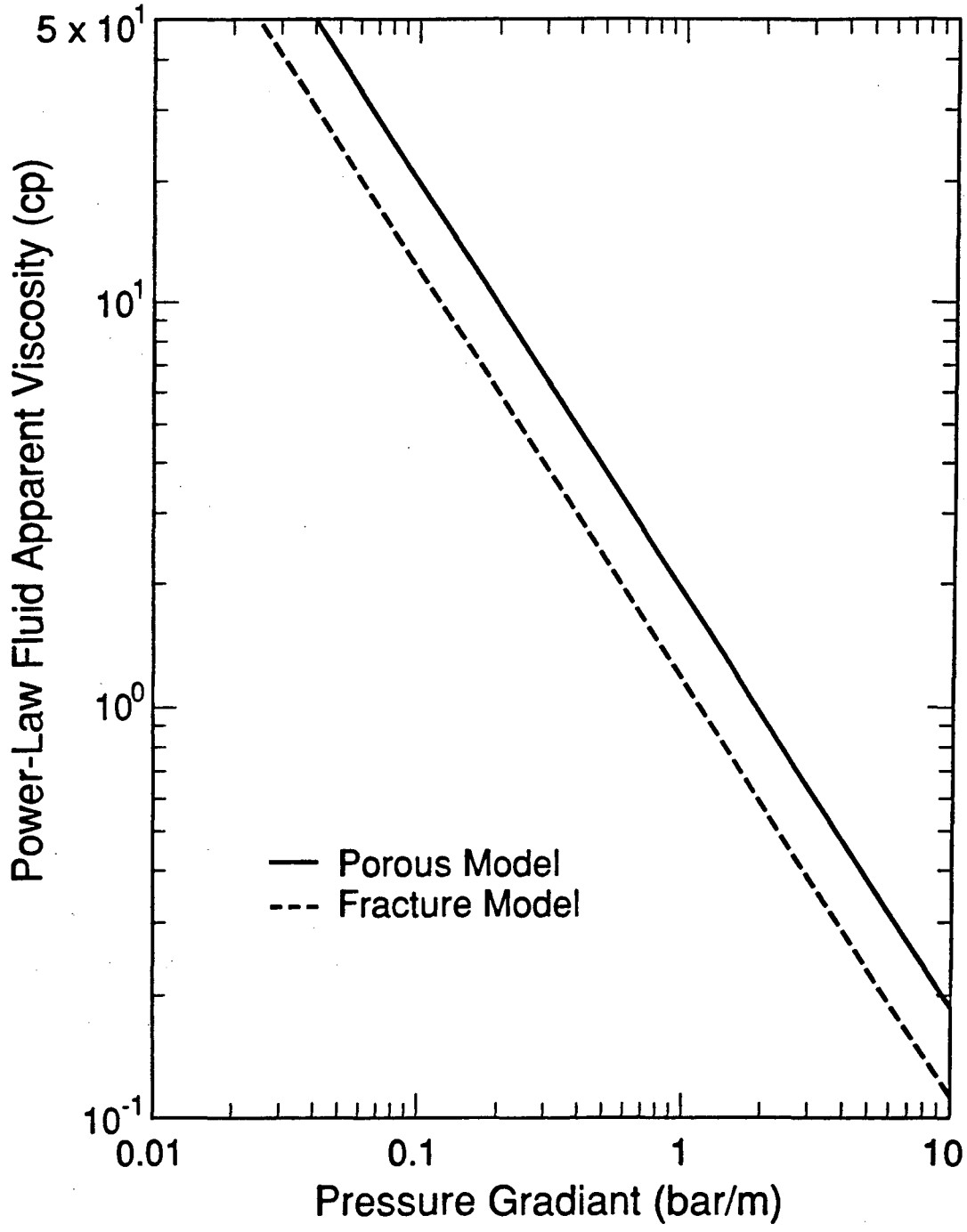

Figure 8.7 Apparent Viscosities of a Power-Law Fluid Calculated from the Porous Model and the Fracture Model.

assumed to be vertical.

The MINC-method contains the double-porosity approximation as a special case by defining only two continua in each primary grid block, representing fracture and matrix, respectively. Therefore, we can check the applicability of the double-porosity concept to the injection of a power-law fluid into a fractured reservoir. The fluid and formation parameters for this power-law fluid injection are given in Table 8.4. A comparison of wellbore injection pressures is shown in Figure 8.8, and were calculated for different levels of subgridding with 2-10 continua. The matrix block was sub-divided into equal-volume subdomains in this calculation, except the element connected with the fracture, whose volume was taken as 1 % of the total matrix volume. It is obvious that the double-porosity approximation (MINC-2) introduces larger errors during the early transient time and only approaches the correct solution at long injection times. As the number of subdivisions in the matrix system increases, the results become more accurate, and little improvement could be obtained after eight sub-domains were used. Therefore, meshes with eight sub-divisions are used in the following study. The reason the double-porosity method is inaccurate for non-Newtonian fluid flow is apparent on Figure 8.9, which gives a distribution of the pressure increases in the fractures after t = 10 seconds. When the number of subdivisions is small, the double-porosity prediction overestimates pressures in the fractures. This indicates that flow into the matrix system is underestimated by the double-porosity approximation, which treats the matrix as a single continuum with locally uniform pressure and fluid distributions. The pressure gradient and pore velocity into the matrix from this calculation are smaller than it should be, and the result is a higher viscosity for this shear-thinning fluid. This phenomenon is similar to that obtained using the double-porosity method for multiple phase flow in fractured reservoirs, as discussed by Wu and Pruess (1986). It is concluded that, in general, the double-porosity method cannot be used for the analysis of non-Newtonian fluid flow in fractured media, and some method of transient interporosity flow, such as MINC,

Table 8.4

Parameters for Power-Law Fluid Injection in a Double-Porosity System

Initial Pressure	$P_i=3\times10^{6}$Pa
Fracture Aperture	$b=2.3\times10^{-4}$m
Half Fracture Spacing	D=0.5m
Matrix Porosity	$\phi_m=0.20$
Fracture Porosity	$\phi_f=2.3\times10^{-4}$
Matrix Permeability	$K_m=9.869\times10^{-15}m^2$
Effective Fracture Permeability	$K_f=1.014\times10^{-12}m^2$
Fluid Compressibility	$C_f=4.557\times10^{-10}Pa^{-1}$
Rock Compressibility	$C_r=5.443\times10^{-10}Pa^{-1}$
Initial Fluid Density	$\rho_i=972.78Kg/m^3$
Injection Rate	$Q_m=2\times10^{-2}Kg/s$
Wellbore Radius	$r_w=0.10m$
Power-Law Index	n=.5
Power-Law Coefficient	$H=0.10Pa\cdot s^n$

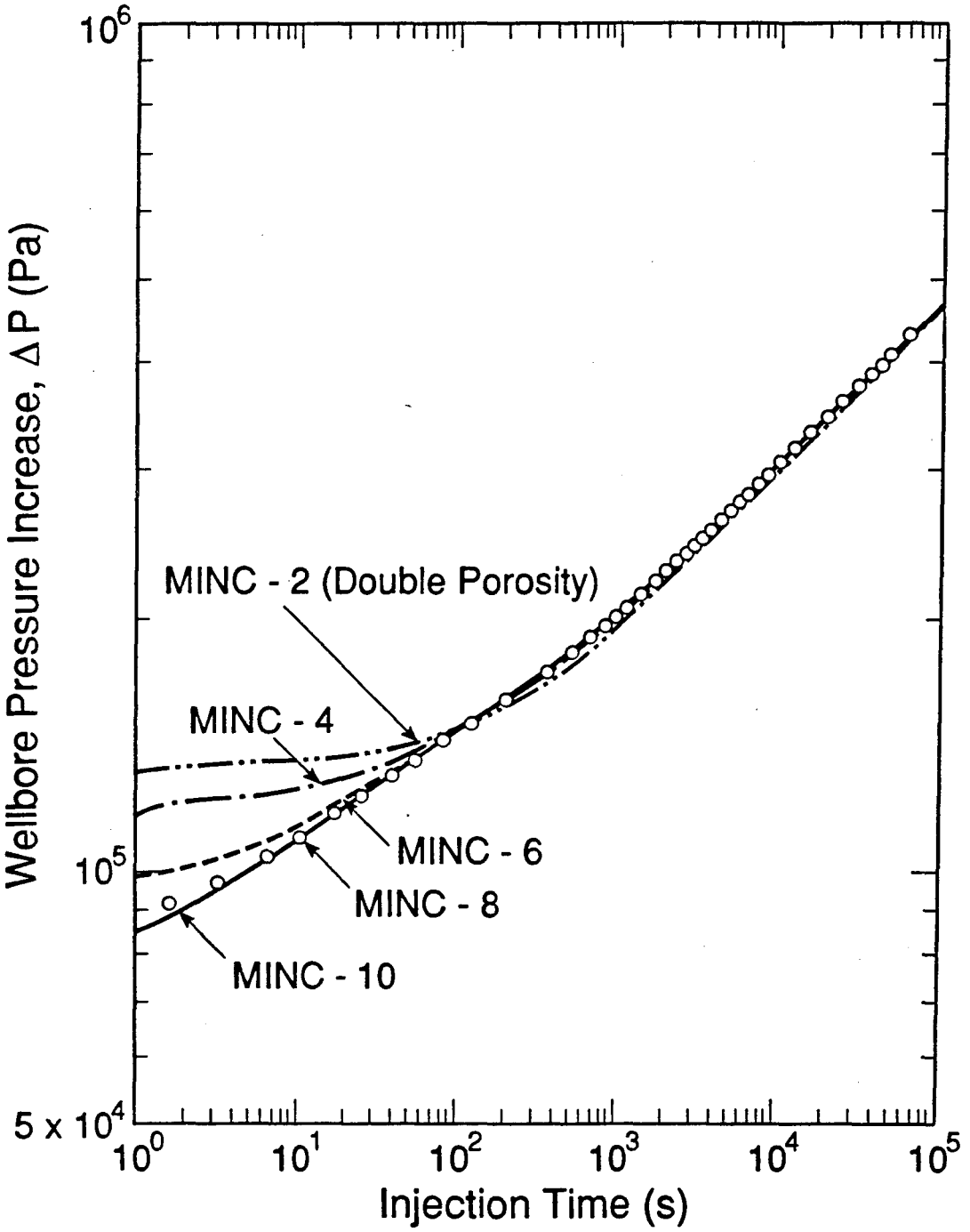

XBL 8912-7917
T.I.D. Illus.88

Figure 8.8 Transient Pressure Responses in a Double-Porosity System during a Power-Law Fluid Injection, Effects of Subdivisions of the Matrix System on Interporosity Flow.

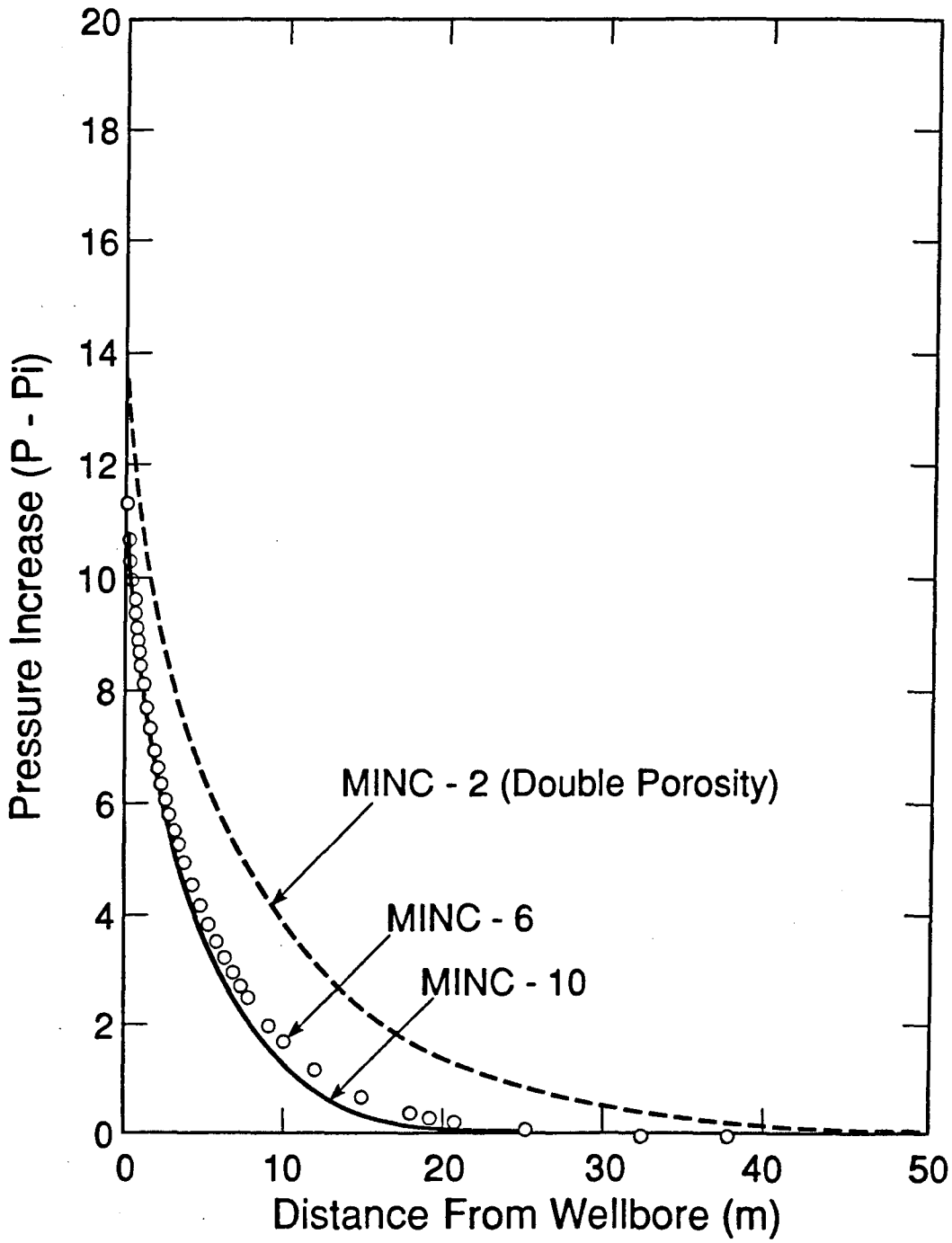

Figure 8.9 Distributions of Pressure Increases in the Fracture System for Different Subdivisions of the Matrix System.

will have to be utilized instead.

As pointed out by Warren and Root (1963), the flow of a Newtonian fluid in fractured reservoirs is indicated on semi-log plots of pressure buildup by two parallel straight lines. This enables one to determine two parameters, the storage coefficient, ω, and the interporosity flow coefficient, λ, which are sufficient to characterize a fractured medium in double-porosity approximation. We shall use the same two parameters to discuss the flow behavior of a power-law fluid in a fractured medium. The storage coefficient is defined (Warren and Root, 1963) as,

$$\omega = \frac{\phi_f C_f}{\phi_m C_m + \phi_f C_f} \tag{8.6}$$

where C_f and C_m are total compressibilities of fracture and matrix systems, respectively. The interporosity coefficient is defined (Lai, 1985) as,

$$\lambda = \frac{r_w^2 K_m}{K_f D^2} \tag{8.7}$$

The characteristic curves of transient pressure behavior for power-law fluid flow in this idealized fracture model, calculated with MINC-8 subgridding, are given in Figures 8.10 and 8.11. The fluid and formation parameters in these calculations are summarized in Table 8.4. Figure 8.10 shows that the flow of a power-law fluid in a fractured medium is now characterized by two parallel log-log straight lines, instead of the semi-log straight lines obtained for Newtonian flow. Interestingly, the slopes of the straight lines of log(ΔP) versus log(t) during the early and long injection times are also described by Equation 8.2 with $m' = 0.20$. This indicates that, at very early times, the pressure responses are dominated by flow only in the fractures; and the behavior approaches that of an equivalent system of a homogeneous reservoir at long times. The results on Figures 8.10 and 8.11 indicate that the power-law flow behavior is also controlled by the same two dimensionless parameters, ω and λ. The coefficient λ governs the

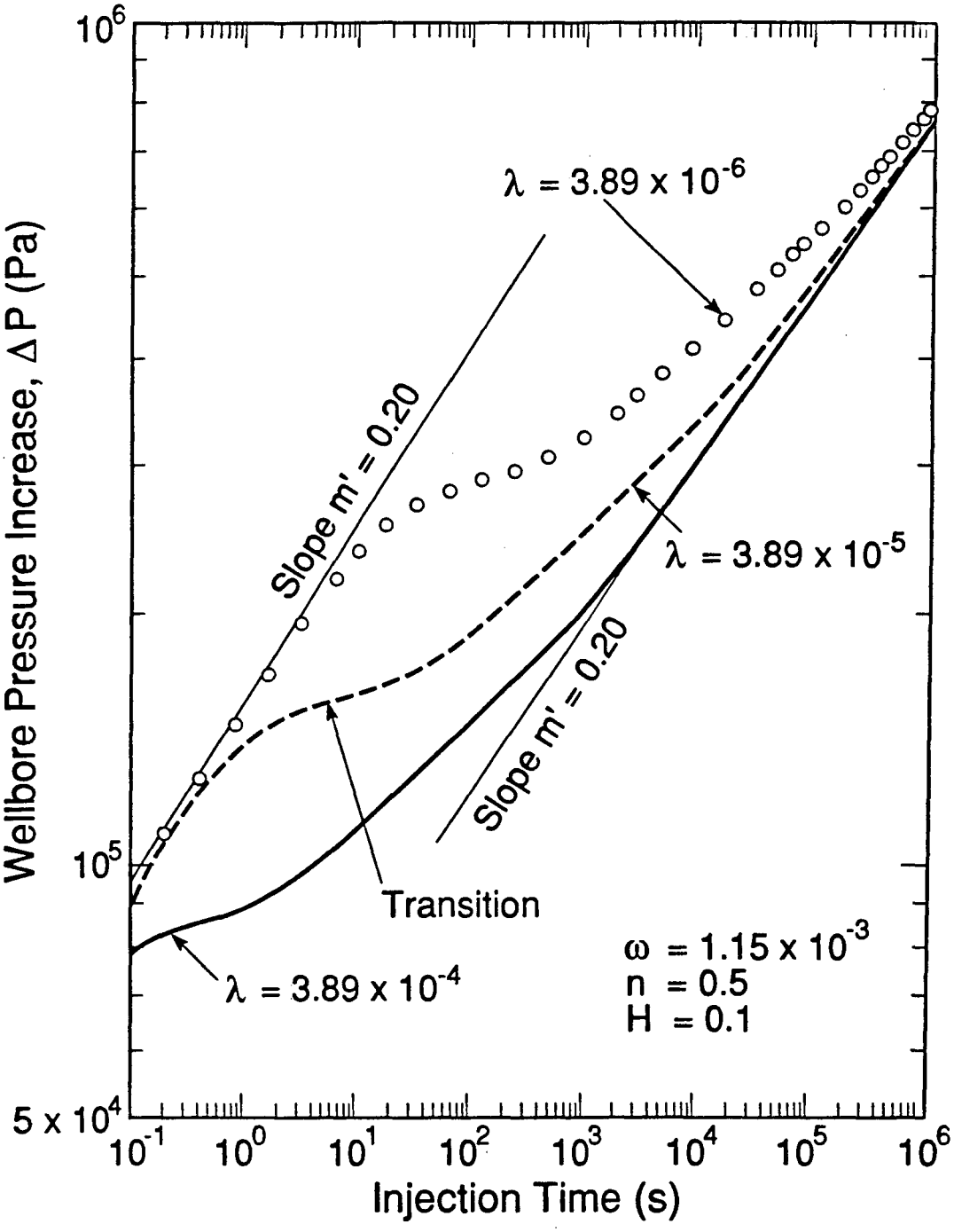

Figure 8.10 Characteristic Curves of Flow Behavior of a Power-Law Fluid through a Double-Porosity Medium, Effects of Interporosity Flow Coefficient λ.

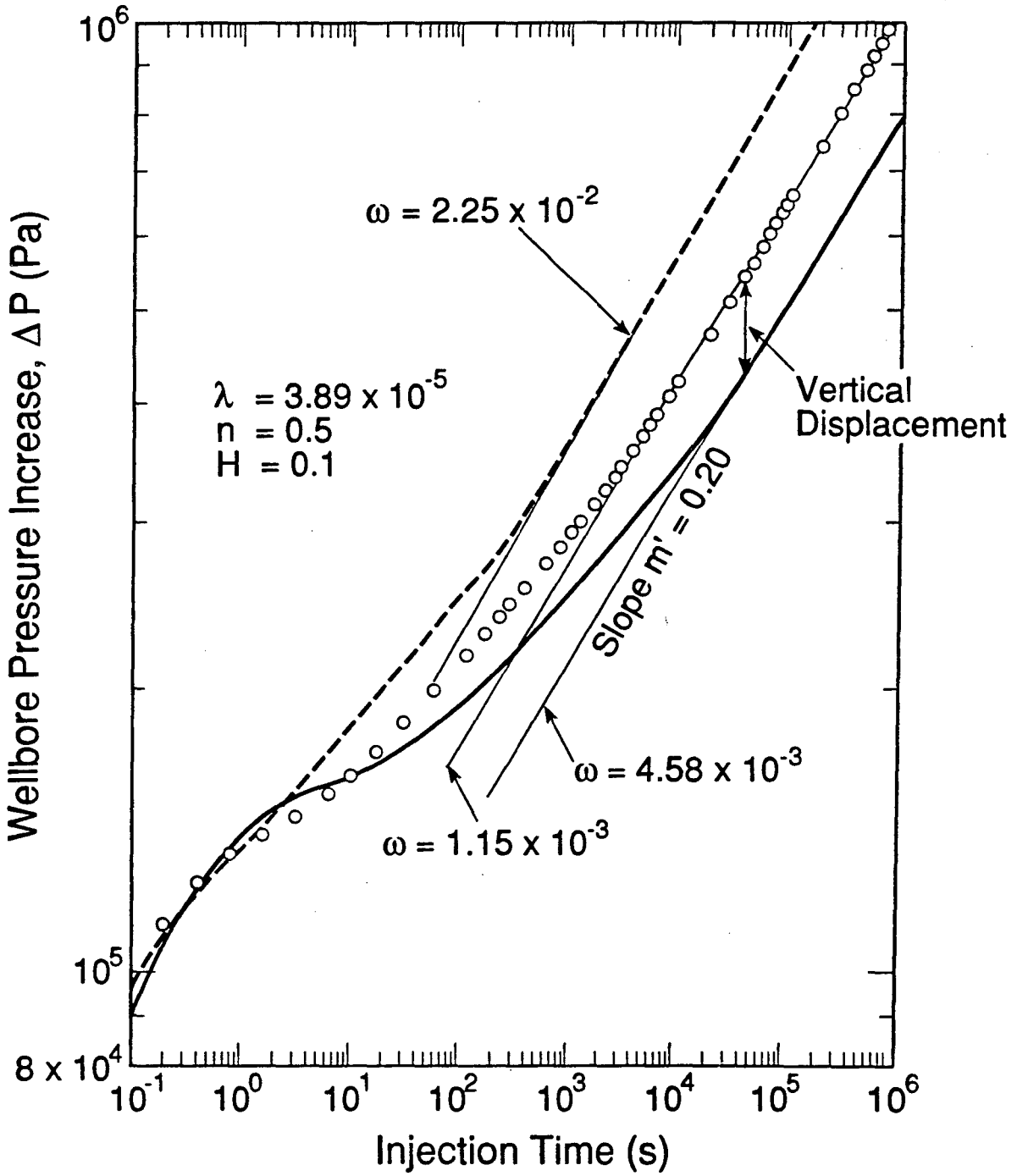

XBL 8912-7920
T.I.D. Illus.88

Figure 8.11 Characteristic Curves of Flow Behavior of a Power-Law Fluid through a Double-Porosity Medium, Effects of Storage Coefficient ω.

interporosity flow and determines the time frame when the transitional period in the pressure plot will occur between the two log-log straight lines, as shown in Figure 8.10. The other parameter ω is the ratio of the storage capacity of the fracture to the total storage capacity of the medium and is related to the vertical displacement between the parallel straight lines (see Figure 8.11).

In a real field test of power-law fluid flow in a fractured reservoir, there may be only one of the two straight lines that develops on the log-log plot, depending on the fluid and formation properties. At early time, the log-log straight lines may not be evident when the interporosity flow parameter λ is large, because of wellbore flow conditions, such as wellbore storage and skin effects. For a finite system with a small value of λ, the long time straight line may never form. Knowing these effects of the two dimensionless parameters, λ and ω, on pressure response helps in the analysis of well test data with power-law fluid flow in fractured reservoirs.

There is a significant difference in the log-log plot for a Newtonian fluid. Figure 8.12 shows the results for pressure increases in the same fracture system with a Newtonian fluid having a constant viscosity $\mu_{ne} = 10$ cp. The difference between Newtonian and power-law non-Newtonian fluid flow is that no straight line develops on the log-log plot for Newtonian flow. For the same fracture system with a Newtonian fluid, the usual semi-log plot of pressure increase versus time will exhibit two parallel straight lines (Kazemi, 1969). It is apparent that flow resistance in the fractured medium increases more rapidly with a power-law fluid than with a Newtonian fluid.

8.4 Flow Behavior of a General Pseudoplastic Non-Newtonian Fluid

The apparent viscosity of a general pseudoplastic fluid is assumed to be described by the Meter four-parameter model, Equation 3.13, (Meter and Bird, 1964). The shear

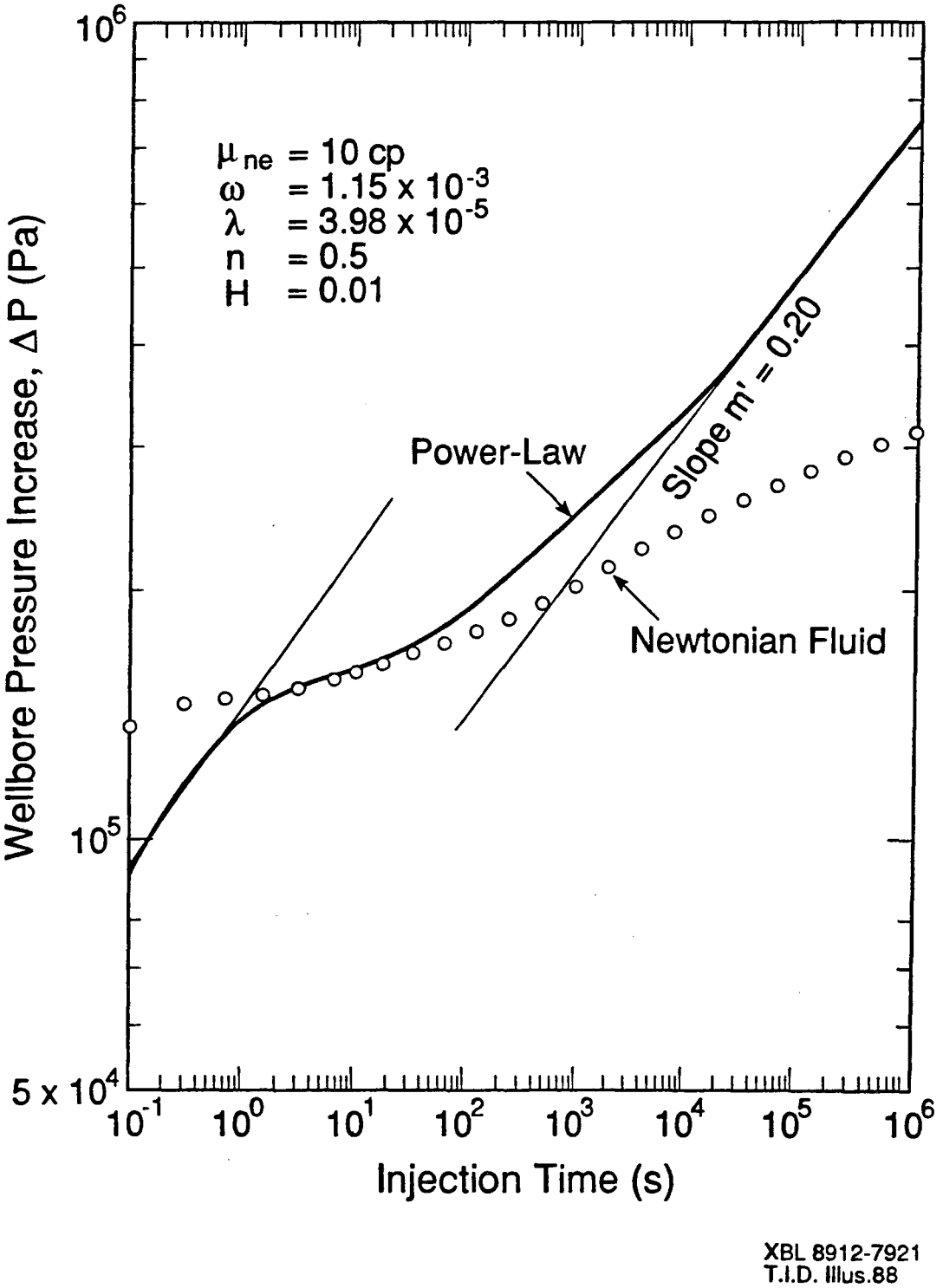

Figure 8.12 Comparison of Pressure Responses between Newtonian and Non-Newtonian Power-Law Fluid through a Double-Porosity System.

rate function, $\dot{\gamma}$, needed in Equation 3.13 for single phase one-dimensional flow of a power law fluid is given by Equation 3.12 (Camilleri et al., 1987a; Hirasaki and Pope, 1974). Then, the viscosity is determined by Equation 4.23. As shown in Figure 8.13, viscosities calculated from Equation 4.23 for the pseudoplastic fluid depend on pressure gradients and approach constants μ_0 and μ_∞, respectively, for small and large values of pressure gradient. This is physically more realistic than the power-law model because the power law predicts an infinite viscosity in the limit of vanishing shear rate.

Let us now consider the problem of injecting a pseudoplastic fluid into a horizontal porous formation through a well. The fluid and formation properties for this study are given in Table 8.5. It should be mentioned that, based on the literature, the non-Newtonian parameters used here are in a reasonable range for polymer solution flow in porous media. A log-log plot of pressure increase versus injection time is given in Figure 8.14, showing the effects of maximum viscosities, μ_0. It is evident that even at large injection times, no log-log straight lines develop on the curves of Figure 8.14. The slopes of the pressure-time curves decrease as injection time increases. As discussed in Section 8.2, a log-log straight line develops on the transient pressure curve at late times for power-law fluids. Therefore, the flow resistance for a power-law fluid increases more rapidly than for a pseudoplastic fluid under the same flow condition. If we keep the maximum viscosity constant at $\mu_0 = 100$ cp, and change the minimum viscosities, μ_∞, a comparison of the pressure responses is given in Figure 8.15. It is evident on this figure that the minimum viscosity parameter, μ_∞, has little influence on wellbore pressure as long as $\mu_\infty << \mu_0$. This simply means that the flow is essentially dominated by the low pore velocity (or shear rate) zone near the pressure penetration front, where the viscosity is close to the maximum viscosity μ_0 for this radial flow case.

The effects of the parameter, $\dot{\gamma}_{1/2}$, are shown in Figures 8.16 and 8.17. It serves as a shift factor on these log-log curves of both viscosity versus pressure gradient and pressure increase versus injection time. The exponential parameter, β, in Equation 3.13,

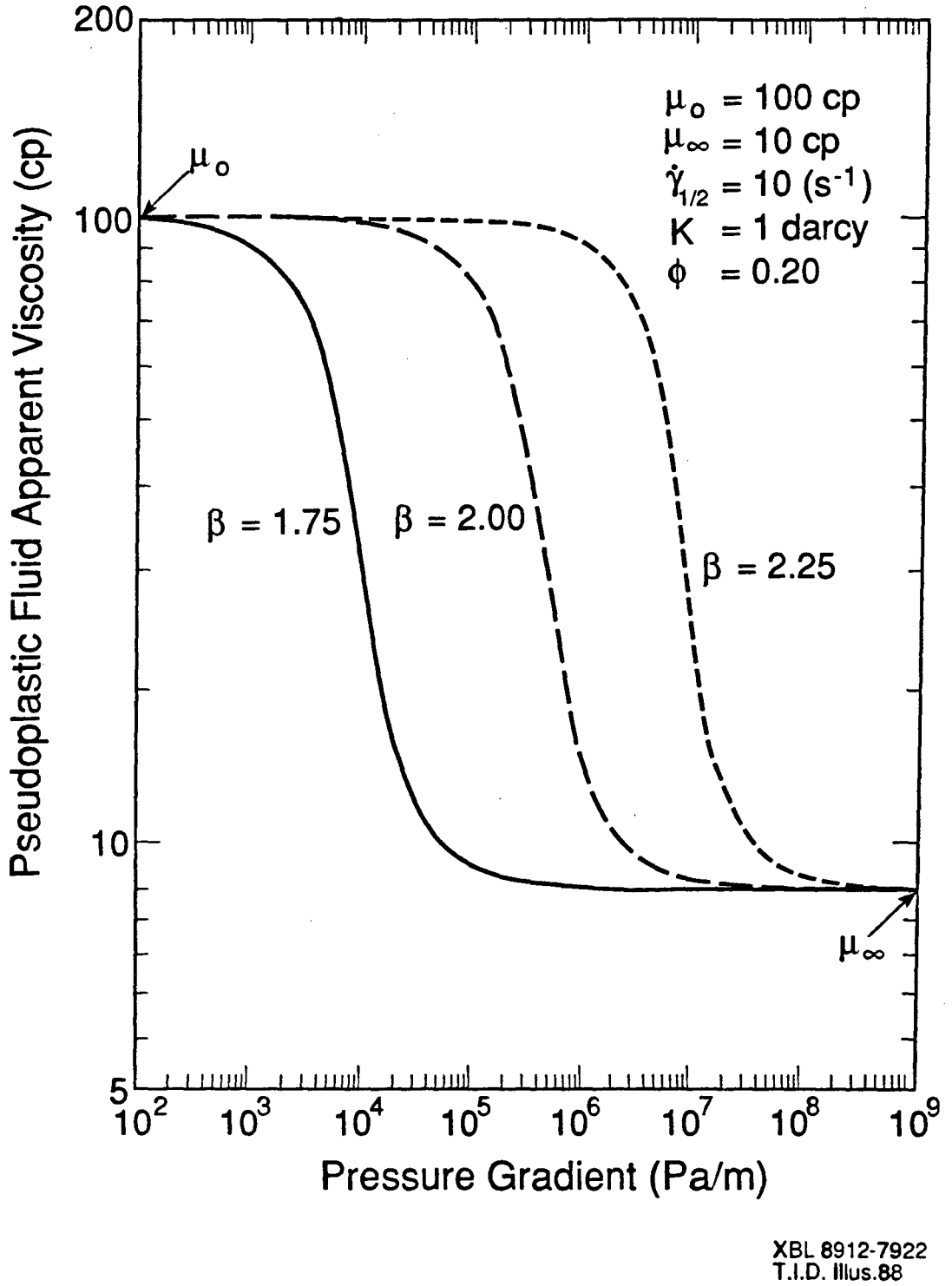

Figure 8.13 Apparent Viscosity Curves of a General Pseudoplastic Fluid, by Meter's Model, Effects of the Exponential Parameter β.

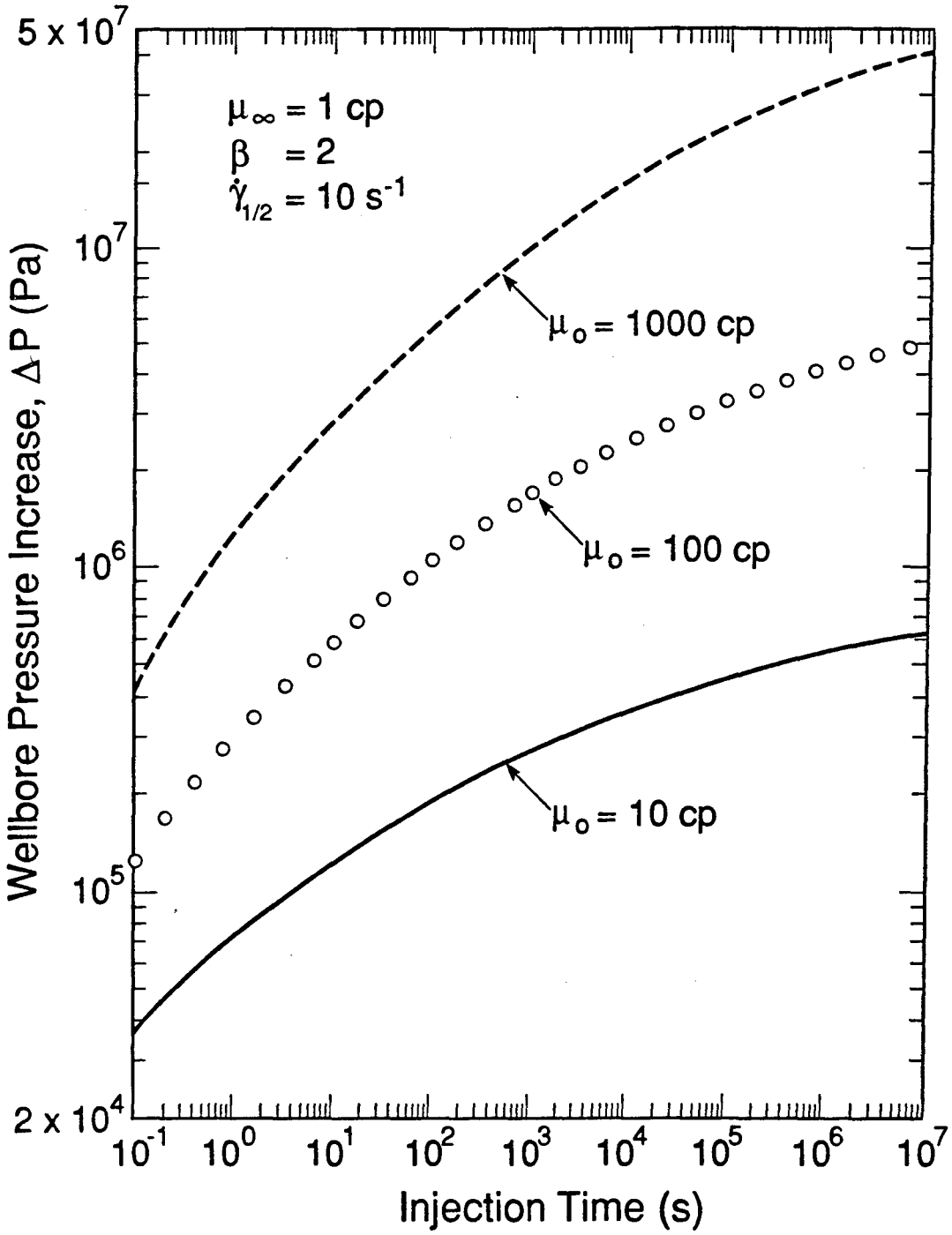

Figure 8.14 Transient Pressure Behavior of Pseudoplastic Fluid Flow in Porous Media, Effects of the Maximum Viscosity μ_0.

Table 8.5

Parameters for Pseudoplastic Fluid Injection in a Porous Medium

Initial Pressure	$P_i=1\times10^7$Pa
Initial Porosity	$\phi_i=0.20$
Formation Thickness	h=1m
Permeability	$K=9.869\times10^{-13}m^2$
Fluid Compressibility	$C_f=4.557\times10^{-10}Pa^{-1}$
Rock Compressibility	$C_r=2\times10^{-10}Pa^{-1}$
Initial Fluid Density	$\rho_i=975.92Kg/m^3$
Injection Rate	$Q_m=0.05Kg/s$
Wellbore Radius	$r_w=0.10m$
Power-Law Index	n=0.5

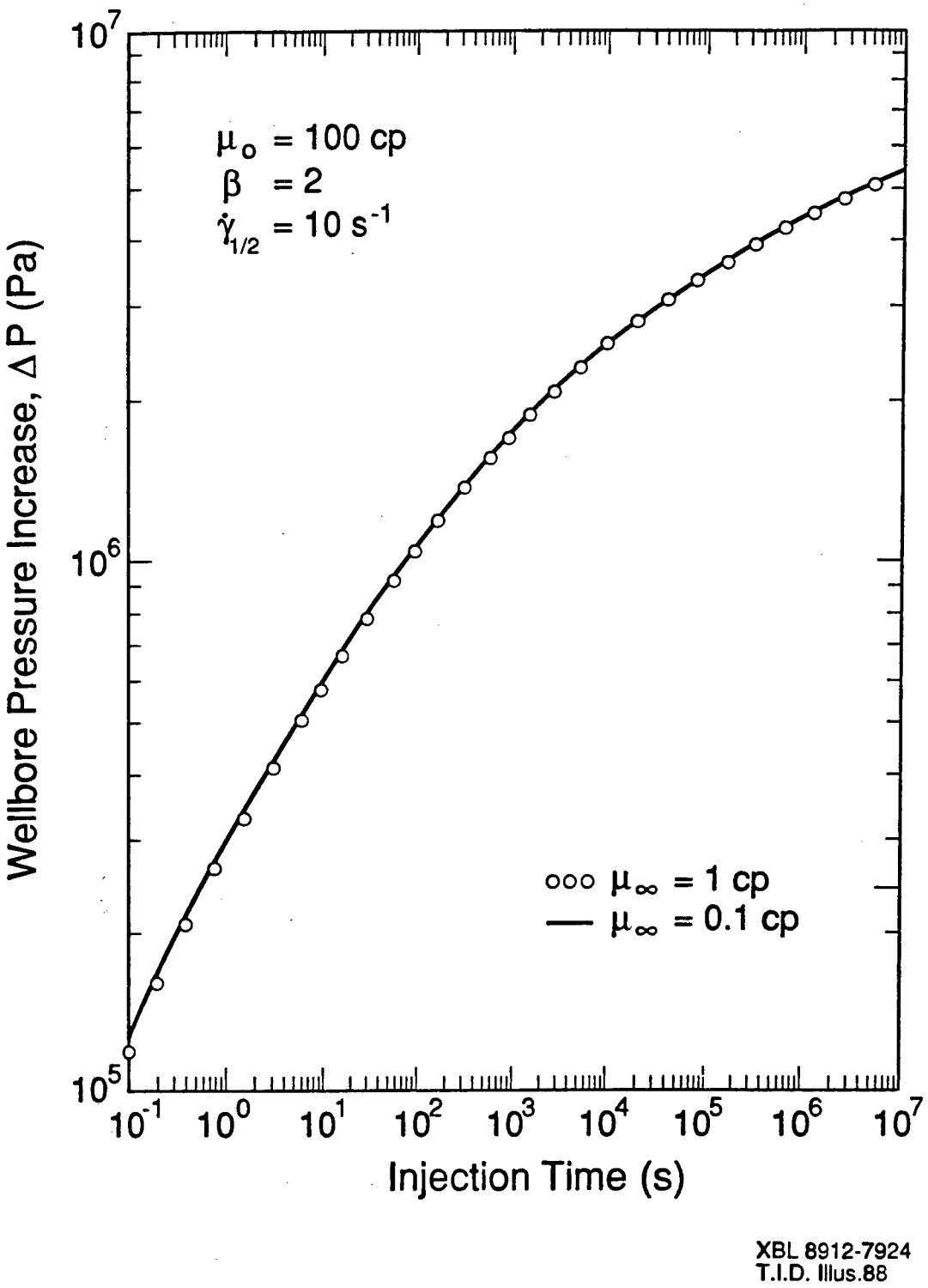

Figure 8.15 Transient Pressure Behavior of Pseudoplastic Fluid Flow in Porous Media, Effects of the Minimum Viscosity μ_∞.

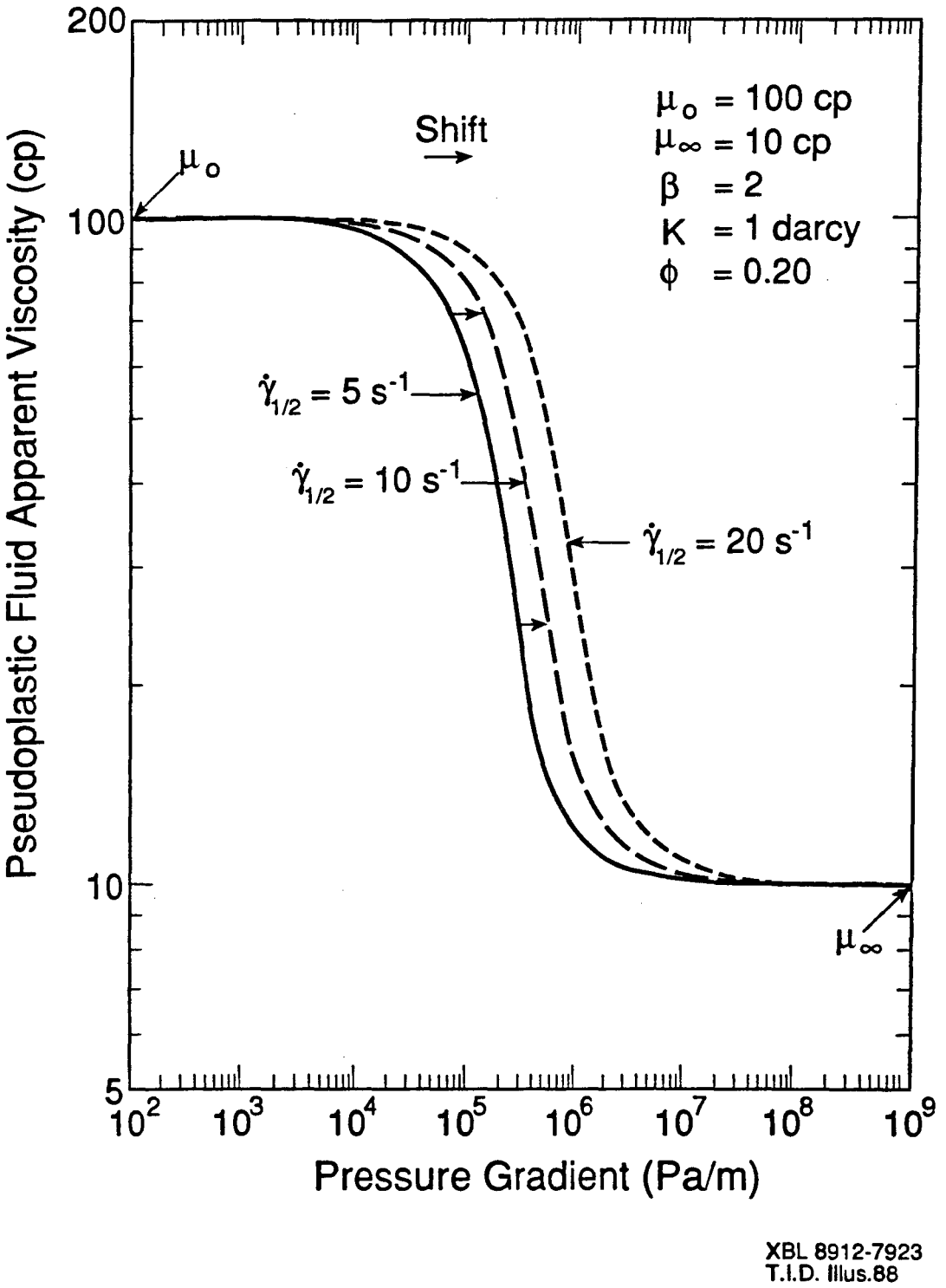

Figure 8.16 Apparent Viscosity Curves of a General Pseudoplastic Fluid, by Meter's Model, Effects of the Coefficient $\gamma_{1/2}$.

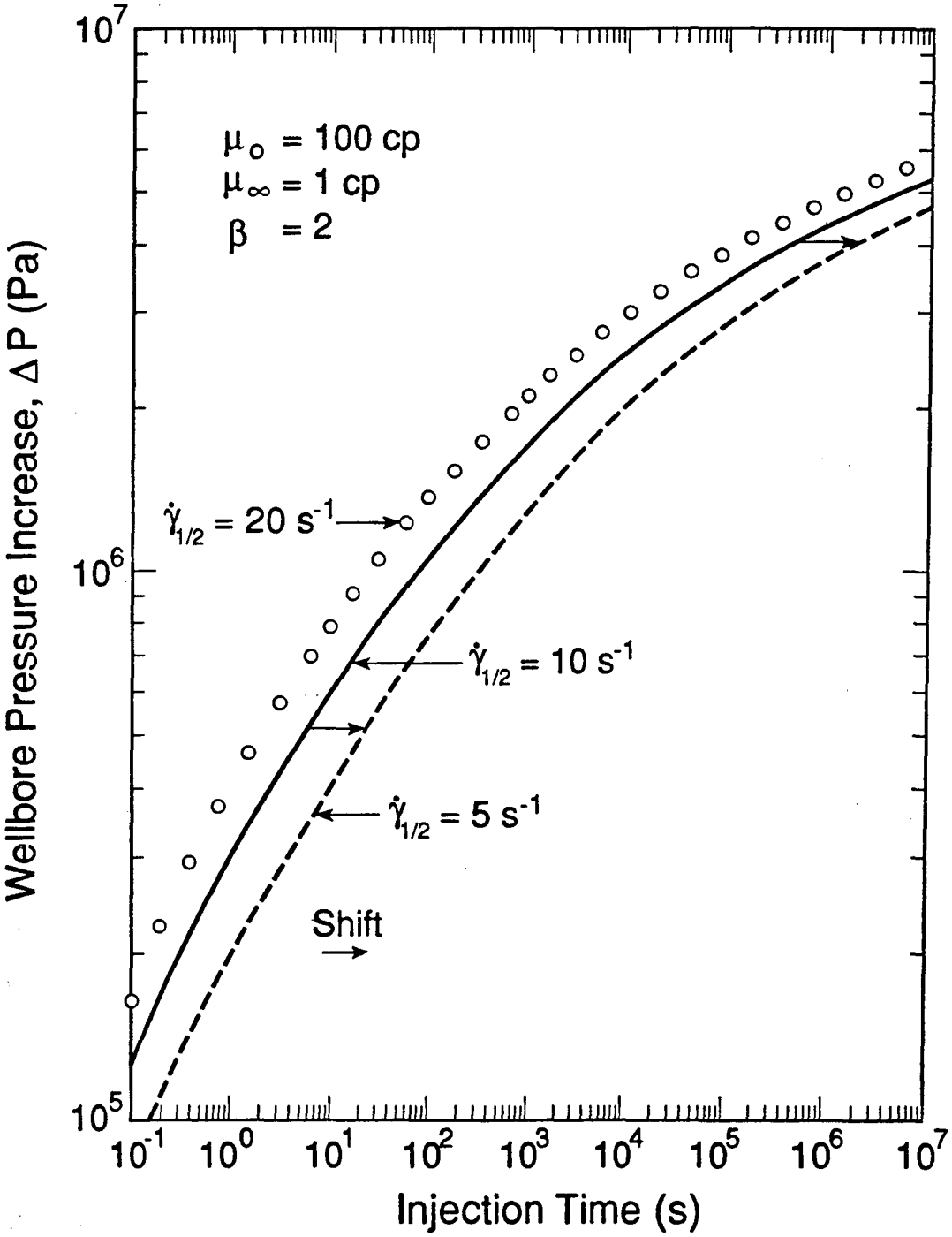

Figure 8.17 Transient Pressure Behavior of Pseudoplastic Fluid Flow in Porous Media, Effects of the Coefficient $\gamma_{1/2}$.

affects the flow behavior more significantly, as shown in Figure 8.18. The magnitude and shapes of the wellbore pressure-time plots both change as β changes.

Meter and Bird (1964) discussed a method for determining the parameters of the four parameter model, Equation 2.8, by analyzing laboratory experiments. However, flow properties obtained from core experiments are usually quite different from those observed for a reservoir in the field. Therefore, well test techniques are used in many applications to find the in-situ flow parameters for the system of interest. As the number of physical parameters increases, analysis of well test data becomes more difficult to perform and the results may not be unique. In practice, it is very important to reduce the number of unknowns so that a successful well test may be obtained.

For the pseudoplastic non-Newtonian fluid flow problem, the semi-log plots of pressure increase versus time are given in Figure 8.19, in which the pressure-time data are the same as those in Figure 8.18. It is encouraging to note that semi-log straight lines develop at long injection times. This indicates that at long time, the behavior of pseudo-plastic fluids tends toward that of a Newtonian fluid. For $\beta = 2$ and 3, the semi-log straight lines are almost parallel to each other; their slopes are measured to be $m|_{\beta=2} = 9.21\times10^5$ Pa, and $m|_{\beta=3} = 9.51\times10^5$ Pa per log-cycle, respectively. By using the standard semi-log analysis method (Earlougher, 1977; Matthews and Russell, 1967), we can calculate the equivalent Newtonian viscosity μ_{eqv} at long times as,

$$\mu_{eqv} = \frac{4\pi Khm}{2.303Q} = \frac{4\times\pi\times9.869\times10^{-13}\times9.51\times10^5}{2.303\times.05/975.92} = 99.95 \text{ (cp)} \qquad (8.8)$$

where Q is the constant volumetric injection rate. This calculated equivalent viscosity value is close to μ_0, i.e., $\mu_{eqv} \approx \mu_0 = 100$ cp. Therefore, this further confirms that the long time flow behavior is controlled by the low flow velocity and high viscosity region far from the well. This indicates that the maximum viscosity parameter μ_0 for flow of a pseudoplastic fluid can be obtained approximately by a semi-log analysis of pressure drawdown tests.

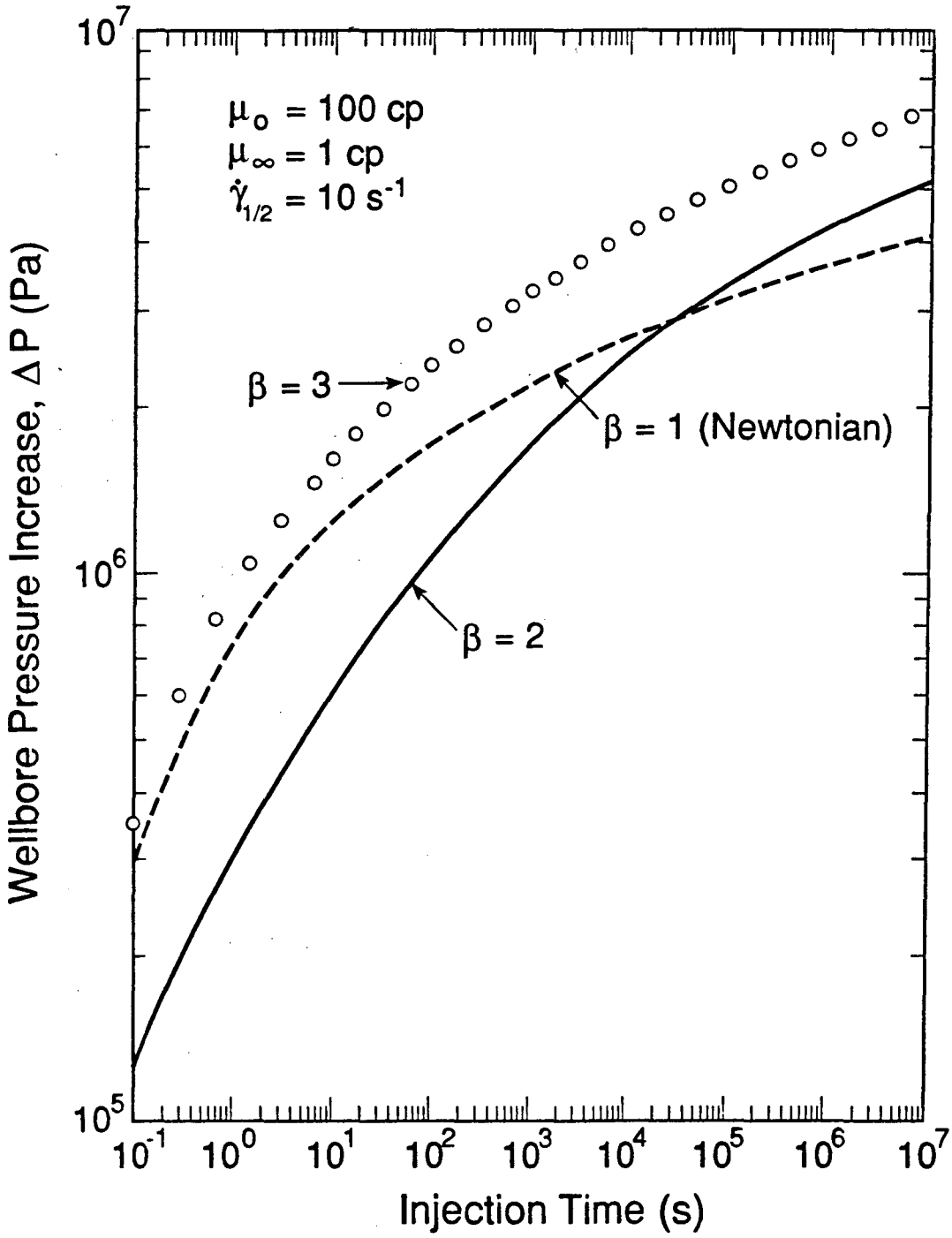

Figure 8.18 Transient Pressure Behavior of Pseudoplastic Fluid Flow in Porous Media, Effects of the Exponential Parameter β.

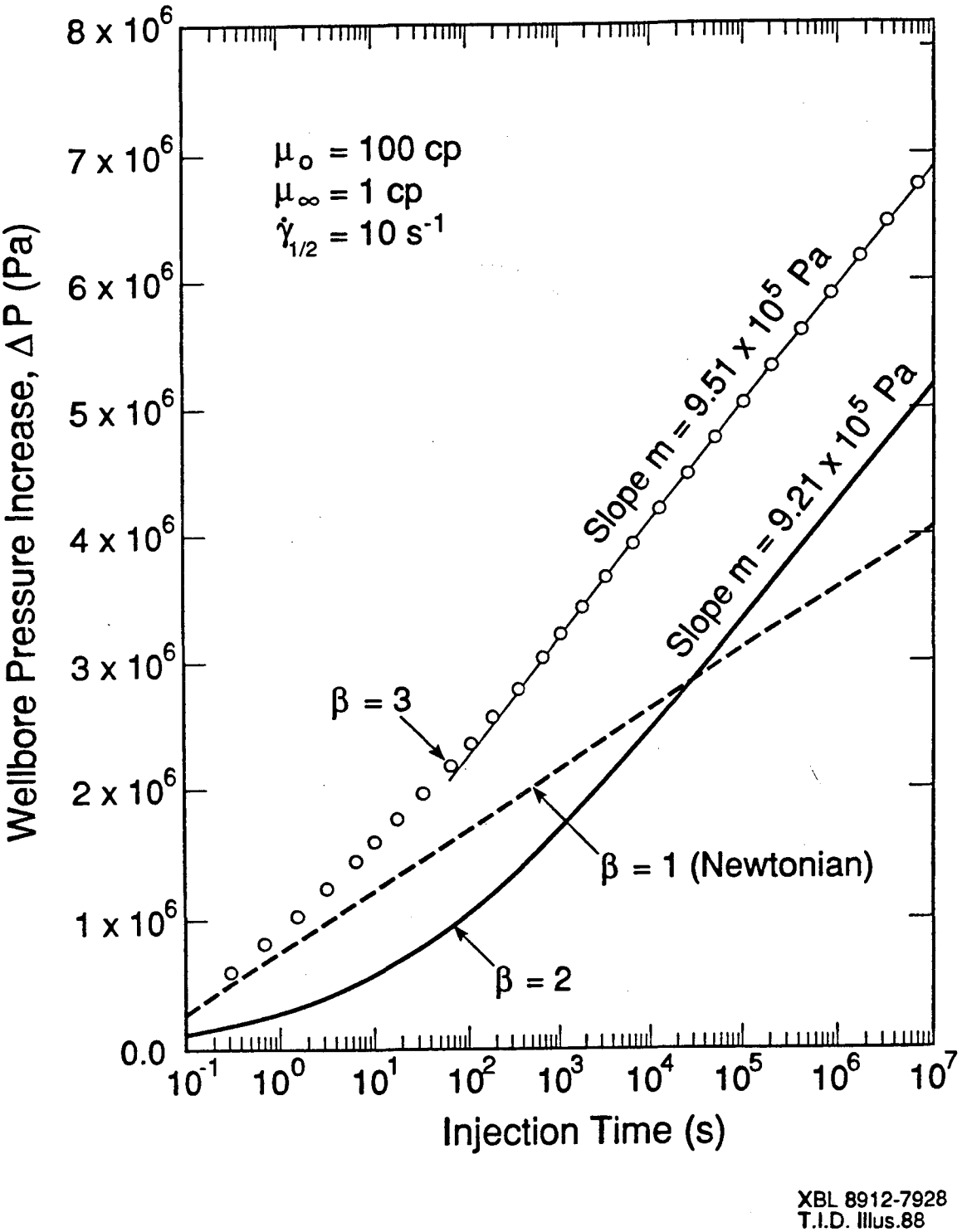

Figure 8.19 Semi-log Plot of Transient Pressure Behavior of Pseudoplastic Fluid Flow in Porous Media.

8.5 Conclusions

A comprehensive numerical study of transient flow of single-phase power-law fluids has been carried out in this chapter. The semi-analytical test analysis method is discussed and recommended for transient pressure analysis of power-low fluid injectivity tests. This method combines the log-log analysis technique by Ikoku and Ramey with numerical simulation. Two published examples of well test data are analyzed by using this method to demonstrate its application to field problems. The results show that considerable improvement on the existing analysis techniques has been obtained for more accurate fluid and formation properties.

By using an idealized fracture model, this study presents the fundamentals of the behavior of power-law fluid flow in a fractured medium. Transient flow of a power-law fluid in a double-porosity system is controlled by the two dimensionless parameters, the storage coefficient ω and the interporosity parameter λ, and is characterized by the two-parallel straight lines on a log-log plot of wellbore pressure increases versus injection time. The slopes of the straight lines are related to the power-law index n. In general, the double-porosity approximation will result in large errors for the early time pressure prediction.

Some insights into transient flow of a general pseudoplastic non-Newtonian fluid in porous medium have also been obtained in this chapter. Unlike power-law fluid flow, no straight lines appear in log-log plots of pressure increase versus injection time during pseudoplastic fluid injection. Instead, semi-log straight lines on the pressure-time plots develop at late times. Therefore, the long time flow behavior of pseudoplastic fluids approaches that of an equivalent Newtonian system and is essentially determined by the low flow velocity and high viscosity zone far from the injection well.

Chapter 9
Transient Flow of a Single-Phase Bingham Non-Newtonian Fluid

9.1 Introduction

Compared with the progress made in analyzing the flow of power-law fluids though porous media, the flow behavior of a Bingham plastic fluid in porous media is very poorly understood. To date research on Bingham fluid flow has been conducted mainly in laboratory experiments and field tests, from which a modified Darcy's law has been derived. Little work on flow and transport behavior through porous media can be found in the literature. To the best of my knowledge, no quantitative analysis has been published on Bingham fluid flow, and there is also no reliable well testing technique available in the petroleum engineering and groundwater literature. Therefore, this chapter is devoted to a systematic study of Bingham fluid flow through a porous medium.

This chapter presents an integral analytical method for analyzing non-linear Bingham fluid flow in porous media. The integral method, which has been widely used in the study of unsteady heat transfer problems (Ozisik, 1980), is applied here to obtain an approximate analytical solution for Bingham fluid flow in porous media. The integral approach to heat conduction utilizes a simple parametric representation of the temperature profile, e.g. by means of a polynomial, which is based on physical concepts such as a time-dependent thermal penetration distance. An approximate solution of the heat transfer problem is then obtained from simple principles of the continuity and conservation of heat flux. This solution satisfies the governing partial differential equation only in an average, integral sense. However, it is encouraging to note that many integral solutions to heat transfer and fluid mechanics problems have an accuracy that is generally acceptable for engineering applications (Ozisik, 1980). When applied to fluid flow

problems in porous media, the integral method consists of assuming a pressure profile in the pressure disturbance zone and determining the coefficients of the profiles by making use of the integral mass balance equation.

The integral solution obtained in this chapter for Bingham fluid flow has been checked by comparison with solutions for a special linear case where the exact solution is available. The numerical code of Chapter 4 is also used to examine the analytical results from the integral solution for general non-linear problems. It is found that the accuracy of the integral solution is surprisingly good when compared with the exact solution and with the numerical results for Bingham fluid flow through an infinite radial system. In addition, a pressure profile for integral solutions is proposed for radial flow in porous media that is better than what is typically recommended for heat conduction in radial flow systems (Lardner and Pohle, 1961). This pressure profile is able to provide very accurate results for transient fluid flow in a radial system.

The effects of non-Newtonian properties on flow behavior during a slightly-compressible Bingham fluid flow are discussed using the integral solution. The analytical results reveal the basic pressure responses in the formation during a Bingham fluid production or injection operation. Based on the analytical and numerical solutions, a new method for well test analysis of Bingham non-Newtonian fluids has been developed, which can be used to determine reservoir fluid and formation properties. In order to demonstrate the use of the new approach, two examples of pressure drawdown and buildup tests are created by the numerical and analytical simulations, and the simulated well test data are analyzed using this new technique.

9.2 Governing Equation and Integral Solution

The problem concerned here is the flow of a Bingham fluid into a fully penetrating well in an infinite horizontal reservoir of constant thickness, where the formation is initially saturated with the same fluid. To formulate the flow problem, the following basic assumptions are made:

1) isothermal, isotropic and homogeneous formation;
2) horizontal flow of a single phase fluid without gravity effects;
3) Darcy's law, Equation 3.7, applies with the viscosity function of (3.14) for the Bingham fluid; and
4) constant fluid properties and formation permeability.

The governing flow equation can be derived by combining Equations 4.5, 4.3 and 3.14, and is expressed in a radial coordinate system as,

$$\frac{K}{r}\frac{\partial}{\partial r}\left\{\frac{\rho(P)}{\mu_b}r\left[\frac{\partial P}{\partial r}-G\right]\right\}=\frac{\partial}{\partial t}[\rho(P)\phi(P)] \tag{9.1}$$

for production of a Bingham fluid. The density, $\rho(P)$, of the Bingham fluid, and the porosity, $\phi(P)$, of formation, are functions of pressure only.

The initial condition is,

$$P(r, t=0) = P_i \text{ (Constant)} \quad (r \geq r_w) \tag{9.2}$$

For the inner boundary at the wellbore, $r = r_w$, the fluid is produced at a given mass production rate $Q_m(t)$,

$$\frac{2\pi r_w K h \rho(P_0)}{\mu_b}\left[\frac{\partial P}{\partial r}-G\right]_{r=r_w} = Q_m(t) \tag{9.3}$$

where $P_0 = P_0(t) = P(r_w, t)$, the wellbore pressure.

The integral solution for the radial flow into a well at a specified mass production rate $Q_m(t)$ is obtained (see Appendix D) as

$$P(r, t) = P_i + (r - r_w\eta)G - \frac{Q_m(t)\mu_b}{2\pi Kh}\frac{1}{\rho(P_0)}\left[\frac{1 + 2\delta(t)/r_w}{2\delta(t)/r_w}\right]\times$$

$$\ln\left[\frac{2r/r_w}{\eta} - \left[\frac{r/r_w}{\eta}\right]^2\right] \tag{9.4}$$

where $\eta = 1+\delta(t)/r_w$. The unknowns, P_0, the wellbore pressure, and $\delta(t)$, the pressure penetration distance, are determined by solving Equation 9.4 by setting $r = r_w$ and the following integral equation simultaneously,

$$\int_{r_w}^{r_w+\delta(t)} 2\pi hr\rho(P)\phi(P)dr = -\int_0^t Q_m(t)dt + \pi h\rho_i\phi_i[(r_w + \delta(t))^2 - r_w^2] \tag{9.5}$$

where $\rho_i = \rho(P_i)$, and $\phi_i = \phi(P_i)$. Equation 9.5 is simply a mass balance equation in the region of pressure disturbance.

For slightly compressible fluid flow, we can obtain the following explicit expression of the integral mass balance equation (see Appendix D) as

$$\int_0^t Q_m(t)dt + \rho_i\phi_i C_t r_w^2\left\{2\pi hr_w G\left[-\frac{1}{6}\eta^3 + \frac{1}{2}\eta - \frac{1}{3}\right]\right.$$

$$+ \frac{Q_m(t)\mu_b}{K\rho(P_0)}\left[\frac{1+2\delta(t)/r_w}{2\delta(t)/r_w}\right]\left[-\frac{3}{2}\eta^2 + \eta + \frac{1}{2} +\right.$$

$$\left.\left.2\eta\ln(\eta) - \frac{1}{2}[1 - 4\eta^2]\ln\left[\frac{2\eta - 1}{\eta^2}\right]\right]\right\} = 0 \tag{9.6}$$

Solving Equations 9.6 and 9.4 with $r = r_w$ simultaneously for $\delta(t)$ and $P_0(t)$ and substituting them into (9.4) give the final solution for Bingham fluid flow in a slightly compressible system.

9.3 Verification of Integral Solutions

The solution from the integral method is approximate and needs to be checked by comparison with an exact solution or with numerical results. The accuracy of the integral solution obtained in Section 9.2 is examined and confirmed by comparison with an exact solution and numerical calculations. It has also been found that the accuracy of integral solutions depends on the choice of forms of pressure profiles for a radial flow problem, among other variables.

9.3.1 Comparison with Exact Solution

For the special case of minimum pressure gradient G = 0, a Bingham fluid becomes Newtonian, and the Theis solution can be used to to check the integral solution. At a first step, the temperature profile, as given in Equation D.9 in Appendix D and as recommended for radial heat conduction problems (Lardner and Pohle, 1961; Ozisik, 1980), has been used to represent the pressure profile for the radial flow of a slightly compressible fluid in porous media. The results for wellbore pressure in a single well injection problem are shown in Figures 9.1 and 9.2, in which first-degree and second-degree polynomials are used, respectively, in Equation D.9. The parameters used for checking the integral solutions with the exact solution are given in Table 9.1. Figure 9.1 indicates that for the linear flow case of G = 0 , the integral solution overestimates injection pressures, by about 5-10%. The distribution of pressures in the formation obtained using Equation D.9 is compared with the exact solution from the Theis equation on Figure 9.2. Up to an injection time of 1,000 seconds, the results expressed in terms of a logarithm multiplied by a first- or second- polynomial do not match very well with the Theis solution. It is apparent that the resulting integral solution introduces large errors into the

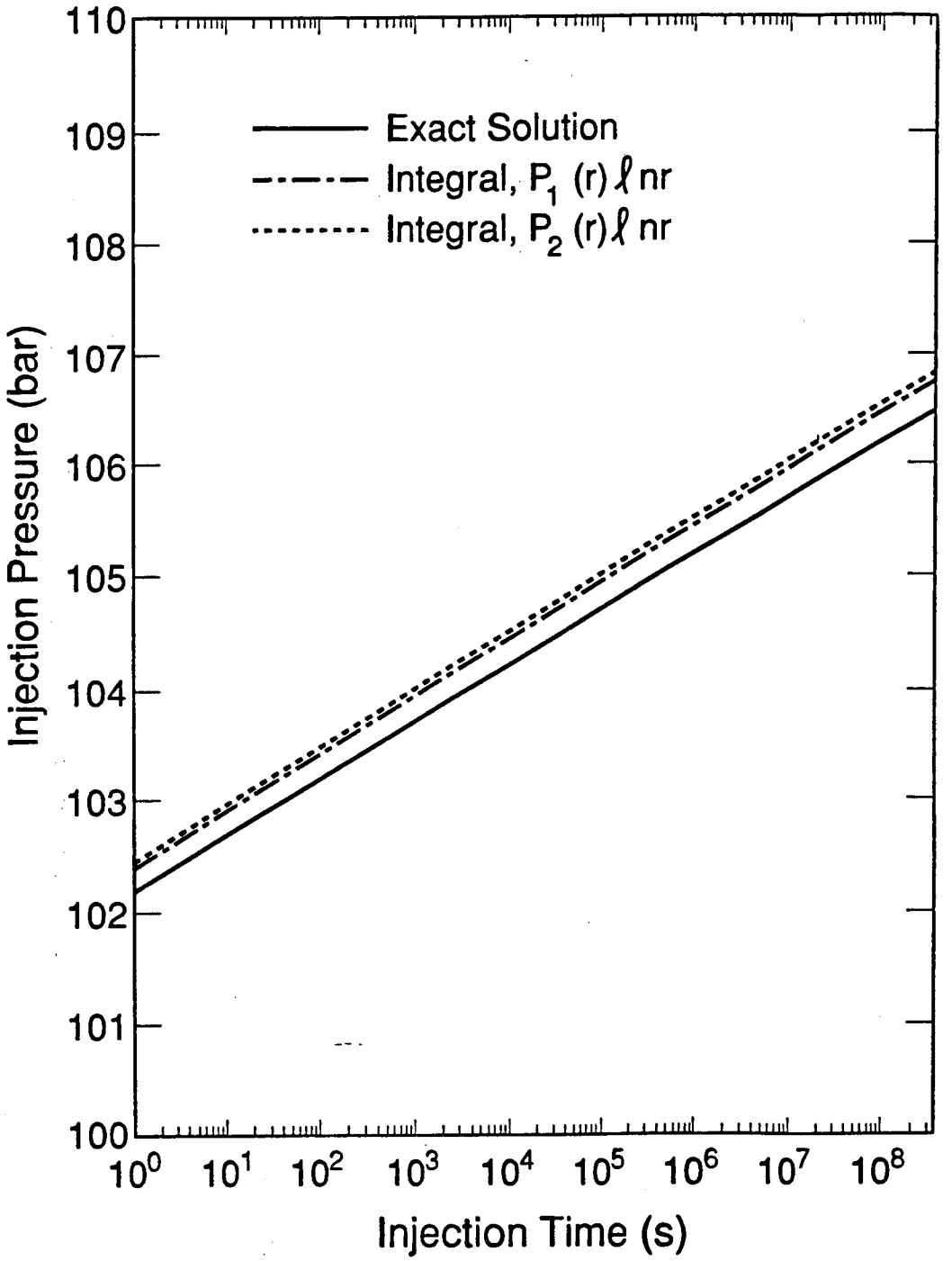

XBL 8911-7879
T.I.D. Illus.88

Figure 9.1 Comparison of Injection Pressures during Newtonian Fluid Injection, Calculated from the Exact Theis Solution and the Integral Solutions with Pressure Profiles Recommended in Heat Transfer.

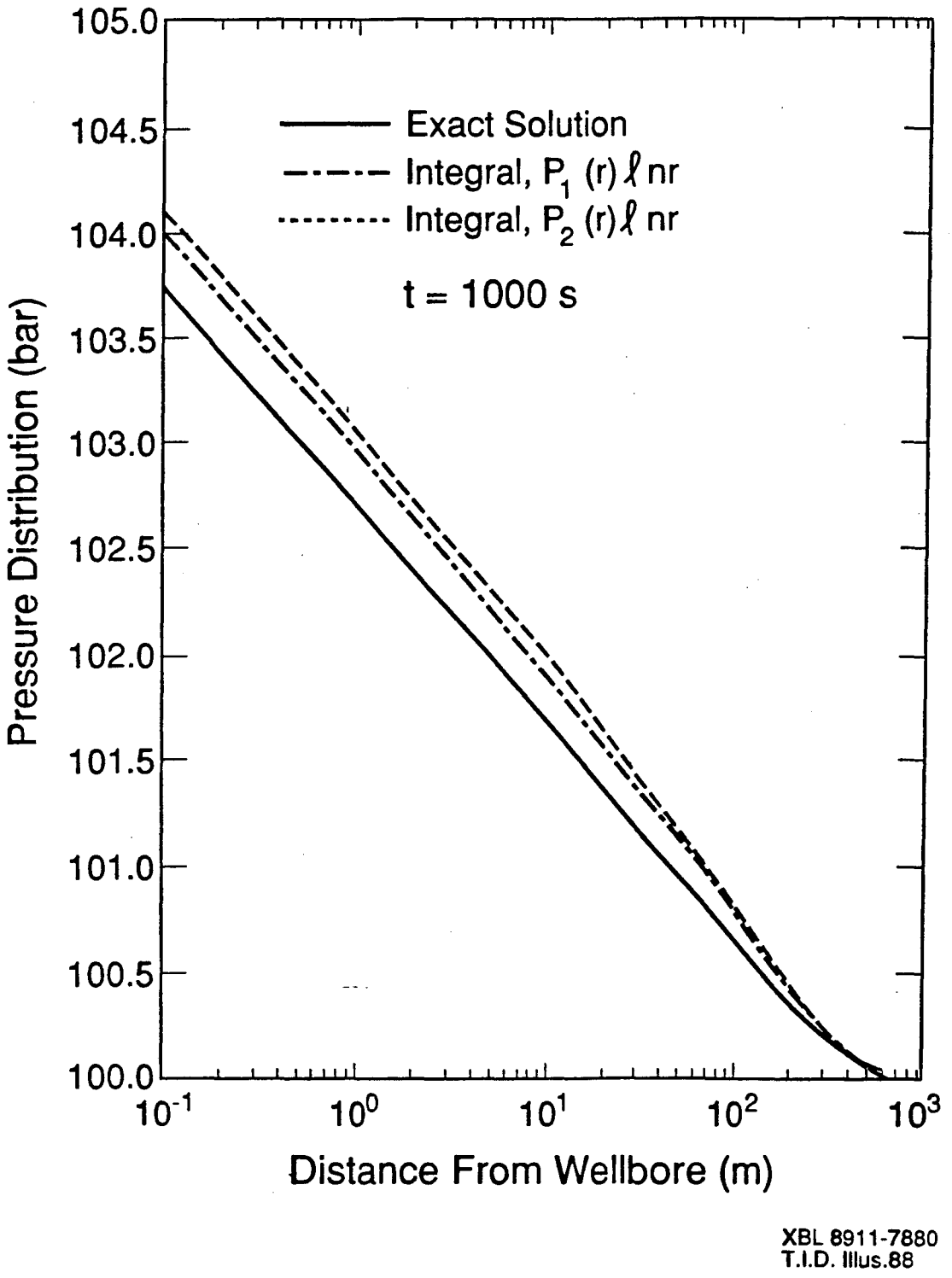

Figure 9.2 Comparison of Pressure Distributions of Newtonian Fluid Injection, Calculated from the Exact Theis Solution and the Integral Solutions with Pressure Profiles Recommended in Heat Transfer.

Table 9.1

Parameters Used for Checking with Exact Solution

Initial pressure	$P_i=10^7$Pa
Initial Porosity	$\phi_i=0.20$
Initial Fluid Density	$\rho_i=975.9$kg/m^3
Formation Thickness	h=1m
Fluid Viscosity	$\mu_f=.35132\times10^{-3}$Pa.s
Fluid Compressibility	$C_f=4.557\times10^{-10}$Pa^{-1}
Rock Compressibility	$C_r=5\times10^{-9}$Pa^{-1}
Mass Injection Rate	Q_m=1kg/s
Permeability	$K=9.869\times10^{-13}$m^2
Wellbore Radius	r_w=0.1m

radial flow results.

If the pressure profile given by Equation D.11 is used, the integral solution given by Equations 9.4-9.6 results. A comparison of the exact Theis solution and the integral solution is presented in Figure 9.3 and 9.4. Here, we see an excellent agreement on Figure 9.3 for the wellbore pressures calculated from the two solutions. There are only minor errors in the pressure profile on Figure 9.4 near the pressure penetration front on the pressure profile after injection of 1,000 seconds. Many tests were performed to compare the integral solution with the Theis solution using different fluid and formation properties, and excellent agreement has been obtained from all the calculations.

9.3.2 Comparison with Numerical Solution

For the radial flow problem during producing a Bingham fluid with $G > 0$, the results from the integral solution have been examined by comparison with a numerical simulation. The input parameters are given in Table 9.2. It should be mentioned that the numerical results are considered reliable for this problem because their accuracy has been verified in many simulations. The wellbore flowing pressures calculated from the integral and numerical solutions are shown in Figures 9.5-9.7 for three values of G, minimum pressure gradient. It is interesting to note that the agreement between the approximate integral and numerical results is excellent over the entire transient flow period. The pressure distribution in the formation after production of 1,000 seconds is shown in Figure 9.8. The integral solution also matches the numerical predictions very well.

It is concluded that the pressure profiles, obtained with Equation D.11, give very accurate results for a radial flow problem with both Newtonian and Bingham fluids. The use of the temperature profile, Equation D.9, recommended in the heat transfer

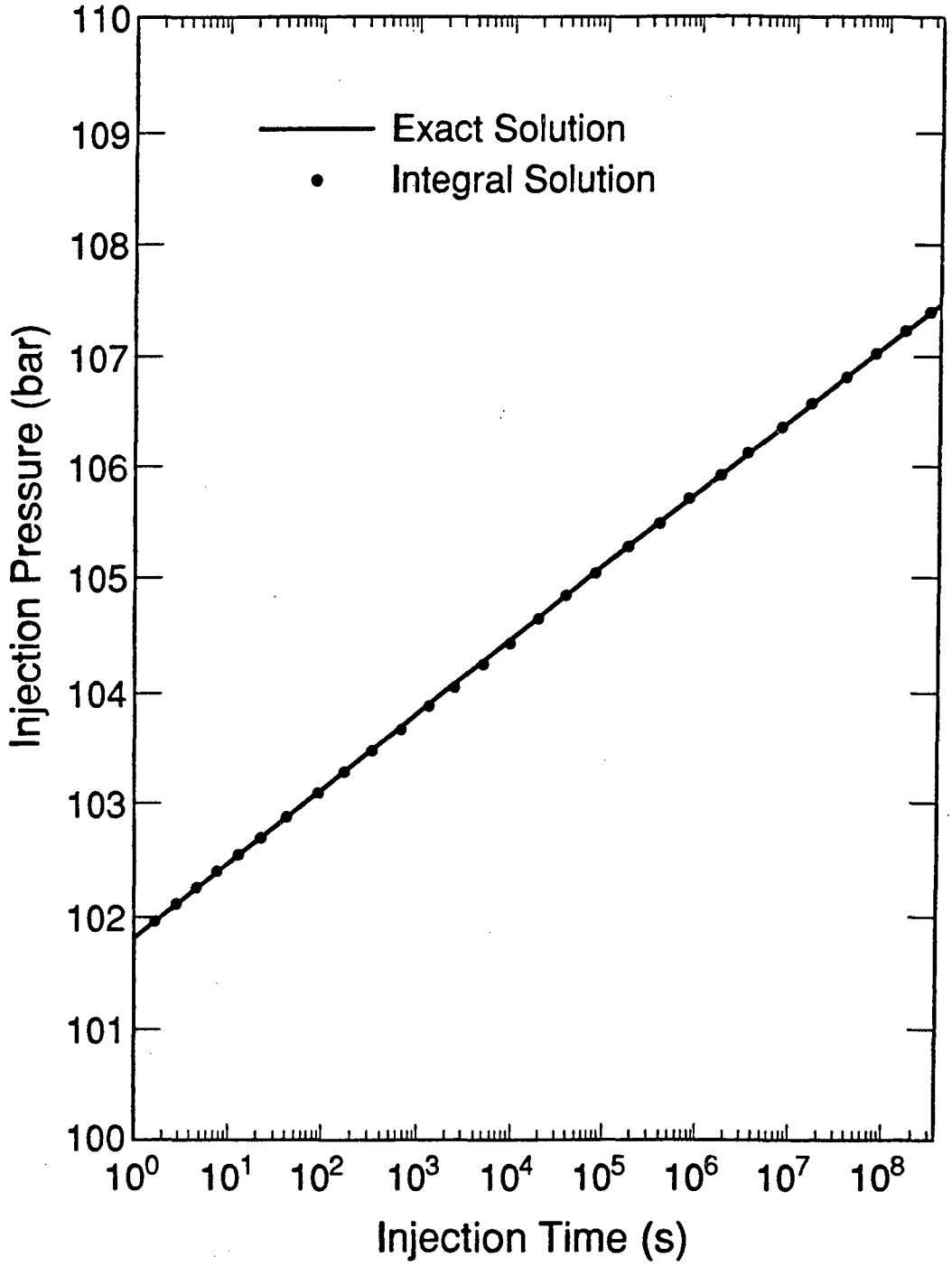

Figure 9.3 Comparison of Injection Pressures during Newtonian Fluid Injection, Calculated from the Exact Theis Solution and the Integral Solutions with Pressure Profiles Recommended in This Work.

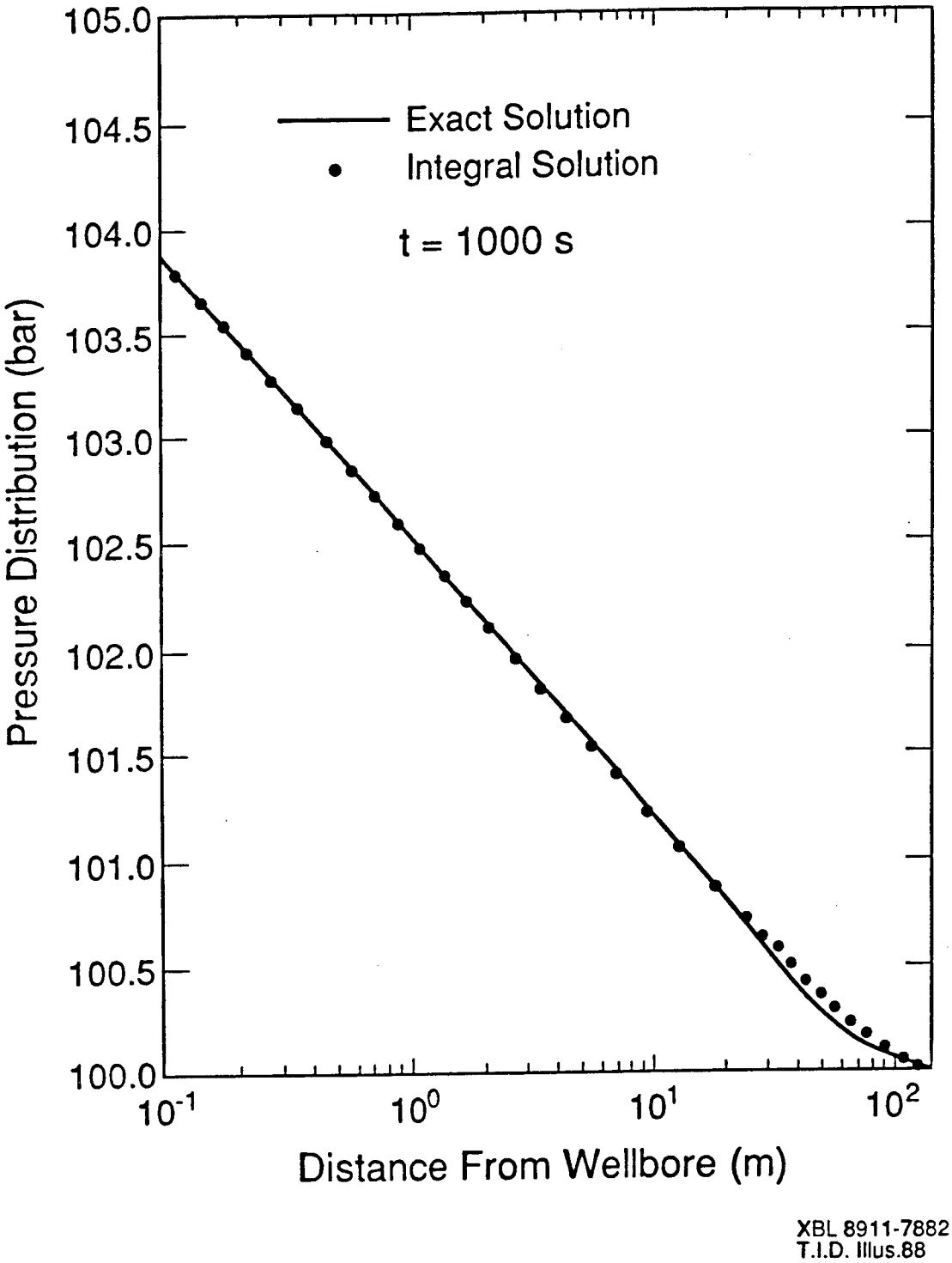

Figure 9.4 Comparison of Pressure Distributions of Newtonian Fluid Injection, Calculated from the Exact Theis Solution and the Integral Solutions with Pressure Profiles Recommended in This Work.

Table 9.2

Parameters Used for Checking with Numerical Solution

Initial pressure	$P_i=10^7$Pa
Initial Porosity	$\phi_i=0.20$
Initial Fluid Density	$\rho_i=975.9$kg/m^3
Formation Thickness	h=1.0m
Bingham Plastic Coefficient	$\mu_b=5\times10^{-3}$Pa.s
Total Compressibility	$C_t=3\times10^{-9}$Pa^{-1}
Mass Production	$Q_m=0.1$kg/s
Permeability	$K=9.869\times10^{-13}$m^2
Wellbore Radius	$r_w=0.1$m
Minimum Pressure Gradient	$G=10^2,10^3,10^4$,Pa/m

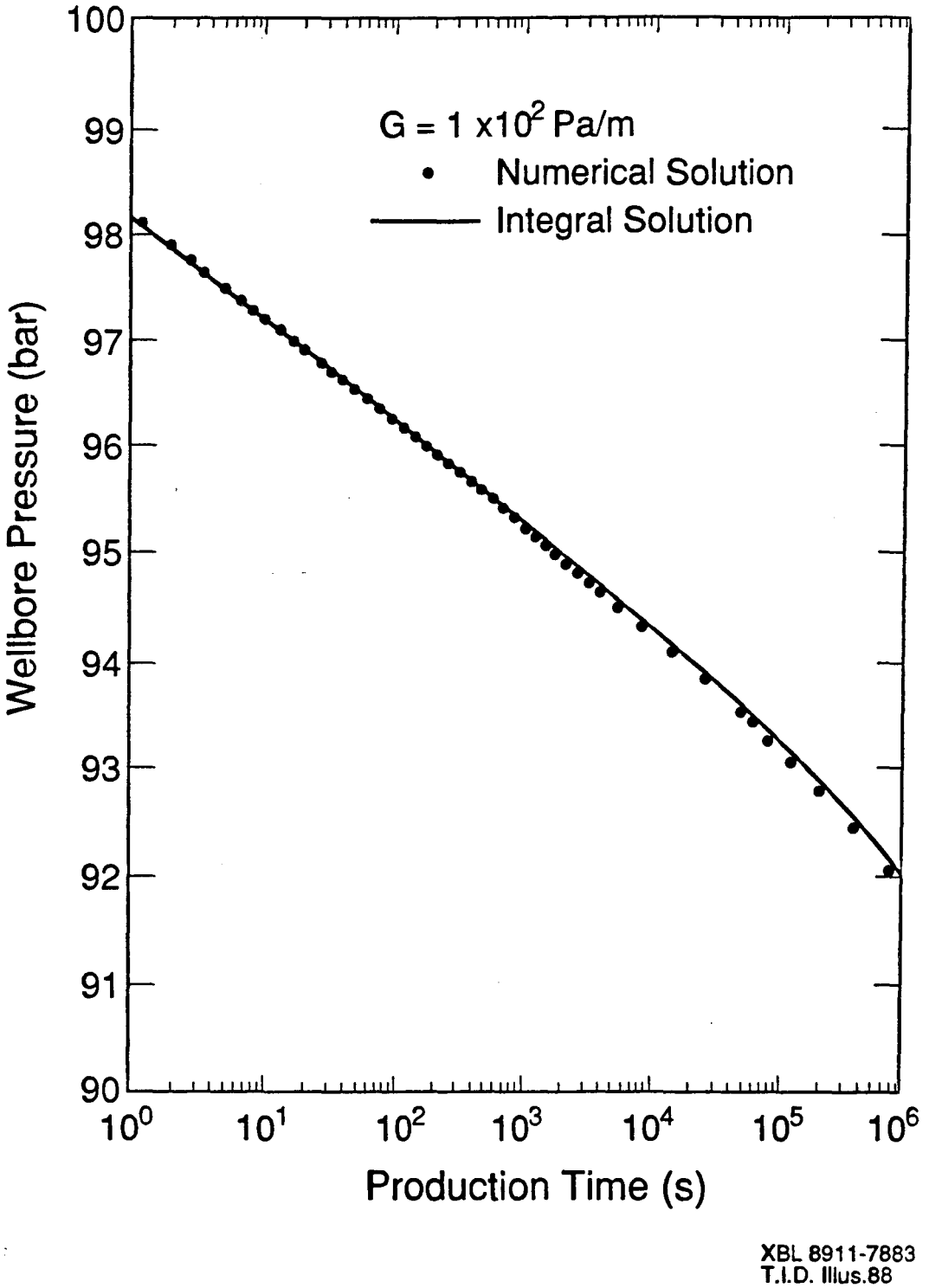

Figure 9.5 Comparison of Wellbore Pressures during Bingham Fluid Production, Calculated from the Numerical Solution and the Integral Solution (G = 100 Pa/m).

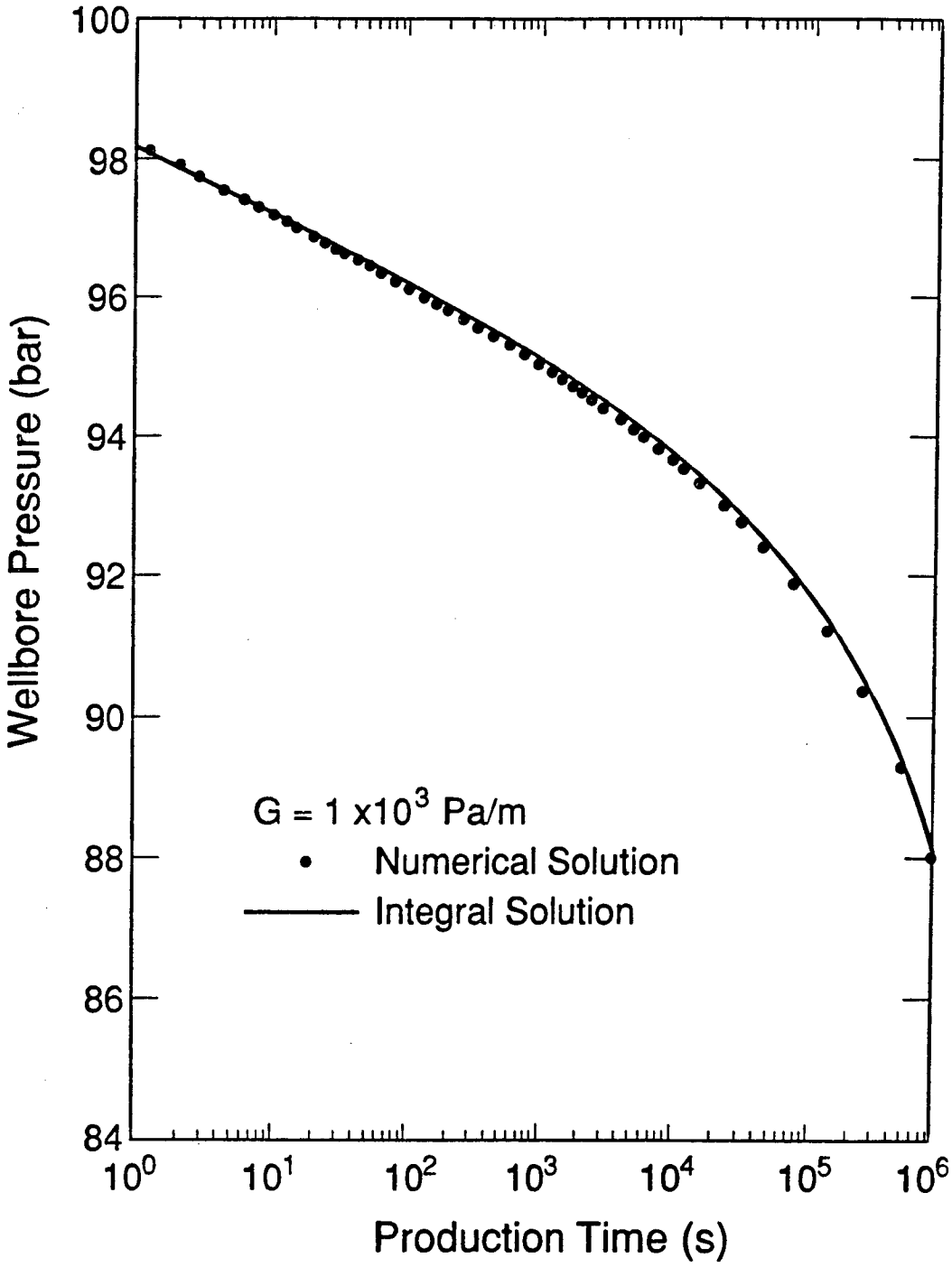

XBL 8911-7884
T.I.D. Illus.88

Figure 9.6 Comparison of Wellbore Pressures during Bingham Fluid Production, Calculated from the Numerical Solution and the Integral Solution (G = 1000 Pa/m).

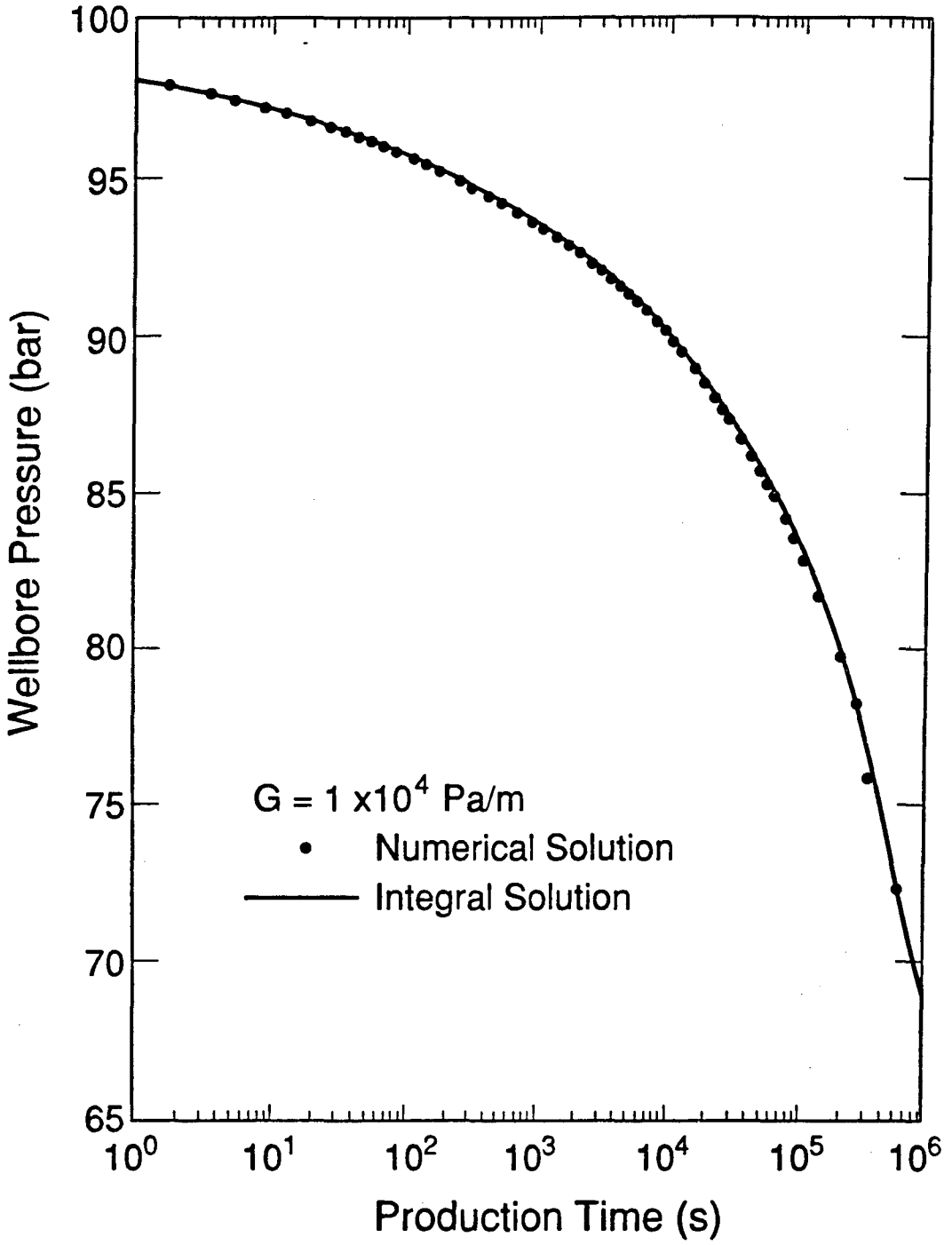

XBL 8911-7885
T.I.D. Illus.88

Figure 9.7 Comparison of Wellbore Pressures during Bingham Fluid Production, Calculated from the Numerical Solution and the Integral Solution (G = 10000 Pa/m).

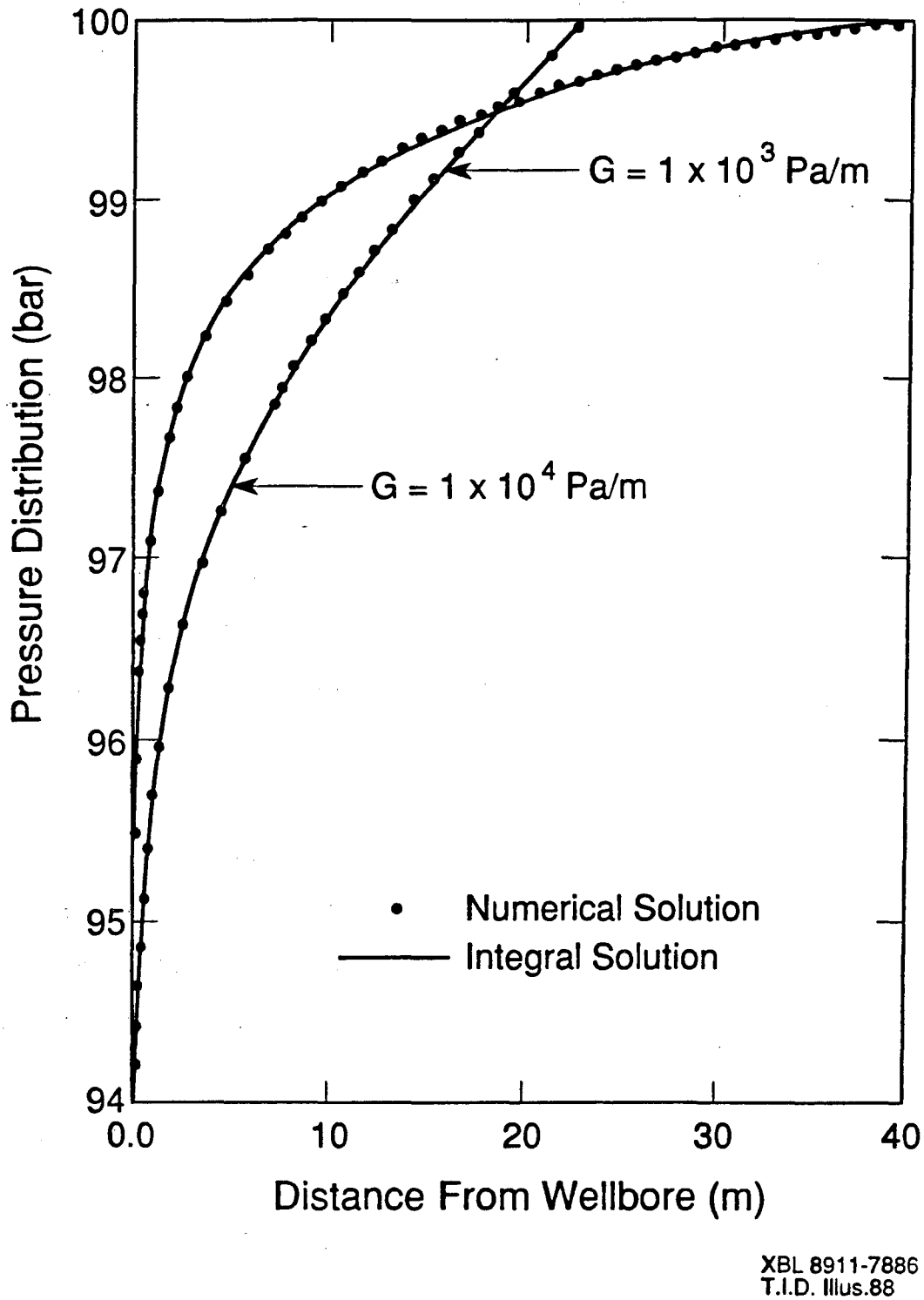

Figure 9.8 Comparison of Pressure Distributions of Bingham Fluid Production, Calculated from the Numerical Solution and the Integral Solution.

literature, is not satisfactory and will result in large errors.

9.4 Flow of a Bingham Fluid through a Porous Medium

The flow of a Bingham fluid in a porous medium is characterized by the two non-Newtonian parameters, the minimum pressure gradient G, and the Bingham plastic coefficient μ_b. The effects of the non-Newtonian rheological properties on the flow behavior in an infinite radial formation can be discussed using the integral solution of Section 9.2, since its accuracy has been confirmed. The input parameters that will be used for the fluid and formation are given in Table 9.3.

Pressure drawdown at the wellbore is shown in Figure 9.9 when a Bingham fluid is produced at a constant mass production rate. Physically, the flow resistance increases with an increase in the minimum pressure gradient G in the reservoir.

It can be seen from Figure 9.9 that in order to maintain the same production rate, the wellbore pressures will decrease more rapidly as G increases. The pressure profiles at different values of G after continuous production of 10 hours are given on Figures 9.10 and 9.11. The pressure drops penetrate less deeply into the formation as the minimum pressure gradient increases. It should be note in the semi-log plot of the pressure distributions on Figure 9.11 that parallel semi-log straight lines of pressure versus log (r) in the formation exist near the wellbore for various values of G. Semi-log straight lines are also developed in the pressure drawdown curves of Figure 9.9. This suggests that the conventional semi-log analysis method to calculate flow and formation properties can be used.

The effects of the Bingham plastic coefficient, μ_b, are shown in Figure 9.12. This coefficient becomes the viscosity of a Newtonian fluid if G = 0. The apparent viscosity

Table 9.3

Parameters for a Bingham fluid Flow through a Porous Medium

Initial Pressure	$P_i=10^7$Pa
Initial Porosity	$\phi_i=0.20$
Initial Fluid Density	$\rho_i=1000.0$up3
Formation thickness	h=1m
Bingham Plastic Coefficient	$\mu_b=1.0\times10^{-3}$Pa.s
Fluid Compressibility	$C_f=4.55575\times10^{-10}Pa^{-1}$
Rock Compressibility	$C_r=2.0\times10^{-10}Pa^{-1}$
Mass Production Rate	Q_m=0.5kg/s
Permeability	$K=9.869\times10^{-13}m^2$
Wellbore Radius	r_w=0.1m
Minimum Pressure Gradient	$G=10^2,10^3,10^4$,Pa/m

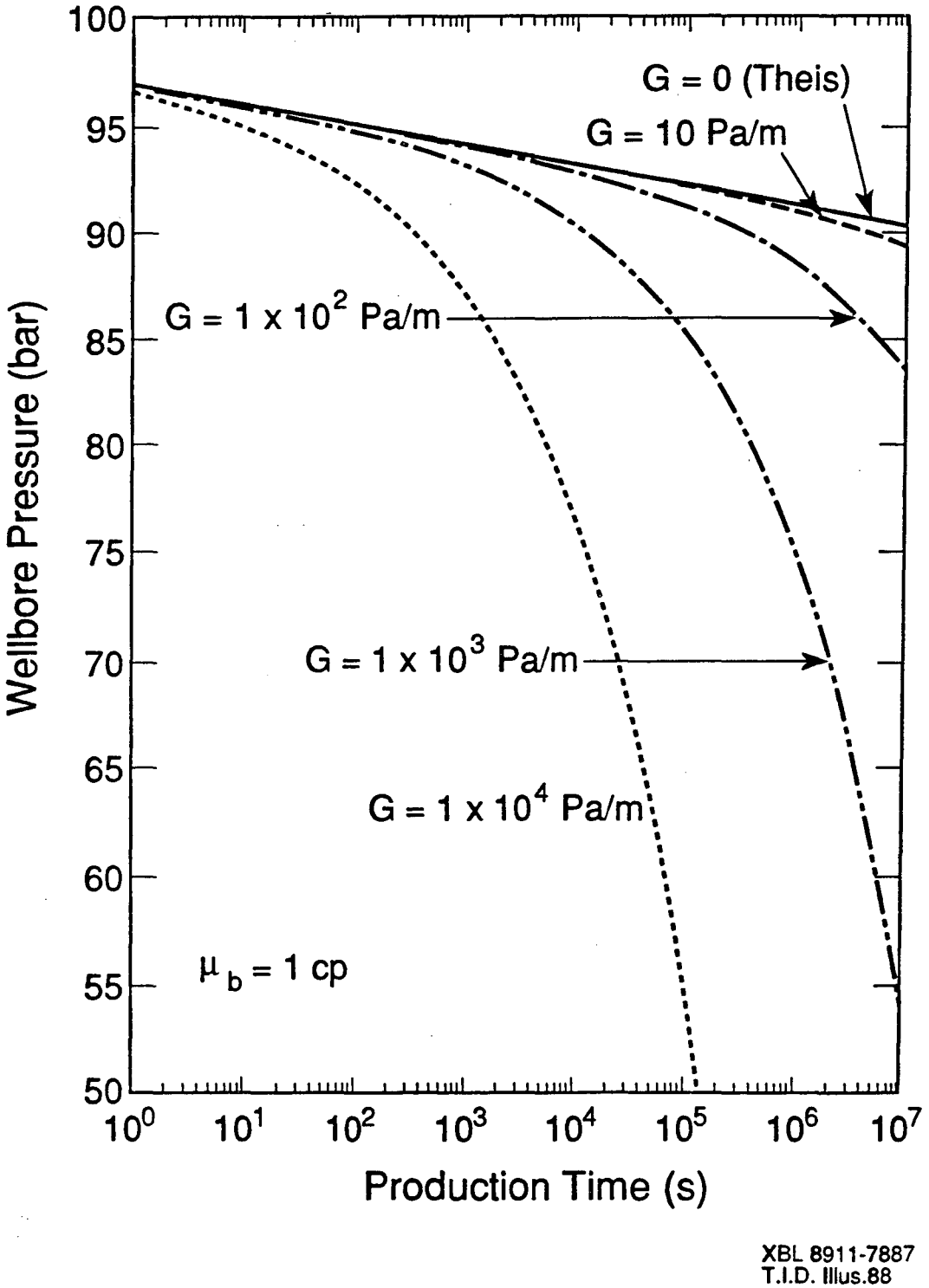

Figure 9.9 Transient Wellbore Pressure Behavior during Bingham Fluid Production, Effects of the Minimum Pressure Gradient.

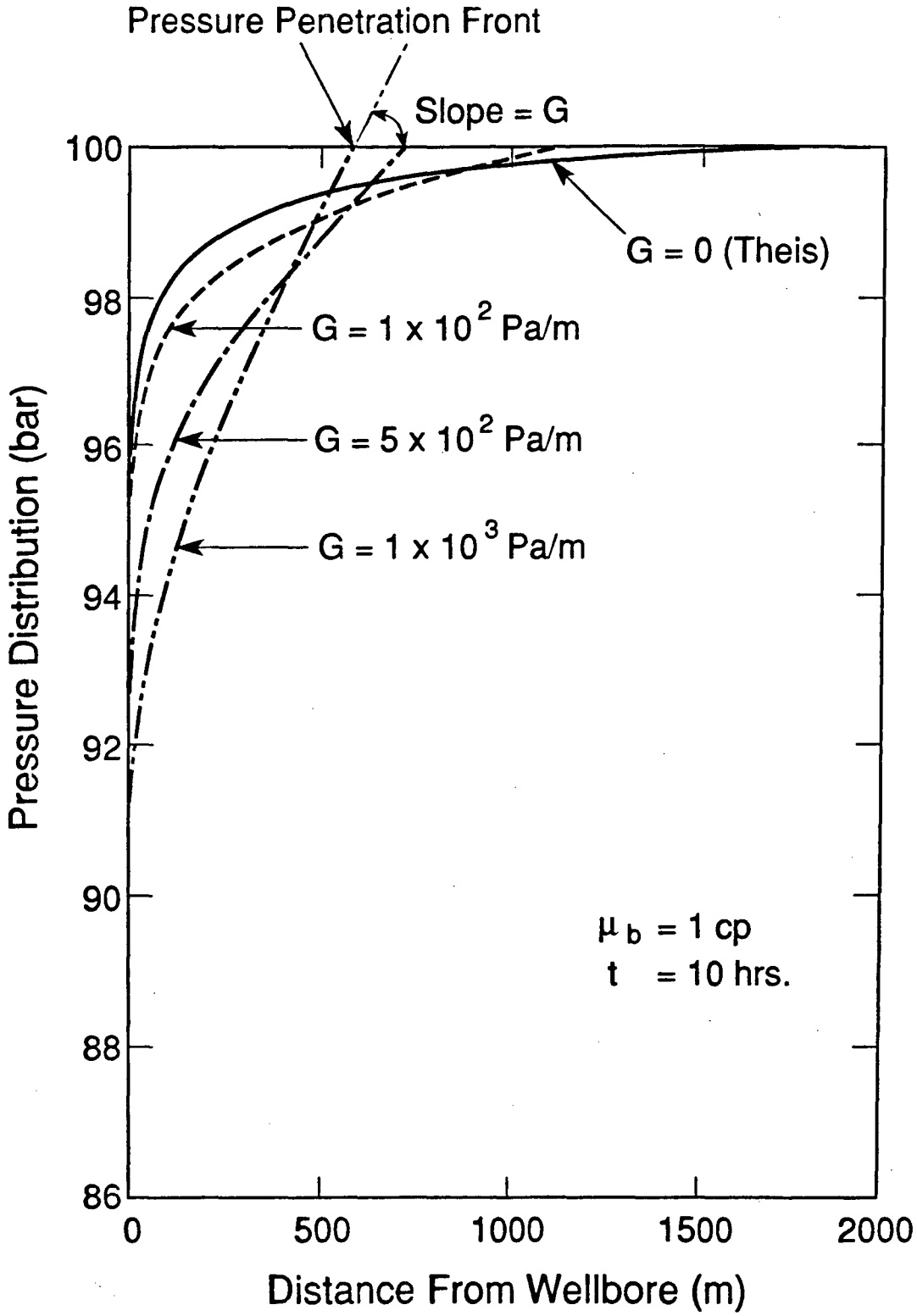

Figure 9.10 Pressure Distributions in a Linear Plot of Bingham Fluid Production, Effects of the Minimum Pressure Gradient.

XBL 8911-7888
T.I.D. Illus.88

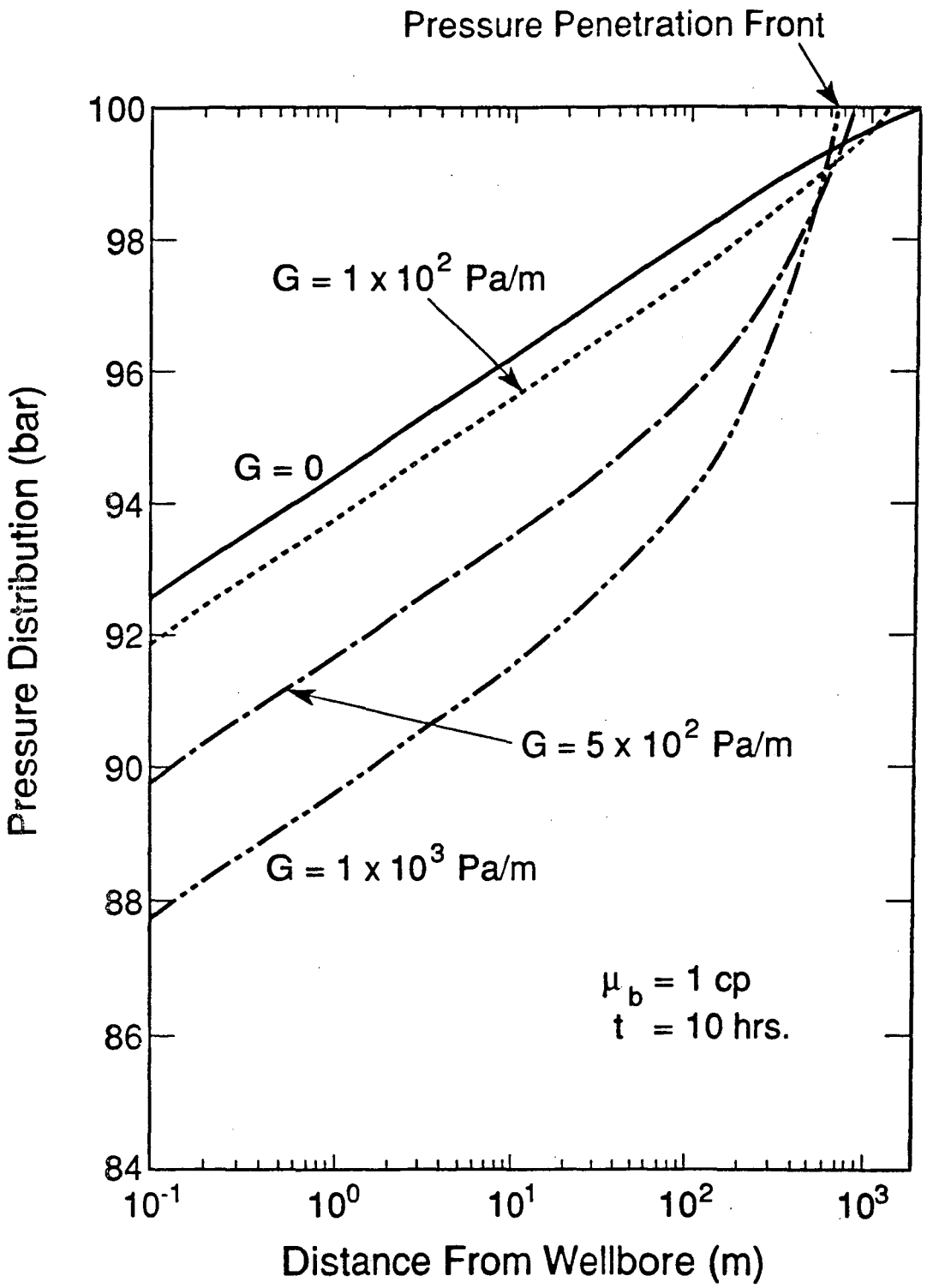

XBL 8911-7889
T.I.D. Illus.88

Figure 9.11 Pressure Distributions in a Semi-Log Plot of Bingham Fluid Production, Effects of the Minimum Pressure Gradient.

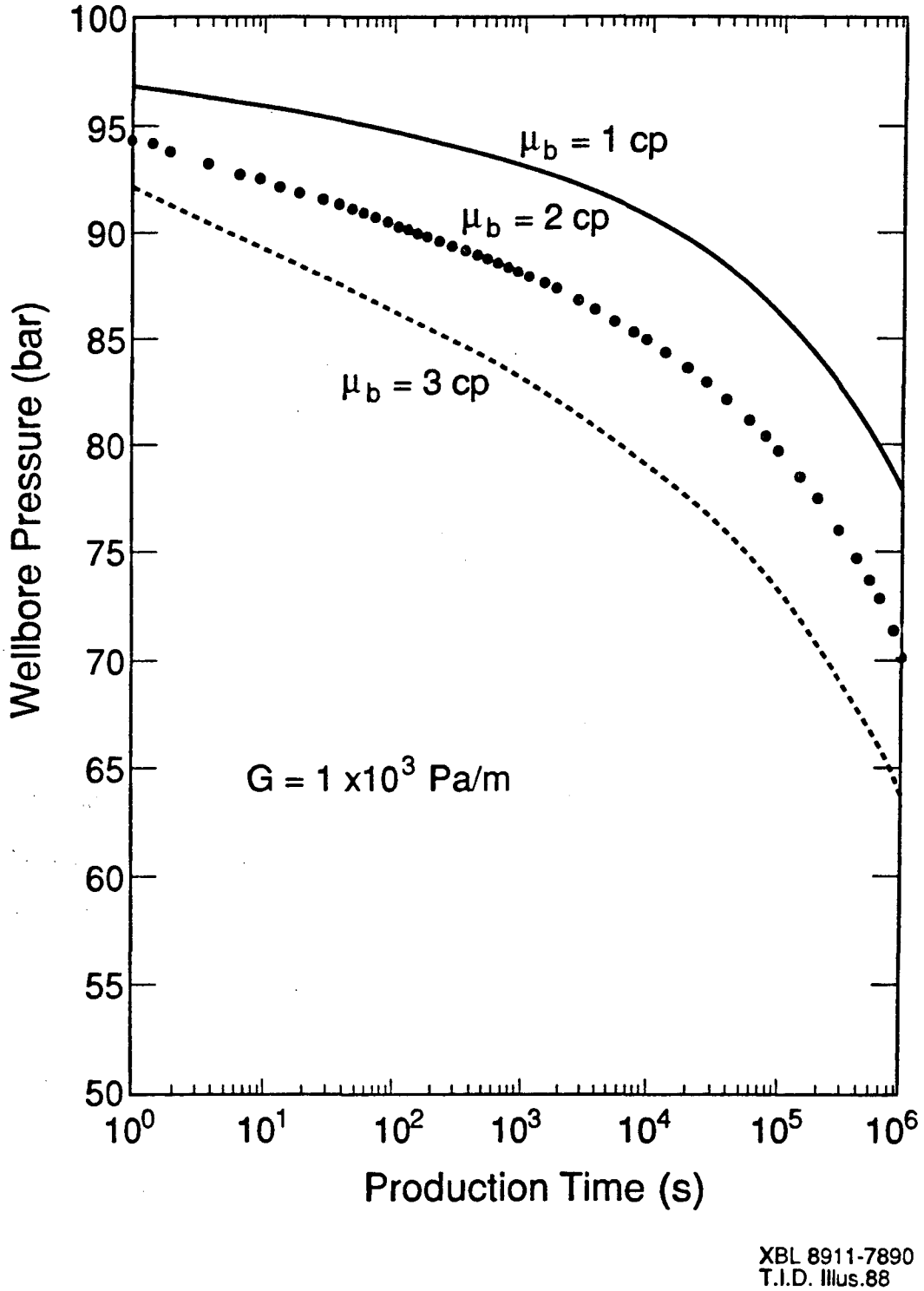

Figure 9.12 Transient Wellbore Pressure Behavior during Bingham Fluid Production, Effects of the Bingham Coefficient μ_b .

of a Bingham fluid is proportional to μ_b , as given by Equation 3.14. Therefore, as μ_b increases, the flow resistance increases, and the pressure drops more rapidly to satisfy the constant production rate at the well. Figure 9.12 also show that semi-log straight lines exist during the earlier transient time which can be used to estimate the value of μ_b.

The pressure changes at r = 100 m from the wellbore during production from the system are given in Figure 9.13. The figure shows that pressures in the formation decrease more dramatically than in the wellbore after a period of time delay. At r = 100 m, there is hardly a straight line developed in the semi-log graph of pressure versus time for $G > 0$.

9.5 Well Testing Analysis of Bingham Fluid Flow

A new method for analysis of transient pressure tests during a Bingham fluid production from and injection into a well can be developed, based on the integral and numerical solutions in this chapter. The most important factors for Bingham fluid flow through porous medium are the two characteristic rheological parameters, the minimum pressure gradient, G, and the coefficient, μ_b. Both of them can be determined by a well-controlled single well pressure test, discussed below. It is always possible to obtain these parameters by trial and error, using the integral or numerical solutions to match the observed pressure data. However, the following approach is more accurate and convenient to use, and therefore is recommended for field applications.

Let us consider the pressure buildup behavior at a producing well in an infinite horizontal formation. After a period of production, the well is shut in. Physically, the pressure in the system after a long enough shut-in period will buildup until a new equilibrium is reached. Then, there is a stable pressure drop formed from wellbore to a

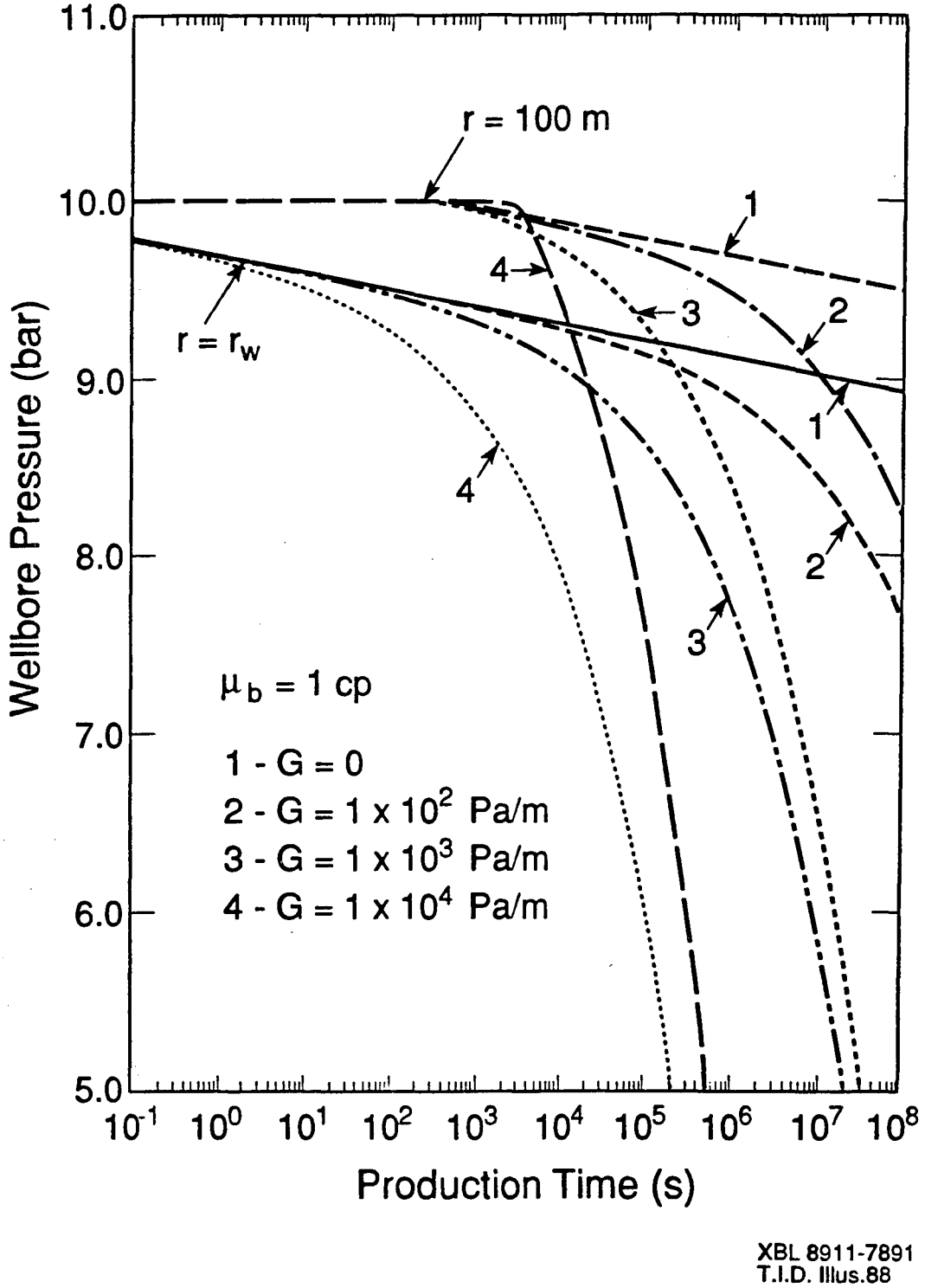

Figure 9.13 Comparison of Wellbore and Formation Pressures during Bingham Fluid Production, Effects of the Minimum Pressure Gradient.

certain pressure penetration distance, and the pressure gradient everywhere in the pressure drop zone is expected to be equal to the minimum pressure gradient. This is confirmed by a numerical study of the pressure buildup, as shown in Figure 9.14, after $t_p = 1{,}000$ seconds of Bingham fluid production from a well. The flow and formation properties used are provided in Table 9.4. If we know the cumulative mass production rate Q_c before the well is shut in, and measure the stable wellbore pressure P_w at a long time after stopping production from the well, the minimum pressure gradient of the system can be calculated (see Appendix E) by

$$G = \frac{1}{2Q_c}\left\{\pi h r_w \rho_i \phi_i C_t (\Delta P)^2 + \left[[\pi h r_w \rho_i \phi_i C_t (\Delta P)^2]^2 + 4\pi h \rho_i \phi_i C_t (\Delta P)^3/3\right]^{1/2}\right\} \quad (9.7)$$

where $\Delta P = P_i - P_w$, the stable pressure drop at wellbore, measured at a long time after well shut-in. It is interesting to note that the minimum pressure gradient determined by the pressure buildup method, Equation 9.7, is independent of the flow properties, such as permeability K, and the coefficient μ_b, since the equilibrium is obtained in the system.

A Bingham fluid buildup test example is here created by the numerical simulator, to illustrate the procedure of calculating the value of G. The input data are from Table 9.4, and the stable wellbore pressure is found to be $P_w = .97474\times10^7$ Pa, at a long well shut-in time from the simulated test. A Bingham fluid is produced at a mass rate $Q_m = 0.1$ Kg/s until the production time $t_p = 1{,}000$ seconds, and then the well is shut in. Thus, the minimum pressure gradient can be calculated by Equation 9.7,

$$G = \frac{1}{200}\times\left[1.1737423\times10^5 + \left[1.377671\times10^8 + 3.953165\times10^{12}\right]^{1/2}\right]$$

$$= 10{,}000.14 \text{ (Pa/m)} \quad (9.8)$$

This is very accurate compared with the input value, G = 10,000 Pa/m, in the numerical calculation. Then, the pressure penetration distance under the equilibrium is,

$$\delta(t) = \frac{\Delta P}{G} = \frac{2.526\times10^5}{10{,}000.14} = 25.26 \text{ (m)} \quad (9.9)$$

Table 9.4
Parameters for Well Testing Analysis

Initial Pressure	$P_i=10^7$Pa
Initial Porosity	$\phi_i=0.20$
Initial Fluid Density	$\rho_i=975.9$kg/m^3
Formation thickness	h=1m
Bingham Plastic Coefficient	$\mu_b=5.0\times10^{-3}$Pa.s
Total Compressibility	$C_t=9.0\times10^{-9}$Pa^{-1}
Mass Production Rate	$Q_m=0.1$kg/s
Permeability	$K=9.869\times10^{-13}$m^2
Minimum Pressure Gradient	$G=1.0\times10^4$Pa/m
Wellbore Radius	$r_w=0.1$m

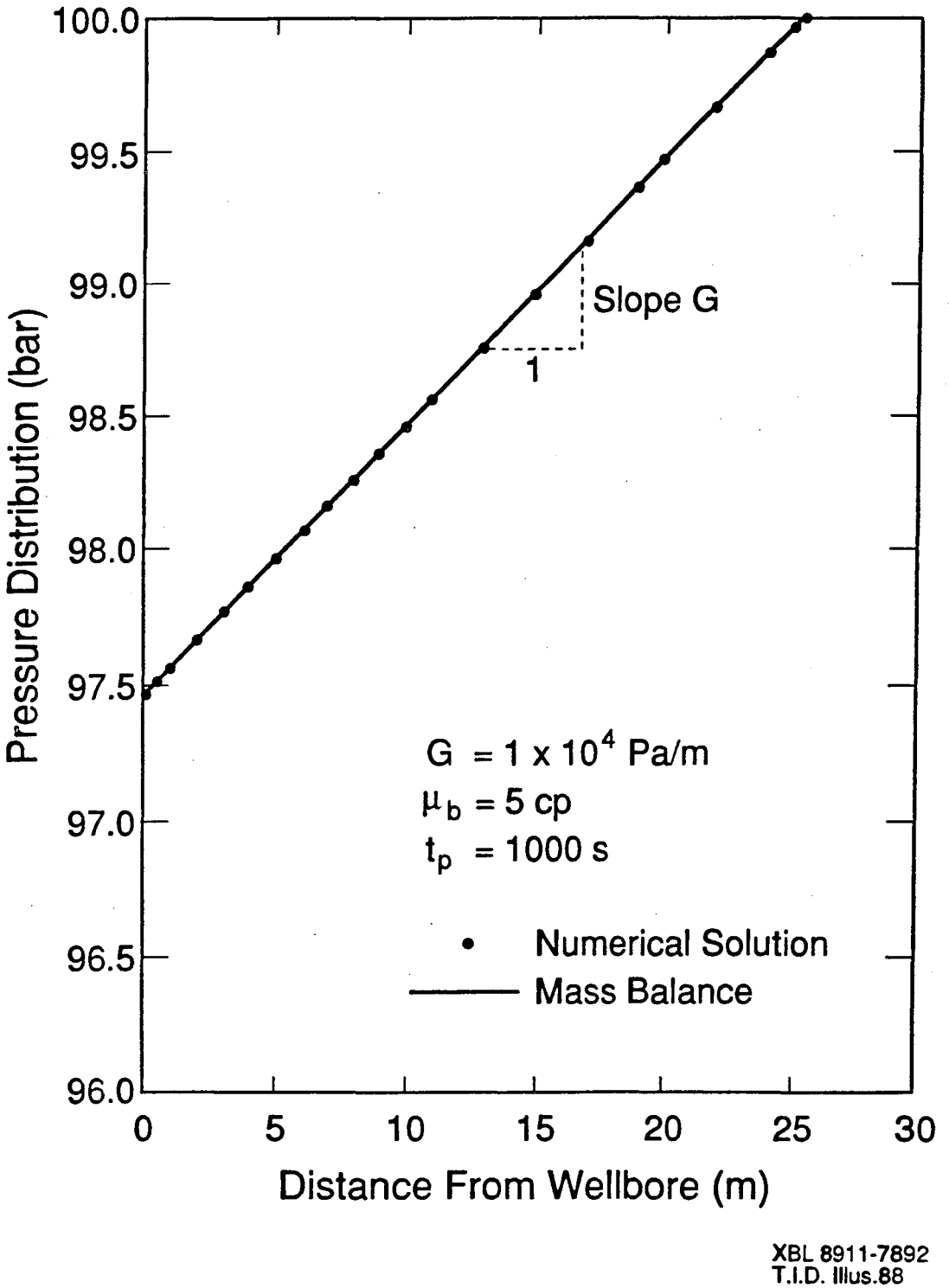

Figure 9.14 Pressure Distribution at Long-Time of Well Shut-in after 1000 Seconds of Bingham Fluid Production.

The pressure distribution after a long time shut-in calculated from the mass balance is also shown in Figure 9.14, by the solid line curve. The analytical and numerical results are essentially identical to each other in the figure.

The apparent mobility, (K/μ_b), is a flow property of the system, and may be determined by only the transient flow tests of pressure drawdown and buildup. As shown in Figures 9.9 and 9.12, the semi-log straight lines occur in the pressure drawdown curves during the early transient period, when minimum pressure gradient, G, is not very large. The semi-log straight lines are almost in parallel with the straight line from the Theis solution (G = 0) on Figure 9.9. Therefore, if the semi-log straight line is developed during the earlier flow time in the transient drawdown analysis plot, the conventional analysis technique of pressure drawdown (Earlougher, 1977; Matthews and Russell, 1967) can be used to estimate the value of (K/μ_b) for a Bingham fluid flow problem,

$$\frac{K}{\mu_b} = \frac{2.303 \times Q}{4\pi hm} \tag{9.10}$$

where m is the slope of the semi-log straight line; and Q is the constant volumetric production rate.

A simulated pressure drawdown test is generated by the integral solution, and the parameters used are the same as in Table 9.3. The pressure drawdown curves of the test are shown in Figure 9.15. The slope m of the semi-log straight line part of the curve G = 100 Pa/m, is measured as 9.24×10^4 Pa/$\log_{10}$–cycle , and the slope of the curve G = 1,000 Pa/m is 9.95×10^4 Pa/$\log_{10}$–cycle . Then, K/μ_b , can be estimated as,

$$\frac{k}{\mu_b} = \frac{2.303\times0.5/1000.0}{4\times3.1415926\times1.0\times9.24\times10^4}$$

$$= 9.92\times10^{-10}\ (m^2/Pa\cdot s) \tag{9.11}$$

from the curve G = 100 Pa/m, and

$$\frac{k}{\mu_b} = \frac{2.303\times0.5/1000.0}{4\times3.1415926\times1.0\times9.95\times10^4}$$

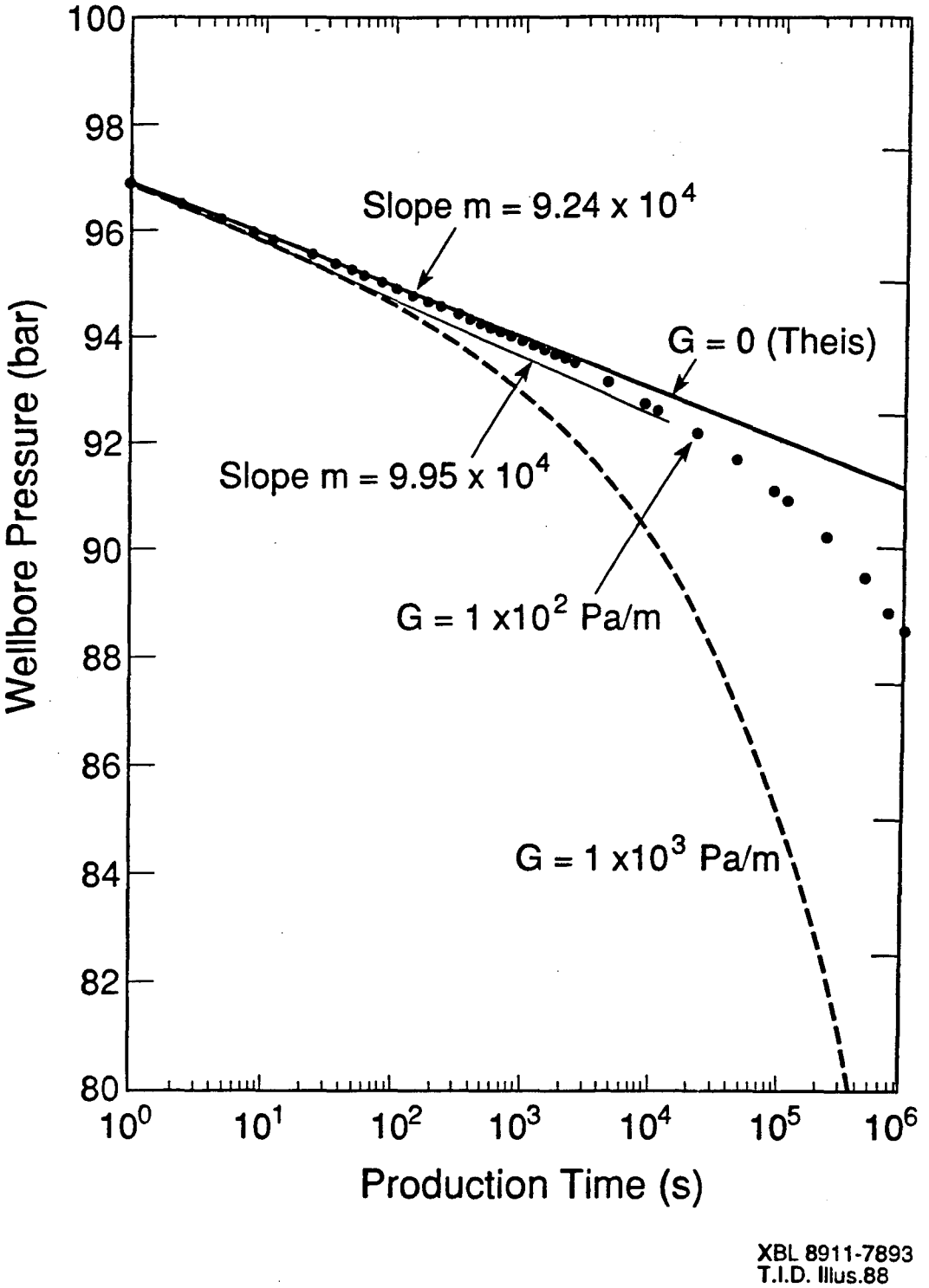

Figure 9.15 Semi-Log Pressure Drawdown Curves for Determining the Apparent Mobility.

$$= 9.21\times10^{-10}\ (m^2/Pa\cdot s) \tag{9.12}$$

From the curve G = 1,000 Pa/m. In the simulated test, the actual input is

$$\frac{K}{\mu_b} = \frac{.9869\times10^{-12}}{1.0\times10^{-3}} = 9.87\times10^{-10}(m^2/Pa\cdot s) \tag{9.13}$$

So, the relative errors introduced into the results are 0.5 % and 6.7 % from the two calculations, respectively. The curve G = 100 Pa/m gives a more accurate prediction.

For a large value of minimum pressure gradient, G, in a system, there hardly exist semi-log straight lines in the pressure drawdown plots of Figure 9.9. However, the pressure buildup curves, as shown in Figures 9.16 and 9.17, do result in a long straight line even for the large minimum pressure gradient, G = 10,000 Pa/m. This pressure buildup test is conducted by the numerical code. The top curve is calculated from the integral solution, based on the superposition principle. It is obvious that the superposition technique cannot be used for this non-linear problem. The slope of the semi-log straight line of Figure 9.16 can be measured, m=9.17×10^4 $\log_{10}$–cycle . Then, we have

$$\frac{K}{\mu_b} = \frac{2.303\times0.1/975.9}{4\times3.1415926\times1.0\times9.17\times10^4} = 2.05\times10^{-10}\ (m^2/Pa\cdot s) \tag{9.14}$$

This value introduces only 3.8 % errors in the result by comparison with the input value, $K/\mu_b = 1.97\times10^{-10}\ m^2/Pa\cdot s$.

If no straight lines have developed in both pressure drawdown and pressure buildup curves in a well test, then the apparent mobility can be obtained by using the integral solution to match the observed transient pressure data. In this procedure, the minimum pressure gradient, G, should be calculated first by the mass balance calculation of Equation 9.7, which is always applicable. Then, the only unknown is the apparent mobility, (K/μ_b), and it will not be very difficult to determine by trial and error.

In general, we cannot separate the permeability K and the Bingham plastic coefficient μ_b by the transient pressure tests only, even though their ratio, apparent

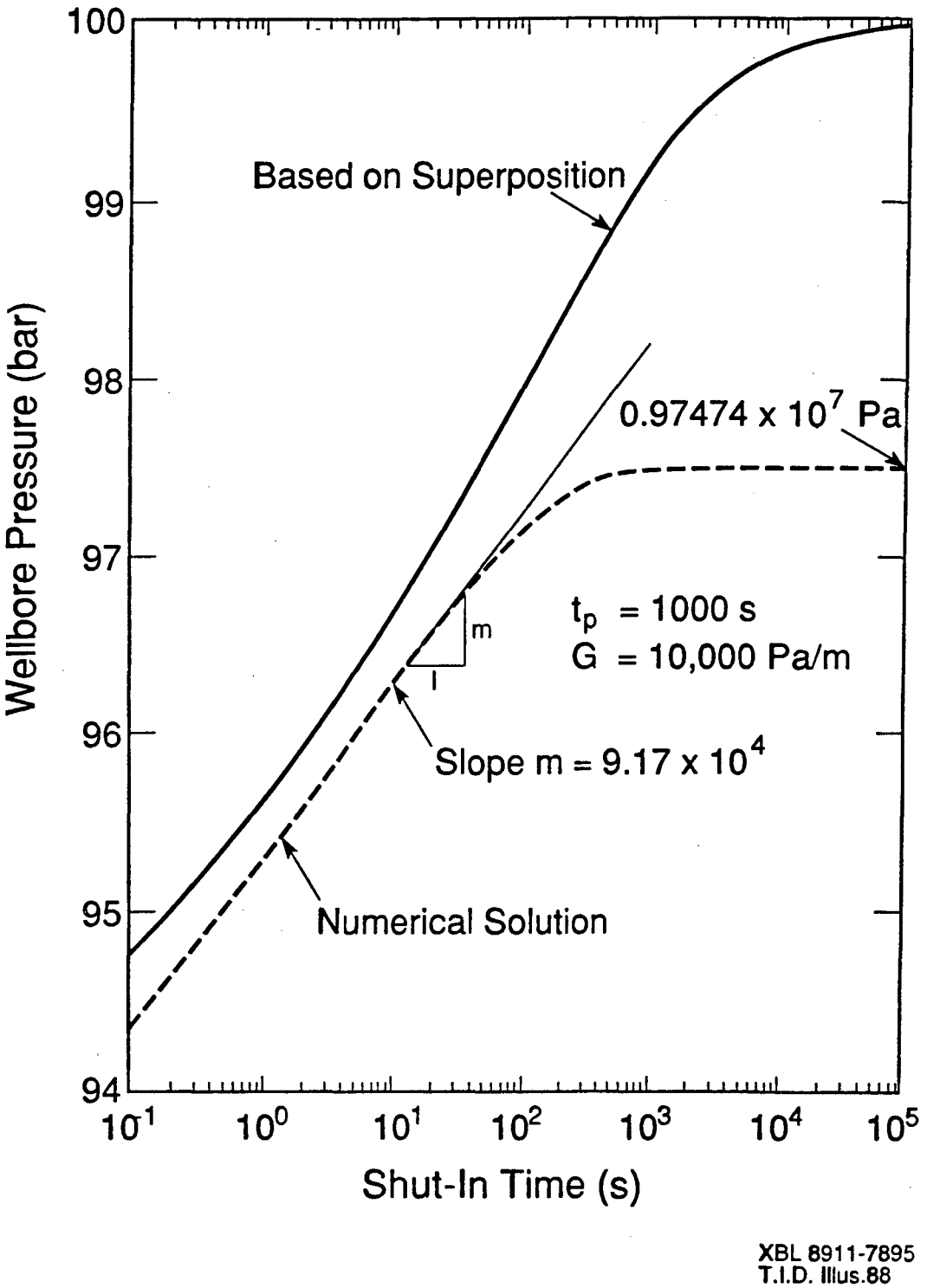

Figure 9.16 Pressure Buildup during Well Shut-in after 1000 Seconds of Bingham Fluid Production.

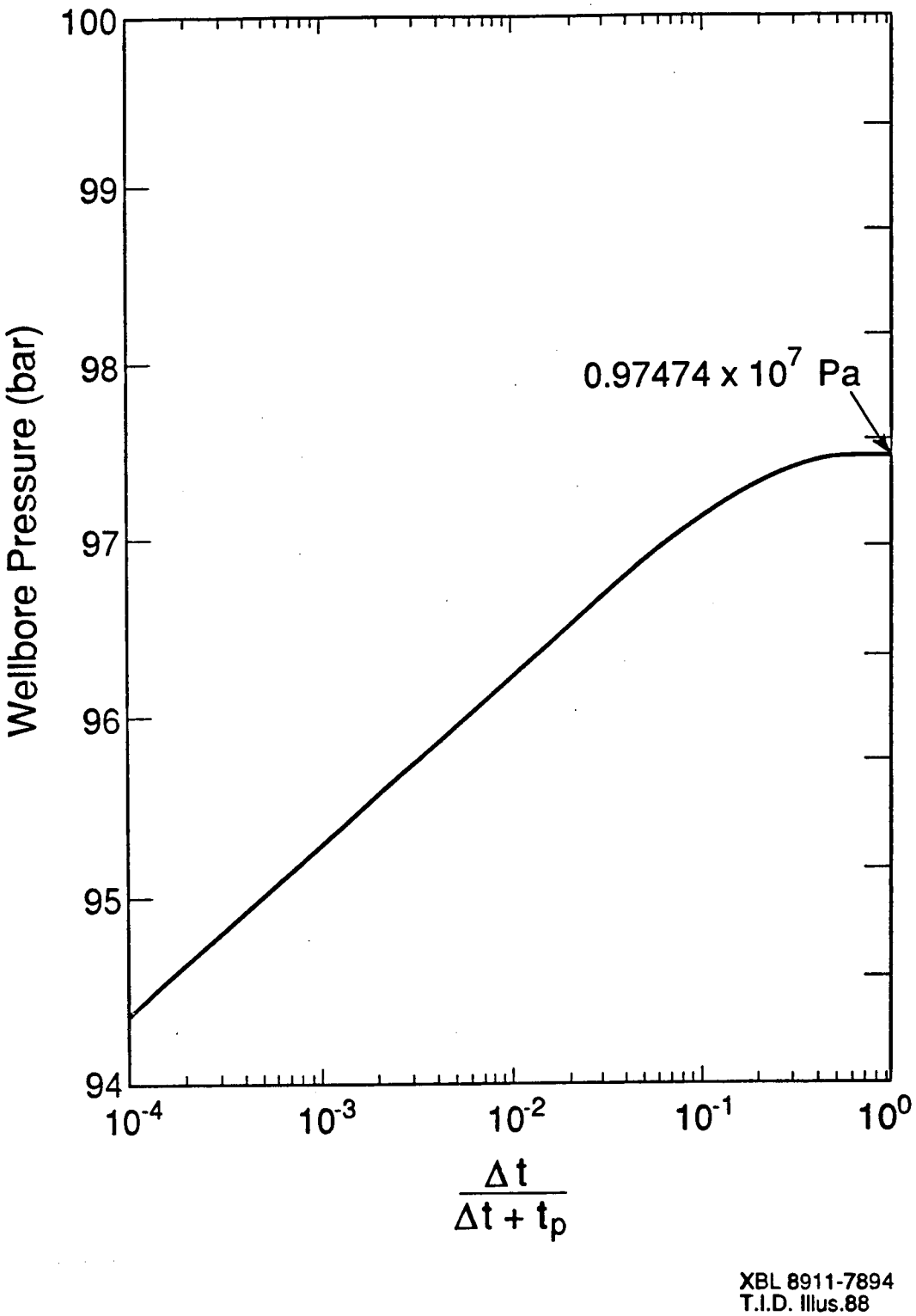

Figure 9.17 Horner Plot of Pressure Buildup during Well Shut-in after 1000 Seconds of Bingham Fluid Production.

mobility, has been determined. In order to estimate the non-Newtonian coefficient μ_b, we need some other techniques, such as core analysis, to find the permeability of the reservoir.

Finally, the effects of wellbore storage and skin have not been considered in this study, which may significantly affect the early pressure transient data in a field test. Since little information about the formation can be obtained from transient test data dominated by the wellbore storage effect, in this case, it will be more complicated to determine the apparent mobility from the early transient data. However, the mass balance calculation of the minimum pressure gradient is not influenced by the storage and skin effects. Also, the integral solution provided in this work have the ability to decrease the effects of wellbore storage on the analytical results by adjusting the production rate as a function of time.

9.6 Conclusions

An integral solution has been obtained for a flow problem of Bingham fluids through a porous medium, and its accuracy is confirmed by comparison of the integral results with the exact and numerical solutions. The analytical and numerical studies show that the transient flow behavior of a slightly compressible Bingham fluid is essentially controlled by the non-Newtonian properties, the minimum pressure gradient G, and the coefficient μ_b. Therefore, the transient pressure data will provide some important information related to the non-Newtonian fluid and formation properties. The well testing analysis technique, developed in this study, uses these flow test data to estimate the non-Newtonian flow properties in the system.

The integral method with the pressure profile used in this work will find more applications for radial flow problems in porous medium. It is especially useful when the

flow equation is non-linear and other analytical approaches cannot apply.

Chapter 10
Conclusions and Recommendations

10.1 Conclusions

The primary objective of the present study was to develop a new methodology to investigate transport phenomena of non-Newtonian fluids through porous media. Whenever non-Newtonian fluids are involved in porous media, the flow problem will become non-linear because the apparent viscosity used in the Darcy equation is a function of shear rate. The viscosity function for a non-Newtonian fluid depends on shear rate, or pore velocity in a porous medium in a complex way. The non-Newtonian rheological behavior is quite different for different fluids and/or for different porous materials. Therefore, it is impossible to develop a universal approach for handling various non-Newtonian fluid flow problems. However, under some special circumstances, analytical solutions have been proven here to be possible for describing non-Newtonian flow in porous media. In this work both analytical and numerical methods have been employed, and major attention has been paid to power-law and Bingham plastic fluids, since they are the most likely to be encountered in reservoirs.

Among the theoretical methods contributed from this work, a fully implicit three-dimensional integral finite difference model has been developed by modifying the general numerical code "MULKOM" to include the effects of non-Newtonian viscosity. This new simulator is capable of modeling both single and multiple phase non-Newtonian fluid flow through porous or fractured media. The numerical model can take account of all the important factors which affect the flow behavior of non-Newtonian and Newtonian fluids, such as capillary pressure, complicated flow domains, inhomogeneous porous media, and various well operation conditions. Different non-Newtonian

rheological models have been incorporated in the code. The validity of the numerical method has been checked by comparing the numerical results with analytical solutions for displacement of a Newtonian fluid by a power-law fluid. In this study, this code has been successfully applied to numerical investigations of transient flow of power-law fluids and to verification of the integral solution for Bingham fluid flow.

Along with the numerical technique, an analytical solution for one-dimensional immiscible displacement of non-Newtonian and Newtonian fluids in porous media has been obtained, in analogy with the Buckley-Leverett theory for Newtonian fluid displacement. The non-Newtonian fluid viscosity is assumed to be a function of the local flow potential gradient and saturation. Therefore, this solution is generally applicable to various non-Newtonian and Newtonian fluid displacement. To apply this theory to a field problem, a graphic procedure for evaluating displacement of non-Newtonian and Newtonian fluids has also been developed from the analytical solution. The resulting method can be regarded as an extension of the Buckley-Leverett-Welge theory to the flow problem of non-Newtonian fluids in porous media. This solution has been used, i) to study the physical mechanisms of immiscible flow with power-law and Bingham fluids; and ii) to verify the numerical code in this work.

An integral method has also been presented for analysis of non-linear single phase Bingham fluid flow through porous media. The integral method, widely used in the study of unsteady heat transfer problems, is applied to derive an approximate analytical solution for radial flow of a Bingham fluid. Using a newly-proposed pressure profile, the integral solution has been examined numerically to give very accurate results for the Bingham fluid flow. Based on the integral solution, a well test analysis method for Bingham fluid flow is constructed to determine the rheological and formation properties. In addition, a general procedure for application of the integral technique to flow problems in porous media has been outlined, which can be applied for analyzing other non-linear flow problems through porous media.

The physical mechanisms of non-capillary displacement with non-Newtonian fluids in porous media are revealed by the Buckley-Leverett type analytical solution. The non-Newtonian immiscible displacement is a complicated process, which is controlled by the rheological properties of the non-Newtonian fluids and the flow condition, in addition to relative permeability. It has been known from Buckley-Leverett theory that injection rate has no effects on displacement efficiency for Newtonian fluids under the stabilized condition. As discussed in this work, a fundamental difference between Newtonian and Non-Newtonian displacement is that the non-Newtonian displacement is flow rate dependent because of changes in non-Newtonian viscosity with pore flow velocity.

Power-law and Bingham plastic fluids are the most commonly encountered non-Newtonian fluids in porous media flow problems. Therefore, a detailed study has been made on the displacement behavior of these two fluids in order to obtain an understanding of the physics behind the immiscible flow process. For displacement of a Newtonian fluid by a shearing-thinning power-law fluid, such as in oil production by polymer flooding, the sweep efficiency can be improved by reducing injection rates of the power-law fluid. As to a Bingham fluid displaced by a Newtonian one, with a practical example of heavy oil recovery by water flooding, the displacement is characterized by an ultimate sweep saturation, and no further improvement can be achieved when the saturation approaches the ultimate saturation under the same flow operation.

A further theoretical study has been performed for transient flow problems of power-law fluids by using the numerical code. In the first place, this numerical investigation has improved the existing well test analysis technique of power-law fluid injectivity tests for general applicability. Secondly, an idealized fracture model has been used to study the transient flow of a power-law fluid through a double-porosity medium. The non-Newtonian behavior is found to be generate two parallel log-log straight lines on a wellbore pressure-time plot, instead of two parallel semi-log straight lines for

Newtonian fluid flow. The third problem is to obtain some insights into pseudoplastic fluid flow through porous media. The Meter four-parameter rheological model was used for calculating apparent viscosity of the pseudoplastic fluid. The finding is that the transient pressure responses in the flow system tend to an equivalent Newtonian system at long times, which is quite different from a power-law flow problem.

A new theory for analyzing single phase Bingham fluid flow in porous media has been developed, based on the integral analytical and numerical solutions. The transient flow of a slightly-compressible Bingham fluid has been shown to be determined essentially by the Bingham rheological properties. Application of the theory has been demonstrated for analysis of two simulated pressure drawdown and buildup tests.

10.2 Recommendations

This work has focused on the theoretical aspects of non-Newtonian fluid transport through porous media, and its emphasis is on the physical insights in "non-Newtonian" behavior. As a result of this, many of the results in the theoretical development depend on the assumptions about rheological properties, which are based on the previous experimental research. Since most of the laboratory studies of non-Newtonian flow in the literature were conducted using only single phase non-Newtonian fluids, there certainly is a need for further experiments under multiple phase flow condition. Such experimental studies should be designed to provide us with rheological models for the non-Newtonian fluid and porous materials of interest. In the present study, the apparent viscosity for multiple phase flow of non-Newtonian fluids is taken as a function of flow potential gradient and saturation. Physically, this is a natural extension of the single phase flow theory to a multiple phase flow problem. However, this assumption needs to be confirmed experimentally. Just as in multiple phase Newtonian fluid flow, the

extension of Darcy's law to multiple phase flow is, in fact, a heuristic procedure suggested by the analogy with single phase flow. Then, experimental work is required to verify this speculation.

Effects of capillary pressure on immiscible non-Newtonian fluid flow have been ignored in the analytical analysis, which is necessary to develop the Buckley-Leverett type solution. For Newtonian displacement, various investigators have concluded that for high flow rates the Buckley-leverett non-capillary theory gives a good approximation of the actual saturation distribution. At low flow rates, the influence of capillary pressure becomes important. For non-Newtonian displacement, similar experimental studies should also be carried out to look at capillary effects. This can be easily done by using the numerical code since it has the ability to include capillary effects, as long as the capillarity data are obtained from experiments.

As an application of the theory developed in this work on the transient flow of Bingham type non-Newtonian fluids in porous media, transient pressure tests are recommended to perform in certain heavy oil reservoirs. Since no well test data are available for Bingham oil flow in the literature, the new analysis method proposed for analyzing Bingham fluid flow was here used to interpret only the simulated well testing examples. Currently, there is no quantitative approach in the petroleum engineering and groundwater literature for well test analysis on Bingham fluid production or injection in reservoirs. Many efforts should be made to obtain flow properties of Bingham fluid in porous media, which is very important for heavy oil development and numerous other applications.

Non-Newtonian fluid flow in porous media usually is affected by the chemical concentration in the fluid. Such as for a polymer solution, changes in polymer concentration will result in changes in its viscosity. The chemical composition effect is not included in this work. It is obvious that the study of non-Newtonian flow coupled with chemical transport is a whole new area for further research efforts in this field. Among other

factors, phenomena of adsorption and dispersion of chemicals in non-Newtonian fluids during flow through porous media must be understood first before a realistic theoretical model can be developed. Such an investigation will depend heavily on experimental and numerical approaches. Even though many results of chemical adsorption during polymer solution flow in porous media can be found in the petroleum literature, very few studies have been reported on dispersion of non-Newtonian fluids in porous media (Payne and Parker, 1973; Wen and Yim, 1971). Many mechanisms which govern non-Newtonian fluid and chemical transport process are very poorly understood. Therefore, a complete understanding of the physics of non-Newtonian fluid flow, coupled with chemical transport, through porous media needs many more experimental and theoretical studies.

References

Albrecht, R. A. and Marsden, S. S. (1970) : "Foams as Blocking Agents in Porous Media," *Soc. Pet. Eng. J.*, 51.

Astarita, G. and Marrucci, G. (1974) : *Principles of Non-Newtonian Fluid Mechanics,*

Aziz, K. and Settari, A. (1979) : *Petroleum Reservoir Simulation,* Applied Science, London.

Barenblatt, G. E., Entov, B. M. and Rizhik, B. M. (1984) : *Flow of Liquids and Gases in Natural Formations,* Nedra, Moscow.

Barenblatt, G. E., Zheltov, I. P. and Kochina, I. N. (1960) : "Basic Concepts in the Theory of Seepage of Homogeneous Liquids in Fissured Rocks," *J. Appl. Math.,* (USSR), Vol. 24, No. 5, 1286-1303.

Bear, J. (1972) : *Dynamics of Fluids in Porous Media,* American Elsevier, New York.

Benis, A. M. (1968) : "Theory of Non-Newtonian Flow through Porous Media in Narrow Three-Dimensional Channels," *Int. J. Non-Linear Mechanics,* Vol.3, 31-46, Pergamon Press, Great Britain.

Bensten, R. G. (1985) : "A New Approach to Instability Theory in Porous Media," *Soc. Pet. Eng. J.*, 765-779

Bird, R. B. (1965) : "Polymer Fluid Dynamics," *Selected Topics in Transport Phenomena,* Chemical Engineering Progress Symposium Series 65, No. 58, Vol. 61, American Inst. of Chemical Engineers.

Bird, R. B. , Stewart, W. E. and Lightfoot, E. N. (1960) : *Transport Phenomena,* Wiley, New York.

Bohme, G. (1987) : *Non-Newtonian Fluid Mechanics,* Vol. 31, North-Holland-Amsterdam, New York.

Bondor, P. L., Hirasaki, G. J. and Tham, M. J. (1972) : "Mathematical Simulation of Polymer Flooding in Complex Reservoirs," *Soc. Pet. Eng. J.*, 369-382.

Buckley, S. E. and Leverett, M. C. (1942) : "Mechanism of Fluid Displacement in Sands," *Trans.*, AIME 146, 107-116.

Camilleri, D., Engelsen, S., Lake, L. W., Lin, E. T., Pope, G. A. and Sepehrnoori, K. (1987a) : "Description of an Improved Compositional Micellar/Polymer Simulator," *SPE Reservoir Engineering*, 427-432.

Camilleri, D., Fil, A., Pope, G. A., Rouse, B. A. and Sepehrnoori, K. (1987b) : "Improvements in Physical-Property Models used in Micellar/Polymer Flooding," *SPE Reservoir Engineering*, 433-440.

Camilleri, D., Fil, A., Pope, G. A., Rouse, B. A. and Sepehrnoori, K. (1987c) : "Comparison of an Improved Compositional Micellar/Polymer Simulator with Laboratory Corefloods," *SPE Reservoir Engineering*, 441-451.

Cardwell, W. T. Jr. (1959) : "the Meaning of the Triple Value in Noncapillary Buckley-Leverett Theory," *Trans.*, AIME, Vol.216, 271-276.

Castagno, R. E., Shupe, R. D., Gregory, M. D. and Lescarboura, J. A. (1987) : "Method for Laboratory and Field Evaluation of a Proposed Polymer Flood," *SPE Reservoir Engineering*, 452-460.

Castagno, R. E., Shupe, R. D., Gregory, M. D. and Lescarboura, J. A. (1984) : "A Method for Laboratory and Field Evaluation of a Proposed Polymer Flood," SPE Paper 13124, Presented at the 59th Annual Technical Conference and Exhibition Held in Houston, Texas.

Chen, Z. X. (1988) : "Some Invariant Solutions to Two-Phase Fluid Displacement Problems Including Capillary Effect," *SPE Reservoir Engineering*, 691-700.

Chen, Z. X. and Whitson, C. H. (1987) : "Generalized Buckley-Leverett Theory of Two-Phase Flow through Porous Media," Division of Petroleum Engineering and

Applied Geophysics, the Norwegian Institute of Technology, the University of Trondheim.

Christopher, R. H. and Middleman, S. (1965) : "Power-Law Flow through a Packed Tube," *I & EC Fundamentals,* Vol.4, No.4, 422-426.

Chu, C. (1987) : "Thermal Recovery," *Petroleum Engineering Handbook,* SPE., Richardson, TX, 46.1-46.46.

Cloud, J. E. and Clark, P. E. (1985) : "Alternatives to the Power-Law Fluid Model for Crosslinked Fluids," *Soc. Pet. Eng. J.,* 935-942.

Coats, K. H. (1987) : "Reservoir Simulation," *Petroleum Engineering Handbook,* SPE., Richardson, TX, 48.1-48.13.

Coats, K. H. (1980) : "In-Situ Combustion Model," *Soc. Pet. Eng. J.,* 533-553.

Coats, K. H. (1978) : "A Highly Implicit Steamflooding Model," *Soc. Pet. Eng. J.,* 369-383.

Coats, K. H., George, W. D., Chu, C. and Marcum, B. E. (1974) : "Three-Dimensional Simulation of Steamflooding," *Soc. Pet. Eng. J.,* 573-592.

Cohen, Y. and Christ, F. R. (1986) : "Polymer Retention and Adsorption in the Flow of Polymer Solutions through Porous Media," *SPE reservoir Engineering,* 113-118.

Collins, R. E. (1961) : *Flow of Fluids through Porous Materials,* Reinhold Publishing Co., New York.

Coulter, A. W. Jr., Martinez, S. J., and Fischer, K. F. (1987) : "Remedial Cleanup, Sand Control, and Other Stimulation Treatments," *Petroleum Engineering Handbook,* Society of Petroleum Engineers, Richardson, TX., 56.1-56.9.

Crochet, M. J., Davies, A. R. and Walters, K. (1984) : *Numerical Simulation of Non-Newtonian Flow,* Rheology Series Vol.1, Elsevier Amsterdam, Oxford.

Dauben, D. L. and Menzie, D. E. (1967) : "Flow of Polymer Solutions through Porous Media," *J. Pet. Tech.,* 1065-1073.

deZabala, E. F., Vislocky, J. M., Rubin, E. and Radke, C. J. (1982) : "A Chemical Theory for Linear Alkaline Flooding," *Soc. Pet. Eng. J.*, 245-258.

Douglas, J. Jr., Peaceman, D. W. and Rachford, H. H. Jr. (1959) : "A Method for Calculating Multidimensional Immiscible Displacement," *Trans.*, AIME 216, 147-155.

Duff, I. S. (1977) : "A Set of FORTRAN Subroutines for Sparse Unsymmetric Linear Equations,"

Earlougher, R. C. Jr. (1977) : *Advances in Well Test Analysis,* SPE Monograph Series, Vol.5.

Fahien, R. W. (1983) : *Fundamentals of Transport Phenomena,* McGraw-Hill, New York

Falls, A. H., Gauglitz, P. A. and Hirasaki, G. J., Miller, D. D., Patzek, T. W. and Ratulowski, J. (1986) : "Development of a Mechanistic Foam Simulator: The Population Balance and Generation by Snap-Off," Paper SPE-14961, Presented at SPE/DOE Enhanced Oil Recovery Symposium, Tulsa, OK.

Falls, A. H., Musters, J. J. and Ratulowski, J. (1986) : "The Apparent Viscosity of Foams in Homogeneous Bead Packs," Submitted to *Soc. Pet. Eng. J.* for Publication.

Fayers, F. J. and Perrine, R. L. (1959) : "Mathematical Description of Detergent Flooding in Oil Reservoirs," *trans.*, AIME., 277-283.

Fayers, F. J. and Sheldon, J. W. (1959) : "The Effect of Capillary Pressure and Gravity on Two-Phase Fluid Flow in a Porous Medium," *Trans.*, AIME 216, 147-155.

Frisch, U., Hasslacher, B. and Pomeau, Y. (1986) : "Lattice Gas Automata for the Navier-Stokes Equation," *Phys. Rev. Letters,* Vol. 56, No. 14, 1505-1507.

Gencer, C. S. and Ikoku, C.U. (1984) : "Well Test Analysis for Two-Phase Flow of Non-Newtonian Power-law and Newtonian Fluids," ASME *Journal of Energy Resources Technology,* Vol. 106, 295-304.

Gogarty, W. B. (1967a) : "Rheological Properties of PseudoPlastic Fluids in Porous Media," *Soc. Pet. Eng. J.*, 149-159.

Gogarty, W. B. (1967b) : "Mobility Control with Polymer Solutions," *Soc. Pet. Eng. J.*, 161-173.

Harvey, A. H. and Menzie, D. E. (1970) : "Polymer Solution Flow in Porous Media," *Soc. Pet. Eng. J.*, 111-118.

Helfferich, F. G. (1981) : "Theory of Multicomponent, Multiphase Displacement in Porous Media," *Soc. Pet. Eng. J.*, 51-62.

Hirasaki, G. J. and Lawson, J. B. (1985) : "Mechanisms of Foam Flow in Porous Media: Apparent Viscosity in Smooth Capillaries," *Soc. Pet. Eng. J.*, 176-190.

Hirasaki, G. J. (1981) : "Application of the Theory of Multicomponent, Multiphase Displacement to Three-Component, Two-Phase Surfactant Flooding," *Soc. Pet. Eng. J.*, 191-204.

Hirasaki, G. J. and Pope, G. A. (1974) : "Analysis of Factors Influencing Mobility and Adsorption in the Flow of Polymer Solution through Porous Media," *Soc. Pet. Eng. J.*, 337-346.

Honarpour, M., Koederitz, L. and Harvey, A. H. (1986) : *Relative Permeability of Petroleum Reservoirs,* CRC Press, Inc., Boca Raton, Florida.

Hovanessian, S. A. and Fayers, F. J. (1961) : "Linear Waterflood with Gravity and Capillary Effects," *Trans.*, AIME 222, 32-36.

Hubbert, M. K. (1956) : "Darcy's Law and Field Equations of Flow of Underground Fluids," *Trans.*, AIME 207, 222-239.

Hughes, W. F. and Brighton, J. A. (1967) : *Theory and Problems of Fluid Dynamics,* Schaum's Outline Series, McGraw-Hill Book Co., 230-241.

Ikoku, C. U. and Ramey, H. J. Jr. (1980) : "Wellbore Storage and Skin Effects during the Transient Flow of Non-Newtonian Power-Law fluids in Porous Media," *Soc.*

Pet. Eng. J., 25-38.

Ikoku, C. U. and Ramey, H. J. Jr. (1979) : "Transient Flow of Non-Newtonian Power-Law Fluids in Porous Media," *Soc. Pet. Eng. J., 164-174.*

International Formulation Committee, (1967) : *A Formulation of the Thermodynamic Properties of Ordinary Water Substance,* IFC Secretariat, Duesseldorf, Germany.

Iyoho, A. W. and Azar, J. J. (1981) : "An Accurate Slot-Flow Model for Non-Newtonian Fluid Flow through Eccentric Annuli," *Soc. Pet. Eng. J.*, 565-572.

Jennings, R. R., Rogers, J. H. and West, Y. J. (1971) : "Factor Influencing Mobility Control by Polymer Solutions," *J. Pet. Tech.*, 391-401.

Karakas, N., Saneie, S. and Yortsos, Y. (1986) : "Displacement of a Viscous Oil by the Combined Injection of Hot Water and Chemical Additive," *SPE Reservoir Engineering,* 391-402.

Kasraie, M. and Farouq Ali, S. M. (1989) : "Role of Foam, Non-Newtonian Flow, and Thermal Upgrading in Steam Injection," Paper SPE 18784, Presented at the 1989 California Regional Meeting of SPE, Bakersfield, CA.

Kazemi, H. (1969) : "Pressure Transient Analysis of Naturally Fractured Reservoirs with Uniform Fractured Distribution," *Soc. Pet. Eng. J., Trans.*, AIME 246, 451-462,

Kozicki, W., Hsu, C. J. and Tiu,.C. (1967) : "Non-Newtonian Flow through Packed Beds and Porous Media," *Chemical Engineering Science,* Pergamon Press Ltd., Oxford, Vol.22, 487-502.

Lai, C. -H. (1985) : "Mathematical Models of Thermal and Chemical Transport in Geologic Media," Ph. D. Thesis, Report LBL-21171, Earth Sciences Division, Lawrence Berkeley Laboratory, Berkeley, CA.

Lake, L. W. (1987) : "Chemical Flooding," *Petroleum Engineering Handbook,* SPE. Richardson, TX., 47.1-47.26.

Lardner, T. J. and Pohle, F. V. (1961) : "Application of the Heat Balance integral to Problems of Cylindrical Geometry," *J. Appl. Mech., Trans.* ASME, 310-312.

Larson, R. G., Davis, H. T. and Scriven, L. E. (1982) : "Elementary Mechanisms of Oil Recovery by Chemical Methods," *Soc. Pet. Eng. J.*, 243-258.

Larson, R. G. and Hirasaki, G. J. (1978) : "Analysis of the Physical mechanisms in Surfactant Flooding," *Soc. Pet. Eng. J.*, 42-58.

Luan, Z. -A. (1981) : "Analytical Solution for Transient Flow of Non-Newtonian Fluids in Naturally Fractured reservoirs," *Acta Petrolei Sinica 2*, No. 4, 75-79 (in Chinese).

Lund, O. and Ikoku, C. U. (1981) : "Pressure Transient Behavior of Non-Newtonian / Newtonian Fluid Composite Reservoirs," *Soc. Pet. Eng. J.*, 271-280.

Mandl, G. and Volek, C. W. (1969) : "Heat and Mass Transport in Steam-Drive Processes," *Soc. Pet. Eng. J.*, 59-79.

Marle, C. M. (1981) : *Multiphase Flow in Porous Media,* Technip, Paris.

Marsily, G. de. (1986) : *Quantitative Hydrogeology* - Groundwater Hydrology for Engineers, Translated by Marsily, G. de., Academic Press Inc., London.

Matthews, C. S. and Russell, D. G. (1967) : *Pressure Buildup and Flow Tests in Wells,* Monograph Series, Vol. 1, Society of Petroleum Engineers AIME, Dallas.

Marx, J. W. and Langenheim, R. N. (1959) : "Reservoir Heating by Hot Fluid Injection," *Trans.*, AIME 216, 312-315.

McDonald, A. E. (1979) : "Approximate Solutions for Flow on Non-Newtonian Power-law Fluids through Porous Media," Paper SPE 7690, Presented at the SPE- AIME Fifth Symposium on Reservoir Simulation, Denver.

McKinley, R. M., Jahns, H. O., Harris, W. W. and Greenkorn, R. A. (1966): "Non-Newtonian Flow in Porous Media," *AIChE Jour.*, Vol. 12, No. 1, 17-20.

Meter, D. M. and Bird, R. B. (1964) : "Tube Flow of Non-Newtonian Polymer Solutions: Part I. Laminar Flow and Rheological Models," *AIChE Jour.*, Vol. 10, No. 6, 878-881.

Mirzadjanzade, A. KH., Amirov, A. D., Akhmedov, Z. M., Barenblatt, G. I., Gurbanov, R. S., Entov, V. M., and Zaitsev, YU. V. (1971) : "On the Special Features of Oil and Gas Field Development Due to Effects of Initial Pressure Gradient," *Preprints of Proceedings of 8th World Petroleum Congress, Special Papers.* Elsevier London.

Mitchell, J. K. (1976) : *Fundamentals of Soil Behavior,* John Wiley & Sons, Inc., New York.

Mungan, N. (1972) : "Shear Viscosities of Ionic Polyacrylamide Solutions," *Soc. Pet. Eng. J.*, 469-473.

Mungan, N., Smith, F. W. and Thompson, J. L. (1966) : "Some Aspects of Polymer Floods," *J. Pet. Tech.*, 1143-1150.

Muskat, M. (1946) : *The Flow of Homogeneous Fluids through Porous Media,* McGraw-Hill, New York.

Narasimhan, T. N. (1982) : *Recent Trends in Hydrogeology,* Special Paper 189, the Geological Society of American.

Narasimhan, N. T. and Witherspoon, P. A. (1976) : "An Integrated Finite Difference Method for Analyzing Fluid Flow in Porous Media," *Water Resources Research,* Vol.12, No.1, 57-64.

Odeh, A. S. and Yang, H. T. (1979) : "Flow of Non-Newtonian Power-Law Fluids through Porous Media," *Soc. Pet. Eng. J., 155-163.*

Ozisik, M. N. (1980): *Heat Conduction,* John Wiley and Sons, New York.

Patton, J. T., Coats, K. H. Colegrove, G. T. (1971) : "Prediction of Polymer Flood Performance," *Soc. Pet. Eng. J., Trans.*, AIME 251, 72-84.

Patton, J. T., Holbrook, S. T. and Hsu, W. (1983) : "Rheology of Mobility-Control Foams," *Soc. Pet. Eng. J.*, 456-460.

Payne, L. W. and Parker, H. W. (1973) : "Axial Dispersion of Non-Newtonian Fluids in Porous Media," *AIChE Jour.*, Vol. 19, No.1, 202-204.

Peaceman, D. W. (1977) : *Fundamentals of Numerical Reservoir simulation,* Elsevier Scientific Publishing Co., Amsterdam.

Peaceman, D. W. and Rachford, H. H. Jr. (1962) : "Numerical Calculation of Multidimesional Miscible Displacement," *Soc. Pet. Eng. J., Trans.*, AIME 225, 327-339.

Pope, G. A. (1980) : "The Application of Fractional Flow Theory to Enhanced Oil Recovery," *Soc. Pet. Eng. J.*, 191-205.

Pruess, K (1988) : "SHAFT, MULKOM, TOUGH: a Set of Numerical Simulators for Multiphase Fluid and Heat Flow," Report LBL-24430, Earth Sciences Division, Lawrence Berkeley Laboratory, Berkeley, CA.

Pruess, K. (1987) : *TOUGH User's Guide* Report LBL-20700, Earth Sciences Division, Lawrence Berkeley Laboratory, Berkeley, CA.

Pruess, K. (1983a) : "Heat Transfer in Fractured Geothermal Reservoirs with Boiling," *Water Resources Research,* Vol. 19, No. 1, 201-208.

Pruess, K. (1983b) : "GMINC - A Mesh Generator for Flow Simulation in Fractured Reservoirs," Lawrence Berkeley Laboratory LBL-15227, Berkeley, CA.

Pruess, K. (1983) : "Development of the General Purpose Simulator MULKOM," *Annual Report,* Earth Sciences Division, Lawrence Berkeley Laboratory, Berkeley CA.

Pruess, K. and Narasimhan, T. N. (1985) : "A Practical Method for Modeling Fluid and Heat Flow in Fractured Porous Media," *Soc. Pet. Eng. J.*, Vol. 25, No. 1, 14-26.

Pruess, K. and Narasimhan, T. N. (1982) : "On Fluid Reserves and the Production of Superheated Steam from Fractured, Vapor-Dominated Geothermal Reservoirs," *J. of Geo. Res.*, Vol. 87, No. B11, 9329-9339.

Pruess, K. and Wu, Y.-S. (1988) : "On PVT-Data, Well Treatment, and Preparation of Input Data for an Isothermal Gas-Water-Foam Version of MULKOM," Report LBL-25783, UC-403, Earth Sciences Division, Lawrence Berkeley Laboratory, Berkeley, CA.

Ramey, H. J. Jr. (1959) : "Discussion of Reservoir Heating of Hot Fluid Injection," *Trans.*, AIME 216, 364-365.

Ransohoff, T. C. and Radke, C. J. (1986) : "Mechanisms of Foam Generation in Glass Bead Packs," Paper SPE-15441, Presented at the 61st Annual Meeting of SPE, New Orleans, LA.

Robertson, R. E. and Stiff, H. A. Jr. (1976) : "An Improved Mathematical Model for Relating Shear Stress to Shear Rate in Drilling Fluids and Cement Slurries," *Soc. Pet. Eng. J.*, 31-36.

Rothman, D. H. (1988) : "Lattice-Gas Automata for Immiscible Two-Phase Flow," *MIT Porous Flow Project,* Report No. 1, 11-26.

Rothman, D. H. and Keller, J. M. (1988) : "Immiscible Cellular-Automaton Fluids," *MIT Porous Flow Project,* Report No. 1, 1-10.

Sadowski, T. J. and Bird, R.B. (1965) : "Non-Newtonian Flow through Porous Media: I Theoretical," *Trans. Society of Rheology,* Vol. 9, No.2, 243-250.

Sadowski, T. J. (1965) : "Non-Newtonian Flow through Porous Media : II experimental," *Trans. Society of Rheology,* Vol. 9, No.2, 251-271.

Savins, J. G. (1969) : "Non-Newtonian Flow through Porous Media," *Ind. Eng. Chem.,* Vol. 61, No. 10, 18-47.

Savins, J. G. (1962) : "The Characterization of Non-Newtonian Systems by a Dual Differentiation-Integration Method," *Soc. Pet. Eng. J.*, 111-119.

Savins, J. G., Wallick, G. C. and Foster, W. R. (1962a) : "The Differentiation Method in Rheology : I. Poiseuille-Type Flow," *Soc. Pet. Eng. J.*, 211-215.

Savins, J. G., Wallick, G. C. and Foster, W. R. (1962b) : "The Differentiation Method in Rheology: II. Characteristic Derivatives of Ideal Models in Poiseuille Flow," *Soc. Pet. Eng. J.*, 309-316.

Savins, J. G., Wallick, G. C. and Foster, W. R. (1962c) : "The Differentiation Method in Rheology: III. Couette Flow," *Soc. Pet. Eng. J.*, 14-18.

Scheidegger, A. E. (1974) : *The Physics of Flow through Porous Media,* University of Toronto Press.

Shah, S. N. (1982) : "Propant Settling Correlations for Non-Newtonian Fluids under Static and Dynamic Conditions," *Soc. Pet. Eng. J.*, 164-170.

Sheldon, J. W., Zondek, B. and Cardwell, W. T. Jr. (1959) : "One-Dimensional, Incompressible, Noncapillary, Two-Phase Fluid Flow in a Porous Medium," *trans.*, AIME 216, 290-296.

Skelland, A. H. P. (1967) : *Non-Newtonian Flow and Heat Transfer,* John Wiley & Sons, Inc. New york, London, and Sydney.

Sorbie, K. S., Parker, A. and Clifford, P. J. (1987) : "Experimental and Theoretical Study of Polymer Flow in Porous Media," *SPE Reservoir Engineering,* 281-304.

Stalkup, F. I. Jr. (1983) : *Miscible Displacement,* SPE Monograph Series, Dallas.

Stehfest, H. (1970) : "Numerical Inversion of Laplace transform," *Communication,* ACM 13, No.1, 47-48.

Taber, J. J., Kamath, I. S. K. and Reed, R. L. (1961) : "Mechanism of Alcohol Displacement of Oil from Porous Media," *Soc. Pet. Eng. J.*, 195-212.

Thomas, G. W. (1982) : *Principles of Hydrocarbon Reservoir Simulation,* International Human Resources Development Co. , Boston.

van Poollen, H. K. and Associates, Inc. (1980) : *Fundamentals of Enhanced Oil Recovery,* PennWell Books, Tulsa, Oklahoma.

van Poollen, H. K. and Jargon, J. R. (1969) : "Steady-State and Unsteady-State Flow of Non-Newtonian Fluids through Porous Media," *Soc. Pet. Eng. J., Trans.,* AIME 246, 80-88.

Vargaftik, N. B. (1975) : *Tables on the Thermophysical Properties of Liquids and Gases,* Second Edition, John Wiley & Sons, New York.

Vongvuthipornchai, S. and Raghavan, R. (1987a) : "Pressure Falloff Behavior in Vertically Fractured Wells: Non-Newtonian Power-Law Fluids," *SPE Formation Evaluation,* 573-589.

Vongvuthipornchai, S. and Raghavan, R. (1987b) : "Well Test Analysis of data Dominated by Storage and Skin: Non-Newtonian Power-Law Fluids," *SPE Formation Evaluation,* 618-628.

Wachmann, C. (1964) : "A Mathematical Theory for the Displacement of Oil and Water by Alcohol," *Soc. Pet. Eng. J.,* 250-266.

Warren, J. E. and Root, P. J. (1963) : "The Behavior of Naturally Fractured Reservoirs," *Soc. Pet. Eng. J., Trans.,* AIME 228, 245-255.

Welge, H. J. (1952) : "A Simplified Method for Computing Oil Recovery by Gas or Water Drive," *Trans.,* AIME 195, 91-98.

Wen, C. Y. and Yim, J. (1971) : "Axial Dispersion of a Non-Newtonian Liquid in a Packed Bed," *AIChE Jour.,* Vol. 17, No.6, 1503-1504.

Willhite, G. P. (1986) : *Waterflooding,* SPE textbook Series, Society of Petroleum Engineers, Richardson, TX.

Wissler, E. H. (1971) : "Viscoelastic Effects in the Flow of Non-Newtonian Fluids though a Porous Medium," *Ind. Eng. Chem. Fundam.*, Vol. 10, No.3, 411-417.

Witherspoon, P. A., Benson, S., Persoff, P., Pruess, K., Radke, C. J. and Y. -S. Wu (1989) : "Feasibility Analysis and Development of Foam Protected Underground Natural Gas Storage Facilities," Final Report, Earth Sciences Division, Lawrence Berkeley Laboratory, CA.

Wu, Y. -S. and Pruess, K. (1986) : "A Multiple-Porosity Method for Simulation of Naturally Fractured Petroleum Reservoirs," SPE Paper 15129, Presented at the 56th California Regional Meeting of SPE, Oakland, CA. *SPE Reservoir Engineering, (1988),* 327-336.

Yortsos, Y. C. and Fokas, A. S. (1983) : "An Analytical Solution for Linear Waterflood Including the Effects of Capillary Pressure," *Sec. Pet. Eng. J.*, 115-124.

Yortsos, Y. C. and Huang, A. B. (1986) : "Linear- Stability Analysis of Immiscible Displacement: Part 1-Simple Basic Flow Profiles," *SPE reservoir Engineering,* 378-390.

Appendix A.
Derivation of Buckley-Leverett Type Solution

The sum of Equations 5.7 and 5.8 gives

$$-\frac{\partial(u_{ne} + u_{nn})}{\partial x} = \phi \frac{\partial}{\partial t} (S_{ne} + S_{nn}) = 0 \qquad (A.1)$$

This means that at a given time, the total volumetric flux through any cross-section in the flow system is independent of the distance coordinate, x.

$$u_{ne} + u_{nn} = u(t) = \frac{q(t)}{A} \qquad (A.2)$$

Physically this follows from the incompressible assumption. Substituting Equations 5.9 and 5.10 into (A.2) leads to Equation 5.21, which is a constraint condition to relate the flow potential gradient and the saturation for the system.

Introducing

$$u_{nn} = u(t)\, f_{nn} \qquad (A.3)$$

into Equation 5.8, for a given time t, it turns out,

$$-\frac{\partial f_{nn}}{\partial x} = \frac{\phi}{u(t)} \frac{\partial S_{nn}}{\partial t}$$

$$= -\left[\frac{\partial f_{nn}}{\partial S_{nn}}\right]_t \left[\frac{\partial S_{nn}}{\partial x}\right]_t \qquad (A.4)$$

since the fractional flow f_{nn} is a function of saturation.

Let us look at a particular saturation at this time, S_{nn} ,

$$S_{nn} = S_{nn}(x, t) \qquad (A.5)$$

The total derivative of S_{nn} ,

$$dS_{nn} = \left[\frac{\partial S_{nn}}{\partial x}\right]_t dx + \left[\frac{\partial S_{nn}}{\partial t}\right]_t dt = 0 \qquad (A.6)$$

After some rearrangement, then we obtain

$$\left[\frac{dx}{dt}\right]_{S_{nn}} = -\frac{\left[\frac{\partial S_{nn}}{\partial t}\right]_x}{\left[\frac{\partial S_{nn}}{\partial x}\right]_t} \qquad (A.7)$$

Substituting Equation A.7 into Equation A.4, it follows that

$$-\left[\frac{df_{nn}}{dS_{nn}}\right]_t \left[\frac{\partial S_{nn}}{\partial x}\right]_t = -\frac{\phi A}{q(t)} \left[\frac{\partial S_{nn}}{\partial x}\right]_t \left[\frac{dx}{dt}\right]_{S_{nn}}$$

This will result in Equation 5.22 by cancelling the same terms $\left[\partial S_{nn}/\partial x\right]_t$ on both sides of the equation.

Appendix B.
Derivation of Graphic Method

The mass conservation of the injected non-Newtonian fluid in the swept zone of system for a given time t of injection gives,

$$Q(t) = \int_0^t q(\lambda)d\lambda = \int_0^{x_f}(S_{nn} - S_{nnir})\phi A dx$$

$$= \phi A x_f(S_f - S_{nnir}) - \int_0^{x_f}\phi A x dS_{nn} \tag{B.1}$$

Substituting Equation 5.24 into (B.1) yields,

$$Q(t) = Q(t)(S_f - S_{nnir})\left[\frac{\partial f_{nn}}{\partial S_{nn}}\right]_{S_f} - Q(t)(f_{nn}|_{S_f} - f_{nn}|_0) \tag{B.2}$$

Noting that at x = 0, $S_{nn} = 1 - S_{neir}$, and $f_{nn} = 1$, therefore,

$$1 = (S_f - S_{nnir})\left[\frac{\partial f_{nn}}{\partial S_{nn}}\right]_{S_f} - f_{nn}|_{S_f} + 1 \tag{B.3}$$

or,

$$\left[\frac{\partial f_{nn}}{\partial S_{nn}}\right]_{S_f} = \frac{f_{nn}|_{S_f} - f_{nn}|_{S_{nnir}}}{S_f - S_{nnir}} \tag{5.26}$$

in which $f_{nn} = 0$ at $S_{nn} = S_{nnir}$ is used, and both f_{nn} and $\partial f_{nn}/\partial S_{nn}$ are evaluated at the shock saturation S_f.

Similarly, the average saturation in the displaced zone is defined as,

$$\bar{S}_{nn} = \frac{\int_0^{x_f} S_{nn}A\phi dx}{\int_0^{x_f} A\phi dx} = \frac{\phi A}{\phi A x_f}\int_0^{x_f} S_{nn}dx \tag{B.4}$$

then

$$\phi A x_f(\bar{S}_{nn} - S_{nnir}) = \phi A \int_0^{x_f} (S_{nn} - S_{nnir})dx = Q(t) \qquad (B.5)$$

Using Equation 5.24 again, we will have,

$$\left[\frac{\partial f_{nn}}{\partial S_{nn}}\right]_{S_f} = \frac{1}{\bar{S}_{nn} - S_{nnir}} \qquad (5.27)$$

Appendix C.

Modified Darcy's Law for Power-Law Fluid Flow in Fractures

A velocity profile for flow of a power-law fluid through a uniform horizontal fracture between two parallel plates is shown in Figure C.1. Under steady state condition, the velocity u_z as a function of the x coordinate can be determined by solving the momentum balance equation (Bird et al., 1960; and Hughes and Brighton, 1967),

$$u_z = \frac{n}{n+1}\frac{1}{H^{1/n}}\left\{1 - \left[\frac{x}{b/2}\right]^{(1+n)/n}\right\}(b/2)^{(1+n)/n}\left[-\frac{\partial P}{\partial z}\right]^{1/n} \tag{C.1}$$

where b is aperture of the fracture; and the pressure gradient is given by (see Figure C.1)

$$-\frac{\partial P}{\partial z} = \frac{P_0 - P_L}{L} \tag{C.2}$$

The average velocity across the fracture can be calculated as

$$\bar{u}_z = \frac{W}{W\,b}\int_{-b/2}^{+b/2} u_z\,dx$$

$$= \frac{n}{2n+1}\frac{1}{H^{1/n}}(b/2)^{(1+n)/n}\left[-\frac{\partial P}{\partial z}\right]^{1/n} \tag{C.3}$$

For flow across a basic section of the fracture system, as shown in Figure 8.5, the total flux from the Darcy's equation should be equal to

$$A_t\,u = A_f\bar{u}_z \tag{C.4}$$

where $A_t = W(2D + b) \approx 2WD$, total cross-sectional area of the basic section; $A_f = W\,b$, cross-sectional area of fracture only. Then, the Darcy's velocity can be derived as

$$u = \frac{A_f}{A_t}\bar{u}_z$$

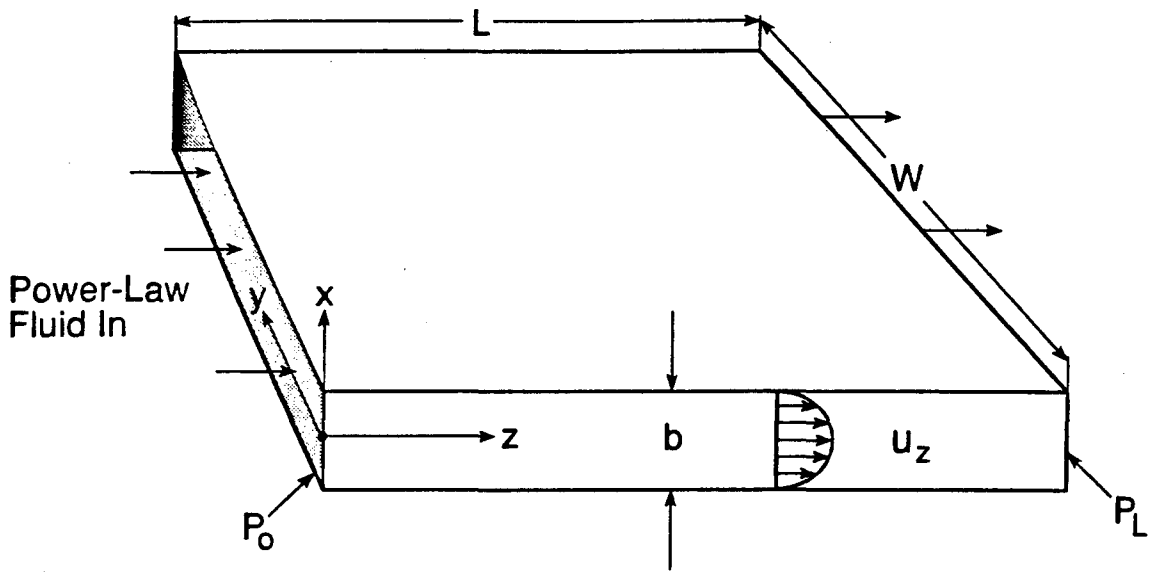

XBL 8912-7930
T.I.D.Illus.88

Figure C.1 Schematic of Power-Law Fluid Flow through a Fracture.

$$= \frac{b}{2D}\,\frac{n}{2n+1}\,\frac{1}{H^{1/n}}(b/2)^{(1+n)/n}\left[-\frac{\partial P}{\partial z}\right]^{1/n} \tag{C.5}$$

If the cubic law is assumed to be valid for describing the permeability of the fracture, the effective permeability used in Darcy's law is

$$K_f = \frac{b^3}{24D} \tag{C.6}$$

Then, let Equation C.5 be equivalent to a Darcy's law in a form:

$$u = -\frac{K_f}{\mu_{nn}}\frac{\partial P}{\partial z} \tag{C.7}$$

A comparison of Equations C.5 and C.7 gives us

$$\mu_{nn} = \frac{H^{1/n}}{3}\,\frac{2n+1}{n}(b/2)^{(n-1)/n}\left[-\frac{\partial P}{\partial z}\right]^{(n-1)/n} \tag{C.8}$$

Equation C.8 can be written in the form of Equation 3.11, and then μ_{eff} in Equation 3.11 is defined by μ_{eff}^{*} in Equation 8.5.

Appendix D.

Derivation of Integral Solution for Production of a Bingham Fluid

A pressure penetration (disturbance) distance is defined at $r = r_w + \delta(t)$, in analogy to the thermal layer thickness in a heat conduction problem (Ozisik, 1980), such that it requires,

$$\delta(t) = 0 \qquad \text{at } t = 0 \tag{D.1}$$

ahead of the pressure penetration front,

$$P(r \geq r_w+\delta(t),\, t) = P_i \tag{D.2}$$

and

$$\left[\frac{\partial P}{\partial r}\right]_{r=r_w+\delta(t)} = G \tag{D.3}$$

the system is undisturbed by production and remains at the initial equilibrium condition.

Define

$$P^*(r,\, t) = P(r,\, t) - P_i + (r_w + \delta(t) - r)G \tag{D.4}$$

Then,

Then, Equation 9.1 becomes

$$\frac{K}{r}\frac{\partial}{\partial r}\left[\frac{\rho(P)}{\mu_b} r \frac{\partial P^*}{\partial r}\right] = \frac{\partial}{\partial t}[\rho(P)\phi(P)] \tag{D.5}$$

The constraint conditions for the pressure penetration distance now become,

$$P^*(r \geq r_w + \delta(t),\, t) = 0 \tag{D.6}$$

$$\left[\frac{\partial P^*}{\partial r}\right]_{r=r_w+\delta(t)} = 0 \tag{D.7}$$

and the specified inner boundary condition, (9.3), gives

$$\frac{2\pi r_w Kh}{\mu_b}\rho(P_0)\left[\frac{\partial P^*}{\partial r}\right]_{r=r_w} = Q_m(t) \qquad (D.8)$$

Since Equation D.5 and the constraint conditions, (D.6)-(D.8) are similar to the heat conduction problem in form, the first pressure profile used in this study to describe the pressure distribution within the pressure disturbance zone, in analogy to the heat conduction problem (Lardner and Pohle, 1961; Ozisik, 1980), is given by

$$P^*(r, t) = [p_n(r)] \ln(r) \qquad (r_w \le r \le r_w + \delta(t)) \qquad (D.9)$$

where $p_n(r)$ is a nth-degree polynomial in r; and the time dependence is implicitly included in the coefficients of the polynomial, which is dependent on the pressure penetration distance. However, it has been found that the solutions in terms of a profile of Equation D.9 are not accurate when compared with the Theis solution, and always introduce 5-10 % errors, as discussed in Section 9.3.

We know, from the Theis solution, that the pressure at a given time for radial flow is distributed as a logarithm in (t/r^2). Thus for $\frac{K\,t}{\phi_i \mu C_t r^2} > 100$, the Theis solution is simplified as (Earlougher, 1977):

$$P(r,t) - P_i = \frac{Q}{4\pi Kh}\left[\ln\frac{Kt}{\phi\mu C_t r^2} + .80907\right] \qquad (D.10)$$

which is very accurate except near the pressure penetration front. This suggests us to look for a pressure profile in r, such as

$$P^*(r, t) = \text{constant} \times \ln[(P_n(r)] \qquad (D.11)$$

instead of the form of Equation D.9 to approximate the pressure profile for our problem. By using Equation D.11 as a pressure profile with $P_n(r)$ being a second-degree polynomial in r, it can be shown that the following solution

$$P^*(r, t) = \frac{Q_m(t)\mu}{2\pi h}\frac{1}{\rho(P_0)k(P_0)}\left[\frac{1 + 2\delta(t)/r_w}{2\delta(t)/r_w}\right]\times$$

$$\ln\left[\frac{2r/r_w}{\eta} - \left[\frac{r/r_w}{\eta}\right]^2\right] \qquad (D.12)$$

satisfies the constraint conditions (D.6)-(D.8).

Performing the integration

$$\int_{r_w}^{r_w+\delta(t)} 2\pi hrdr$$

on both sides of Equation D.5 and use Equation D.7, we will have,

$$-Q_m(t) = 2\pi h \int_{r_w}^{r_w+\delta(t)} r\frac{\partial}{\partial t}[\rho(P)\phi(P)]dr$$

$$= \frac{d}{dt}\left\{\int_{r_w}^{r_w+\delta(t)} 2\pi hr\rho(P)\phi(P)dr - \pi h\left[r_w + \delta(t)\right]^2\rho_i\phi_i\right\} \qquad (D.13)$$

Integrating Equation D.13 with respect to t from t = 0 to t = t, and using $\delta(t) = 0$ for t = 0, we have the integral mass balance, Equation 9.5.

For "slightly compressible" fluid and rock, compressibilities C_f and C_r are very small constants. We have

$$\rho(P) = \rho_i e^{C_f(P-P_i)} \approx \rho_i[1 + C_f(P - P_i)] \qquad (D.14)$$

and

$$\phi(P) = \phi_i e^{C_r(P-P_i)} \approx \phi_i[1 + C_r(P - P_i)] \qquad (D.15)$$

So,

$$\rho(P)\phi(P) \approx \rho_i\phi_i[1 + C_t(P - P_i)] \qquad (D.16)$$

where $C_t = C_f + C_r$, total compressibility of the system.

Then, we can calculate the integral in Equation 9.5 by using the pressure profile given by Equation 9.4,

$$\int_{r_w}^{r_w+\delta(t)} 2\pi hr\rho\phi dr \approx \pi h\rho_i\phi_i[(r_w + \delta(t))^2 - r^2_w] + 2\pi h\rho_i\phi_i C_t\left\{Gr_w{}^3\left[-\frac{1}{6}(\eta)^3 + \frac{1}{2}\eta - \frac{1}{3}\right] - \frac{r_w{}^2\mu_b Q_m(t)}{2\pi Kh\rho(P_0)}\left[\frac{1 + 2\delta(t)/r_w}{2\delta(t)/r_w}\right]\right.$$

$$\left[-\frac{3}{2}(\eta)^2 + \eta + \frac{1}{2} + 2(\eta)^2\ln(\eta)\right.$$

$$\left.\left. - \frac{1}{2}\left[1 - 4(\eta)^2\right]\ln\left[\frac{2(\eta) - 1}{(\eta)^2}\right]\right]\right\} \qquad \text{(D.17)}$$

Substituting (D.17) into (9.5), we have the mass balance equation 9.6 for the flow of a slightly compressible Bingham fluid. The complete integral solution consists of Equations 9.4 and 9.6.

Appendix E.

Mass Balance Calculation of Minimum Pressure Gradient

The pressure gradient in the entire pressure drop zone at the well shut-in time is larger that the minimum pressure gradient G. As shown in Figure E.1, the fluid masses should be equal to each other in the shadowed regions of the figure, and there is a linear relationship of pressure and radial distance with a slope G, if the equilibrium is achieved,

$$P = P_w + G[r - r_w] \quad \text{for } r_w \le r \le r_w+\delta(t) \tag{E.1}$$

and the minimum pressure gradient G and the final pressure penetration distance $\delta(t)$ at equilibrium are related by

$$\delta(t) = \frac{P_i - P_w}{G} \tag{E.2}$$

The mass balance in the pressure zone under the equilibrium condition gives

$$\pi h\rho_i\phi_i[(r_w+\delta(t))^2 + r_w^2] - \int_0^t Q_m(t)dt = 2\pi h \int_{r_w}^{r_w+\delta(t)} r\rho\phi dr \tag{E.3}$$

For a slightly compressible system, using Equations D.16 and E.1 in the integral of the right hand side of equation E.3, we will obtain the mass balance as

$$2\pi h \int_{r_w}^{r_w+\delta(t)} r\rho\phi dr = 2\pi h\rho_i\phi_i C_t\left[-\frac{1}{2}(\Delta P + r_w G)[(r_w+\delta(t))^2 - r_w^2]\right.$$

$$\left. + \frac{1}{3}[(r_w+\delta(t)]^3 - r_w^3]\right] \tag{E.4}$$

Substituting Equation E.2 into E.4, and solving the resulting algebraic equation for G, we will have Equation 9.7.

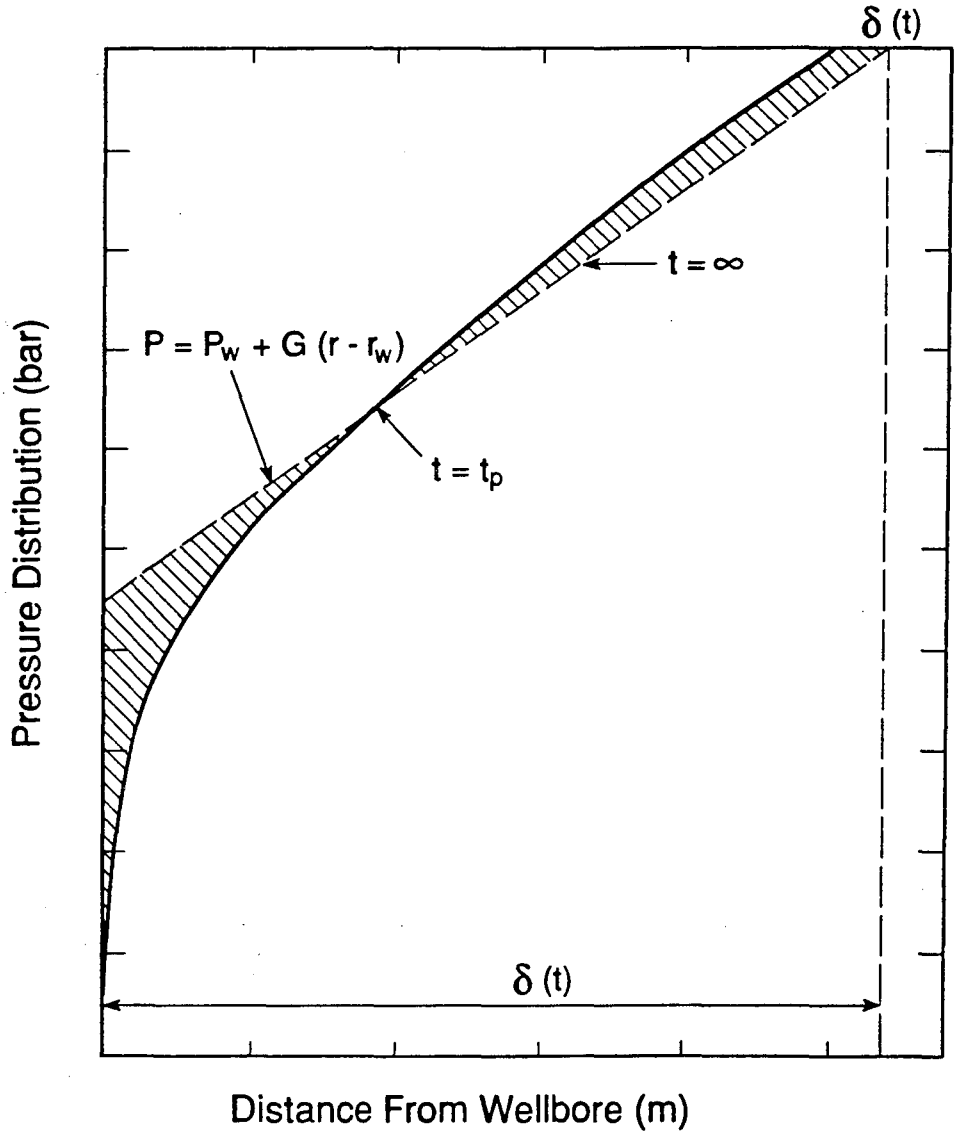

Figure E.1 Schematic of Pressure Distributions at Well Shut-in and Equilibrium Long Time after Well Shut-in after a Period of Time of Bingham Fluid Production.

Appendix F.

Subroutines for Treatment of Non-Newtonian Behavior

The viscosity of non-Newtonian fluids in porous media is a flow property, and the numerical treatment of effects of non-Newtonian viscosities is included in the Subroutine "MULTI" of a modified version of MULKOM, since MULTI handles the flow-terms in the code (Pruess, 1987). The use and input data of the modified version of MULKOM for non-Newtonian flow are similar to those of the code "MULKOM-GWF" (Pruess and Wu, 1988). The following three subroutines have been incorporated in MULTI for power-law, Bingham plastic, and general pseudoplastic non-Newtonian fluids, respectively.

F.1 Subroutine for Viscosity of Power-Law Fluids

```
      FUNCTION VISPOW(DPDX, PERM, PHI)
C-----CALCULATION OF VISCOSITY OF A POWER-LAW FLUID
C-----BY EQUATION 3.11
C-----DPDX - ABSOLUTE VALUE OF FLOW POTENTIAL GRADIENT (Pa/m).
C-----PERM - PERMEABILITY (m**2).
C-----PHI - POROSITY.
      COMMON/REOLG/ALPHA,BETA1,VISI,DPB,QF,RMWF
C-----ALPHA - H, POWER-LAW CONSISTENCE (Pa·s**n).
C-----BETA1 - n, POWER-LAW INDEX.
C-----VISI - δ2, LINEAR INTERPOLATION PARAMETER (Pa/m).
C-----DPB - δ1, LINEAR INTERPOLATION PARAMETER (Pa/m).
C-----QF AND RMWF - NOT USED.
      VISEFF=ALPHA*/12.*(9.+3./BETA1)**BETA1*(150.*PERM*PHI)**
     1 ((1.-BETA1)/2.)
      Y=(BETA1-1.)/BETA1
      IF(DPDX.GT.DPB) VISPOW=VISEFF*(PERM/VISEFF*DPDX)**Y
      IF(DPDX.LE.DPB) THEN
```

```
    VIS1=VISEFF*(PERM/VISEFF*DPB)**Y
    VIS2=VISEFF*(PERM/VISEFF*VISI)**Y
    VISPOW=VIS1+(VIS1-VIS2)/(DPB-VISI)*(DPDX-DPB)
    ENDIF
    RETURN
    END
```

F.2 Subroutine for Equivalent Potential Gradient of Bingham Fluids

```
C-----ADJUSTMENT OF POTENTIAL GRADIENT BY EQUATION 4.21.
    FUNCTION EPG(DPDX, VISBIN)
C-----DPDX - ABSOLUTE VALUE OF FLOW POTENTIAL GRADIENT (Pa/m).
C-----VISBIN - EQUIVALENT VISCOSITY (Pa·s).
    COMMON/REOLG/ALPHA,BETA1,VISI,DPB,QF,RMWF
C-----ALPHA - μb, BINGHAM COEFFICIENT (Pa·s)
C-----DPB - G, MINIMUM PRESSURE GRADIENT
C-----BETA1, VISI, QF, AND RMWF, NOT USED.
    VISBIN=ALPHA
    DPBN=-DPB
    IF(DPDX.GT.DPB) EPG=DPDX-DPB
    IF(DPDX.LT.DPBN) EPG=DPDX+DPB
    IF(DPDX.LE.DPB.AND.DPDX.GE.DPBN) EPG=0.
    RETURN
    END
```

F.3 Subroutine for Viscosity of General Pseudoplastic Fluids

```
C-----CALCULATION OF VISCOSITY OF GENERAL PSEUDOPLASTIC FLUIDS
C-----BY EQUATION 4.23.
    FUNCTION VISGPF(DPDX, PERM, PHI)
C-----DPDX - ABSOLUTE VALUE OF FLOW POTENTIAL GRADIENT (Pa/m).
C-----PERM - PERMEABILITY (m2).
C-----PHI - POROSITY.
    COMMON/REOLG/ALPHA,BETA1,VISI,DPB,QF,RMWF
```

```
C-----ALPHA - μ0, MAXIMUM VISCOSITY AT LOW SHEAR RATE (Pa·s).
C-----BETA1 - β, EXPONENTIAL IN EQUATION 3.13.
C-----VISI - μ∞, MINIMUM VISCOSITY AT HIGH SHEAR RATE (Pa·s).
C-----DPB - [(3n+1)/4n]^(n/(n-1))/γ̇½,
      n - POWER-LAW INDEX;
      γ̇½ - COEFFICIENT IN EQUATION 3.13 (s^-1).
C-----QF AND RMWF - NOT USED.
      VISGPF=ROOTV(DPDX, PERM, PHI)
      RETURN
      END
C-----CALCULATION OF VISCOSITY AS ROOT OF EQUATION 4.23.
C-----BY BISECTIONAL TECHNIQUE.
      FUNCTION ROOTV(DPDX, PERM, PHI)
      COMMON/REOLG/ALPHA,BETA1,VISI,DPB,QF,RMWF
      AA=VISI
      BB=ALPHA
      N=0
      X2=1.E30
1     X1=.5*(AA+BB)
      Z=VISEQN(X1, DPDX, PERM, PHI)
      N=N+1
      IF(Z.LT.0.) AA=X1
      IF(Z.GT.0.) BB=X1
      IF(Z.EQ.0.) GOTO 10
      IF(N.GE.100) GOTO 5
      DX=ABS(X2-X1)
      IF(DX.LE.1.E-5) GOTO 10
      GOTO 1
5     PRINT 20,X1
      GOTO 25
10    CONTINUE
      ROOTV=X1
20    FORMAT(2X,F20.10,10X,'NOT-CONVERGENCE')
25    CONTINUE
      RETURN
      END
```

```
C-----EQUATION 4.23 FOR CALCULATION VISCOSITY FROM
C-----FLOW POTENTIAL GRADIENT.
      VISEQN(X, DPDX, PERM, PHI)
      COMMON/REOLG/ALPHA,BETA1,VISI,DPB,QF,RMWF
      BETA2=BETA1-1.
      CM=(DPB*SQRT(2.*PERM/PHI))**BETA2
      Y=X**BETA2*CM
      VISEQN=X**BETA1+Y*X-ALPHA*X**BETA2-VISI*Y
      RETURN
      END
```

F.4 Subroutine of "MULTI" in "MULKOM"

```
C-----IMPROVED ON MAY 10,1988 FOR THE DOCUMENTATION OF THE GAS-
C----- FOAM-WATER FLOW CODE FOR GRI.
C-----MOP(19)=0, DEFAULT,KRW &KRG INPUT FROM TABULAR DATA, KRF
IS
C     CALCULATED FROM STONE'S FUNCTION;
C-----MOP(19)=1,FOR WATER AND GAS TWO PHASE FLOW,KRW & KRG ARE
C     DETERMINED BY TNE INTERNAL FUNCTION
C-----MOP(19)=2, SHARP-FRONT TRACKING TECHNIQUE USED FOR GAS-
C     FOAM-WATER FLOW
C
      SUBROUTINE MULTI
      COMMON/E1/ELEM(1)
      COMMON/E2/MATX(1)
      COMMON/E3/EVOL(1)
      COMMON/E4/PHI(1)
      COMMON/E5/P(1)
      COMMON/E6/T(1)
      COMMON/P1/X(1)
      COMMON/P2/DX(1)
      COMMON/P3/DELX(1)
      COMMON/P4/R(1)
      COMMON/P5/DOLD(1)
```

```
COMMON/C1/NEX1(1)
COMMON/C2/NEX2(1)
COMMON/C3/DEL1(1)
COMMON/C4/DEL2(1)
COMMON/C5/AREA(1)
COMMON/C6/BETA(1)
COMMON/C7/ISOX(1)
COMMON/C8/GLO(1)
COMMON/C9/ELEM1(1)
COMMON/C10/ELEM2(1)
COMMON/SECOND/PAR(1)
COMMON/COMPO/FLO(1)
COMMON/SOLID/NM,MAT(2,27),DM(27),POR(27),PER(3,27),CM(27),CH(27)
COMMON/SOLI/COM(27),EXPAN(27),NADF(27)
COMMON/L1/IRN(1)
COMMON/L2/ICN(1)
COMMON/L3/CO(1)
COMMON/L4/WKAREA(1)
COMMON/L5/IKEEP(1)
COMMON/L6/IW(1)
COMMON/L7/JVECT(1)
COMMON/AMMIS/MA,IPIV,U,IAB,NZ
COMMON/CYC/KCYC,ITER,ITERC,TIMIN,SUMTIM,GF,TIMOUT
COMMON/CONTST/RE1,RE2,RERM,NER,KER,DFAC
COMMON/NN/NEL,NCON,NOGN,NK,NEQ,NPH,NB,NK1,NEQ1,NBK,NSEC,NFLUX
COMMON/DM/DELTEN,DELTEX,FOR,FORD
COMMON/KONIT/KON,DELT,IGOOD
COMMON/DG/WUP,WNR
COMMON/SVZ/NOITE,MOP(24)
COMMON/PATCH/SING
COMMON/MODREL/MODE,IDIM,IREL,REL(7),REDLT,RINCR
COMMON/LIQVIS/NTLIQV,NX1LIQV,TLIQV(15),VISLT(15),
AX1LIQV(10),VISLX1(10)
COMMON/FOAMV/vf(1001)
COMMON/REOLG/ALPHA,BETA1,VISI,DPB,TI,QF,IZFOAM,RMWF
COMMON/RELATW/ASW(20,10),AKRW(20,10),AKRH(20,10),PCF(20,10)
```

```
      COMMON/RELATG/ASG(20,10),AKRG(20,10),AKRO(20,10),PCG(20,10)
      DIMENSION D(11,12),F(11,23)
      data imul/1/
      if(imul.gt.1) goto 99
      imul=imul+1
      delta=1.e-10**(1./beta1)
      renn=1./(1.+beta1)
      exnn=(renn-1.)/(2.*renn)
 99   continue
      NZ=0
      IF(MOP(3).GE.1)WRITE(6,201)KCYC,ITER 201   FORMAT(/39H  SUBROUTINE
     MULTI ,24H  ---  [KC
     AYC,ITER] = [,I4,1H,,I3,1H]/)
      DO 100 N=1,NEL
      NLOC=(N-1)*NEQ
      NLOC2=(N-1)*NSEC*NEQ1
      DO 20 K=1,NEQ
 20   R(NLOC+K)=0.
      PHIN=PHI(N)
      NMAT=MATX(N)
      CD=CH(NMAT)*DM(NMAT)*(1.-POR(NMAT))
      DO 101 M=1,NEQ1
      NLM2=NLOC2+(M-1)*NSEC
      DO 1011 K=1,NEQ
 1011 D(K,M)=0.
      DPRES=0.
      IF(M.EQ.2) DPRES=DELX(NLOC+1)
      PRES=X(NLOC+1)+DX(NLOC+1)+DPRES
      DPHI=PHIN*(COM(NMAT)*(PRES-P(N))+EXPAN(NMAT)*(PAR(NLM2+NSEC-
     1)
     A-T(N)))
      PHINN=PHIN+DPHI
      DO 102 NP=1,NPH
      NL2NP=NLM2+(NP-1)*NBK
      SNP=PAR(NL2NP+1)
      IF(SNP.EQ.0.) GOTO 102
```

```
      RHONP=PAR(NL2NP+4)
      PHISRO=PHINN*SNP*RHONP
      DO 103 K=1,NK
      XNPKM=PAR(NL2NP+NB+K)
  103 D(K,M)=D(K,M)+XNPKM*PHISRO
  102 CONTINUE
  101 CONTINUE
      IF(MOP(3).GE.4)WRITE(6,200)ELEM(N),((D(K,M),K=1,NK1),M=1,NEQ1)
  200 FORMAT(/31H ACCUMULATION TERMS AT ELEMENT ,A5/(10(1X,E12.5)))
      DO 105 K=1,NEQ
      IF(ITER.NE.1)
     AR(NLOC+K)=R(NLOC+K)+D(K,1)-DOLD(NLOC+K)
      IF(ITER.EQ.1) DOLD(NLOC+K)=D(K,1)
      DO 106 L=1,NEQ
      IRN(NZ+1)=NLOC+K
      IF(IAB.EQ.0) ICN(NZ+1)=NLOC+L
      IF(IAB.NE.0) JVECT(NZ+1)=NLOC+L
      CO(NZ+1)=-(D(K,L+1)-D(K,1))/DELX(NLOC+L)
      IF(PHINN.EQ.0..AND.K.EQ.L.AND.K.NE.NEQ) CO(NZ+1)=1.
  106 NZ=NZ+1
  105 CONTINUE
  202 FORMAT(/22H RESIDUALS AT ELEMENT ,A5/(10(1X,E12.5)))
  100 CONTINUE
      DO1 N=1,NCON
      vf(n)=0.
      N1=NEX1(N)
      N2=NEX2(N)
      IF(N1.EQ.0.OR.N2.EQ.0) GOTO 1
      N1LOC=(N1-1)*NEQ
      N2LOC=(N2-1)*NEQ
      N1LOC2=(N1-1)*NSEC*NEQ1
      N2LOC2=(N2-1)*NSEC*NEQ1
      D1=DEL1(N)
      D2=DEL2(N)
      WT1=D2/(D1+D2)
      WT2=1.-WT1
```

```
      NMAT1=MATX(N1)
      NMAT2=MATX(N2)
      PO1=POR(NMAT1)
      PO2=POR(NMAT2)
      poa=.5*(po1+po2)
      ISO=ISOX(N)
      GX=BETA(N)*GF
      AX=AREA(N)
      PER1=PER(ISO,NMAT1)
      PER2=PER(ISO,NMAT2)
      DPERI=WT1*PER1+WT2*PER2
      PERI=0.
      IF(DPERI.NE.0.) PERI=PER1*PER2/DPERI
      FAC1=FORD/EVOL(N1)
      FAC2=FORD/EVOL(N2)
      DPX0=X(N2LOC+1)+DX(N2LOC+1)-X(N1LOC+1)-DX(N1LOC+1)
      DPX0=DPX0/(D1+D2)
      IF(MOP(3).GE.5)WRITE(6,199)N,ELEM(N1),ELEM(N2),FAC1,FAC2
  199 FORMAT(/11H CONNECTION,I5,13H  ELEMENTS (,A5,1H,,A5,11H)  FAC1 =
     A ,E12.5,10H  FAC2 = ,E12.5)
      DO 2 M=1,NFLUX
      DPRES1=0.
      DPRES2=0.
      IF(M.EQ.2) DPRES1=DELX(N1LOC+1)
      IF(M.EQ.NEQ+2) DPRES2=DELX(N2LOC+1)
      PRES1=X(N1LOC+1)+DX(N1LOC+1)+DPRES1
      PRES2=X(N2LOC+1)+DX(N2LOC+1)+DPRES2
      DPX=(PRES2-PRES1)/(D1+D2)
      M2=2
      IF(M.EQ.1) M2=0
      IF(2.LE.M.AND.M.LE.NEQ1) M2=1
      N1LM2=N1LOC2+MOD(M2,2)*(M-1)*NSEC
      N2LM2=N2LOC2+(M2/2)*(M-NEQ1)*NSEC
      DO 21 K=1,NEQ
   21 F(K,M)=0.
      IF(MOP(3).GE.6)WRITE(6,198)M,N1LM2,N2LM2,PRES1,PRES2,DPX
```

```
198  FORMAT(/9H FLUX NO.,I3,22H   SECONDARY INDICES (,I5,1H,,I5,12H)
   APRES1 = ,E12.5,11H   PRES2 = ,E12.5,9H   DPX = ,E12.5)
    IF(MOP(3).GE.6)WRITE(6,197)CONI,PAR(N1LM2+NSEC-1),
   APAR(N2LM2+NSEC-1),DTX,F(NK1,M)
197  FORMAT(8H CONI = ,E12.5,11H   TEMP1 = ,E12.5,11H   TEMP2 = ,E12.5,
   A9H   DTX = ,E12.5,10H   FNK1 = ,E12.5)
    DO 3 NP=1,NPH
    N1L2NP=N1LM2+(NP-1)*NBK
    N2L2NP=N2LM2+(NP-1)*NBK
    REL1=PAR(N1L2NP+2)
    REL2=PAR(N2L2NP+2)
    FNPM=0.
    IF(REL1.EQ.0..AND.REL2.EQ.0..AND.NP.NE.3) GOTO31
    S1=PAR(N1L2NP+1)
    VIS1=PAR(N1L2NP+3)
    RHO1=PAR(N1L2NP+4)
    RHO10=PAR(N1LOC2+(NP-1)*NBK+4)
    PCAP1=PAR(N1L2NP+6)
    PCAP10=PAR(N1LOC2+(NP-1)*NBK+6)
    S2=PAR(N2L2NP+1)
    VIS2=PAR(N2L2NP+3)
    RHO2=PAR(N2L2NP+4)
    RHO20=PAR(N2LOC2+(NP-1)*NBK+4)
    PCAP2=PAR(N2L2NP+6)
    PCAP20=PAR(N2LOC2+(NP-1)*NBK+6)
    W1=0.5
    IF(RHO1.EQ.0.) W1=0.
    IF(RHO2.EQ.0.) W1=1.
    W2=1.-W1
    RHOX=W1*RHO1+W2*RHO2
    RHOX0=W1*RHO10+W2*RHO20
    DR=(PCAP2-PCAP1)/(D1+D2)-RHOX*GX
    DR=DR+DPX
    DR0=(PCAP20-PCAP10)/(D1+D2)-RHOX0*GX
    DR0=DR0+DPX0
```

C-for calculation of Bingham fluid flow-10-6-89

```
      if(np.eq.3) then
      dr=epg(dr0,visf)
      endif
C
      IF(DR.GT.0..AND.S2.EQ.0.) GOTO 31
      IF(DR.LT.0..AND.S1.EQ.0.) GOTO 31
      IF(MOP(11).GE.1) WM1=W1
      IF(MOP(11).EQ.0.AND.DR0.GT.0.) WM1=1.-WUP
      IF(MOP(11).EQ.0.AND.DR0.LE.0.) WM1=WUP
      IF(RHO1.EQ.0.) WM1=0.
      IF(RHO2.EQ.0.) WM1=1.
      WM2=1.-WM1
      if(mop(19).ne.2) goto 50
      nfun1=nadf(nmat1)
      nfun2=nadf(nmat2)
      if(np.ne.3) then
      if((dr0.le.0.0.and.np.eq.1).or.(dr0.gt.0.0.and.np.eq.2)) then
      sd1=1.-asg(2,nfun1)
      sd2=1.-asg(1,nfun1)
      if(np.eq.2) sd1=1.-asw(2,nfun1)
      if(np.eq.2) sd2=1.-asw(1,nfun1)
      rel1=0.
      rel2=0.
      if(s1.ge.sd2) rel1=1.
      if(s2.ge.sd2) rel2=1.
      if(s1.gt.sd1.and.s1.lt.sd2) rel1=1.+(s1-sd2)/(sd2-sd1)
      if(s2.gt.sd1.and.s2.lt.sd2) rel2=1.+(s2-sd2)/(sd2-sd1)
      endif
      if((dr0.ge.0.0.and.np.eq.1).or.(dr0.le.0.0.and.np.eq.2)) then
      sd1=asg(1,nfun1)
      sd2=asg(2,nfun1)
      if(np.eq.2) sd1=asw(1,nfun1)
      if(np.eq.2) sd2=asw(2,nfun1)
      rel1=0.
      rel2=0.
      if(s1.ge.sd2) rel1=1.
```

```
if(s2.ge.sd2) rel2=1.
if(s1.lt.sd2.and.s1.gt.sd1) rel1=1.+(s1-sd2)/(sd2-sd1)
if(s2.lt.sd2.and.s2.gt.sd1) rel2=1.+(s2-sd2)/(sd2-sd1)
endif
endif
if(rel1.gt.1.) rel1=1.
if(rel1.lt.0.) rel1=0.
if(rel2.gt.1.) rel2=1.
if(rel2.lt.0.) rel2=0.
if(np.ne.3) goto 60
if(beta(n).ne.0) goto 53
swd=par(n1loc2+nbk+1)
if(dr0.lt.0.) swd=par(n2loc2+nbk+1)
ity=1
if(swd.gt..5) ity=2
sd1=asw(1,nfun1)
sd2=asw(2,nfun1)
if(ity.eq.1) then
rel1=0.
rel2=0.
if(s1.ge.sd2) rel1=1.
if(s2.ge.sd2) rel2=1.
if(s1.gt.sd1.and.s1.lt.sd2) rel1=1.+(s1-sd2)/(sd2-sd1)
if(s2.gt.sd1.and.s2.lt.sd2) rel2=1.+(s2-sd2)/(sd2-sd1)
endif
if(ity.eq.2) then
rel1=0.
rel2=0.
sd3=1.-sd2
sd4=1.-sd1
if(s1.ge.sd4) rel1=1.
if(s2.ge.sd4) rel2=1.
if(s1.lt.sd4.and.s1.gt.sd3) rel1=1.+(s1-sd4)/(sd2-sd1)
if(s2.lt.sd4.and.s2.gt.sd3) rel2=1.+(s2-sd4)/(sd2-sd1)
endif
52  continue
```

```
      if(rel1.gt.1.) rel1=1.
      if(rel1.lt.0.) rel1=0.
      if(rel2.gt.1.) rel2=1.
      if(rel2.lt.0.) rel2=0.
      goto 50
   53 continue
      rel1=s1
      rel2=s2
   50 continue
      if(rel1.gt.par(n1l2np+2)) par(n1l2np+2)=rel1
      if(rel2.gt.par(n2l2np+2)) par(n2l2np+2)=rel2
      if(np.ne.3) goto 60
c-----calculation of viscosity of power-law fluids
      visf=vispw(dr,dperi,poa) c-----calculation of viscosity of general pseudoplastic fluids
      visf=visgpe(dr,dperi,poa)
      if(visf.lt.par(n1l2np+3)) par(n1l2np+3)=visf
      if(visf.lt.par(n2l2pn+3)) par(n2l2np+3)=visf
      if(m.eq.1) vf(n)=visf
   60 continue
      DMOBI=(WM1*REL1/VIS1+WM2*REL2/VIS2)*PERI
      if(np.eq.3) dmobi=(wm1*rel1+wm2*rel2)*peri/visf
      RHOX=WM1*RHO1+WM2*RHO2
      FNPM=DMOBI*RHOX*DR*AX
      DO 4 K=1,NK
      XNPMK=WM1*PAR(N1L2NP+NB+K)+WM2*PAR(N2L2NP+NB+K)
    4 F(K,M)=F(K,M)+XNPMK*FNPM
   31 CONTINUE
      IF(MOP(3).LT.7) GOTO 190
      WRITE(6,196)NP,N1L2NP,N2L2NP
  196 FORMAT(/5H NP =,I3,22H  SECONDARY INDICES (,I5,1H,,I5,1H))
      WRITE(6,195)S1,REL1,VIS1,RHO1,H1,PCAP1
  195 FORMAT(5H S1 =,E12.5,8H  REL1 =,E12.5,8H  VIS1 =,E12.5,8H  RHO1 =,
     AE12.5,6H  H1 =,E12.5,9H  PCAP1 =,E12.5)
      WRITE(6,194)S2,REL2,VIS2,RHO2,H2,PCAP2
  194 FORMAT(5H S2 =,E12.5,8H  REL2 =,E12.5,8H  VIS2 =,E12.5,8H  RHO2 =,
     AE12.5,6H  H2 =,E12.5,9H  PCAP2 =,E12.5)
```

```
      WRITE(6,193)DMOBI,RHOX,DR,FNPM,HNPM,VISF
  193 FORMAT(8H DMOBI =,E12.5,8H  RHOX =,E12.5,6H  DR =,E12.5,8H
     A, FNPM =, E12.5,8H  HNPM =,E12.5,'  VISF=',E12.5)
  190 CONTINUE
      IF(MOP(3).GE.6)WRITE(6,192)(F(K,M),K=1,NK1)
  192 FORMAT(/11H FLOW TERMS/(10(1X,E12.5)))
      IF(M.NE.1) GOTO 3
      FLO((N-1)*NPH+NP)=FNPM
    3 CONTINUE
    2 CONTINUE
      DO 5 K=1,NEQ
      R(N1LOC+K)=R(N1LOC+K)-FAC1*F(K,1)
      R(N2LOC+K)=R(N2LOC+K)+FAC2*F(K,1)
      DO 6 L=1,NEQ
      IRN(NZ+1)=N1LOC+K
      IF(IAB.EQ.0) ICN(NZ+1)=N2LOC+L
      IF(IAB.NE.0) JVECT(NZ+1)=N2LOC+L
      CO(NZ+1)=FAC1*(F(K,L+1+NEQ)-F(K,1))/DELX(N2LOC+L)
      IF(CO(NZ+1).EQ.0.) CO(NZ+1)=SING
      IF(MOP(8).EQ.0.OR.CO(NZ+1).NE.0.) GOTO 40
      NZ=NZ-1
   40 CONTINUE
      IRN(NZ+2)=N2LOC+K
      IF(IAB.EQ.0) ICN(NZ+2)=N1LOC+L
      IF(IAB.NE.0) JVECT(NZ+2)=N1LOC+L
      CO(NZ+2)=-FAC2*(F(K,L+1)-F(K,1))/DELX(N1LOC+L)
      IF(CO(NZ+2).EQ.0.) CO(NZ+2)=SING
      IF(MOP(8).EQ.0.OR.CO(NZ+2).NE.0.) GOTO 41
      NZ=NZ-1
   41 CONTINUE
      NZ=NZ+2
      N1KL=(N1-1)*NEQ*NEQ+(K-1)*NEQ+L
      CO(N1KL)=CO(N1KL)+FAC1*(F(K,L+1)-F(K,1))/DELX(N1LOC+L)
      N2KL=(N2-1)*NEQ*NEQ+(K-1)*NEQ+L
      CO(N2KL)=CO(N2KL)-FAC2*(F(K,L+1+NEQ)-F(K,1))/DELX(N2LOC+L)
    6 CONTINUE
```

```
5   CONTINUE
1   CONTINUE
    IF(NOGN.NE.0) CALL QU
    IF(IGOOD.EQ.3) RETURN
    RERM=0.
    DO10 N=1,NEL
    NLOC=(N-1)*NEQ
    IF(MOP(3).GE.4)WRITE(6,202)ELEM(N),(R(NLOC+K),K=1,NEQ)
    DO10 K=1,NEQ
    NLM=NLOC+K
    DOA=ABS(DOLD(NLM))
    IF(DOA.LT.RE2) RER=R(NLM)/RE2
    IF(DOA.GE.RE2) RER=R(NLM)/DOLD(NLM)
    IF(ABS(RER).LE.RERM) GOTO 10
    RERM=ABS(RER)
    NER=N
    KER=K
10  CONTINUE
    RETURN
    END
```

LAWRENCE BERKELEY LABORATORY
TECHNICAL INFORMATION DEPARTMENT
1 CYCLOTRON ROAD
BERKELEY, CALIFORNIA 94720